

Vol. 61C

# Boletín *de la* Asociación Argentina *de* Astronomía

2020

Boletín de artículos científicos XVI Latin American Regional Meeting  
International Astronomical Union  
Antofagasta, Chile, noviembre de 2019



# Boletín de la Asociación Argentina de Astronomía

BAAA, Vol. 61C



Asociación Argentina de Astronomía. Comité Editorial BAAA Vol. 61C, correspondiente a la XVI LARIM:  
Alberto Marcos Vásquez (Editor en Jefe), Patricia B. Tissera (Editora Invitada),  
Elena Jiménez Bailon (Editora Invitada), Jaime E. Forero-Romero (Editor Invitado),  
Francisco Andrés Iglesias (Secretario Editorial) y Mario Agustín Sgró (Técnico Editorial).



## **Asociación Argentina de Astronomía**

Fundada en 1958

Personería jurídica 11811 (Buenos Aires)

### **Comisión Directiva**

Leonardo J. Pellizza (presidente)  
Susana E. Pedrosa (vicepresidente)  
Rodrigo F. Díaz (secretario)  
Daniel D. Carpintero (tesorero)  
Andrea V. Ahumada (vocal 1)  
Andrea P. Buccino (vocal 2)  
Georgina Coldwell (1er suplente)  
Hebe Cremades (2do suplente)

### **Comisión Revisora de Cuentas**

Sofía A. Cora  
Gerardo Juan M. Luna  
Luis R. Vega

### **Comité Nacional de Astronomía**

Cristina Mandrini (secretaria)  
Lydia Cidale  
Hebe Cremades  
Federico González  
Hernán Muriel

#### **Publicado por**

Asociación Argentina de Astronomía  
Paseo del Bosque s/n, La Plata, Buenos Aires, Argentina

ISSN 1669-9521 (versión digital)  
ISSN 0571-3285 (versión impresa)

#### **Créditos:**

Diseño de portada: Adrián Rovero y Andrea León  
Foto grupal: Cronómetro Producciones  
Confeccionado con la clase "confproc" en L<sup>A</sup>T<sub>E</sub>X

Impreso en Buenos Aires, agosto de 2020

## **Sociedad Chilena de Astronomía**

Fundada en 2000

<https://sochias.cl>

## **XVI Latin American Regional IAU Meeting**

Antofagasta, 3 - 8 November, 2019

Organized by the Chilean Astronomical Society - SOCHIAS.

### **Comisión Directiva**

Monica Rubio Lopez (presidenta)  
Daniela Paola Barría Díaz (1ra vicepresidenta)  
Márcio Catelan (2do vicepresidente)  
Eduardo Ibar Plasser (director ejecutivo)  
María del Carmen Argudo Fernández (secretaria)  
Claudio Cáceres Acevedo (tesorero)  
Patricio Rojo (presidente anterior)

### **Scientific Organizing Committee**

Amelia Bayo (UV/NPF, Chile)  
Reinaldo de Carvalho (INPE, Brazil)  
Carlos Feinstein (IALP/UNLP, Argentina)  
Jaime E. Forero-Romero (UAndes, Colombia)  
Arturo Gomez Ruiz (INAOE, Mexico)  
Guillermo Hägele (IALP/UNLP, Argentina)  
Elena Jiménez Bailon (UNAM, Mexico)  
Elisabete M. de Gouveia Dal Pino (USP, Brazil)  
Monica Rubio (UCHile, Chile)  
Gonzalo Tancredi (UdelaR, Uruguay)  
Patricia B. Tissera (UNAB, Chile) (Chair)  
Katherine Vieira (CIDA, Venezuela)

### **Local Organizing Committee**

Javier Alonso-García (Universidad de Antofagasta)  
Douglas Geisler (Universidad de Concepción)  
Paula Jofré (Universidad Diego Portales)  
Paulina Lira (Universidad de Chile)  
Francesco Mauro (Universidad Católica del Norte)  
Christian Moni (Universidad Católica del Norte)  
Alicia Reyes (Antofagasta Convention Bureau)  
Linda Schmidtbreick (European Southern Observatory)  
Eduardo Unda-Sanzana (Universidad de Antofagasta) (Chair)  
Manuela Zoccali (Pontificia Universidad Católica de Chile)

La organización agradece al Gobierno Regional de Antofagasta y la Agrupación Científico-Cultural Likancabur.

## **Nota inicial**

Estimados lectores:

Esta edición constituye un importante hito para el Boletín de la Asociación Argentina de Astronomía, ya que por primera vez está dedicado a las memorias de una Reunión Regional Latinoamericana de la Unión Astronómica Internacional. Por la propia naturaleza de dicha reunión, a diferencia de los números anteriores del Boletín, en esta edición las secciones, las contribuciones y el prefacio de los editores se encuentran redactados en idioma inglés. El resto del material se encuentra redactado en idioma castellano, como corresponde al diseño usual del Boletín.

Habiendo aceptado el desafío que supone concretar con éxito una empresa tan significativa, surgió la necesidad de decidir la numeración que debe corresponder a este número de excepción, un tema no menor dados los esfuerzos realizados en los últimos años para que dicha numeración quede coordinada con la correspondiente a las Reuniones Anuales de la Asociación Argentina de Astronomía, después de muchos años de desfasaje.

La numeración “61C” que se ha dado a este número del Boletín responde entonces a una doble necesidad. Por un lado, se ha querido utilizar una numeración que se corresponda con la cronología de la edición de los Boletines. Así, este número sigue al “61B”, antecediendo a su vez al próximo número 62 que estará dedicado a la 62<sup>a</sup> Reunión Anual de la Asociación Argentina de Astronomía. Por otra parte, el agregado del sufijo “C” asegura la futura coordinación de la numeración de los BAAA con los ordinales de las Reuniones de la AAA. Cabe destacar que el sufijo “B” fue asignado al número anterior con el mismo objetivo.

Comisión Directiva

Asociación Argentina de Astronomía



## **Prefacio**

Siguiendo la tradición iniciada en 1978 en Chile con la primera Reunión Regional de la Unión Astronómica Internacional en Latinoamérica (LARIM), colegas de esta región se congregaron una vez más para la XVI LARIM. En esta oportunidad, la reunión se realizó en Antofagasta, del 3 al 9 de noviembre de 2019. El evento, al que concurrieron un total de 293 participantes de 11 países diferentes, fue financiado por la Unión, el Gobierno Regional de Antofagasta, organizaciones nacionales y regionales, así como también observatorios internacionales presentes en Chile como ALMA-CONICYT y el Comité Conjunto ESO-Chile.

La XVI LARIM constituyó una oportunidad favorable, no solamente para discutir proyectos actuales y resultados conseguidos por colegas de la región, sino también para imaginar posibles nuevos caminos de colaboración que promuevan el campo de la astronomía en Latinoamérica. Agradecemos a la Sociedad Chilena de Astronomía, y los Comités Organizadores Local y Científico por organizar una exitosa reunión. Vaya nuestro reconocimiento a conferencistas y participantes de la XVI LARIM (<http://www.sochias.cl/larim2019/results/>) por sus destacadas contribuciones.

Esperamos reencontrarnos en la XVII LARIM, que se celebrará en Uruguay en 2022.

Santiago de Chile, 3 de agosto de 2020.

*Patricia B. Tissera*

Editora Invitada

*Elena Jiménez Bailon*

Editora Invitada

*Jaime E. Forero-Romero*

Editor Invitado

*Alberto Marcos Vásquez*

Editor en Jefe

*Francisco Andrés Iglesias*

Secretario Editorial

*Mario Agustín Sgró*

Técnico Editorial

## Foreword

In accordance with the tradition initiated in 1978, in Chile, with the first Regional Meeting of the International Astronomical Union in Latin America (LARIM), astronomers from this area of the world congregated once again for the XVI LARIM. In this opportunity, the meeting was held in Antofagasta, between the 3rd and the 9th of November, 2019. A total of 293 participants from 11 different countries attended the event. The occasion was supported by the Union, the Regional Government of Antofagasta, and both national and regional organizations, as well as international observatories present in Chile such as ALMA-CONICYT and Joint Committee ESO-Chile.

The XVI LARIM constituted a favourable opportunity not only for discussion of on-going projects and results achieved by researchers in the region, but also to envisage possible new routes of collaboration which would strengthen the field of astronomy in Latin America. We thank the Chilean Astronomical Society, and the Local and Scientific Organizing Committees for the organization of a successful meeting. We acknowledge the outstanding contributions of the invited reviewers, speakers and all participants to the XVI LARIM (<http://www.sochias.cl/larim2019/results/>).

Looking forward to seeing you in the XVII LARIM which will be held in Uruguay in 2022.

Santiago de Chile, August 3, 2020.

*Patricia B. Tissera*

Invited Editor

*Elena Jiménez Bailon*

Invited Editor

*Jaime E. Forero-Romero*

Invited Editor

*Alberto Marcos Vásquez*

Editor-in-Chief

*Francisco Andrés Iglesias*

Editorial Secretary

*Mario Agustín Sgró*

Editorial Technician





# Índice general

Nota inicial. . . . .	V
Prefacio . . . . .	VII
Foreword . . . . .	VIII
Foto grupal. . . . .	IX
<b>Review talks</b>	<b>1</b>
Spatially resolved evolution of galaxies	
<i>J.K. Barrera-Ballesteros</i> . . . . .	1
Evolution of low and intermediate-mass stars in binary systems with neutron stars	
<i>O.G. Benvenuto</i> . . . . .	6
On the origin of stellar associations The impact of <i>Gaia</i> DR2	
<i>G. Carraro</i> . . . . .	11
<b>Keynote talks</b>	<b>16</b>
Investigating central massive black hole feedback in galaxies using cosmological hydrodynamical simulations	
<i>P. Barai</i> . . . . .	16
Science with the Cherenkov Telescope Array	
<i>U. Barres de Almeida &amp; for the CTA Consortium</i> . . . . .	19
The challenges of measuring the star formation rate of galaxies	
<i>M. Boquien</i> . . . . .	22
Dynamical effects of an eccentric giant planet on outer small body reservoirs	
<i>G.C. de Elía</i> . . . . .	25
Deciphering the accretion history of galaxies: insights from stellar halos	
<i>A. Monachesi</i> . . . . .	28
100th anniversary of the International Astronomical Union	
<i>S. Torres-Peimbert</i> . . . . .	31
Solar corona tomography	
<i>A.M. Vásquez</i> . . . . .	34
<b>Contributed talks</b>	<b>37</b>

Chemodynamic structures in dwarf galaxy Leo I Chemodynamical tracers for the formation of dSph <i>A.G. Alarcón Jara, M. Fellhauer, J.D. Simon &amp; A. del Pino</i> . . . . .	37
STARHORSE photo-astrometric distances, extinctions, and astrophysical parameters for <i>Gaia</i> DR2 stars <i>F. Anders, A. Khalatyan, C. Chiappini, A.B.A. Queiroz &amp; B.X. Santiago</i> . . . . .	38
Characterizing the iron $K\alpha$ line variability in a large sample of AGNs <i>C. Andonie &amp; F. Bauer</i> . . . . .	39
The formation of ultra-faint dwarf spheroidal galaxies <i>C.A. Aravena, M. Fellhauer, F. Urrutia Zapata &amp; A.G. Alarcón Jara</i> . . . . .	40
Analytical solutions for radiation-driven winds in massive stars. II: The $\delta$ -slow regime <i>I. Araya, A. Christen, M. Curé, L. Cidale, H. Clavería, R. Venero, M. Haucke &amp; C. Arcos</i> . . . . .	41
A MaNGA-View on how isolated galaxies formed and evolved <i>M. Argudo-Fernández, M. Boquien, F. Yuan, S. Shen, J. Yin &amp; R. Chang</i> . . . . .	42
Helium abundance in horizontal branch stars in M28 <i>D. Barría &amp; C. Moni Bidin</i> . . . . .	43
Scaling relations for globular cluster systems in early-type galaxies <i>J.P. Caso, B.J. De Bórtoli, A.I. Ennis &amp; L.P. Bassino</i> . . . . .	44
Kinematic asymmetries in dark matter dominated galaxies <i>L. Chemin, P. Amram, C. Carignan, C. Balkowski &amp; B. Épinat</i> . . . . .	45
Feeding and feedback in local radio galaxies <i>G.S. Couto, T. Storchi-Bergmann, A. Robinson, R.A. Riffel, P. Kharb, D. Lena &amp; A. Schnorr-Müller</i> . . . . .	46
Search, spectral classification and benchmarking of brown dwarfs <i>M. dal Ponte, B. Santiago, A. Carnero Rosell &amp; B. Burningham</i> . . . . .	47
A panchromatic study of the stellar populations in NGC 4303 <i>N.Z. Dametto, R. Riffel, L. Colina, R.A. Riffel &amp; M. Boquien</i> . . . . .	48
The role of radiation backgrounds in the direct collapse scenario <i>V.B. Díaz, D.R.G. Schleicher, S. Bovino, S. Vanaverbeke, R. Riaz &amp; M.Z.C. Vergara</i> . . . . .	49
Neutron escape from microquasar jets <i>G.J. Escobar, L.J. Pellizza &amp; G.E. Romero</i> . . . . .	50
Formation scenarios of dSph galaxies <i>M. Fellhauer, A.G. Alarcon Jara, C. Aravena, F. Urrutia Zapata, D.R. Matus Carrillo &amp; M.C.B. Morales Inostroza</i> .	51

Deuteration chemistry in massive star-forming regions	
<i>S. Ferrada-Chamorro, S. Bovino, A. Lupi &amp; D.R.G. Schleicher</i>	52
Comparative study of activity of the near-parabolic orbitcomet C/1977 R1 (Kohler)	
<i>L.F. de Araújo, A.A. de Almeida &amp; G.C. Sanzovo</i>	53
<i>Kepler</i> photometry and spectroscopic observations of the $\delta$ Scuti / $\gamma$ Doradus hybrid candidate star KIC 4920125	
<i>L. Fox-Machado &amp; J. Higuera</i>	54
Orbital light-curve changes in DPVs related with the long cycle	
<i>J. Garcés, R.E. Mennickent &amp; G. Djurašević</i>	55
Gas velocity structure of the Orion A integral-shaped filament	
<i>V. González Lobos &amp; A.M. Stutz</i>	56
Collisional blue stragglers as the “top of the iceberg” of modified stars in globular clusters	
<i>V.V. Kravtsov</i>	57
Link between filaments and star formation: kinematics	
<i>H.-L. Liu &amp; A. Stutz</i>	58
Introducing the new photometric PYTHON3 package SKZPIPE	
<i>F. Mauro</i>	59
A speckle survey of binary stars in the southern sky	
<i>R.A. Mendez and E. Costa</i>	60
Cluster galaxies in the cosmic afternoon with SpARCS and GOGREEN	
<i>J. Nantais, R. Demarco, P. Cerulo, G. Wilson, M. Balogh, A. Muzzin, G. Rudnick, A. Noble, L. Old, R. van der Burg, SpARCS Collaboration &amp; GOGREEN Collaboration</i>	61
The Orion luminosity/mass function revisited	
<i>K. Peña Ramírez</i>	62
Chemical gradients in the disk galaxies M33 and NGC 300	
<i>M. Peña &amp; S. Flores-Durán</i>	63
Non-porphyrinic chondrules in unequilibrated chondrites (CO) from Atacama Desert	
<i>G.A. Pinto, M.E. Varela &amp; R. Martínez</i>	64
Design and analysis of a prototype antenna for the low-frequency radio telescope MIST	
<i>O.A. Restrepo, F.I. Lucero, R. Molina, G. Chaparro, F.P. Mena &amp; R. Bustos</i>	65

A MUSE study of the Seyfert 1 galaxy NGC 7469: Spatially resolved star-formation and AGN-driven winds <i>A.C. Robledo-Orús, J.P. Torres-Papaqui, A.L. Longinotti, R.A. Ortega-Minakata, S.F. Sánchez, Y. Ascasibar, E. Bellocchi, L. Galbany, M. Chow-Martínez, J.J. Trejo-Alonso, A. Morales-Vargas &amp; F.A. Romero-Cruz</i> . . . . .	66
Improving FOF galaxy group finder <i>F. Rodríguez &amp; M. Merchán</i> . . . . .	67
Hierarchical star formation in nearby galaxies <i>M.J. Rodríguez, G. Baume &amp; C. Feinstein</i> . . . . .	68
Uncertainties in quantitative spectroscopy of O-type stars <i>C. Sabín-Sanjulián</i> . . . . .	69
Evaluating ‘twin’parallaxes for binary stars <i>A. Samadi-Ghadim &amp; P. Jofré</i> . . . . .	70
Torques on low-mass objects embedded in discs in eccentric orbits <i>F.J. Sánchez-Salcedo</i> . . . . .	71
Tidal effects in potentially habitable planets at the sub-stellar mass limit <i>M.B. Sánchez, G.C. de Elía &amp; J.J. Downes</i> . . . . .	72
What obscures a galaxy? <i>J.H. Barbosa-Santos &amp; G.B. Lima Neto</i> . . . . .	73
Formation of massive black holes: interplay of collisions and accretion <i>D.R.G. Schleicher, P.J. Alister Seguel, B. Reinoso, M.Z.C. Vergara, T. Boekholt, M.A. Fellhauer, R.S. Klessen, N. Leigh, C. Olave, V.B. Díaz, C. Bravo-Castillo, R. Riaz, B. Bandyopadhyay &amp; L. Haemmerle</i> . . . . .	74
Star formation history of Canis Major OB1 II: a bimodal X-ray population revealed by <i>XMM-Newton</i> <i>T. Santos-Silva, J. Gregorio-Hetem, T. Montmerle &amp; B. Fernandes</i> . . . . .	75
With a view to ELT: the <i>Primera Luz</i> outreach initiative <i>E. Unda-Sanzana</i> . . . . .	76
A new formation scenario for compact ellipticals <i>F. Urrutia Zapata, M. Fellhauer, A.G. Alarcón Jara, D.R. Matus Carrillo &amp; C.A. Aravena</i> . . . . .	77
Asteroseismic analysis of subdwarf B variable stars: what we have learned from the recent space missions <i>M. Uzundag &amp; M. Vučković</i> . . . . .	78
New cycle period in chromospherically active stars, characterized by some activity index <i>F.A. Villegas, R.E. Mennickent &amp; J. Garcés</i> . . . . .	79

<b>Posters</b>	<b>80</b>
Cosmic magnetic fields from cosmological simulations	
<i>S. Adduci Faria, P. Barai &amp; E.M. de Gouveia Dal Pino</i> . . . . .	80
Massive open clusters in VVV data using unsupervised clustering algorithms	
<i>J. Anais Vilchez, S. Ramírez-Alegría &amp; K. Peña-Ramírez</i> . . . . .	80
Heating of protostellar accretion discs associated with plasma inhomogeneities	
<i>N.F.S. Andrade &amp; V. Jatenco-Pereira</i> . . . . .	81
The lithium–rotation connection in the Psc–Eri stream	
<i>J. Arancibia, J. Bouvier, A. Bayo, P.A.B. Galli, W. Brandner, H. Bouy &amp; D. Barrado</i> . . . . .	81
Atmospheric chemistry of a free-floating planet’s exomoon	
<i>P.J. Ávila, S. Bovino &amp; T. Grassi</i> . . . . .	82
Alternative classification diagrams for AGN/SBGs	
<i>C.P. Aydar, J.E. Steiner &amp; D. May</i> . . . . .	82
Stellar magnetic activity in the Orion star-formation complex	
<i>M.G. Batista, G. Pinzón &amp; J. Hernández</i> . . . . .	83
Multiwavelength analysis of brightness variations in FSRQs	
<i>P.P.B. Beaklini, T.P. Dominici, Z. Abraham &amp; J.C. Motter</i> . . . . .	83
Time evolution of rotating and magnetized white dwarf stars	
<i>L. Becerra, K. Boshkayev, J.A. Rueda &amp; R. Ruffini</i> . . . . .	84
Five new young cluster candidates in VVVX disc area	
<i>S. Bernal, J. Borissova &amp; R. Kurtev</i> . . . . .	84
Atomic/molecular opacities and globular cluster spectra	
<i>V. Branco &amp; P.R.T. Coelho</i> . . . . .	85
Investigating the 21 cm signal from the reionization epoch	
<i>C. Bravo-Castillo &amp; D.R.G. Schleicher</i> . . . . .	85
Ionospheric absorption with a 38 MHz ROACH-based array	
<i>G. Burgos, R. Reeves, A. Foppiano, R. Rodríguez, J. Parra, K. Cortes, D. Arroyo &amp; K. Makita</i> . . . . .	86
Best dSph candidates for indirect dark matter detection	
<i>C. Calderón-Galaz, N.D. Padilla &amp; A. Reisenegger</i> . . . . .	86
Study of the binary system TYC 7398-2542-1	
<i>P.A. Calderón &amp; R.E. Mennickent</i> . . . . .	87

Virial factor and Buckingham's $\Pi$ theorem	
<i>G. Cardona &amp; M.-A. Higuera-G</i> . . . . .	87
Recovering Algol-type eclipsing binaries in the CRTS	
<i>A. Carmo, C.E. Ferreira Lopes, A. Papageorgiou, F.J. Jablonski, C.V. Rodrigues, A.J. Drake, N.J.G. Cross &amp; M. Catelan</i> . . . . .	88
Material heritage of the history of radioastronomy in Brazil	
<i>T.P. Dominici, D.A. da Silva Mesquita, C.P. dos Santos, M.C.M. Casimiro &amp; Y.C.P. Mariano</i> . . . . .	88
Deformations of NSs as a source of gravitational waves	
<i>F. Espinoza-Arancibia &amp; A. Reisenegger.</i> . . . .	89
Optical classification and dynamical study of the OH megamaser galaxy IRAS 11506-3851	
<i>L.M. Gatto &amp; D. Sales</i> . . . . .	89
A detailed re-analysis of the planetary system around Gl 832	
<i>P. Gorrini &amp; N. Astudillo-Defru</i> . . . . .	90
Terzan 5, a fossil relic of the Galactic bulge	
<i>V. Gotta, F. Mauro, C. Moni Bidin, D. Geisler &amp; F. Ferraro</i> . . . . .	90
Effect of the inclination of the BLR on the virial factor	
<i>M.-A. Higuera-G. &amp; G. Cardona</i> . . . . .	91
LLAMA, a sub-mm radiotelescope in the Andes	
<i>J. Lepine, Z. Abraham, G.G. Castro, J.J. Larrarte, E. Rasztrocky, G. Gancio, T. Dominici, P. Beaklini, F. Correria, W. Beccari, M. Luqueze, S. Verri, D. Zanella, J. Kooi &amp; D. Ronsó.</i> . . . .	91
IVIA: Ibero-American VLBI Initiative	
<i>J. Lepine, J-P. Raulin, T. Dominici, G.G. Castro, F. Roig, A. Wiermann, R. Hadano, S. Lucena, M. Garcia, F. Correria, W. Beccari, M. Luqueze, S. Verri, D. Zanella, K. Melendez-Delmestre, T. Gonçalves, U. Barres, M. Borges &amp; M. Figueredo</i> . . . . .	92
Unveiling the properties of strong emission-line galaxies at redshift 2–4	
<i>M. Llerena &amp; R. Amorín</i> . . . . .	92
Magnetic accretion in SW Sextantis stars	
<i>I.J. Lima, C.V. Rodrigues, P. Szkody, C.E.F. Lopes, F.J. Jablonski, K.M.G. Silva, A.S. Oliveira, M.S. Palhares &amp; S. Shugarov</i> . . . . .	93
Cataclysmic variables with enhanced emission regions	
<i>P. Longa-Peña, D. Barría, H. Salas, M. Romero &amp; D. Herrera.</i> . . . .	93

Diffraction in stellar occultations reproduced in laboratory	
<i>L.E. Manzano &amp; J. H. Castro-Chacón</i> . . . . .	94
Binary interactions in a static filament	
<i>M.C. Morales &amp; M. Fellhauer</i> . . . . .	94
Five-year spectral monitoring of Alpha Sco	
<i>B. Oostra, M.G. Batista &amp; L.F. Rodríguez</i> . . . . .	95
The 3D positions of gas and dust clouds in the Galactic centre	
<i>C. Ordenes-Huanca, J. Cuadra &amp; Q.D. Wang</i> . . . . .	95
Search of exoplanets around evolved binary stars	
<i>E.S. Pereira, L.A. Almeida, M.G. Pereira &amp; T.A. Michtchenko</i> . . . . .	96
GW170817-like events in Chandra X-ray catalog	
<i>J. Quirola-Vásquez &amp; F.E. Bauer</i> . . . . .	96
The Universe as a statistical ensemble	
<i>N.B. Razo López &amp; A.M. Cervantes Contreras</i> . . . . .	97
Kinematical analysis of lines in high-ADF planetary nebulae	
<i>F. Ruiz-Escobedo &amp; M. Peña</i> . . . . .	97
A new family of analytical potential–density pairs for galaxy models with thin disks and spheroidal halos	
<i>Y.F. Santos, O.M. Pimentel &amp; G.A. González</i> . . . . .	98
The VISCACHA survey - structure of outer MC star clusters	
<i>J.F.C. Santos Jr. , F. Maia, B. Dias, L. Kerber, A. Piatti, E. Bica &amp; the VISCACHA team</i> . . . . .	98
VHE $\gamma$ -rays from the Galactic center generated by cosmic rays	
<i>A. Scherer, A. Reisenegger &amp; J. Cuadra</i> . . . . .	99
Characterization of young stellar clusters and star-forming regions using S-PLUS	
<i>T. Santos-Silva, J. Gregorio-Hetem, V. Jatenco-Pereira &amp; S-PLUS collaboration</i> . . . . .	99
Non-spherical distribution of rotational velocities of Be stars via Tikhonov deconvolution	
<i>M. Solar, M. Curé, D. Rial, A. Christen &amp; J. Cassetti</i> . . . . .	100
Atacama region as a planetary analog for astrobiology	
<i>A. Tavernier, M. Barbieri, R. Oses, A. Garcia &amp; C. Ulloa</i> . . . . .	100
“Noche de las Estrellas”: a success story in Mexico and in other countries	
<i>S. Torres-Peimbert, B. Arias, E. Velarde &amp; J. Franco</i> . . . . .	101

Revista Mexicana de Astronomía y Astrofísica:	
<i>S. Torres-Peimbert &amp; C. Allen</i> . . . . .	101
Pathway to black hole formation in protostar clusters	
<i>M.Z.C. Vergara, D.R.G. Schleicher, T. Boekholt, B. Reinoso, M. Fellhauer, R.S. Klessen, N. Leigh &amp; V.B. Díaz</i> . . . . .	102
Bayes-based estimation of orbital parameters in hierarchical triple stellar systems	
<i>C.L. Villegas, R.A. Méndez, M.E. Orchard &amp; J.F. Silva</i> . . . . .	102
<b>Índice de autores</b>	<b>103</b>



# Spatially resolved evolution of galaxies

J.K. Barrera-Ballesteros<sup>1</sup>

<sup>1</sup> *Instituto de Astronomía, Universidad Nacional Autónoma de México, México, D.F., Mexico*

*Contact* / jkbarrerab@astro.unam.mx

**Abstract** / Projected in the sky, galaxies are spatially-resolved objects. To understand how they formed and evolve it is necessary to study the spatial distribution of their observables. In this review talk, we briefly describe some scaling relations used to understand the physical processes that drive galaxy evolution, in particular for disc-like star-forming galaxies. First, we explore the relations derived using integrated galactic properties, then we introduce the scaling relations at kpc scales derived using the technique called Integral Field Spectroscopy (IFS) for large samples of galaxies in the nearby Universe. The very existence of scaling relations at kpc scales is a strong evidence that any physical scenario that explains the observed global scaling relations must be able to also explain their local counterpart.

*Keywords* / galaxies: evolution — galaxies: formation — galaxies: structure

## 1. Introduction

One of the most powerful tools that astronomers have to understand how galaxies form and evolve is through the so called scaling relations. These relations link different observational properties, depending on how tight they are, what dynamical range they cover, and their similarity across cosmic times; they give crucial information about the scenarios galaxies form and evolve.

Historically, one of the first studies that described the spatial distribution of light in galaxies was the morphological classification of galaxies by E. Hubble (Hubble, 1926). In this scheme, galaxies are classified basically in two large families of morphologies: reddish or yellowish spheroidals with non-existing substructures and bluish disk-like galaxies with a wide variety of structures. In the last decade, with the use of the IFS observational technique in extensive samples of galaxies it has been possible to determine the relation between observables at kpc-scales. In the next section (Sec. 2.) we will describe the main scaling relations for star-forming galaxies. This is a fundamental step to understand the scaling relations for star-forming regions derived at kpc scales (Sec. 3.). A recent detailed review of scaling relations at kpc scales is presented by Sanchez (2019).

To display both the global and scaling relations we will use throughout this article the dataset from the Sloan Digital Sky Survey SDSS-IV MaNGA survey (Mapping Nearby Galaxies at Apache Point, Bundy et al., 2015) in its 9th data release. This sample consists of more than 8000 galaxies located in the nearby Universe ( $z < 0.15$ ) covering a wide range of stellar masses and morphologies. Therefore this sample can be considered as representative of the local Universe. The analysis of this dataset was performed by the analysis pipeline PIPE3D (Sánchez et al., 2016).

## 2. Scaling relations for global galactic properties

Prior to acquisition of large datasets from spectroscopic surveys, photometric studies already revealed important information of the physical properties of galaxies. With large samples of galaxies it was evident that galaxies follow a clear relation in a color-magnitude diagram (CMD). Red galaxies follow a clear correlation with their luminosity. High-luminosity galaxies tend to be redder than low-luminosity ones following a tight correlation (known as the “Red Sequence of Galaxies”), whereas blue galaxies are located in the so-called “Blue Cloud”. More than a mere classification tool, the CMD has been thought as an *evolutionary plane* where young galaxies in the Blue Cloud evolve moving from this cloud to a intermediate zone called the “Green Valley”. When aging, galaxies end up in the red-sequence. What are the exact physical processes that lead to this possible evolutionary path, and what are the timescales in which they operate are still to a large extent open questions for which astronomers are still looking for comprehensive answers.

With the appearance of large spectroscopic surveys such as the Sloan Digital Sky Survey (SDSS), it was possible to determine scaling relations in large samples of galaxies using other observables. other structural properties of the galaxies. In this section we will describe three fundamental scaling relations derived using integrated properties for star-forming galaxies: The star-formation law (Sec. 2.1.), the star-formation main sequence (Sec. 2.2.), and the mass-metallicity relations (Sec. 2.3.).

### 2.1. The star-formation (Kennicutt-Schmidt) law

The star-formation law (also referred as the Kennicutt-Schmidt law, KS-law) correlates the star-formation rate

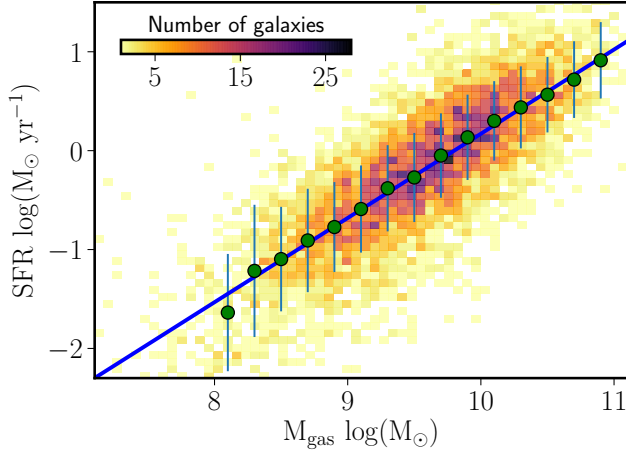


Figure 1: The integrated star-formation law for 5600 galaxies included in the MaNGA survey. Both parameters are derived using optical observables (see Sec. 2.1. for details). The blue line is an ODR fitting of the median values of SFR at different bins of  $M_{\text{gas}}$  (green circles). The slope of this line match the slope using different observables for SFR and  $M_{\text{gas}}$  (Gao & Solomon, 2004; Kennicutt & Evans, 2012).

(SFR) with the amount of cold gas. For a detailed review on the topic, the reader is referred to Kennicutt & Evans (2012). Projected in the sky, this relation is measured in surface densities ( $\Sigma_{\text{SFR}} = \Sigma_{\text{gas}}^N$ ); depending on the scales, different components of the cold gas are measured (i.e. neutral, molecular, and dense), and the proxy for SFR, the index  $N$ , varies (Kennicutt & Evans, 2012). This law is also presented in terms of extensive terms.

In Fig. 1, we plot the relation between the integrated SFR and the molecular gas ( $M_{\text{gas}}$ ) for a sample of 5600 galaxies included in the latest internal MaNGA data release where it was possible to determine  $M_{\text{gas}}$ . SFR is derived using the dust-corrected luminosity of the  $\text{H}\alpha$  line, whereas the gas mass ( $M_{\text{gas}}$ ) is obtained using as calibrator the optical extinction ( $A_V$ ) from the  $\text{H}\alpha/\text{H}\beta$  Balmer decrement, following Barrera-Ballesteros et al. (2019). The two-dimensional histogram shows the trend of these two parameters with SFR increasing for galaxies with large  $M_{\text{gas}}$ . The green circles represent the median SFR for different bins of  $M_{\text{gas}}$ , their error bars representing the standard deviation of the SFR at each of those bins. The blue line shows the best Orthogonal Distance Regression (ODR) fit of a linear fit to these median values. The best relation is described as

$$\log \frac{\text{SFR}}{M_{\odot} \text{ yr}^{-1}} = a + b \times \log \frac{M_{\text{gas}}}{M_{\odot}}, \quad (1)$$

with  $a = -8.34 \pm 0.16$  and  $b = 0.85 \pm 0.1$ . We note that the slope of this relation is in very good agreement with the one derived using direct observations of the cold dense gas and SFR with IR observables in spiral galaxies (e.g. Gao & Solomon, 2004; Kennicutt & Evans, 2012). This strong correlation suggests the deep interplay between the amount of gas available to produce new generations of stars and the amount of those stars. As we will see below, as these relations holds at

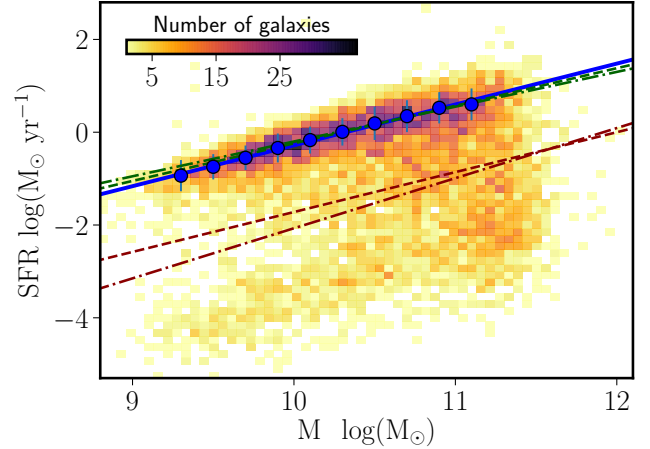


Figure 2: Integrated SFR against the total stellar mass ( $M_*$ ) for 8000 galaxies included in the MaNGA survey. The blue line is an ODR fitting of the median values of SFR at different bins of  $M_*$  (green circles). To perform the ODR fitting, we select those galaxies with  $\text{H}\alpha$  equivalent width  $\text{EW}(\text{H}\alpha) > 10 \text{ \AA}$ . The slope of this line matches the trend derived for different studies using star-forming galaxies observed within different IFS surveys. Green and red dashed lines show the SFMS and RGS derived for the CALIFA survey (Cano-Díaz et al., 2016). Green and red dot-dashed lines represent the best fit derived using the MaNGA survey (Cano-Díaz et al., 2019).

kpc scales, the physical interpretation has to be related to scale-independent processes.

## 2.2. The star-formation main sequence (SFMS)

With large data sets from spectroscopic surveys emerged clearly the analogous of the CMD. In Fig. 2 we plot the relation between the SFR and the total stellar mass ( $M_*$ ) for 8004 MaNGA galaxies. As with the color in the CMD, different authors have noticed that there is a clear bimodality in the SFR (e.g. Kauffmann et al., 2003a; Baldry et al., 2004; Brinchmann et al., 2004). Galaxies with high SFR are well described by a tight correlation (known as the star-formation main sequence, SFMS); as  $M_*$  increases, the population of galaxies is divided between galaxies located in the SFMS and those with much less SFR for the same  $M_*$ . Galaxies located in this region of the SFR– $M_*$  distribution are considered as part of the “Retired Galaxies Sequence” (RGS, e.g. Cano-Díaz et al., 2016).

Different authors have noticed that an excellent parameter to differentiate galaxies from the SFMS and the RGS is the equivalent width of the  $\text{H}\alpha$  emission line ( $\text{EW}(\text{H}\alpha)$ , e.g. Cid Fernandes et al., 2010; Sánchez et al., 2013). Galaxies/regions with large values of  $\text{EW}(\text{H}\alpha)$  are actively star forming. To derive the best fit of the SFMS we select those galaxies with  $\text{EW}(\text{H}\alpha) > 10 \text{ \AA}$  measured at their effective radius (3903 galaxies). In Fig. 2 we show the best ODR fit to the SFMS for the MaNGA sample. The best fit is in very good agreement with previous estimations of the SFMS using different IFS samples (see reference in Fig. 2). Since the SFR– $M_*$

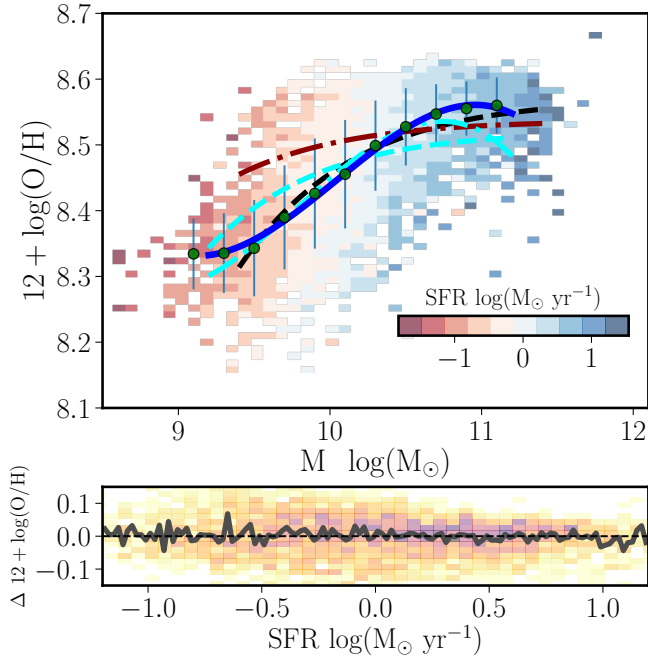


Figure 3: The mass-metallicity relation (MZR) for 3310 galaxies included in the MaNGA survey is shown in the top panel. The relation is colored by the SFR of the galaxies. Note the almost vertical lines in color for a given SFR bin. The blue line is a fourth-degree polynomial fitting of the median values of metallicity at different bins of  $M_*$  (green circles). The black dashed, red dot-dashed, cyan dashed, and cyan dot-dashed lines represent descriptions of the MZR for previous studies using IFS datasets (MaNGA, CALIFA, and SAMI; Barrera-Ballesteros et al., 2017; Sánchez et al., 2017, 2019, respectively). The bottom panel shows the distribution of the residuals of the MZR against SFR. The black line represents the median residual. No significant trend is found between the residuals of the MZR and the SFR.

plane compares the recent star formation with the integral of the star-formation history (SFH) across cosmic times, the existence of a bimodality can be considered as a record of two different channels of galaxy evolution. Massive galaxies tend to exhibit a sharp SFH in comparison to low-mass galaxies; this effect is known as downsizing (Thomas et al., 2005; Cimatti et al., 2006; Fontanot et al., 2009). Similar to the CMD (Schawinski et al., 2014), the location of a galaxy in the SFR– $M_*$  plane is strongly dependent of the morphology (e.g. Bluck et al., 2019).

### 2.3. The mass–metallicity relation (MZR)

Four decades ago, it was evident the close relation between the ionized gas metallicity derived from emission lines in H II regions/galaxies and the total stellar mass (e.g. Lequeux et al., 1979; Skillman et al., 1989; Zaritsky et al., 1994). In the seminal study by Tremonti et al. (2004), using single-fiber spectroscopy for more than 53000 star-forming galaxies included in the SDSS survey, they found a very tight correlation (scatter  $\sim 0.1$  dex) between the metallicity ( $12 + \log(\text{O}/\text{H})$ ) and  $M_*$  covering several orders of magnitude in stellar mass.

In Fig. 3 we plot the MZR relation for 3310 star-forming galaxies selected previously in Sec. 2.2.. The trend of the metallicity observed here is very similar as the one studied by Tremonti et al. (2004). As  $M_*$  increases so does the metallicity, reaching a plateau at massive galaxies ( $\log(M_*/M_{\odot}) \sim 10.5$ ). Following Barrera-Ballesteros et al. (2017), we measure the metallicity at the effective radius of the selected MaNGA galaxies. To estimate the metallicity we use the strong-line calibrator derived by Marino et al. (2013). We also overplot different estimations of the MZR following a homogeneous procedure as the one used here for different IFS surveys (see caption in Fig. 3). This comparison highlights the robustness of the MZR despite the sample of selected galaxies.

Using the same SDSS it has also been proposed a secondary correlation between the SFR and the MZR (Ellison et al., 2008). Later, different authors called this relation a fundamental metallicity relation or plane (FMR, Mannucci et al., 2010; Lara-López et al., 2010; Maiolino & Mannucci, 2019). In this scenario, the scatter of the MZR is driven by the SFR. For a given stellar mass, galaxies with large SFR tend to have low metallicities in comparison to galaxies with low SFR. In Fig. 3, we color the galaxies in the MZR for different SFR bins. We note that for a given  $M_*$  the SFR color is rather constant for different metallicities. To further quantify the possible impact of the SFR in the MZR we plot in the bottom panel of Fig. 3 its residual (with respect to the best fourth-degree polynomial fit, blue line) against the SFR. We find that the median value of the scatter does not strongly correlate with the SFR. In other words, this implies that introducing the SFR as a secondary parameter does not reduce the observed scatter of the MZR. This lack or small impact of the SFR in the MZR has been observed in different works (e.g. Kashino et al., 2016; Telford et al., 2016). In particular, we have explored this dependence (or lack of thereof) for galaxies within all large IFS surveys using a heterogeneous set of calibrators (MaNGA, CALIFA, and SAMI; Barrera-Ballesteros et al., 2017; Sánchez et al., 2017, 2019, respectively). We find little to none relation of the SFR or specific SFR (SSFR) to the MZR. Including the SFR as second parameter does not reduce the scatter of the MZR. Our results suggest that rather than the metallicity be regulated by global flows of gas (thus related with recent global SFR), it has a local origin (see Sec. 3.3.). Possibly the ionized gas metallicity is a record of the local SFH.

## 3. Scaling relations at kpc scales

### 3.1. The resolved star-formation law

With radio telescopes in interferometric mode it has been possible to trace the distribution of the cold gas component at kpc scales ( $\Sigma_{\text{gas}}$ ) in nearby galaxies as well as the SFR density ( $\Sigma_{\text{SFR}}$ ). This allows to explore the KS-law at (sub-)kpc scales in extragalactic objects (e.g. Bigiel et al., 2008; Leroy et al., 2008; Kennicutt & Evans, 2012). In Fig. 4 we plot this relation for more than  $2.38 \times 10^6$  regions (or spaxels). As in Sec. 2.1., we

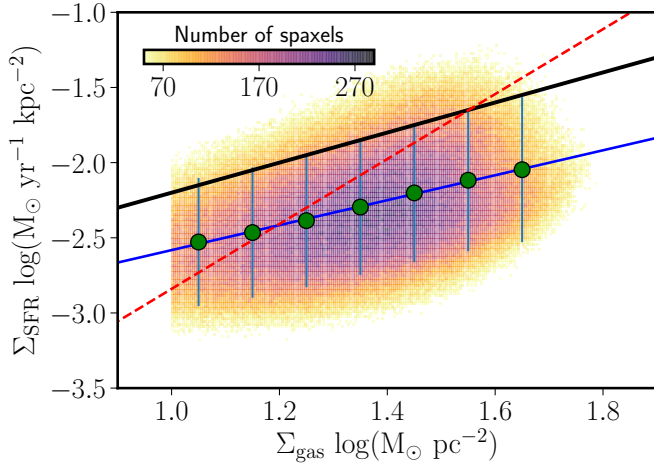


Figure 4: The star-formation law for  $2.38 \times 10^6$  spaxels located in 5382 MaNGA galaxies.  $\Sigma_{\text{gas}}$  is derived using as proxy the optical extinction (see details in Sec. 2.1.). The derived KS law follows a similar trend as those derived using direct observations of molecular gas (black-solid line, EDGE survey; Bolatto et al., 2017), and those using other IFS surveys (red dashed line, CALIFA survey; Barrera-Ballesteros et al., 2019).

use the  $A_V$  as a proxy for  $\Sigma_{\text{gas}}$ . Similar to the extensive properties,  $\Sigma_{\text{SFR}}$  tightly correlates with  $\Sigma_{\text{gas}}$ . The KS-law derived here is similar as those derived using direct observations of molecular gas (Bolatto et al., 2017).

As mentioned in the review by Kennicutt & Evans (2012), the existence of a kpc and global KS-law in extragalactic targets may just be due to averaging in large scales of physical processes occurring at scales of pcs. Even more, as they argue, there are two possible, maybe competing, scenarios that explain the scaling relations observed at pc scales in the Milky Way. In the first scenario star formation is locally controlled within molecular clouds. Therefore, the properties and amount of gas in molecular clouds control the efficiency with which they form new stars (e.g. Krumholz & McKee, 2005). In the other scenario, star formation is controlled mainly by galactic-scale processes, in particular dynamic ones (e.g. Ostriker et al., 2010).

### 3.2. The resolved star-formation and retired sequences

Similar to what we observe above in the SFR– $M_*$  plane (see Sec. 2.2.), there is a clear bimodality observed in the SFR surface density  $\Sigma_{\text{SFR}}$  plotted against the stellar mass density  $\Sigma_*$  at kpc scales in the nearby Universe (see Fig. 5). As for the SFMS and RGS, a good proxy to differentiate the resolved star-formation sequence (rSFS) and the retired sequence (rRS) is via the  $\text{EW}(\text{H}\alpha)$ . Following Cano-Díaz et al. (2016), we select spaxels with  $\text{EW}(\text{H}\alpha) > 6 \text{ \AA}$  as part of the rSFS; spaxels with smaller  $\text{EW}(\text{H}\alpha)$  are considered as rRS spaxels. The best fit of both relations are in very good agreement with other studies, even using different IFS surveys (see caption of Fig. 5 for details). Different studies have suggested also the strong impact of the morphology and spatial dis-

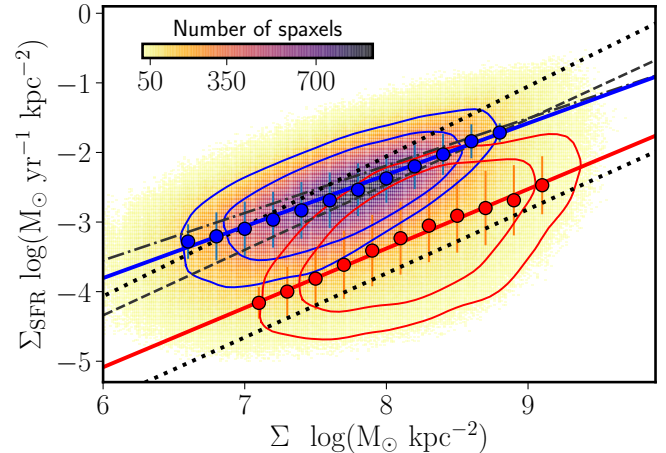


Figure 5:  $\Sigma_{\text{SFR}}$  against  $\Sigma_*$  for  $6.06 \times 10^6$  spaxels located in 7687 galaxies included in the MaNGA survey. The distribution is color-coded according to the density of spaxels. Each of the blue and red contours enclose 80% and 60% of the so called resolved star-formation (rSFS) and resolved retired sequences (rRS), respectively (see details in the text). Blue and red lines represent the best fits of the medians of  $\Sigma_{\text{SFR}}$  for bins of  $\Sigma_*$  for the rSFS and rRS, respectively. We overplot the estimation of the rSFS from other IFS studies (dot-dashed, dashed and dotted lines represent the fits from the CALIFA, and MaNGA studies; Cano-Díaz et al., 2016, 2019; Hsieh et al., 2017, respectively) as well as the estimation of the rRS (lower dotted line Hsieh et al., 2017). As for the integrated properties (see Fig. 2), the bimodality is also present at kpc scales.

tribution of the rSFS and rRS (e.g. Medling et al., 2018; Cano-Díaz et al., 2019). These trends suggest that the processes responsible for controlling SF are of a local nature (self-regulation, local outflows) whereas quenching processes may be due to galaxy-scale processes (Sanchez, 2019).

### 3.3. The resolved mass–metallicity relation

In the top panel of Fig. 6 we plot the relation of the local metallicity—using the same calibrator as in Sec. 2.3.—and  $\Sigma_*$  (rMZR) for the sample of *bona fide* star-forming regions (i.e. spaxels with line ratios below the Kauffmann et al. (2003b) demarcation line and  $\text{EW}(\text{H}\alpha) > 10 \text{ \AA}$ ). It is evident the similarity in shape with the global MZR (see Sec. 2.3.). In fact, the MZR can be recovered by integrating from the rMZR (Rosales-Ortega et al., 2012; Barrera-Ballesteros et al., 2016). Using an exponential function (red solid line), the best fit to the median values of the rMZR is in very good agreement with previous estimations of the rMZR (see caption of Fig. 6 for details). A fourth-degree polynomial was also fitted to the data (solid blue line) yielding a more tight fit to the median values. The rMZR has been found to be fairly independent of the total stellar mass—except for the less massive galaxies—and it does explain fairly well the observed metallicity gradients in star-forming galaxies (Barrera-Ballesteros et al., 2016).

Recently, different authors have explored the pos-

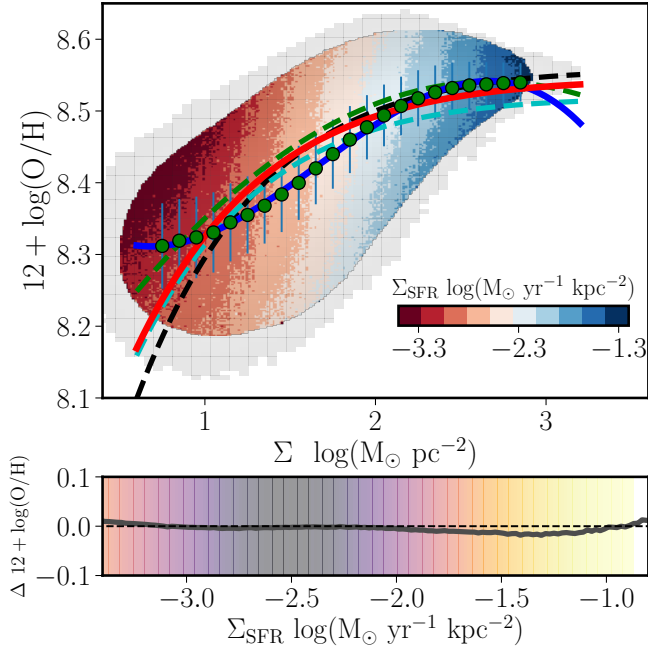


Figure 6: *Top panel:* The spatially-resolved mass-metallicity relation (rMZR) for  $3.59 \times 10^6$  spaxels located in 4904 galaxies included in the MaNGA survey. The 80% of the distribution of the rMZR is color-coded with their respective  $\Sigma_{\text{SFR}}$ . For a given  $\Sigma_*$  bin there is little variation of  $\Sigma_{\text{SFR}}$  in the rMZR plane. The blue and red lines represent different fitted functions commonly used. The fit is done for the median metallicities (green circles). The green, cyan, and black dashed lines represent the best fit derived in different IFS surveys (PINGS, CALIFA, MaNGA; Rosales-Ortega et al., 2012; Sánchez et al., 2013; Barrera-Ballesteros et al., 2016, respectively). *Bottom panel:* The residuals of the rMZR (with respect to the blue solid line) against  $\Sigma_{\text{SFR}}$ . As for the MZR, the median residuals show a flat trend, indicating that  $\Sigma_{\text{SFR}}$  does not reduce the scatter of the rMZR.

sible secondary dependence of the metallicity on  $\Sigma_{\text{SFR}}$  (e.g. Maiolino & Mannucci, 2019; Sánchez-Menguiano et al., 2019). In other words, a resolved FMR. In contrast to these studies, we find that for a given  $\Sigma_*$ ,  $\Sigma_{\text{SFR}}$  is rather constant (see color distribution in Fig. 6). We further quantify this possible relation by plotting the scatter of the relation with respect the blue solid line. We find that the residuals of the rMZR does not correlate with  $\Sigma_{\text{SFR}}$ . Using the exponential fit to derive the residual may yield a mild positive relation of the scatter only for spaxels with very low  $\Sigma_{\text{SFR}}$  ( $\log(\Sigma_{\text{SFR}} M_{\odot}^{-1} \text{ yr kpc}^2) < -3.0$ ). These results suggest that as for the integrated relation there is no clear evidence of a resolved FMR or a secondary relation of the rMZR with  $\Sigma_{\text{SFR}}$ . The existence of a local counterpart of the MZR (largely independent of the morphology and the stellar mass) suggests that the physical process(es) responsible for this scaling relation has a local origin. Even more, the lack of relation with the  $\Sigma_{\text{SFR}}$  indicates that other parameters may play an important role shaping the local abundance in star-forming galaxies (e.g. gas fraction, mass-loading factor; Barrera-Ballesteros et al., 2018).

*Acknowledgements:* The author is grateful with the LOC/SOC of the XVI LARIM, without their support it would not been possible for him to assist. The author thanks S. Sánchez for providing the data analysis products of the MaNGA datacubes to present the plots in this proceeding. The author acknowledges support from the CONACYT grant CB-285080 and FC-2016-01-1916, and funding from the PAPIIT-DGAPA-IA101217 and PAPIIT-DGAPA-IA100420 (UNAM) projects.

## References

- Baldry I.K., et al., 2004, ApJ, 600, 681  
 Barrera-Ballesteros J.K., et al., 2016, MNRAS, 463, 2513  
 Barrera-Ballesteros J.K., et al., 2017, ApJ, 844, 80  
 Barrera-Ballesteros J.K., et al., 2018, ApJ, 852, 74  
 Barrera-Ballesteros J.K., et al., 2019, arXiv e-prints, arXiv:1911.09677  
 Bigiel F., et al., 2008, AJ, 136, 2846  
 Bluck A.F.L., et al., 2019, MNRAS, 2839  
 Bolatto A.D., et al., 2017, ApJ, 846, 159  
 Brinchmann J., et al., 2004, MNRAS, 351, 1151  
 Bundy K., et al., 2015, ApJ, 798, 7  
 Cano-Díaz M., et al., 2016, ApJL, 821, L26  
 Cano-Díaz M., et al., 2019, MNRAS, 488, 3929  
 Cid Fernandes R., et al., 2010, MNRAS, 403, 1036  
 Cimatti A., Daddi E., Renzini A., 2006, A&A, 453, L29  
 Ellison S.L., et al., 2008, ApJL, 672, L107  
 Fontanot F., et al., 2009, MNRAS, 397, 1776  
 Gao Y., Solomon P.M., 2004, ApJ, 606, 271  
 Hsieh B.C., et al., 2017, ApJL, 851, L24  
 Hubble E.P., 1926, ApJ, 64, 321  
 Kashino D., et al., 2016, ApJL, 823, L24  
 Kauffmann G., et al., 2003a, MNRAS, 341, 54  
 Kauffmann G., et al., 2003b, MNRAS, 346, 1055  
 Kennicutt R.C., Evans N.J., 2012, ARA&A, 50, 531  
 Krumholz M.R., McKee C.F., 2005, ApJ, 630, 250  
 Lara-López M.A., et al., 2010, A&A, 521, L53  
 Lequeux J., et al., 1979, A&A, 500, 145  
 Leroy A.K., et al., 2008, AJ, 136, 2782  
 Maiolino R., Mannucci F., 2019, A&A Rv, 27, 3  
 Mannucci F., et al., 2010, MNRAS, 408, 2115  
 Marino R.A., et al., 2013, A&A, 559, A114  
 Medling A.M., et al., 2018, MNRAS, 475, 5194  
 Ostriker E.C., McKee C.F., Leroy A.K., 2010, ApJ, 721, 975  
 Rosales-Ortega F.F., et al., 2012, ApJL, 756, L31  
 Sanchez S.F., 2019, arXiv e-prints, arXiv:1911.06925  
 Sánchez S.F., et al., 2013, A&A, 554, A58  
 Sánchez S.F., et al., 2016, RMxAA, 52, 171  
 Sánchez S.F., et al., 2017, MNRAS, 469, 2121  
 Sánchez S.F., et al., 2019, MNRAS, 484, 3042  
 Sánchez-Menguiano L., et al., 2019, ApJ, 882, 9  
 Schawinski K., et al., 2014, MNRAS, 440, 889  
 Skillman E.D., Kennicutt R.C., Hodge P.W., 1989, ApJ, 347, 875  
 Telford O.G., et al., 2016, ApJ, 827, 35  
 Thomas D., et al., 2005, ApJ, 621, 673  
 Tremonti C.A., et al., 2004, ApJ, 613, 898  
 Zaritsky D., Kennicutt R.C.J., Huchra J.P., 1994, ApJ, 420, 87



# Evolution of low and intermediate-mass stars in binary systems with neutron stars

O.G. Benvenuto<sup>1,2</sup>

<sup>1</sup> *Instituto de Astrofísica de La Plata, IALP, CCT-CONICET-UNLP, Argentina*

<sup>2</sup> *Facultad de Ciencias Astronómicas y Geofísicas, Universidad Nacional de La Plata (UNLP), La Plata, Argentina*

Contact / obenvenu@fcaglp.unlp.edu.ar

**Abstract** / We discuss the evolution of low and intermediate-mass stars in close binary systems with neutron star companions. If the orbital period is short enough, the standard scenario predicts the occurrence of one (or more) long-standing Roche lobe overflow(s) of the donor star, feeding and spinning up the neutron star. When detached, we should be able to observe it as a pulsar; while during mass transfer we should detect it as a low-mass X-ray binary. Eventually, a fraction of the transferred material is accreted by the neutron star whereas the rest is lost from the system. From the study of eclipsing millisecond pulsars in binary systems it has emerged evidence for the existence of two well separate families: black widows and redbacks. Both have circular orbits with periods of 0.1–1.0 day but very different companion masses: 0.1–0.7  $M_{\odot}$  for redbacks and lighter than 0.05  $M_{\odot}$  for black widows. Standard models are in trouble to account for the existence of these objects. Models beyond standard, including irradiation feedback and evaporation, are helpful to understand the evolution of both families. Recently, it has been detected a new class of 'transitional' objects that switch between low-mass X-ray binaries and redbacks on a very short time scale of months/years. Constructing a model able to undergo this phenomenology is the next challenge in the study of this kind of close binary systems.

*Keywords* / binaries: close — pulsars: general — stars: evolution — stars: neutron

## 1. Introduction

Close binary systems (CBSs) are very relevant for the understanding of many astrophysical problems. Isolated stars have no size limitation and can swell up to very large radii. If stars belong to binary systems with large orbital periods  $P_{\text{orb}}$ , stellar evolution proceeds as if the components of the pair were isolated. However, in the case of CBSs if  $P_{\text{orb}}$  is short enough, stars may reach sizes comparable with the maximum allowed volume which corresponds to the famous Roche lobe. If we consider a three-body system in which two stars are point masses moving along a circular orbit together with a massless particle, we are in the conditions of the 'restricted three-body problem'. If the CBS has a circular orbit, any portion of the stellar envelopes will feel an effective potential very similar to that corresponding to the restricted three-body problem. Among the five Lagrangian points in which the effective force on the massless point vanish, the most relevant for binary evolution is the one that locates in between the stars, usually called  $L_1$ . This point is on the equipotential surface that defines the Roche lobes of each star. When one component of the pair reaches a size equal to that of the Roche lobe, it cannot remain in hydrostatic equilibrium and begins to shed mass across the 'pipe' given by  $L_1$  (Paczynski, 1971). This material will have a large intrinsic angular momentum. So, if the companion star is small enough it will form an accretion disc (AD). Depending on the characteristics of the system, the mate-

rial may be accreted by the companion or ejected from the CBS.

When one of the stars (hereafter "the donor") fills its Roche lobe, mass transfer starts out and the stars evolve to conditions that are not accessible to isolated objects. From that moment on, the evolution of the CBS depends on how the system reacts to mass transfer. It is suitable to define the following coefficients that quantify the reaction of the donor to the occurrence of mass transfer:

$$\zeta_{\text{ad}} = \left( \frac{\partial \log R}{\partial \log M} \right) \Big|_{\text{ad}}, \quad (1)$$

$$\zeta_{\text{th}} = \left( \frac{\partial \log R}{\partial \log M} \right) \Big|_{\text{th}}, \quad (2)$$

$$\zeta_{\text{rl}} = \left( \frac{\partial \log R_{\text{rl}}}{\partial \log M} \right). \quad (3)$$

$\zeta_{\text{ad}}$  describes the reaction of the radius of the donor to adiabatic mass loss,  $\zeta_{\text{th}}$  corresponds to the case in which the star is in thermal equilibrium, and  $\zeta_{\text{rl}}$  describes the reaction of the Roche lobe. If  $\zeta_{\text{rl}} > \zeta_{\text{ad}}$  the lobe shrinks faster than the star, no hydrostatic equilibrium is possible and mass transfer is unstable. If  $\zeta_{\text{ad}} > \zeta_{\text{rl}} > \zeta_{\text{th}}$  mass transfer will be stable and occurs on the thermal time scale of the donor star. In this work we are interested on systems that are able to undergo stable mass transfer episodes.

Among the variety of binary systems occurring in nature, here we are interested in the case of a normal

donor star orbiting together with a neutron star (NS). This case is relevant for the understanding of the so called low and intermediate-mass X-ray binaries, usually referred in the literature as LMXBs and IMXBs respectively, and also binary pulsars. Here we shall not treat the case of NS-NS pairs like the Hulse-Taylor pulsar PSR1913+16. It is the aim of this presentation to briefly review the main characteristics of the evolution of this kind of objects.

The remainder of this presentation is organised as follows: In Section 2. we review the main results associated to the standard treatment of the evolution of this kind of CBSs, and the difficulties it faces to account for the existence and characteristics of some binary pulsars. In Section 3. we present the modifications of the evolution induced by the inclusion of irradiation feedback (IFB) and evaporation. In Section 4. we discuss the observation of a very massive neutron star, and in Section 5. we present some concluding remarks.

## 2. Binary systems with one neutron star: the standard model

In the standard treatment of the evolution of these objects (see, e.g., Podsiadlowski et al. 2002; Benvenuto & De Vito 2005) it is considered that the system is on a circular and synchronised orbit (i.e. it is assumed that tidal coupling is instantaneous). This condition is necessary for the validity of the Roche lobe construction. The structure of the star is described by the standard evolution equations (see, e.g., Clayton 1968 and Kippenhahn & Weigert 1990), departures from spherical symmetry are neglected and the size of the lobe is described by a sphere with the volume of the lobe (Eggleton, 1983). In order to solve for the evolution it is considered the conservation of orbital angular momentum as in Rappaport et al. (1983). In particular, it is usual to assume that the NS companion will accrete a fraction  $\beta$  of the material transferred from the donor star, being the Eddington rate its absolute upper limit  $\dot{M}_{\text{Edd}} \approx 2 \times 10^{-8} M_{\odot} \text{ yr}^{-1}$ . The material lost from the system carries away the specific angular momentum of the NS. Other relevant sinks of angular momentum are magnetic braking (Verbunt & Zwaan, 1981) and gravitational radiation (Landau & Lifshitz, 1975). Let us remark that magnetic braking acts if the donor star has an outer convective envelope (but it is not fully convective), braking the donor. Then, the loss of orbital angular momentum is due to tidal coupling effects.

If the initial  $P_{\text{orb}}$  is short enough, the donor star fills its Roche lobe during its evolution and then a mass-transfer episode establishes. Usually, this process has a time scale of several million years and the final resulting configuration largely depends on the donor mass and the initial  $P_{\text{orb}}$  of the pair. Typically, for initial  $P_{\text{orb}}$  of the order of a day and masses of  $1 - 3 M_{\odot}$  the result is a helium core white dwarf (WD) that will be on a well defined mass-period relation that slightly depends on the metallicity (Tauris & Savonije 1999; De Vito & Benvenuto 2012). If donor masses are larger, we expect the occurrence of carbon-oxygen WDs, while if  $P_{\text{orb}} <$

1 day we expect the formation of ultra-compact binary systems (Sengar et al., 2017). For further details, see Podsiadlowski et al. (2002) and Benvenuto & De Vito (2005).

Recently, two families of binary eclipsing pulsars have been discovered (Roberts, 2013), these are redbacks (RBs) and black widows (BWs). RBs have  $P_{\text{orb}}$  in the range of 0.1 to 1 day and the companion mass  $M_2$  is  $M_2 = 0.1 - 0.7 M_{\odot}$ . BWs have the same range of  $P_{\text{orb}}$  but companions are much lighter, with  $M_2 < 0.05 M_{\odot}$ . Remarkably, standard models of binary evolution for systems with one NS are in trouble to account for the existence of these binary pulsar families. For example, the range of period and masses in which RBs are observed corresponds to a long-standing mass-transfer episode. Thus, we would expect to see a LMXB or IMXB but *not* a binary pulsar. Regarding BWs the situation is analogous. For so low-mass companions, standard models predict  $P_{\text{orb}}$  values smaller than observations.

## 3. Non-standard models: irradiation feedback and evaporation

There are two processes that are usually not considered in standard binary evolution, that have been proven to be relevant: these are IFB (Büning & Ritter, 2004) and evaporation (Stevens et al., 1992). When the NS accretes material, it irradiates X-rays that illuminate the donor star. Usually we consider  $L_{\text{IFB}} = \alpha_{\text{irrad}} GM_1 \dot{M}_1 / R_1$ , where  $L_{\text{IFB}}$  is the accretion luminosity that effectively produces the IFB phenomenon,  $\alpha_{\text{irrad}}$  is a coupling constant expected to be  $\alpha_{\text{irrad}} \leq 1$ ,  $G$  is the gravitational constant,  $M_1$  is the mass of the NS,  $R_1$  its radius and  $\dot{M}_1$  its accretion rate. If the donor star has a thick enough outer convective envelope, irradiation changes the temperature gradient of the outermost layers. This makes the irradiated portion of the surface to partially lose its ability to release energy coming from the stellar interior. Thus, the effective surface of the star will be smaller than  $4\pi R_2^2$ , where  $R_2$  is the radius of the donor star (Hameury & Ritter, 1997). So, the outer boundary condition is no longer  $L_2 = 4\pi R_2^2 \sigma T_{\text{eff},2}^4$  where  $L_2$  is the luminosity of the donor,  $T_{\text{eff},2}$  its effective temperature, and  $\sigma$  is the Stefan-Boltzmann constant. The consequences of considering IFB during mass transfer are sometimes rather drastic.

In sharp contrast with the standard scenario in which we expect long-standing continuous mass-transfer episodes, Büning & Ritter (2004) discovered that under adequate conditions IFB may lead to the occurrence of cyclic mass transfer episodes. In each of these cycles most of the time the donor is slightly detached from its lobe ('quasi Roche lobe overflow', Benvenuto et al. 2015 with no mass transfer) and sometime later, the donor may get in contact again (because of its internal evolution or angular momentum losses) and mass transfer reestablishes. During detachment the system may be detected as a binary pulsar while when mass transfer occurs, it should be observed as a LMXB.

The evolution of CBSs including IFB and evaporation has been considered by Benvenuto et al. (2014). In

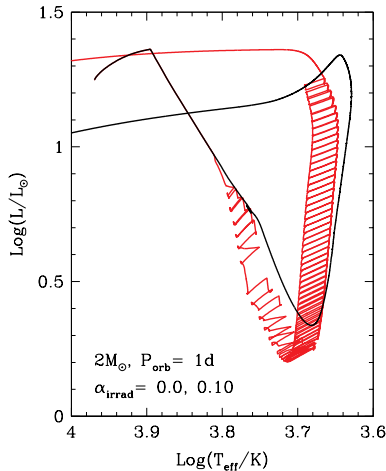


Figure 1: The evolution of the donor star of a close binary system formed by a solar-composition  $2 M_{\odot}$  star together with a  $1.4 M_{\odot}$  NS on an orbit with a period of 1 day. The red line corresponds to the irradiated system whereas the black, smooth line corresponds to the non-irradiated model.

that paper it has been shown that there is a wide variety of conditions in which cyclic mass transfer is expected (see especially their Fig. 3).

As an example of the differences between standard calculations and those considering IFB we present the case of a solar composition  $2 M_{\odot}$  donor star in a 1-day orbit with a  $1.4 M_{\odot}$  NS. These calculations have been performed with our stellar binary code (Benvenuto & De Vito 2003; Benvenuto et al. 2012) which is based on the description presented in Kippenhahn et al. (1967), but modified to consider  $\dot{M}$  as another variable which is iterated together with the stellar structure\*. For the case with IFB we assumed  $\alpha_{\text{irrad}} = 0.1$ . In Figs. 1–4 we present the evolutionary track on the Hertzsprung-Russell diagram, the mass transfer rate and donor mass as a function of time, and the evolution of  $P_{\text{orb}}$  as a function of the donor mass, respectively. Evolutionary tracks (Fig. 1) depart each other when the outer convective zone of the donor has grown thick enough for IFB effects to become appreciable. Since then on, while for the standard model mass transfer is long standing and continuous, the irradiated model undergoes several mass-transfer cycles (Fig. 2). Despite these large differences, remarkably, the mass of the resulting object after the end of mass transfer is approximately the same (Fig. 3); also the dependence of  $P_{\text{orb}}$  on the donor mass is only slight (Fig. 4).

It is worth to remark that moderate evaporation has been usually considered as the key phenomenon to account for the characteristics of BWs (see, e.g., Benvenuto et al. 2012).

As an application to a particular RB system, Benvenuto et al. (2015) have studied the case of the binary pulsar PSR J1723-2837 based on the observations

\*This provides an enhanced numerical stability that is very helpful for computing mass-transfer cycles.

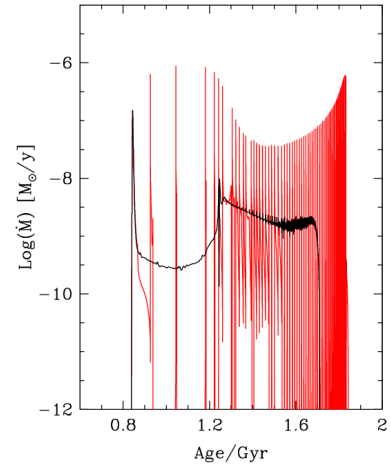


Figure 2: The mass transfer rate as a function of time for the systems presented in Fig. 1. The red (black) line corresponds to the model with (without) IFB.

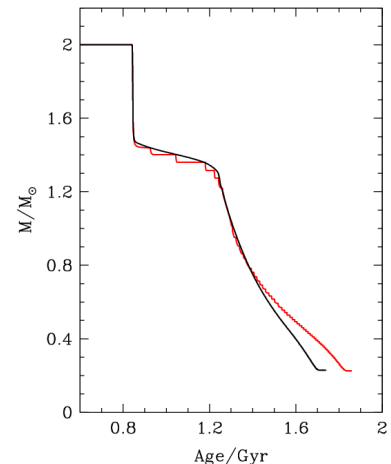


Figure 3: The mass of the donor star as a function of time for the systems presented in Fig. 1. The red (black) line corresponds to the model with (without) IFB.

of Crawford et al. (2013). Performing an exploration of the parameter space of the model (masses of the components, initial  $P_{\text{orb}}$ , metallicity, and  $\alpha_{\text{irrad}}$ ; evaporation is not relevant in our calculations) we found that a CBS with a  $1.25 M_{\odot}$  donor together with a  $1.4 M_{\odot}$  NS on a 0.75 day orbit and  $\alpha_{\text{irrad}} = 0.1$  successfully accounts for many of the characteristics of the observed system. However, the detected secular change of  $P_{\text{orb}}$ ,  $\dot{P}_{\text{orb}} = -3.50(12) \times 10^{-9}$  is far larger than that predicted by our model. In our opinion, this is a clear indication that some key physics is still lacking in our model.

### 3.1. Strong evaporation and reback formation

Other authors have addressed the problem of RBs formation. In particular, Chen et al. (2013) have consid-

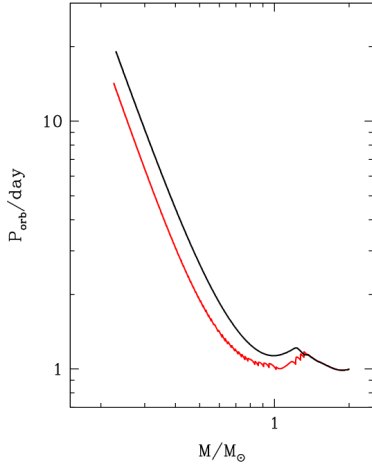


Figure 4: The evolution in the plane  $P_{\text{orb}}$  vs. mass for the binary systems presented in Fig. 1. The red (black) line corresponds to the model with (without) IFB.

ered the possibility of forming RB systems by a strong evaporation regime. When a star is undergoing mass transfer and reaches a very low mass value (typically  $M \lesssim 0.3 M_{\odot}$ ), it becomes fully convective. At that moment, magnetic braking ceases to act as an angular momentum sink and the system reacts by detaching the donor from its Roche lobe. If pulsar emission starts out, it may lead to an evaporation of the donor and even to inhibit further accretion onto the NS component of the system. Then, evaporation leads to an orbital widening, making the system to have masses and  $P_{\text{orb}}$  values compatible with those expected for RBs. De Vito et al. (2019) have explored the viability of the strong evaporation scenario. They found that the model presented by Chen et al. (2013) can account only for the low-mass part of the RBs region, and that in order to reach periods in the observed RBs range, the fraction of the Roche lobe that is occupied by the donor, i.e., *the filling factor* (FF) must be rather low. In this scenario, high FFs are expected only if systems are observed little time after detachment. However, in sharp contrast with these results, most of the measured FFs are rather high. So, observations indicate that the scenario of heavy evaporation for RBs is hardly tenable.

### 3.2. The role of accretion discs

In models with IFB, mass transfer cycles occur on the thermal time scale of the donor envelope. This is of the order of  $\approx 10^5$  yr. Thus, the IFB process is unable to account for the existence of some CBSs that have undergone their transformation from LMXB to binary pulsar and vice versa (Papitto et al., 2013) on time scales of months to years. This enormous difference in time scales clearly indicates that this swinging should be due not to the donor star but to another part of the binary system. The obvious candidate is the AD that surrounds the NS. Although it is usual not to include

explicitly a detailed treatment of ADs in evolutionary calculations, they should play a central role in this problem. Despite ADs have been studied since long ago (see, e.g., Shakura & Sunyaev, 1973; Pringle, 1981), they are still not fully understood. One of the key ingredients is the viscosity that largely determines the evolution of the AD. Many models have been constructed using the “ $\alpha$  prescription” of Shakura and Sunyaev, while others consider the magneto-rotational instability (Balbus & Hawley, 1998). In the context of transitional RBs we expect the occurrence of some instability in the AD. In particular we consider that the X-ray radiation should have a sizeable effect on the AD to eventually remove the material present in its inner part. This behaviour would be sufficient (or at least helpful) to account for the observed swinging behaviour. However, a detailed model is not yet available.

### 3.3. Changes in the orbital period

Another important quantity that allows us to investigate the evolutionary status of these binary systems is  $\dot{P}_{\text{orb}}$ . This has been detected in some systems thanks to the extraordinary accuracy of pulsar observations. In some cases models face serious difficulties to account for the observations (e.g. PSR J1723-2837, see above). Usually, it is considered that during mass transfer, the donor star remains synchronised to the orbit. In other words, the donor star rotates with an angular velocity equal to that of the whole system. This is due to the strong tidal interaction present in semidetached conditions. Usually researchers consider the Hut (1981) equations. These are a system of non-linear differential equations that describe the evolution of the semi-axis and eccentricity of the orbit together with the rotation rate and the inclination of its axis with respect to the orbital plane\*\*. Tides do not act on the NS component of the pair due to its extremely small radius ( $R_1 \approx 10$  km). Some authors, e.g., Repetto & Nelemans (2014) have considered the Hut’s equations up to the moment in which the donor star fills its Roche lobe. In any case, we should remark that Hut (1981) considered only quadrupolar terms as a perturbation to a pure central force field. So, while for well separated objects this is a good approximation, for stars nearly filling their Roche lobe (as it is the case of RBs) it should represent a much poorer treatment. Indeed, for this situation tidal coupling should be appreciably stronger than predicted by Hut’s equations. No doubt, much work remains to be done in order to interpret  $\dot{P}_{\text{orb}}$  observations in terms of detailed binary evolutionary models properly.

## 4. An extremely massive neutron star

Shortly before the LARIM meeting it has been announced the observation of the most massive NS detected to date. Employing Shapiro delay observations, Cromartie et al. (2019) have determined the mass of the

\*\*Of course, if the system were formed by two stars of sizeable radius, they would provide the rotation rate and inclination of the axes of each star.

NS in PSR J0740+6620 to be of  $2.14_{-0.09}^{+0.10} M_{\odot}$ . This pulsar has a spin period of 2.88 ms,  $P_{\text{orb}} = 4.7669$  days and a very cool, He-dominated atmosphere (Beronya et al., 2019) companion of  $0.258(8) M_{\odot}$ . The very existence of this object poses a serious challenge to the study of NS structure, since (obviously) a cold NS should support such a large mass against gravitational collapse. It is well known that, despite the present uncertainties in our knowledge of the cold nuclear matter equation of state (EOS), NSs must have a maximum mass equivalent to the Chandrasekhar's mass for WDs. If we assume a standard EOS below a density of  $\rho = 4.6 \times 10^{14} \text{ g cm}^{-3}$  and a causal one above ( $P = \rho c^2$  where  $P$  is the pressure,  $\rho$  the density and  $c$  the speed of light), the absolute maximum mass for a non-rotating NSs is  $\approx 3.2 M_{\odot}$  (Shapiro & Teukolsky, 1983). Many proposed nuclear EOSs are unable to support a mass of  $2.14 M_{\odot}$  against collapse and must be discarded (see, e.g., Lattimer & Prakash 2004).

From a different point of view, another interesting problem directly related with the main topic of this work is how a binary system can evolve to give rise to such a massive NS together with a low mass, very cool He WD. Work in progress indicates that it is possible to form such a massive NS in the frame of a low mass system with a donor of  $1 M_{\odot}$  and a NS of  $1.4 M_{\odot}$ , if mass transfer is conservative and metallicity is very low ( $Z = 10^{-4}$ ). Such a low donor mass is important since if it were more massive, mass transfer would initially overflow the Eddington rate, forcing a non conservative transfer. Remarkably, it is possible to account for the masses of the components and  $P_{\text{orb}}$  of this system, but for getting a so cold WD, its atmosphere should be devoid of hydrogen. Otherwise it would be hotter, in conflict with Beronya et al. (2019) observations regarding its composition and temperature.

## 5. Conclusions

In this talk I have presented the main results on the evolution of low and intermediate-mass binary systems composed by a normal donor star together with a neutron star (NS). This problem represents a far more challenging problem than that of single stellar evolution. Not surprisingly, while some properties of the evolution of these objects are well understood, others remain as open problems. For example, standard models are in serious difficulties to account for the existence of the redback and black widow families of eclipsing pulsars. Models including evaporation and irradiation feedback are more physically plausible. However, our understanding of these phenomena is still poor. Even more challenging is the observation of systems swinging between LMXB and pulsar on a very short time scale. This is a clear indication that some phenomenology is associated to the accretion disc that surrounds the NS (pulsar); and that the inclusion of detailed models of these discs should be considered.

*Acknowledgements:* The author wants to thank the SOC and LOC for their invitation to give this talk and for the financial support that allowed him to assist to the meeting. Also, he thanks

for their help to make it possible an unforgettable visit to Cerro Paranal.

The author wants to thank Drs. María Alejandra De Vito and Jorge E. Horvath for the collaboration in the study of these objects. The points of view presented in this talk are largely due to the work the author has performed with them. Also, OGB wants to thank our PhD students Lics. Maite Echeveste and Leonela Novarino for their effort.

OGB is member of the Carrera del Investigador Científico of the Comisión de Investigaciones Científicas de la Provincia de Buenos Aires.

## References

- Balbus S.A., Hawley J.F., 1998, *Reviews of Modern Physics*, 70, 1
- Benvenuto O.G., De Vito M.A., 2003, *MNRAS*, 342, 50
- Benvenuto O.G., De Vito M.A., 2005, *MNRAS*, 362, 891
- Benvenuto O.G., De Vito M.A., Horvath J.E., 2012, *ApJL*, 753, L33
- Benvenuto O.G., De Vito M.A., Horvath J.E., 2014, *ApJL*, 786, L7
- Benvenuto O.G., De Vito M.A., Horvath J.E., 2015, *ApJ*, 798, 44
- Beronya D.M., et al., 2019, *MNRAS*, 485, 3715
- Büning A., Ritter H., 2004, *A&A*, 423, 281
- Chen H.L., et al., 2013, *ApJ*, 775, 27
- Clayton D.D., 1968, *Principles of stellar evolution and nucleosynthesis*, University of Chicago Press
- Crawford F., et al., 2013, *ApJ*, 776, 20
- Cromartie H.T., et al., 2019, *Nature Astronomy*, 439
- De Vito M.A., Benvenuto O.G., 2012, *MNRAS*, 421, 2206
- De Vito M.A., Benvenuto O.G., Horvath J.E., 2019, *MNRAS*
- Eggleton P.P., 1983, *ApJ*, 268, 368
- Hameury J.M., Ritter H., 1997, *A&AS*, 123, 273
- Hut P., 1981, *A&A*, 99, 126
- Kippenhahn R., Weigert A., 1990, *Stellar Structure and Evolution*, Springer Verlag
- Kippenhahn R., Weigert A., Hofmeister E., 1967, *Methods in Computational Physics*, 7, 129
- Landau L.D., Lifshitz E.M., 1975, *The classical theory of fields*, Pergamon Press
- Lattimer J.M., Prakash M., 2004, *Science*, 304, 536
- Paczyński B., 1971, *ARA&A*, 9, 183
- Papitto A., et al., 2013, *Nature*, 501, 517
- Podsiadlowski P., Rappaport S., Pfahl E.D., 2002, *ApJ*, 565, 1107
- Pringle J.E., 1981, *ARA&A*, 19, 137
- Rappaport S., Verbunt F., Joss P.C., 1983, *ApJ*, 275, 713
- Repetto S., Nelemans G., 2014, *MNRAS*, 444, 542
- Roberts M.S.E., 2013, J. van Leeuwen (Ed.), *Neutron Stars and Pulsars: Challenges and Opportunities after 80 years*, *IAU Symposium*, vol. 291, 127–132
- Sengar R., et al., 2017, *MNRAS*, 470, L6
- Shakura N.I., Sunyaev R.A., 1973, *A&A*, 500, 33
- Shapiro S.L., Teukolsky S.A., 1983, *Black holes, white dwarfs, and neutron stars : the physics of compact objects*, Wiley
- Stevens I.R., Rees M.J., Podsiadlowski P., 1992, *MNRAS*, 254, 19P
- Tauris T.M., Savonije G.J., 1999, *A&A*, 350, 928
- Verbunt F., Zwaan C., 1981, *A&A*, 100, L7



# On the origin of stellar associations The impact of *Gaia* DR2

G. Carraro<sup>1</sup>

<sup>1</sup> *Dipartimento di Fisica e Astronomia Galileo Galilei, Padova, Italy*

Contact / giovanni.carraro@unipd.it

**Abstract** / In this review I discuss different theories of the formation of OB associations in the Milky Way, and provide the observational evidences in support of them. In fact, the second release of *Gaia* astrometric data (April 2018) is revolutionising the field, because it allows us to unravel the 3D structure and kinematics of stellar associations with unprecedented details by providing precise distances and a solid membership assessment. As an illustration, I summarise some recent studies on three OB associations: Cygnus OB2, Vela OB2, and Scorpius OB1, focussing in more detail to Sco OB1. A multi-wavelength study, in tandem with astrometric and kinematic data from *Gaia* DR2, seems to lend support, at least in this case, to a scenario in which star formation is not monolithic. As a matter of fact, besides one conspicuous star cluster, NGC 6231, and the very sparse star cluster Trumpler 24, there are several smaller groups of young OB and pre-main sequence stars across the association, indicating that star formation is highly structured and with no preferred scale. A new revolution is expected with the incoming much awaited third release of *Gaia* data.

*Keywords* / open clusters and associations: general — stars: formation

## 1. Introduction

Stellar associations (a term introduced by Ambartsumian, 1947) are unbound loose ensembles of young stars (see Gouliermis, 2018, for an exhaustive recent review on this subject). They are dominated by OB stars, which are so bright to be often visible even at optical wavelengths, in spite of the patchy and obscured environment in which they form and spend most of their short life. As expected, they are rich in pre-main sequence stars (Damiani, 2018) as well. Being very young, they should keep a vivid memory of the star formation (SF) event from which they formed and therefore are ideal tracers to study different modes of SF. It is unclear whether stellar (OB or T) associations are a direct product of star formation, or, more conservatively, an intermediate dynamical stage during the early evolution of young star clusters, soon after their formation, and before their final dissolution.

In the first scenario the actual spatial distribution of stars is the one at birth. Since they do not show any special shape, SF is expected to occur at any scale, from very large scale, as large as a galaxy, down to scales as small as individual young stellar objects. SF is then hierarchical, and the stellar structures which emerge from it are often fractally organized. Efremov (1989) identifies associations, aggregates, complexes and super-complexes. There is no preferred scale, and whatever density peak in the interstellar medium (ISM) can generate stars, from cluster size all the way to even individual stars.

In the second scenario, stars form in star clusters (Lada & Lada, 2003) which are initially embedded, and

made of 50 stars or more. They are formed then in the upper part of the molecular cloud mass distribution. Then stellar winds, UV flux, and eventually SNe explosions from the most massive stars in the pristine cluster remove the gas not processed by SF and, in this way, move the star cluster out of virial equilibrium. The cluster becomes loose and turns into an OB association. Associations in this scenario are then the final stage of the evolution of star clusters before dissolution in the general Galactic field. Being the time scale of this process short compared with the average age of Milky Way open clusters, this is normally referred to it as cluster “infant mortality”. From an observational point of view, the 3D kinematics of stars should show some indication of global expansion, in other words, some relationships between radial velocity and radius.

As mentioned in a recent study by Ward et al. (2020), this monolithic scenario does not seem to be supported by *Gaia* DR2 (Gaia Collaboration et al., 2018) data. These authors do not find any significant correlation between radial velocity and radius in most OB associations which, therefore, do not show dominant expansion signatures confirming earlier results by (Mel’nik & Dambis, 2018). Instead, they seem to be dominated by other large scale motions, which indicate that the velocity field is highly structured and cannot be reconciled with a monolithic collapse. To cast additional light on this topic, ideally one should study in detail many OB associations, coupling multi-wavelength campaigns with kinematical and astrometric data from *Gaia* DR2. Studies of this type have been recently performed for some associations, like Cygnus

OB2 (Berlanas et al., 2019), Vela OB2 (Beccari et al., 2018; Cantat-Gaudin et al., 2019) and Scorpius OB1 (Damiani, 2018; Yalyalieva et al., 2020), to give a few examples. In all cases, as I will outline below in more detail, the evidence is that SF is highly structured.

## 2. Recent results from *Gaia* DR2 data exploitation

The second release of *Gaia* astrometric data prompted an intense investigation of stellar associations in the Milky Way. I provide here a couple of illuminating examples of recent studies: Cygnus OB2 and Vela OB2. A full section will then be devoted to Scorpius OB1, in the study of which I was personally involved.

### 2.1. Cygnus OB2

Berlanas et al. (2019) recently studied the young OB association Cygnus OB2 (Wright et al., 2016) and found that this association is composed of two spatially separated, coeval, groups of stars. One main group is located at about 1760 pc, while a second, less prominent, group is located closer, at about 1350 pc. Besides, they find that the bulk of the association is more distant than previously thought. This points to a scenario in which SF occurred at the same time but with different intensity in at least two different, detached, regions of the association.

### 2.2. Vela OB2

More interesting is the case of the Vela OB2 association presented in Beccari et al. (2018). Following up previous suggestions (Jeffries et al., 2014; Damiani et al., 2017) that Vela OB2 is composed of two distinct stellar populations, Beccari et al. (2018) identified six independent physical groups with different distances, ages and kinematics (see Fig. 1). This identification was done using photometry with the wide field camera OmegaCAM mounted at the VLT survey telescope on Paranal (Chile), spectroscopy from the *Gaia*-ESO survey (Randich et al., 2013), and parallaxes and proper motion components from *Gaia* DR2 (Gaia Collaboration et al., 2018). The various groups can be assigned to two different populations. Four of them (they are named Cl 1, Cl 2, Cl 4 and Cl 5) are 10 Myr old, while the other two, Cl 3 and Cl 6, are older (30 Myr). Cl 3 coincides with the young star cluster NGC 2547, and Cl 4 with the very young star cluster  $\gamma$  Velorum, two very well known and widely studied star clusters. The other 4 are newly discovered physical groups. NGC 2547 (Cl 3) would be located at a distance of 393 pc, while  $\gamma$  Velorum (Cl 4) would be at a distance of 391 pc, therefore closer than NGC 2547. As a consequence, the two different populations are separated by about 40 pc. The other groups, although sharing similarities in age either with NGC 2547 or  $\gamma$  Velorum, are located at different distances and therefore they are not associated with the two more prominent clusters. In conclusion, Vela OB2 is quite a complex OB association. It is very difficult to

provide a comprehensive picture since radial velocities are available only for a small group of stars preventing a full 3D characterisation of the association. The authors finally underline that by tracing back the velocity vector it is not possible to find a common spatial origin for the six groups. Nonetheless, it seems that the origin of the Vela OB2 association is linked to the so-called *IRAS* Vela shell, which defines the edge of the association and it is made of dust and gas and with which the various detected stellar groups seem to be associated. According to Cantat-Gaudin et al. (2019), who looked in detail at the spatial distribution and kinematics of Vela OB2, a SN event occurred before the formation of Vela OBs triggered a SF burst which eventually generated it. The SN in this scenario was a massive star from the 30 Myr population whose main representative is NGC 2547. This is a reasonable and appealing scenario, which can be confirmed once radial velocities will be available for a much larger fraction of stars. These, together with more precise age estimates, would allow to integrate back the orbit of the stars and search for a possible common birthplace. In the case that such a common birthplace is found, this would support the proposed SN expansion mechanism.

## 3. The OB association Sco 1

Recent studies on this OB association have been performed by Damiani (2018); Kuhn et al. (2019), and Yalyalieva et al. (2020), using *Gaia* DR2 and multi-wavelength photometry. Sco 1 is a very rich and complex stellar association (Damiani, 2018). The spectacular H II region G345.45+1.50 is situated in the northern part of the field, while the most prominent young star cluster, NGC 6231, is located in the southern part. I will summarise here the results of Yalyalieva et al. (2020), who are not covering NGC 6231 (see Fig. 2), but concentrate on the northern and central region. Here, the most interesting structure is certainly Trumpler 24. This is thought to be a young open cluster with poorly defined boundaries and complex structure belonging to Sco OB1 (Heske & Wendker, 1984). Besides, the area under investigation is rich in pre-main sequence stars (Heske & Wendker, 1984; Damiani, 2018), which indicates active/recent star formation.

The area shown in Fig. 2 was surveyed with multi-colour *UBVI* photometry (Yalyalieva et al., 2020) from the Las Campanas Henrietta Swope 1.0-meter telescope. Then, by cross-correlating with *Gaia* DR2 data, the existence of different physical stellar groupings was searched for.

The clustering algorithm adopted is based on the DBSCAN (Density-Based Spatial Clustering of Applications with Noise) technique. The algorithm uses the clustering module of the machine learning library SCIKIT-LEARN (Pedregosa et al., 2011) as its basis. Nine different groups were found and characterised (see Table 1 and Fig. 3) in some detail, depending on the number of recovered members.

Table 1: Fundamental parameters of the detected groups in the Sco1 OB association by Yalyalieva et al. (2020).  $R_V$  indicates the ratio of total to selective absorption in the direction of each group.

Group	$E(B - V)$ mag	$\sigma_{E(B - V)}$ mag	Distance pc	$\log(\text{Age})$ dex	$R_V$	$\sigma_{R_V}$	$A_V$
A	0.55	0.7	$1608^{+36}_{-35}$	8.75	3.0	0.20	1.650
B1	0.36	0.1	$1549^{+131}_{-47}$	6.50	3.2	0.20	1.152
B2	0.39	0.3	$1644^{+82}_{-78}$	6.75	3.1	0.20	1.209
B3	0.38	0.2	$1629^{+44}_{-21}$	6.95	3.5	0.20	1.330
C	0.57	0.3	$1578^{+85}_{-11}$	6.85	2.8	0.25	1.596
D	0.58	0.3	$1761^{+139}_{-36}$	8.00	3.1	0.25	1.798
E	0.57	0.3	$1249^{+61}_{-58}$	8.15	3.2	0.25	1.824
F	0.47	0.1	$1682^{+137}_{-54}$	>6.60	2.9	0.20	1.363
G	0.40	0.9	$1524^{+135}_{-54}$	6.70	2.5	0.20	1.000

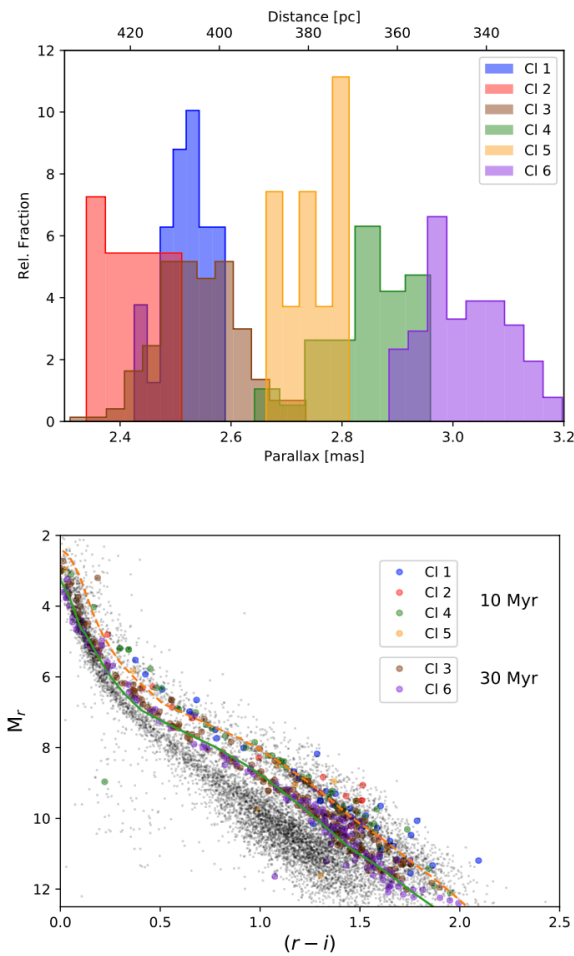


Figure 1: Stellar aggregates identified in the Vela OB2 associations by Beccari et al. (2018). They have different heliocentric distances and form two age groups. Taken from *A sextet of clusters in the Vela OB2 region revealed by Gaia*, Beccari et al. (2018), Oxford University Press.

### 3.1. Group A

Group A evidently coincides with the intermediate-age open cluster VdB-Hagen 202 (van den Bergh & Ha-

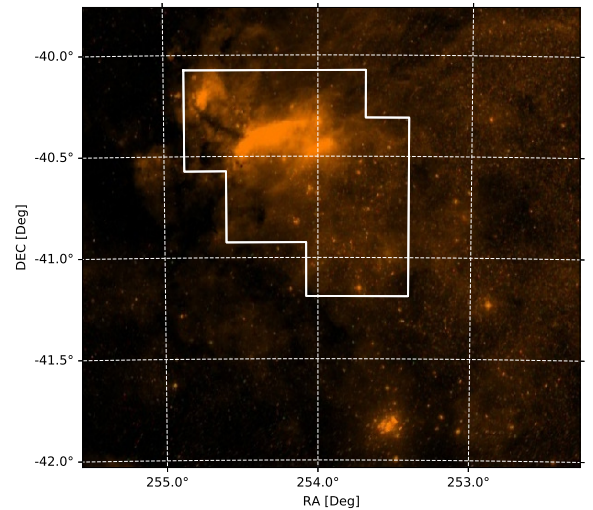


Figure 2: A DSS map of the region of the Sco 1 association. The white area is the one covered by *UBVI* photometry. It includes Trumpler 24 in its totality, the bright H II region mentioned in the text and several other groups. The prominent cluster in the south-west corner is NGC 6231. Taken from *A new look at Sco OB1 association with Gaia DR2*, Yalyalieva et al. (2020), Oxford University Press.

gen, 1975). These authors describe it as a poor red cluster embedded in some nebulosity. It is by far the richest group detected in the covered area. It has also the largest tangential velocity and the oldest age. Our isochrone fit in fact yields an age of 500 Myr, while both the astrometric and the photometric analysis support a heliocentric distance of 1.65 kpc. This group has not been detected by Damiani (2018), possibly because it does not contain young pre-main sequence M stars. On the other hand, close to this position Kuhn et al. (2019) found two rich groups (3 and 5, according to their numbering) of young stars slightly to the north of our group A, possibly our group F (see below). In all cases, the large age (compared with the rest of the groups) and

significantly diverse tangential motion lends support to a picture in which this cluster does not pertain to the association, but it is probably caught in the act of passing through it. The groups D and E (see below) share the same properties of this group A.

### 3.2. Group B

This group is located in the southern edge of the H II region G345.45+1.50, and appears very scattered. DBSCAN returns three different density peaks, that we indicate as B1, B2, and B3, but the area roughly corresponds to the very young star cluster Trumpler 24. Seggewiss (1968) also identified this group, which he indicated as group Trumpler 24 III. It is separated by a gap from the other groups identified in this study (see below). Besides the location, these three groups share the same age and kinematics. In the literature, the distance to Trumpler 24 ranges from 1.6 to 2.2 kpc (Seggewiss, 1968; Heske & Wendker, 1984). Our study favours the shortest distance, both from photometry and from *Gaia* DR2 parallaxes. This group has clear counterparts both in Kuhn et al. (2019) and Damiani (2018).

### 3.3. Group C

This is a very poor group located in the south-west corner of the field we covered. It is essentially composed by early type stars (early B spectral type, judging from the colour-colour diagram), and therefore it shares the same age as Trumpler 24 (group B). Kinematics also is closer to Trumpler 24 than to VdB-Hagen 202.

### 3.4. Group D

In spite of its vicinity to the previous group C, this group appears to be significantly different. It does not contain very young stars, and its kinematics is closer to the star cluster VdB-Hagen 202 (group A) than to Trumpler 24 (group B). It seems also to be positioned somewhat in the background with respect to Trumpler 24. We propose that this group is a part of the group A.

### 3.5. Group E

This scarcely populated group shares the same kinematics as the previous group D, and is situated very close to VdB-Hagen 202. Its paucity of stars prevents us from computing an accurate age for the group. Nonetheless, it seems plausible to adopt an age close to that of group D. We will propose (see below) that this group, and group D as well, are pieces of the group A (the stellar cluster VdB-Hagen 202).

### 3.6. Group F

This group possesses the same properties as group C. It coincides with Kuhn et al. (2019) group 3. The few identified early type stars show age, kinematics, and distance consistent with Trumpler 24. It appears to coincide with Seggewiss (1968) Trumpler 24 II group.

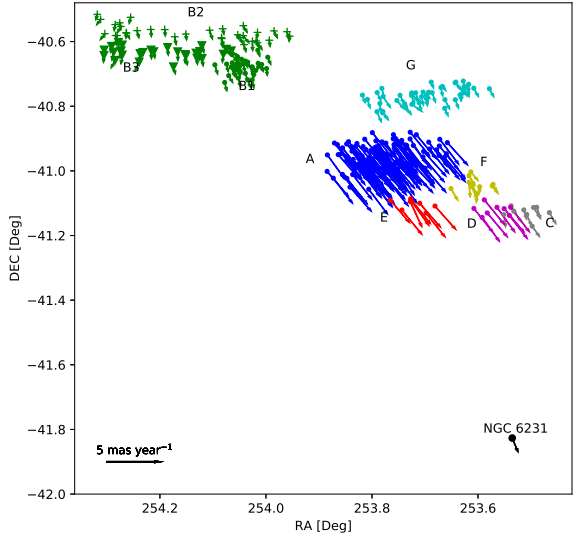


Figure 3: Tangential velocities for the various groups identified in the Sco 1 association. In the lower right corner we indicate the tangential motion of NGC 6231 for comparison. Adapted from Yalyalieva et al. (2020), op. cit.

### 3.7. Group G

This corresponds to Seggewiss (1968) group Trumpler 24 II. Similar to the C and F groups, this group is young. Even if it is situated right to the north of the old A group (VdB-Hagen 202), it possesses mean proper motion components very close to Trumpler 24.

### 3.8. Group families

In full generality, the detailed analysis of the detected groups leads us to separate them in two different families:

Family I: B (B1, B2 and B3), C, F and G groups have colour-colour diagrams typical of a very young population, and show the presence of pre-main sequence stars in the colour-magnitude diagram. They share similar proper motion components:  $\mu_\alpha = -0.3 \text{ mas yr}^{-1}$ ,  $\mu_\delta = -1.3 \text{ mas yr}^{-1}$ .

Family II: A, D and (maybe) E groups are significantly older and have compatible proper motion components:  $\mu_\alpha = -1.7 \text{ mas yr}^{-1}$ ,  $\mu_\delta = -3.7 \text{ mas yr}^{-1}$ . They have distances on average larger than family I.

Family II clearly has nothing to do with the Sco 1 OB association. It is quite reasonable to assume that the three groups are in fact just different portions of the very same star cluster, VdB-Hagen 202, which is undergoing tidal disruption while it is crossing the OB association. Fig. 4 shows the distribution of family I stars. In the lower panel, two density peaks are clearly visible, separated by a decrease in density, a sort of gap. It is tempting to associate this density gap to the recent passage of the old star cluster VdB-Hagen 202 through the Sco 1 association.

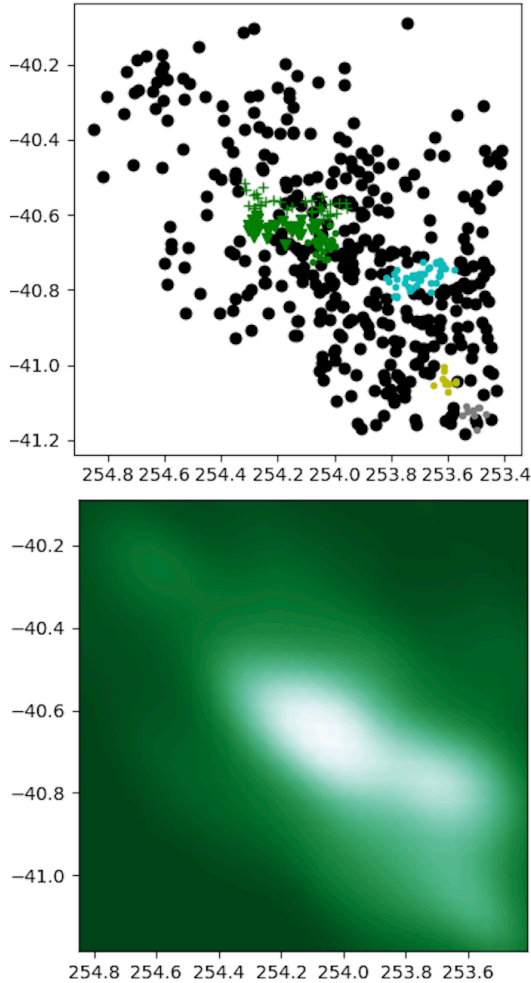


Figure 4: Distribution of family I stars (upper panel) and 2D density contour (lower panel). One can clearly notice two main concentrations separated by a density gap. Adapted from Yalalyeva et al. (2020), op. cit.

In conclusion, also ScoI OB association exhibits quite a complex structure, and it is not easy to depict a formation scenario for it. Here as well, as in the case of the previous examples, the lack of radial velocity data is limiting the study of the region significantly.

#### 4. Conclusions

In this review, I discussed in some detail the two major theories of the formation of OB associations in the Milky Way: the monolithic collapse theory, and the fractal theory of SF. These two theories predict different formation scenarios for the appearance of stellar (OB or T) associations. In the first case, an association is simply a dynamical stage of young star cluster evolution, caused by gas expulsion driven by massive stars evolution. In the second case, associations are the direct product of SF and therefore they reveal the ISM density peak distribution prior to the onset of the SF process. I then described in some detail observational material on three recently studied OB associations, namely Cygnus OB2, Vela OB2, and Scorpius OB1. Multi-colour photometry

are typically combined with *Gaia* DR2 data (parallaxes and proper motion components) which are allowing the investigation of stellar OB associations with much more detail than in the pre-*Gaia* era. In all three cases the observational data outline the high complexity of these associations. Several stellar groups are found with different spatial, kinematical and age properties. Two groups are found in Cygnus OB2, six groups in Vela OB2, and nine groups in Scorpius OB1. Interestingly, in these cases ages, spatial positions, and kinematics combine in very diverse fashions. Based on these preliminary results it is tempting to conclude that SF occurred in a highly structured ISM, and involved molecular clouds with widely different masses and differently distributed (in number and mass) pre-stellar cores. These are of course preliminary conclusions, since many more OB associations await such detailed studies in the future. In any case, these studies show the impressive impact that *Gaia* is providing in the investigation of SF and OB associations in the Milky Way. It is anyway recommendable to couple at some point *Gaia* data with precise radial velocity measurements of a sizeable number of stars, as the *Gaia*-ESO (Randich et al., 2013) survey has been partially doing. Only in this way, in fact, a real 3D kinematical study can be performed, and much more solid conclusions can be drawn on the origin and early evolution of stellar associations.

*Acknowledgements:* I sincerely thank the organisers of the XVI LARIM conference for inviting me in Antofagasta to deliver this review. I also express my gratitude to Lidia Yalalyeva (Lomonosov Moscow University, Russian Federation) and Rubén A. Vázquez (Universidad de La Plata, Argentina) for their help in the assembly of this material.

#### References

- Ambartsumian V.A., 1947, *The evolution of stars and astrophysics*  
 Beccari G., et al., 2018, MNRAS, 481, L11  
 Berlanas S.R., et al., 2019, MNRAS, 484, 1838  
 Cantat-Gaudin T., et al., 2019, A&A, 626, A17  
 Damiani F., 2018, A&A, 615, A148  
 Damiani F., et al., 2017, A&A, 602, L1  
 Efremov Y.N., 1989, *Astrophysics and Space Science Review*, 7, 107  
 Gaia Collaboration, et al., 2018, A&A, 616, A1  
 Gouliermis D.A., 2018, PASP, 130, 072001  
 Heske A., Wendker H.J., 1984, A&AS, 57, 205  
 Jeffries R.D., et al., 2014, A&A, 563, A94  
 Kuhn M.A., et al., 2019, ApJ, 870, 32  
 Lada C.J., Lada E.A., 2003, ARA&A, 41, 57  
 Mel'nik A.M., Dambis A.K., 2018, *Astronomy Reports*, 62, 998  
 Pedregosa F., et al., 2011, *Journal of Machine Learning Research*, 12, 2825  
 Randich S., Gilmore G., Gaia-ESO Consortium, 2013, *The Messenger*, 154, 47  
 Seggewiss W., 1968, ZA, 68, 142  
 van den Bergh S., Hagen G.L., 1975, AJ, 80, 11  
 Ward J.L., Kruijssen J.M.D., Rix H.W., 2020, MNRAS, 495, 663  
 Wright N.J., et al., 2016, MNRAS, 460, 2593  
 Yalalyeva L., et al., 2020, MNRAS, 495, 1349



# Investigating central massive black hole feedback in galaxies using cosmological hydrodynamical simulations

P. Barai<sup>1</sup>

<sup>1</sup> *Instituto de Astronomia, Geofísica e Ciências Atmosféricas - Universidade de São Paulo (IAG-USP), Brasil*

Contact / paramita.barai@iag.usp.br

**Abstract** / Feedback from central massive black holes (BHs) in galaxies widely influence their host galaxies as well as the large scale environment. Energy output from super-massive BHs (SMBHs: mass  $M_{\text{BH}} \geq 10^6 M_{\odot}$ ) existing at the centers of active galactic nuclei (AGN), often generates powerful outflows observed in a wide variety of forms at multi-wavelengths. Recently, intermediate-mass BHs (IMBHs:  $M_{\text{BH}} = 100 - 10^6 M_{\odot}$ ) are being observed hosted at the centers of dwarf galaxies (DGs). Some of the central IMBHs in DGs show signatures of activity in the form of low-luminosity AGN. I will present results from state-of-art cosmological hydrodynamical simulations performed using novel baryonic feedback models: radiative cooling, star formation, chemical enrichment, stellar evolution, supernova feedback, AGN accretion and feedback. The growth and feedback of the central BHs are investigated from the simulation output, as well as their co-evolution with the host galaxies.

*Keywords* / galaxies: active — galaxies: high-redshift — galaxies: dwarf — quasars: supermassive black holes

## 1. Introduction

Accretion of gas onto central supermassive black holes (SMBHs) of active galactic nuclei (AGN) emit enormous amounts of feedback energy (e.g., Rees, 1984). Quasars are powerful AGN existing more commonly at high redshifts than in the local Universe. Multi-wavelength observations have started to discover an increasing number of quasars at  $z \geq 6$  (e.g., Fan, 2006). SMBHs of mass  $M_{\text{BH}} \geq 10^9 M_{\odot}$  are observed to be in place in luminous quasars by  $z \sim 6$ , when the Universe was less than 1 Gyr old (e.g., Wu et al., 2015). It is difficult to understand how these early SMBHs formed over such short time scales, and there are open issues with various plausible scenarios (e.g., Matsumoto et al., 2015). One possibility is the presence of massive black-hole (BH) seed candidates of mass  $M_{\text{BH}} \sim 10^5 M_{\odot}$  at  $z > 6$ , possibly direct-collapse BHs.

BHs are usually observed to belong to two populations: stellar-mass BHs ( $M_{\text{BH}} \leq 10 - 100 M_{\odot}$ ), and SMBHs ( $M_{\text{BH}} \geq 10^6 M_{\odot}$ ). By natural extension, there should be a population of intermediate-mass BHs (IMBHs:  $M_{\text{BH}} = 100 - 10^6 M_{\odot}$ ) in the Universe. AGN feedback mechanisms have recently started to be observed in low-mass galaxies (e.g., Marleau et al., 2017; Penny et al., 2018). The concordance  $\Lambda$ -Cold Dark Matter ( $\Lambda$ CDM) cosmological scenario presents multiple challenges in the dwarf galaxy mass range. Recently Silk (2017) made an exciting claim that the presence of IMBHs at the centers of dwarf galaxies (DGs) can potentially solve the problems. Feedback mechanisms from these IMBHs output energy and affect the gas-rich DGs at  $z = 5 - 8$ . They can quench star-formation and reduce the number of DGs already in the early Universe.

Concordance  $\Lambda$ CDM cosmological galaxy formation

Table 1: Zoom-in simulations (for SMBHs)

Run name	Reposition BH to pot-min	Feedback geometry	Cone half opening
<i>noAGN</i>	–	–	–
<i>AGNoffset</i>	No	Bi-Cone	45°
<i>AGNcone</i>	Yes	Bi-Cone	45°
<i>AGNsphere</i>	Yes	Sphere	90°

simulations widely invoke AGN feedback as a crucial ingredient to self-regulate galaxy and central SMBH growth (e.g., Di Matteo et al., 2008). However, the analogous intermediate-mass regime for central BHs has not been explored in hydrodynamical simulations. In this work we address both the mass regimes of BHs, and present numerical-simulation results of the growth and feedback of SMBHs in AGN and IMBHs in DGs.

Table 2: Periodic-box simulations (for IMBHs)

Run name	BH present	$M_{\text{HaloMin}} M_{\odot}$	$M_{\text{BHseed}} M_{\odot}$	$v_w \text{ km s}^{-1}$
<i>SN</i>	No	–	–	–
<i>BHs2h1e6</i>	Yes	$h^{-1} \times 10^6$	$10^2$	2000
<i>BHs2h7e7</i>	Yes	$5h^{-1} \times 10^7$	$10^2$	2000
<i>BHs3h1e7</i>	Yes	$1 \times 10^7$	$10^3$	2000
<i>BHs3h2e7</i>	Yes	$2 \times 10^7$	$10^3$	2000
<i>BHs3h3e7</i>	Yes	$3 \times 10^7$	$10^3$	2000
<i>BHs3h4e7</i>	Yes	$4 \times 10^7$	$10^3$	2000
<i>BHs3h4e7v5</i>	Yes	$4 \times 10^7$	$10^3$	5000
<i>BHs3h5e7</i>	Yes	$5 \times 10^7$	$10^3$	2000
<i>BHs4h4e7</i>	Yes	$4 \times 10^7$	$10^4$	2000

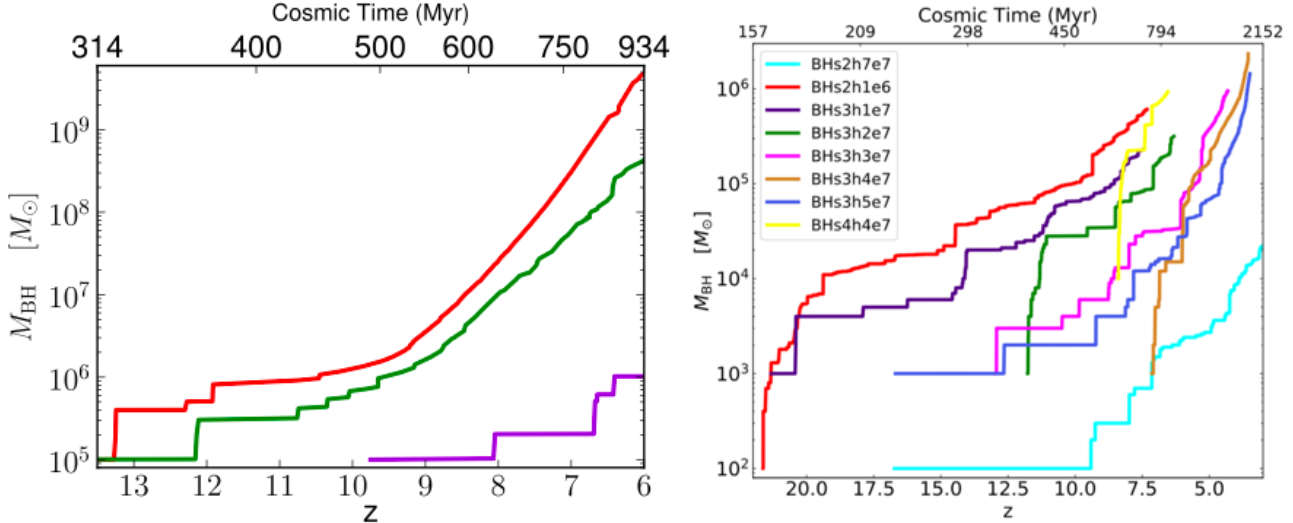


Figure 1: BH mass growth with redshift of the most-massive BH in each run. Left panel: Zoom-in cosmological simulations showing growth of SMBHs. The different colours discriminate the various runs: *AGNoffset* (violet), *AGNcone* (red), *AGNsphere* (green). Taken from *Quasar outflows at  $z \geq 6$ : the impact on the host galaxies*, Barai et al. (2018), Oxford University Press. Right panel: Periodic-box cosmological simulations showing growth of IMBHs. The colours indicate the runs: *BHs2h7e7* (cyan), *BHs2h1e6* (red), *BHs3h1e7* (indigo), *BHs3h2e7* (green), *BHs3h3e7* (magenta), *BHs3h4e7* (brown), *BHs3h5e7* (blue), *BHs4h4e7* (yellow).

## 2. Numerical method and simulations

We perform cosmological hydrodynamical simulations using the code GADGET-3 (Springel, 2005). The initial conditions at  $z = 100$  are generated using the MUSIC\* software (Hahn & Abel, 2011). A BH (initial mass  $M_{\text{BHseed}}$ ) is seeded at the center of each galaxy (not containing a BH already) more massive than a total mass  $M_{\text{HaloMin}}$ . The subgrid prescriptions for BH feedback are adopted from Barai et al. (2014, 2016).

We executed 4 zoom-in cosmological hydrodynamical simulations, with characteristics listed in Table 1. All the runs incorporate metal cooling, chemical enrichment, star formation and supernova feedback. We performed 10 cosmological hydrodynamical simulations of small-sized boxes with periodic boundary conditions, to probe dwarf galaxies at high redshifts, as listed in Table 2. In each series, one run has no BH included, while the other runs explore different BH feedback models.

## 3. Results and discussion

### 3.1. Black hole accretion and growth

Fig. 1 shows the growth of the most-massive BHs versus redshift (lower scale for abscissas) and versus cosmic time (upper scale) in our simulations. We find that the first BHs are seeded at different cosmic times depending on when the halos reach the threshold mass for BH seeding. The seed BHs grow subsequently by merger with other BHs and by accreting gas.

Each SMBH (left panel of Fig. 1 presenting the results of the zoom-in cosmological simulations) is seeded at  $z \sim 14$  in the runs *AGNcone* and *AGNsphere* ( $z \sim 10$

in *AGNoffset*) as  $M_{\text{BH}} = 10^5 M_{\odot}$ . They grow maximally by accreting gas at the Eddington rate over the redshifts  $z = 9 - 6$  in runs *AGNcone* and *AGNsphere*. The  $M_{\text{BH}}$  has a power-law increase, and the SMBH mass increases by a factor  $\sim 10^3$ . In run *AGNcone* (red curve), the SMBH has grown to  $M_{\text{BH}} = 4 \times 10^9 M_{\odot}$  and an accretion rate  $\dot{M}_{\text{BH}} = 100 M_{\odot} \text{yr}^{-1}$  at  $z = 6$ . The SMBH grows 10 times more massive at  $z = 6$  in the *AGNcone* case than in the *AGNsphere* run, because more gas can inflow along the direction perpendicular to the feedback output bi-cone, and accrete onto the SMBH.

The right panel of Fig. 1 shows that the seeding epoch of the IMBHs varies between  $z \sim 22$  to  $z \sim 16$  in our periodic-box cosmological simulations. This is the epoch when the first halos reach  $M_{\text{halo}} = 10^6 h^{-1} M_{\odot}$  to  $M_{\text{halo}} = 5 \times 10^7 h^{-1} M_{\odot}$ . We find that, when seeded in larger halos, IMBHs start to grow later and have an overall smaller growth at the same redshift (compare indigo and magenta curves). Also a IMBH can grow similarly when seeded in smaller halos with a smaller seed mass (red curve), as in larger halos with a higher seed mass (indigo curve). The most-massive IMBH, considering all the runs, has grown to  $M_{\text{BH}} = 2 \times 10^6 M_{\odot}$  at  $z = 5$  in run *BHs3h4e7* (brown curve).

### 3.2. Black-hole mass – galaxy mass correlation

The BH mass versus galaxy stellar mass correlation is presented in Fig. 2. The top row shows the results obtained in the zoom-in cosmological simulations at the epochs  $z = 10, 8, 6$ . Observational data are overplotted as the black lines indicating the BH mass versus stellar-bulge mass relations of local  $z = 0$  galaxies as the black, dashed line:  $M_{\text{BH}}/M_{\star} = 0.002$  (Marconi & Hunt, 2003), and  $z \sim 6$  quasars as the black, solid line:  $M_{\text{BH}}/M_{\star} = 0.022$  (Wang et al., 2010).

\*MUSIC - Multi-scale Initial Conditions for Cosmological Simulations: <https://bitbucket.org/ohahn/music>

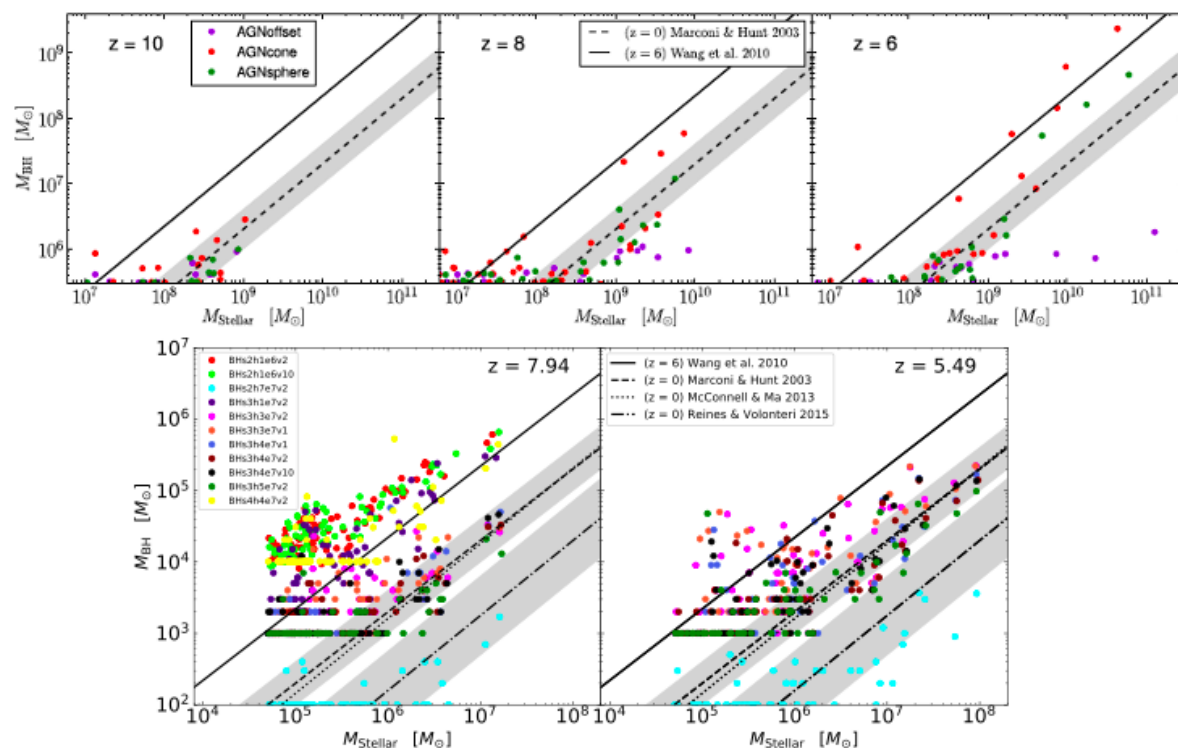


Figure 2: BH mass versus stellar mass of all the galaxies in the zoom-in cosmological simulations at  $z = 10, 8, 6$  (top row), taken from *Quasar outflows at  $z \geq 6$ : the impact on the host galaxies*, Barai et al. (2018), Oxford University Press, and the periodic-box cosmological simulations at  $z = 7.94, 5.49$  (bottom row), taken from *Intermediate-mass black hole growth and feedback in dwarf galaxies at high redshifts*, Barai & de Gouveia Dal Pino (2019), Oxford University Press.

Our simulations *AGNcone* and *AGNsphere* show that, at  $z \sim 6$  massive galaxies ( $M_* > 10^9 M_\odot$ ) contain SMBHs ( $M_{\text{BH}} > 10^7 M_\odot$ ) more massive than expected from the local relation. This suggests that SMBHs grow faster than their host galaxies at high redshifts. We see a dependence on the BH mass: less-massive BHs with  $M_{\text{BH}} < 10^7 M_\odot$  lie on the local relation, while they *migrate* to the  $z = 6$  correlation as they grow.

The bottom row of Fig. 2 shows the BH – galaxy correlation obtained in our periodic-box cosmological simulations. In the runs *BHs2h1e6v2* (red symbols) and *BHs3h1e7v2* (indigo symbols), dwarf galaxies with stellar masses between  $M_* = 10^4 - 10^7 M_\odot$  contain BHs in the range  $M_{\text{BH}} = 10^3 - 10^5 M_\odot$  at  $z = 7.9$ . These IMBHs are hence already more massive than BHs following the local relation as well as BHs in  $z \sim 6$  quasars. Our results suggest that central IMBHs grow faster than their host dwarf galaxies at high redshifts.

#### 4. Conclusions

We investigate outflows in quasar-host galaxies at  $z \geq 6$  by performing cosmological hydrodynamical simulations (details in Barai et al., 2018). We simulate a  $2 \times 10^{12} M_\odot$  halo at  $z = 6$ , inside a  $(500 \text{ Mpc})^3$  comoving volume, using the zoom-in technique. We find that, starting from  $10^5 M_\odot$  seeds SMBHs can grow to  $10^9 M_\odot$  in cosmological environments.

IMBHs ( $M_{\text{BH}} = 100 - 10^6 M_\odot$ ) have started to be observed at the centers of dwarf galaxies. We perform cosmological hydrodynamical simulations of  $(2h^{-1} \text{ Mpc})^3$

comoving boxes, to probe DGs and central IMBHs at high redshifts (details in Barai & de Gouveia Dal Pino, 2019). We conclude that IMBHs at DG centers grow from  $10^2 - 10^3 M_\odot$  to  $10^5 - 10^6 M_\odot$  by  $z \sim 4$  in cosmological environments.

Our simulations indicate that both central IMBHs and SMBHs grow faster than their host galaxies at high redshifts.

*Acknowledgements:* This work is supported by the Brazilian Funding Agency FAPESP (grants 2016/01355-5, 2016/22183-8).

#### References

- Barai P., de Gouveia Dal Pino E.M., 2019, MNRAS, 487, 5549
- Barai P., et al., 2014, MNRAS, 437, 1456
- Barai P., et al., 2016, MNRAS, 461, 1548
- Barai P., et al., 2018, MNRAS, 473, 4003
- Di Matteo T., et al., 2008, ApJ, 676, 33
- Fan X., 2006, NewAR, 50, 665
- Hahn O., Abel T., 2011, MNRAS, 415, 2101
- Marconi A., Hunt L.K., 2003, ApJL, 589, L21
- Marleau F.R., et al., 2017, A&A, 602, A28
- Matsumoto T., et al., 2015, ApJ, 810, 64
- Penny S.J., et al., 2018, MNRAS, 476, 979
- Rees M.J., 1984, ARA&A, 22, 471
- Silk J., 2017, ApJL, 839, L13
- Springel V., 2005, MNRAS, 364, 1105
- Wang R., et al., 2010, ApJ, 714, 699
- Wu X.B., et al., 2015, Nature, 518, 512



# Science with the Cherenkov Telescope Array

U. Barres de Almeida<sup>1</sup>, for the CTA Consortium

<sup>1</sup> *Brazilian Center for Physics Research (CBPF), Rio de Janeiro, Brazil*

*Contact / ulisses@cbpf.br*

**Abstract /** The Cherenkov Telescope Array (CTA) will be the next major ground-based observatory for gamma-ray astronomy at very high energies. It will be an explorer of the extreme Universe, operational in the energy range from 20 GeV to over 300 TeV, with unprecedented sensitivity as well as energy and angular resolutions. With more than 100 telescopes of three different types, it will be located in two sites: in the Northern Hemisphere at La Palma, Spain, and in the Southern Hemisphere at Cerro Paranal, in Chile. CTA will be one of the large astronomical infrastructures in the world in the next decade, and will operate as the first open ground-based gamma-ray observatory. In scientific terms, it will conduct important astronomical surveys of the Galaxy and the extragalactic sky, and will address both astrophysical and fundamental physics questions. This paper briefly presents the CTA concept, focusing on its science and the perspectives for multi-wavelength and multi-messenger cooperations, with a special view to the Latin American context.

*Keywords /* astroparticle physics — methods: observational — gamma-rays: general

## 1. The Cherenkov Telescope Array

Very-high-energy (VHE,  $E_\gamma > 100$  GeV) gamma-ray photons are detected indirectly by ground-based observatories. In the case of the atmospheric Cherenkov telescopes, of which CTA will be the most prominent future example, this is achieved by the observation of the Cherenkov radiation emitted when the air-shower's secondary particles pass through the atmosphere. CTA will be the first open observatory of its kind, with arrays in two sites, in the Northern and Southern Hemispheres. It will be characterised by a very wide energy coverage, from 20 GeV to 300 TeV, being composed of three different types of instruments to collectively achieve this goal. The CTA telescopes will have wide fields of view, varying from  $\sim 4.5^\circ$  to  $8^\circ$ , well tuned for conducting surveys and the imaging of extended sources. CTA will represent a dramatic increase in the point source sensitivity with respect to current instruments, of a factor of  $\sim 10$ , with much impact in the study of transients. Similar improvements are foreseen for its angular and energy resolutions.

## 2. Overview of CTA science

The core of the CTA science is detailed in a publication by the Cherenkov Telescope Array Consortium et al. (2019), and focuses on the understanding of the origin and role of relativistic cosmic particles, which play a central part in a range of astrophysical phenomena, from supernova remnants to active galactic nuclei (AGN). CTA will address these questions and the mechanisms for particle acceleration through the double approach of a census of particle accelerators in the Universe, via comprehensive surveys of the Galaxy and the extragalactic sky, and precision measurements of archetypal

sources.

The study of particle acceleration to VHEs is directly associated to that of extreme environments, such as those close to neutron stars or black holes, as well as relativistic outflows or explosions. In this domain, CTA will observe supermassive black holes and their associated jets in AGN, as well as accreting stellar mass black hole systems, and the environment around neutron stars, via pulsed gamma-ray emission from pulsar magnetospheres and their associated ultra-relativistic outflows.

The reach of CTA will also encompass a large discovery potential in fields of fundamental physics. A major question that CTA will address is the nature of dark matter (DM), a phenomenon for which there is abundant astrophysical evidence in multiple scales, but for which fundamental direct evidence lacks. Obtaining convincing evidence for dark matter from excesses in the measured energy spectrum of gamma-rays will need careful assessment of the astrophysical backgrounds as well as deep understanding of the astrophysical and DM dynamics within the various potential sources. In this respect, the Galactic center will be a prime region for the CTA DM searches, where CTA is expected to reach a sensitivity much beyond what is currently attainable, and well within the range of predicted annihilation cross sections of canonical models (Morselli & Consortium, 2017).

Over the lifetime of CTA, most of the available observation time will be divided into open time, allocated to projects proposed via a Guest Observer Programme, and a Core Programme consisting of so-called Key Science Projects (KSPs). These will be carried out by the CTA Consortium over the first 10 years of operations of the observatory, and will consist on the production of legacy datasets which will advance the state of the

art beyond the current status of the field (Cherenkov Telescope Array Consortium et al., 2019). The KSPs will involve large scale projects, associated to surveys, and will be demanding in terms of observing hours and technical complexity, requiring intense multi-wavelength (MWL) and multi-messenger cooperation for which a brief panorama is presented next.

### 3. MWL and multi-messenger synergies

CTA will have important synergies with many of the next-generation astronomical and astroparticle observatories, from radio to high energies. Such synergies are globally summarised in Fig. 1, for each of the main science cases among the CTA KSPs.

Until the advent of high-energy astrophysics, the radio band provided the main window to the non-thermal universe, with the observation of synchrotron emission from highly energetic electron populations, and it remains to date a main counterpart to the study of the emission from relativistic particles. In this regard, the radio bands have a tremendous advantage for localising acceleration zones, thanks to the angular resolution provided by very-long baseline interferometry, which can be as precise as tens of microarcseconds, and are therefore an invaluable complement to the gamma-ray data (e.g., Orienti et al. (2013)).

The next most evident MWL synergy for CTA comes from X-rays, as phenomena which result in sufficiently high temperatures for thermal X-ray emission are also often associated with shock processes which accelerate non-thermal particles. Over the last decade, the fruitful synergy between X-rays and gamma-rays was emphatically demonstrated by major missions such as *Chandra* and *XMM-Newton*, as well as timing observatories such as *RXTE* and *Swift*, for the variable sky. New missions, such as *eROSITA* and *ATHENA*, are expected to continue this cooperation over the next decade, overlapping CTA operations (e.g., Takahashi et al. (2013)). Finally, the MeV-GeV domain presents very strong synergies with CTA, thanks to the complementarity in the observational techniques and energy range between ground-based and satellite-based gamma-ray observatories.

The last few years have revealed that many compact, high-energy sources, emit detectable levels of synchrotron emission in the optical-IR (OIR) domain, which can also display high variability. Some examples include blazars, microquasars and pulsar wind-nebulae, all of which are prominent VHE emitters. Additionally, OIR studies of non-radiative shocks in supernovae remnants can provide useful constraints on particle acceleration, to mention only a few examples. As is clear from Fig. 2, Latin America hosts a wealth of facilities that can closely cooperate with CTA on many fronts.

In addition to all these synergies, a fundamentally new observational domain has been opened, in which high-energy gamma-ray observations play a central role: that of multi-messenger astrophysics. Throughout this decade, new astronomical messengers such as ultra-high-energy cosmic rays, high-energy neutrinos and gravitational waves have brought us previously undisclosed information about the cosmos, and the recent discovery of

the first electromagnetic (EM) counterparts to some of these events have enabled the start of a real astronomical investigation into the astro-particle physics domain. In the remainder of this contribution we will look into the two such major synergies for VHE astronomy and the future CTA.

#### 3.1. Neutrinos and cosmic-ray accelerators

Neutrinos are crucial messengers for astroparticle physics because they can only originate where protons are accelerated to produce pions and other particles that later decay. Neutrinos can then unequivocally signal cosmic-ray acceleration sites. Despite a number of high-energy neutrinos of likely astrophysical origin have been detected by the IceCube Neutrino observatory over the past decade, the sole event to date with a potential counterpart identification is the 290 TeV neutrino IceCube-170922A. This event, spatially coincident with the blazar TXS 0506+056, was putatively associated to this source after concomitant detection of a flaring state in gamma-rays by *Fermi*-LAT. The source was later detected by MAGIC and identified as a luminous blazar source with energetics in principle capable of accommodating the production of such very-high-energy neutrinos, even if the details have still to be better worked out (IceCube Collaboration et al., 2018).

Despite the isolated case, this likely multi-messenger cross-identification opens up promising avenues for future research, as larger and more sensitive instruments, such as CTA, will be able to scrutinise deeper, and follow-up a larger number of neutrino alerts, probing further the nature of their astrophysical counterparts. Likewise, a broader view of the populations of extragalactic sources, and specially of high-synchrotron-peaked blazars, that CTA should achieve, will improve the possibilities for population cross-matching and counterpart identifications for the entire catalogue of high-energy neutrinos (Schüssler, 2019).

#### 3.2. The gravitational wave connection

Gamma-ray bursts are one of the most interesting phenomena of the high-energy sky. They are characterised by short and sudden EM signals, with peak energy output in the gamma-ray band outshining all other sources in the Universe for the brief moments of their violent outbursts. They are regularly detected (at an average cadence of  $\sim 1+$  per day) by satellites in the keV and MeV bands, and have a bi-modal distribution of the prompt emission duration (short GRBs, lasting for  $< 2$  s, and long GRBs, lasting up to  $\sim 2$  min). Thanks to improved source localisation firstly provided by the *BeppoSAX* X-ray satellite (1996-2003), and the instruments that followed, as well as an efficient real-time global burst alert system, the *Gamma-ray Coordinates Network* (GCN)\*, the multi-band follow-up of GRBs was possible, and their afterglow emission was discovered. This allowed a gradual unveiling of their nature through the accumulation of observational evidence, which cul-

\*<https://gcn.gsfc.nasa.gov>

Band or Messenger	Astrophysical Probes	Galactic Plane Survey	LMC & SFRs	CRs & Diffuse Emission	Galactic Transients	Starburst & Galaxy Clusters	GRBs	AGNs	Radio Galaxies	Redshifts	GWs & Neutrinos
Radio	Particle and magnetic-field density probe. Transients. Pulsar timing.	●	●	●	●	●	●	●			●
(Sub)Millimetre	Interstellar gas mapping. Matter ionisation levels. High-res interferometry.	●	●		●	●	●	●	●		
IR/Optical	Thermal emission. Variable non-thermal emission. Polarisation.	●	●		●	●	●	●	●	●	●
Transient Factories	Wide-field monitoring & transients detection. Multi-messenger follow-ups.				●		●	●			●
X-rays	Accretion and outflows. Particle acceleration. Plasma properties.	●	●	●	●	●	●	●	●		●
MeV-GeV Gamma-rays	High-energy transients. Pion-decay signature. Inverse-Compton process	●	●		●	●	●	●	●		●
Other VHE	Particle detectors for 100% duty cycle monitoring of TeV sky.	●	●		●	●	●	●			●
Neutrinos	Probe of cosmic-ray acceleration sites. Probe of PeV energy processes.	●	●	●		●	●	●			●
Gravitational Waves	Mergers of compact objects (Neutron Stars). Gamma-ray Bursts.						●				●

Figure 1: Matrix of CTA MWL and multi-messenger synergies with respect to the different science cases of the Key Science Programme (KSP). Green dots indicate complementary data which is essential to achieve the CTA science goals in question; yellow dots indicate important complementary data; and red dots indicate useful but non-crucial complementarity.



Figure 2: Example of major Latin American facilities and observatories with potential observational synergies with CTA.

minated in the discovery, by the MAGIC and H.E.S.S. collaborations in 2019, of two instances of sub-TeV emission from the afterglow of two long GRB events\*\*. Such breakthrough discoveries demonstrate the strong prospects for GRB observations with CTA.

The astrophysical nature of long-duration GRBs is firmly associated to supernovae events, as revealed by a number of optical counterpart identifications. More re-

\*\*GRB 190114C (MAGIC Collaboration et al., 2019), GRB 180720 (Abdalla et al., 2019).

cently, the first evidence for short-duration GRBs as being associated to NS-NS mergers was established by the multi-messenger detection of gravitational wave emission and a kilonova associated with the afterglow of GRB 170817 (Smartt et al., 2017). This event opened a new observational window in astrophysics, and a new chapter in the studies of GRBs, and also established a bridge for the multi-messenger observations of GW events for CTA – a connection that has been reinforced by the recent announcement by MAGIC of a 4- $\sigma$  hint signal from the short GRB 160821B (Inoue et al., 2019), associated to a kilonova event (Troja et al., 2019). All this considered, the prospects for CTA observations of counterpart VHE emission from GW events are more promising than ever.

### References

Abdalla H., et al., 2019, *Nature*, 575, 464  
 Cherenkov Telescope Array Consortium, et al., 2019, *Science with the Cherenkov Telescope Array*, World Scientific  
 IceCube Collaboration, et al., 2018, *Science*, 361, eaat1378  
 Inoue S., et al., 2019, *36th International Cosmic Ray Conference (ICRC2019)*, vol. 36, 703  
 MAGIC Collaboration, et al., 2019, *Nature*, 575, 459  
 Morselli A., Consortium C., 2017, *35th International Cosmic Ray Conference (ICRC2017)*, vol. 301, 921  
 Orienti M., et al., 2013, *MNRAS*, 428, 2418  
 Schüssler F., 2019, *36th International Cosmic Ray Conference (ICRC2019)*, vol. 36, 788  
 Smartt S.J., et al., 2017, *Nature*, 551, 75  
 Takahashi T., Uchiyama Y., Stawarz L., 2013, *Astroparticle Physics*, 43, 142  
 Troja E., et al., 2019, *MNRAS*, 489, 2104



# The challenges of measuring the star formation rate of galaxies

M. Boquien<sup>1</sup>

<sup>1</sup> *Centro de astronomía (CITEVA), Universidad de Antofagasta, Antofagasta, Chile*

*Contact / mederic.boquien@uantof.cl*

**Abstract** / Star formation is one of the most important processes driving the formation and evolution of galaxies across the Universe. Yet, measuring star formation in galaxies is a surprisingly difficult task. We present here some of the main principles and assumptions upon which star formation rate estimators are based along with recent improvements on our techniques to measure star formation in galaxies from adaptive hybrid estimators to spectro-photometric modeling.

*Keywords* / galaxies: star formation

## 1. Introduction

Star formation is one of the key processes driving the transformation of baryonic matter across the Universe. By converting their gas reservoir into stars, it has a considerable effect on the formation and evolution of galaxies, their appearance, and their fate. In turn, through the course of their evolution stars produce metals that are the building blocks of dust grains. Both metals and dust are essential for allowing the gas to cool down and for atomic gas to transform into  $H_2$ , the phase in which stars form. As stars explode into supernovae they not only disperse metals and dust across the interstellar medium, the corresponding mechanical feedback can also have a strong down-regulating effect, quenching star formation for a time. Ultimately if we want to constrain detailed models of galaxy evolution, we need to be in a position to measure star formation as reliably as possible in galaxies.

Our most direct tracer of star formation is the UV photospheric emission of massive stars. Because they are short-lived, typically a few hundred million years at most, they dominate the UV spectral domain in star-forming galaxies. A slightly more indirect way is through recombination lines. The most massive stars, which live a few ten million years at most, emit an important number of Lyman continuum photons that ionize the surrounding gas. This gas emits series of emission lines when recombining, which can then be used as star formation tracers, in particular hydrogen lines. A complication to tracing star formation in the UV or from recombination lines such as  $H\alpha$  is that galaxies contain dust. Even if it accounts for generally less than 1% of the mass of the interstellar medium (Rémy-Ruyer et al., 2014), dust has a very strong effect on the emerging radiation of galaxies, absorbing an important fraction of energetic photons over a broad range of redshifts (Burgarella et al., 2013). In some galaxies the dust absorbs a large enough fraction of UV photons that it becomes a

good tracer of the luminosity of massive stars and thus a star formation tracer in its own right.

At first sight, estimating the star formation rate (SFR) of a galaxy may appear relatively easy. The SFR should be proportional to the number of massive stars. Then one would just have to find the appropriate coefficient to convert their luminosity to their SFR. However determining this conversion coefficient is far from trivial and relies on multiple assumptions. In Sec. 2. we describe some of the main assumptions behind monochromatic SFR estimators and what their impact is. Then in Sec. 3. we describe hybrid SFR estimators that combine different estimators to correct for dust attenuation. Finally we present in Sec. 4. how spectro-photometric modeling can be used to waive some of the basic assumptions made to build SFR estimators and alleviate some of their usual limits.

## 2. Various assumptions behind SFR estimators

The most common SFR estimators are monochromatic. That is, the luminosity in a single band is directly converted to an SFR. This step strongly depends on a number of assumptions: the mass distribution of stars at birth, the stellar populations models (stellar atmosphere, stellar evolution, metallicity, etc.), when stars were formed, etc. Here we describe in more detail a few of these assumptions and what their effects are.

### 2.1. Initial mass function

Star formation tracers rely, either directly or indirectly, on the emission of massive stars. However even though they are luminous, they only represent a minor fraction of the total stellar mass formed. It is therefore necessary to assume a certain initial mass function (IMF) to extrapolate the total mass from the emission of the

massive stars. The effect of the IMF can be important. For instance, for a given far-ultraviolet (FUV) luminosity, assuming a Chabrier (2003) IMF would yield a SFR that is  $\sim 40\%$  lower than for a Salpeter (1955) IMF.

In the previous case we assumed that the IMF is fully sampled. However that may not always be true, in particular in the case of galaxies with a low SFR. It can be easily understood that it is unlikely that a low mass gas cloud is going to form many massive stars. It may form fewer or even none at all. This case generates considerable biases that can reach 0.5 dex (da Silva et al., 2014).

## 2.2. Stellar population models

The second key ingredient is the choice of the stellar population models. The constitution of these models is particularly complex and the different assumptions on stellar atmospheres, stellar evolution tracks, stellar rotation, binary evolution, etc. can lead to important differences between models. This naturally has direct consequences on the estimation of the general physical properties and the SFR in particular. For instance the inclusion of stellar rotation in models (e.g. Ekström et al., 2012) can increase the Lyman photon production rate by almost a factor two. The effect of binary evolution is more modest. For the BPASS models (Eldridge & Stanway, 2009; Eldridge et al., 2017) for instance, binary evolution increases the production of Lyman continuum photons by around 20%.

Another important assumption is that of the stellar metallicity. The presence of metals affects both the stellar atmosphere and the stellar evolution. The effect can be very important in particular for recombination lines. For instance the Lyman continuum photon production in a stellar population at  $Z = 0.0001$  is twice that of a stellar population at  $Z = 0.02$ , considering the stellar models of Bruzual & Charlot (2003).

## 2.3. Star formation history

As the emission of a single stellar population evolves rapidly as it ages, in particular in star-formation tracing bands, the star formation history has a considerable importance to estimate the SFR. The most common assumption is probably that of a “constant SFR over 100 Myr” (Kennicutt, 1998; Kennicutt & Evans, 2012). The idea of a constant SFR is probably reasonable for large isolated galaxies evolving secularly, where we expect the SFR to vary only slowly. However, it may not be appropriate for instance in strongly interacting galaxies where large and rapid variations of the SFR can be expected. An implicit but very important part of this assumption is that there is not any star older than 100 Myr. In practice if the specific SFR is at a very high level, the stars born over the last 100 Myr will dominate in star formation tracing bands. However, if it is not the case then we can expect that there will be an additional contribution due to longer lived stars that will contaminate star formation tracers, leading to an overestimate of the SFR that can reach several 10%

in standard cases (Boquien et al., 2014) but that can be considerably higher in extreme situations. Overall, any deviation from the “constant SFR over 100 Myr” is going to have a strong effect on the estimated SFR.

## 3. Dust attenuation and hybrid SFR estimators

As mentioned earlier, dust can have an important consequence on our ability to measure star formation in galaxies. Unfortunately, correcting for dust attenuation is an arduous task. In the absence of infrared observations of the dust emission, a standard technique is to rely on the slope of the UV spectrum. The idea is simple: under the assumptions described in the previous section, it is possible to compute the theoretical spectrum of a star-forming galaxy in the absence of dust. A key characteristic of dust is that the attenuation diminishes with increasing wavelength. This has the practical effect of reddening the spectrum of galaxies. The color of the spectrum will then be indicative of the amount of attenuation. This method works remarkably well for starburst galaxies (Meurer et al., 1999) but it unfortunately fails for more normal star-forming galaxies (e.g. Kong et al., 2004). Various reasons have been advanced, involving mainly deviations on the assumptions on the star formation history and/or the shape of the dust attenuation curve (e.g. Boquien et al., 2009, 2012; Salim & Boquien, 2019, and many others).

Rather than attempting to correct the rest-frame UV emission or the  $H\alpha$  for the attenuation by dust, another idea has been to combine the UV or  $H\alpha$ , which trace the non-attenuated fraction of star formation, with the IR, which traces attenuated star formation. The principle is that the weighted sum of the attenuated and non-attenuated luminosities would correspond to the intrinsic UV (or  $H\alpha$ ) luminosity:

$$L_{UV,intrinsic} = L_{UV,observed} + k \times L_{IR,observed}, \quad (1)$$

with  $L$  the luminosity and  $k$  the calibrated scaling coefficient that depends on the considered IR band. Then this luminosity can be transformed into a SFR in the usual way. Various attempts have been carried out in the literature yielding generally good results (Buat et al., 1999, 2005; Calzetti et al., 2007; Zhu et al., 2008; Kennicutt et al., 2009), but sometimes with non-trivial discrepancies (Hao et al., 2011; Liu et al., 2011). In such a situation it is not obvious to know what should be the value of  $k$  and under which circumstances.

To answer this question, in Boquien et al. (2016) we studied a small sample of KINGFISH (Kennicutt et al., 2011) galaxies. We carefully modeled them from the far-UV to the far-IR in a spatially resolved way with the CIGALE (Burgarella et al., 2005; Noll et al., 2009; Boquien et al., 2019) spectral energy distribution modeling code in order to measure their physical properties. It turned out that hybrid SFR estimators are very dependent on the stellar mass surface density, suggesting a contamination of dust emission originating from heating by evolved stars. However, measuring stellar mass is relatively straightforward even with a single near-IR band. We have therefore derived a new class of adaptive

hybrid SFR estimators. The value of  $k$  is automatically adapted based on the near-infrared emission so that the excess of IR emission generated by evolved stellar populations is eliminated, removing one possible bias.

#### 4. Spectro-photometric modeling

Even though adaptive hybrid SFR estimators represent an important progress, they still suffer from many of the same assumptions as monochromatic estimators. Deviating from these assumptions leads to biases in SFR estimates. To address this problem, one of the solutions lies in spectro-photometric modeling. The fundamental idea is that a number of these assumptions are made because the information brought by one (in the case of monochromatic estimators) or two/three (in the case of [adaptive] hybrid SFR estimators) bands is limited and does not allow to actually constrain the parameters that had to be assumed. With spectro-photometric modeling, we can combine data over a broad range of wavelengths, bringing sufficient information to allow us to relax some of the assumptions such as the star formation history or the shape of the attenuation curve for instance. This in principle should allow us to derive much more reliable estimates not just on SFR but also on many of the physical properties of galaxies.

With this aim in mind, we have developed CIGALE (see Fig. 1). Its latest generation is a fast, easy-to-use, modular spectro-photometric modeling code written in modern PYTHON (Boquien et al., 2019). The key idea behind it is energy balance. The idea is simple: the energy absorbed by dust is re-emitted self-consistently at longer wavelengths. Ideally, computing the spectrum of a dusty galaxy requires solving the radiation transfer equation, a computationally expensive operation. The energy balance principle allows us to compute the spectrum with good accuracy from a tiny fraction of the cost. Computing a single far-UV to far-IR model can take the order of 1 ms per core. This speed allows for a change of scale. A standard desktop computer can rapidly compute millions of models and fit them to observations in order to estimate the physical properties. Because many models can be a good fit to the data, the model minimizing the  $\chi^2$  is not necessarily the most appropriate. To estimate physical properties and their uncertainties CIGALE computes the likelihood-weighted means and standard deviations. The code covers the electromagnetic range from X-rays (Yang et al., 2020) to radio frequencies, and includes diverse stellar populations models, flexible star formation histories, nebular emission, many different prescriptions of dust in attenuation and in emission, and even models of active nuclei. The code is freely available\* and its development is fully open with a public git repository.

The use of modeling codes such as CIGALE allows for important improvements on the measurement of physical properties, in particular in the case of galaxies that do not lend themselves to the usual assumptions of classical estimators (Hunt et al., 2019). Whenever sufficient

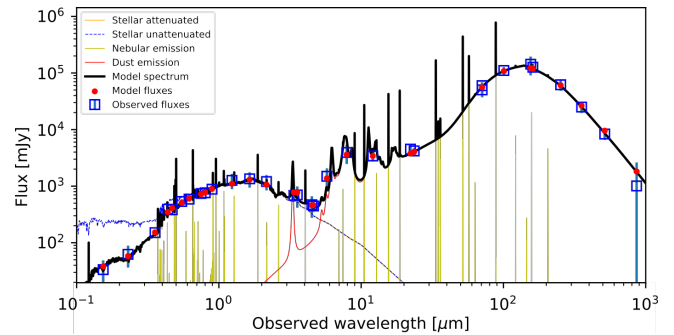


Figure 1: We see CIGALE in action as it is measuring the physical properties of the galaxy NGC 4254 while taking into account complex stellar populations, ionized gas, and dust in absorption and emission. Spectro-photometric codes such as CIGALE fully exploit multi-wavelength data to measure with greater reliability physical properties in general and the SFR in particular. It is open source and publicly available at <https://cigale.lam.fr/>.

data are available, they should be preferred over classical estimators.

*Acknowledgements:* We acknowledge partial support from the FONDECYT regular project 1170618.

#### References

- Boquien M., Buat V., Perret V., 2014, *A&A*, 571, A72
- Boquien M., et al., 2009, *AJ*, 137, 4561
- Boquien M., et al., 2012, *A&A*, 539, A145
- Boquien M., et al., 2016, *A&A*, 591, A6
- Boquien M., et al., 2019, *A&A*, 622, A103
- Bruzual G., Charlot S., 2003, *MNRAS*, 344, 1000
- Buat V., et al., 1999, *A&A*, 352, 371
- Buat V., et al., 2005, *ApJL*, 619, L51
- Burgarella D., Buat V., Iglesias-Páramo J., 2005, *MNRAS*, 360, 1413
- Burgarella D., et al., 2013, *A&A*, 554, A70
- Calzetti D., et al., 2007, *ApJ*, 666, 870
- Chabrier G., 2003, *ApJL*, 586, L133
- da Silva R.L., Fumagalli M., Krumholz M.R., 2014, *MNRAS*, 444, 3275
- Ekström S., et al., 2012, *A&A*, 537, A146
- Eldridge J.J., Stanway E.R., 2009, *MNRAS*, 400, 1019
- Eldridge J.J., et al., 2017, *PASA*, 34, e058
- Hao C.N., et al., 2011, *ApJ*, 741, 124
- Hunt L.K., et al., 2019, *A&A*, 621, A51
- Kennicutt R.C., Evans N.J., 2012, *ARA&A*, 50, 531
- Kennicutt R.C., et al., 2009, *ApJ*, 703, 1672
- Kennicutt R.C., et al., 2011, *PASP*, 123, 1347
- Kennicutt Jr. R.C., 1998, *ARA&A*, 36, 189
- Kong X., et al., 2004, *MNRAS*, 349, 769
- Liu G., et al., 2011, *ApJ*, 735, 63
- Meurer G.R., Heckman T.M., Calzetti D., 1999, *ApJ*, 521, 64
- Noll S., et al., 2009, *A&A*, 507, 1793
- Rémy-Ruyer A., et al., 2014, *A&A*, 563, A31
- Salim S., Boquien M., 2019, *ApJ*, 872, 23
- Salpeter E.E., 1955, *ApJ*, 121, 161
- Yang G., et al., 2020, *MNRAS*, 491, 740
- Zhu Y., et al., 2008, *ApJ*, 686, 155

\*<https://cigale.lam.fr>



# Dynamical effects of an eccentric giant planet on outer small body reservoirs

G.C. de Elía<sup>1</sup>

<sup>1</sup> *Instituto de Astrofísica de La Plata, CCT La Plata-CONICET-UNLP, La Plata, Argentina*

<sup>2</sup> *Facultad de Ciencias Astronómicas y Geofísicas, UNLP, La Plata, Argentina*

Contact / gdeelia@fcaglp.unlp.edu.ar

**Abstract** / The last 25 years of investigations concerning planetary sciences have led to a real explosion of new discoveries in extrasolar planets. In fact, the number of confirmed planets discovered to date outside the Solar System amounts to about 4150, which show a wide diversity of physical and dynamical properties. In particular, giant gaseous exoplanets exist on diverse orbits with small, moderate, and high eccentricities, which even reach values of up to 0.97. The dynamical structure of planetary systems that host a massive eccentric perturber is complex. Here, we combine analytical criteria and  $N$ -body numerical experiments in order to analyze the dynamical properties of outer test particles in the elliptical restricted three-body problem. In particular, we describe the orbit-flipping resonance that leads to librations of the ascending node longitude  $\Omega$ , and the inverse Lidov-Kozai resonance associated with librations of the argument of pericenter  $\omega$ , for different values associated with the eccentricity of the inner massive perturber. The dynamics discussed in this research could play a key role in understanding the evolution of debris discs associated with extrasolar systems that host an inner and eccentric giant planet.

**Keywords** / planets and satellites: dynamical evolution and stability — minor planets, asteroids: general — methods: numerical

## 1. Introduction

The dynamics of an outer test particle perturbed by an inner binary in the elliptical restricted three-body problem is a topic of special interest for a wide diversity of astrophysical problems. In this work, we study the dynamical effects of an eccentric giant planet on outer small body reservoirs resulting from planetary scattering scenarios. In particular, our analysis focuses on the orbit-flipping resonance and the inverse Lidov-Kozai resonance, which are associated with librations of the longitude of the ascending node  $\Omega$  and the argument of the pericenter  $\omega$  of the outer test particle, respectively, as a function of the eccentricity of the inner perturber. We have carried out this investigation using analytical criteria and  $N$ -body simulations, and our main results are described in detail in Naoz et al. (2017), Zanardi et al. (2017), Zanardi et al. (2018), and de Elía et al. (2019).

## 2. Numerical model

We carry out  $N$ -body experiments aimed at studying the evolution of outer small body reservoirs in systems that suffer strong planetary scattering events. To do this, we model systems initially composed of three Jupiter-mass planets located close to their dynamical instability limit (Marzari, 2014), and an outer disk of 1000 massless particles on orbits with low initial eccentricities and inclinations around stars of  $0.5 M_{\odot}$  and  $1 M_{\odot}$ . In particular, the present research focuses on the dynamical properties of those systems in which a single

giant planet survives after the instability event.

The numerical simulations were developed using the RA15 version of the RADAU integrator included in the MERCURY code (Chambers, 1999). We remark that the orbital elements of the planet and the test particles that survive in each  $N$ -body experiment were referenced to the invariant plane of the system, whose  $x$ -axis is oriented towards the pericenter of the planet.

## 3. Results

In this section, we describe the orbit-flipping ( $\Omega$ ) resonance and the inverse Lidov-Kozai ( $\omega$ ) resonance that experience outer test particles, which evolve under the effects of an inner eccentric Jupiter.

### 3.1. The orbit-flipping resonance

Such as was discussed by Zanardi et al. (2017), in general terms, the outer small body reservoirs resulting from the  $N$ -body experiments can be composed of three different kind of particles:

- *Type-P* particles, with inclinations  $i < 90^{\circ}$  and circulations of the longitude of the ascending node  $\Omega$ ;
- *Type-R* particles, with inclinations  $i > 90^{\circ}$  and circulations of the longitude of the ascending node  $\Omega$ ;
- *Type-F* particles, whose orbital planes flip from prograde to retrograde and back again experiencing librations of the longitude of the ascending node  $\Omega$  around  $90^{\circ}$  or  $270^{\circ}$ . Thus, these particles experience

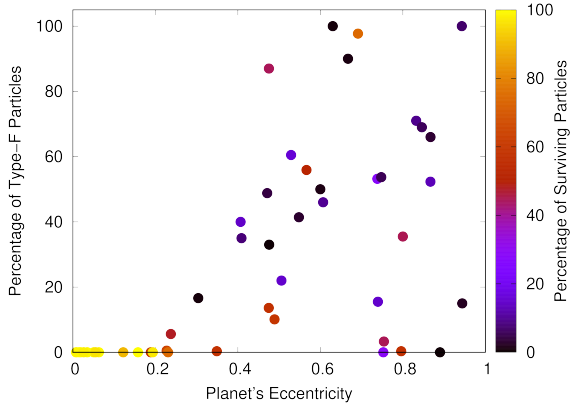


Figure 1: Percentage of *Type-F* particles at 100 Myr as a function of the eccentricity of the planet, in systems around stars of  $0.5 M_{\odot}$  and  $1 M_{\odot}$ . The color palette illustrates the percentage of the initial particles that survive.

an orbit-flipping resonance with nodal librations.

Figure 1 illustrates the percentage of *Type-F* particles in the resulting systems at 100 Myr as a function of the eccentricity of the planet, where the color palette represents the percentage of surviving particles respect to the initial number. In general terms, systems that harbor a planet with an orbital eccentricity less than  $\sim 0.2$  maintain more than 95% of the initial particles, while there are no *Type-F* particles in the resulting reservoirs. For greater values of the eccentricity of the planet, the results are very different. On the one hand, the percentage of surviving particles significantly decreases, ranging between 0.3% and 74.5% with a median value of 14.4%. On the other hand, the production of *Type-F* particles becomes a very efficient process.

The link between *Type-F* particles and the eccentricity of the planet can be understood from the use of analytical prescriptions. In fact, the  $\Omega$  resonance appears at quadrupole order in the secular Hamiltonian of an outer test particle in the elliptical restricted three-body problem (Ziglin, 1975; Farago & Laskar, 2010; Naoz et al., 2017; Vinson & Chiang, 2018). According to this, it is possible to derive analytical expressions, from which the results of our  $N$ -body experiments can be analyzed. From Ziglin (1975), the range of inclinations that lead to libration trajectories of  $\Omega$  has a width  $\Delta i$  given by

$$\Delta i = 2 \arccos \left\{ \sqrt{\frac{1 - e_{\text{pla}}^2}{1 + 4e_{\text{pla}}^2}} \right\}, \quad (1)$$

where  $e_{\text{pla}}$  is the eccentricity of the planet. This expression allows us to infer two important results. First, the greater the eccentricity of the planet, the larger the range of inclinations that leads to nodal librations of the outer test particle. Second, the orbit-flipping resonance that involves librations of  $\Omega$  requires a planet on a non-circular orbit, since the width  $\Delta i = 0^\circ$  for  $e_{\text{pla}} = 0$ .

The top and bottom panels of Fig. 2 show the evolutionary trajectories in a  $(\Omega, i)$  plane of *Type-P* (green curve), *Type-R* (yellow curve), and *Type-F* (black curve) representative particles associated with systems around a  $0.5 M_{\odot}$  star that harbor a Jupiter-

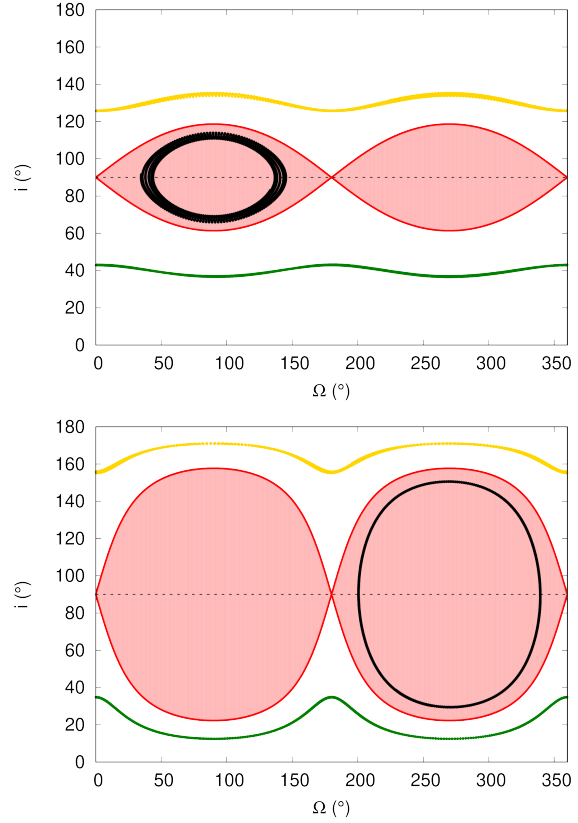


Figure 2: Evolutionary trajectories in the  $(\Omega, i)$  plane of *Type-P* (green curves), *Type-R* (yellow curves), and *Type-F* (black curves) representative particles in systems around a  $0.5 M_{\odot}$  star with  $e_{\text{pla}} = 0.24$  (top panel) and  $0.74$  (bottom panel). In each panel, the red shaded region represents the values that lead to nodal librations.

mass planet with eccentricities of 0.24 and 0.74, respectively. In both panels, the red curve illustrates the separatrix of the system, which divides circulation from libration trajectories of  $\Omega$ , while the red shaded region represents the pairs  $(\Omega, i)$  that lead to the orbit-flipping resonance. It is evident that the more eccentric the planet, the larger the range of inclinations that lead to the generation of *Type-F* particles.

Recently, Zanardi et al. (2018) studied how General Relativity (GR) affects the dynamical evolution of outer test particles in the elliptical restricted three-body problem. The authors showed that, if GR is included in the model, the range of prograde (retrograde) inclinations that lead to nodal librations is reduced (increased) with respect to that derived in absence of GR. Future studies aimed at describing the dynamical structure of debris discs associated with systems of the observed sample that host an inner eccentric giant planet should take into account this result.

### 3.2. The inverse Lidov-Kozai resonance

The inverse Lidov-Kozai resonance is associated with librations of the argument of pericenter  $\omega$  around  $90^\circ$  or  $270^\circ$  of an outer test particle in the elliptical restricted

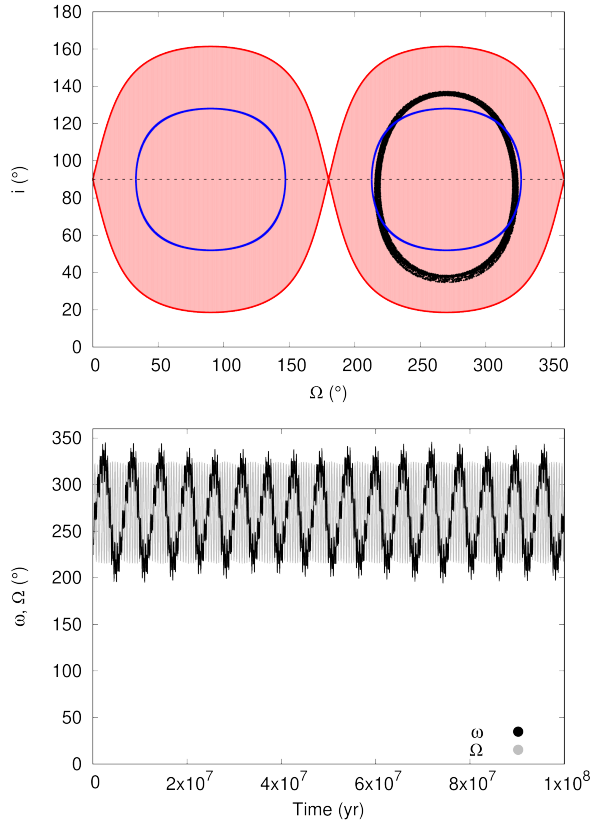


Figure 3: Top panel: Evolutionary trajectory in the  $(\Omega, i)$  plane of a *Type-F* particle (black curve) that experience the inverse Lidov-Kozai resonance in a system around a  $0.5 M_{\odot}$  star with  $e_{\text{pla}} = 0.8$ . The blue curve represents the values that lead to the vanishing of the  $\omega$  quadrupole precession rate. The red shaded region illustrates the pairs  $(\Omega, i)$  associated with the orbit-flipping ( $\Omega$ ) resonance. Bottom panel: Temporal evolution of  $\omega$  (black curve) and  $\Omega$  (gray curve).

three-body problem. According to Vinson & Chiang (2018), such a resonance appears at hexadecapole order in the secular Hamiltonian, for which the derivation of a resonant condition as a function of the orbital elements of the test particle and the planet is not an easy task. Recently, de Elía et al. (2019) showed that the pairs  $(\Omega, i)$  that lead to the vanishing of the quadrupole precession rate of the argument of pericenter  $\omega$  of an outer test particle satisfy the condition

$$i = \arccos \left\{ \pm \sqrt{\frac{2 + 3e_{\text{pla}}^2 [1 - 5 \cos(2\Omega)]}{10 + 5e_{\text{pla}}^2 [3 - 5 \cos(2\Omega)]}} \right\}. \quad (2)$$

From this and the condition derived by Ziglin (1975) for the orbit-flipping resonance, the  $\omega$  quadrupole precession rate vanishes for outer particles that only experience nodal circulations (librations) for a planet eccentricity  $e_{\text{pla}} < 0.25$  ( $> 0.40825$ ).

A very interesting result inferred by de Elía et al. (2019) suggests that Eq. 2 gives a condition close to the inverse Lidov-Kozai resonance. From this and that mentioned in the above paragraph, it was possible to find the inverse Lidov-Kozai resonance for outer test particles on nodal circulation trajectories for  $e_{\text{pla}} < 0.25$ , and for outer test particles on nodal libration trajectories for

$e_{\text{pla}} > 0.40825$  in our  $N$ -body experiments. According to this, systems with  $e_{\text{pla}} > 0.40825$  show relevant dynamical features since test particles with simultaneous librations of  $\Omega$  and  $\omega$  can be found in the outer reservoirs. Figure 3 shows a clear example of this kind of particles in a system with  $e_{\text{pla}} = 0.8$  around a  $0.5 M_{\odot}$  star. In such a figure, the top panel shows the evolutionary trajectory of the test particle (black curve) in the  $(\Omega, i)$  plane, together with the values that lead to the vanishing of the  $\omega$  quadrupole precession rate of the test particle for  $e_{\text{pla}} = 0.8$  given by Eq. 2 (blue curve). The bottom panel illustrates the simultaneous librations of  $\Omega$  and  $\omega$  around  $270^\circ$  as a function of time for the test particle under consideration.

Finally, it is necessary to mention that the conditions that lead to the inverse Lidov-Kozai resonance are more restrictive than those related to the orbit-flipping resonance associated with nodal librations. This allows us to understand the low number of particles that experience the inverse Lidov-Kozai resonance in comparison with the number of *Type-F* particles in our  $N$ -body experiments. Beyond this, we must remark that the inverse Lidov-Kozai resonance is possible for small, moderate, and even high values of the eccentricity of the planet.

## 4. Conclusions

This work is part of an investigation aimed at analyzing the dynamical properties of planetary systems that host an inner eccentric massive perturber. In particular, we focus on the secular resonances of outer test particles that evolve under the effects of an inner and eccentric Jupiter-mass planet in systems that suffered strong scattering events. We remark that the conditions that lead to the orbit-flipping ( $\Omega$ ) resonance and the inverse Lidov-Kozai ( $\omega$ ) resonance for the outer test particles are strongly dependent on the eccentricity of the planet.

Our analytical and numerical results are important since they have potential application to the study of outer debris discs in extrasolar systems and circumbinary planets.

*Acknowledgements:* I thank the SOC and LOC of XVI LARIM for the invitation to the meeting and the financial support. I specially acknowledge Dr. Patricia B. Tissera and Dr. Eduardo Unda-Sanzana for the kind treatment received. I also thank the financial support by Agencia Nacional de Promoción Científica y Tecnológica (ANPCyT) through PICT 201-0505. Finally, I acknowledge Dr. Macarena Zanardi for her work in this research and valuable discussions.

## References

- Chambers J.E., 1999, MNRAS, 304, 793
- de Elía G.C., et al., 2019, A&A, 627, A17
- Farago F., Laskar J., 2010, MNRAS, 401, 1189
- Marzari F., 2014, MNRAS, 442, 1110
- Naoz S., et al., 2017, AJ, 154, 18
- Vinson B.R., Chiang E., 2018, MNRAS, 474, 4855
- Zanardi M., et al., 2017, A&A, 605, A64
- Zanardi M., et al., 2018, A&A, 615, A21
- Ziglin S.L., 1975, Soviet Astronomy Letters, 1, 194



# Deciphering the accretion history of galaxies: insights from stellar halos

A. Monachesi<sup>1,2</sup>

<sup>1</sup> *Instituto de Investigación Multidisciplinar en Ciencia y Tecnología, Universidad de La Serena, Chile*

<sup>2</sup> *Departamento de Astronomía, Universidad de La Serena, Chile*

Contact / amonachesi@userena.cl

**Abstract** / During the last decade, significant progress has been made to resolve the halos of nearby galaxies. In this proceeding we mostly focus on the results from the GHOSTS survey, an *HST* imaging survey of nearby galaxies. Stellar halos show a large diversity in their properties for Milky Way-like galaxies that are alike in terms of total luminosity and stellar mass. Another important result from this survey is the discovery of a stellar halo mass–metallicity relation, which allows to constrain the mass and metallicity of the most massive accreted satellite. We also discuss the results from the stellar halos of the Auriga simulations, a suite of forty cosmological magneto-hydrodynamical zoom-in simulations of Milky Way-mass galaxies. A comparison between the results from the Auriga simulations with those obtained from observations of nearby galaxies shows a good agreement. We discuss observational signatures of stellar halos that allow us to decode the accretion and merger history of observed galaxies. In particular, the stellar mass and metallicity of the halos at 30 kpc reflect the properties of the most massive accreted satellite, and strong metallicity gradients are found when the stellar halo is built from few (one to four) significant progenitors.

*Keywords* / galaxies: halos — galaxies: stellar content — galaxies: structure — galaxies: evolution

## 1. Introduction

Within the currently favored  $\Lambda$ -Cold Dark Matter cosmological model, stellar halos of Milky Way (MW)-mass galaxies grow in mass hierarchically through the accretion of smaller objects that, due to gravity, merge together to form the larger systems we see today (Searle & Zinn, 1978). Tidal debris from this merging and accretion process forms a stellar halo extending to large radii that remains very structured owing to long dynamical times (e.g. Bullock & Johnston, 2005). Thus, the outskirts of galaxies are the best place to look at in order to gain some insight into the accretion and growth history of galaxies. If we are able to study the stellar properties of halos such as age and metallicity, and characterize their accreted satellites, we will have a powerful tool to constrain the origin of stellar halos and test model predictions.

However, observing and characterizing stellar halos is extremely challenging, due to their faintness (reaching surface brightnesses of  $\mu_V \sim 35$  mag/arcsec<sup>2</sup>) and extension (out to 100 to 200 kpc from the galactic center) around a MW-sized galaxy, which prevented until now the use of stellar halos as quantitative measures of merger history. This stellar component also represents only a small fraction (one to few percent) of the total stellar mass and light of a MW-like galaxy. Until very recently, only the stellar halos of our own Galaxy and that of M31 have been studied, due to their proximity. These two halos, although show qualitatively similar properties, exhibit significant differences (e.g. Bell

et al. 2010; Xue et al. 2015 for MW; Gilbert et al. 2014; Ibata et al. 2014 for M31). In addition, models predict substantial galaxy-to-galaxy scatter in halo properties, motivating study of other external stellar halos.

Over the last decade, great effort and progress has been made both observationally, particularly to resolve the stellar halos of galaxies, and theoretically with improved and higher resolution simulations, which allow us to use stellar halos to quantitatively measure the most massive accretion of a galaxy. In this proceeding we show advances on both fronts that allowed connecting the observable properties that we get from stellar halos with the merger and accretion history of galaxies.

On the observational side, we focus on the GHOSTS survey (Radburn-Smith et al., 2011) from which we gain a greater insight into the physical properties of halos, since it resolves their stellar populations. The GHOSTS survey is a *Hubble Space Telescope* (*HST*) survey imaging the outskirts of more than 16 nearby disk galaxies with a range of masses and luminosities, located most of them out to 6 Mpc, the farthest one out to 15 Mpc. It is the largest study of the resolved stellar populations in the outer disks and halos of nearby disk galaxies.

On the theoretical side, we focus here on the results from the Auriga simulations (Grand et al., 2017). The Auriga simulations are a suite of forty cosmological magneto-hydrodynamical zoom simulations of the formation of galaxies in isolated Milky Way mass dark halos. These were carried out with the moving mesh code AREPO, together with a comprehensive model for galaxy formation physics, including AGN feedback and

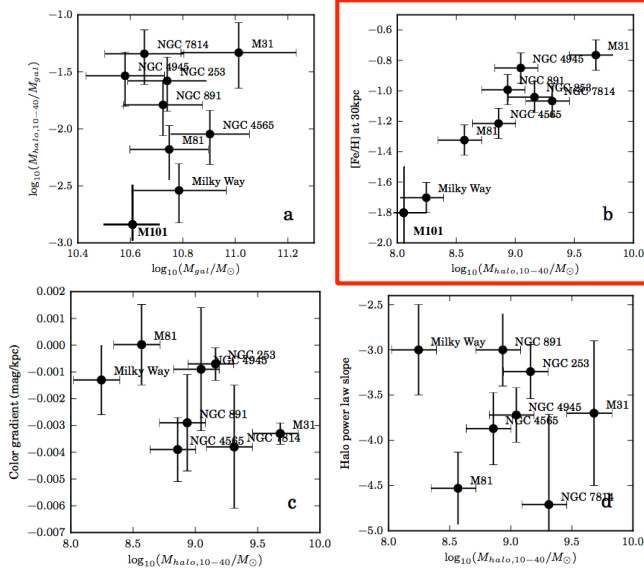


Figure 1: Correlations between inferred stellar halo properties of the GHOSTS galaxies as well as M31 and the MW. Top-left: Fraction of stellar halo mass vs. total stellar mass. Top-right: stellar halo metallicity at 30 kpc on the minor axis vs. stellar halo mass. Bottom-left: color gradient vs. stellar halo mass. Bottom-right: power-law slope vs. stellar halo mass. The strongest correlation that we find, highlighted in red, is the stellar halo mass–metallicity relation. Adapted from *Diverse stellar haloes in nearby Milky Way mass disc galaxies*, Harmsen et al. (2017), Oxford University Press.

magnetic fields, which produces realistic galaxy populations in large cosmological simulations. These simulations reproduce a wide range of present-day observables, in particular, two-component disk-dominated galaxies with appropriate stellar masses, sizes, rotation curves, star formation rates and metallicities.

## 2. Results

### 2.1. Observations

We show here the results that we obtained from the seven most massive MW-like galaxies of GHOSTS. For each of these galaxies we have observed several *HST* fields along their minor and major axes, in two filters, providing star counts and color-magnitude diagrams of the outer disk and halo of each galaxy. Our GHOSTS observations typically reach 1.5 to 2 mag below the tip of the red giant branch (RGB) with  $S/N = 7$ . We focus on the fields along the minor axis, because this gives us the clearest information about the accretion history of stellar halos for disk galaxies. Comparison with models strongly suggests that the minor axis at  $> 10$  kpc for MW-like galaxies is accretion-dominated (Monachesi et al., 2016a). We use the RGB stars as tracers of the faint underlying population to obtain information about the galactic stellar halos, such as their metallicities and stellar surface density along the minor axis profiles. We construct color (a proxy for metallicity) and surface brightness profiles of each galaxy along the minor axis out to approximately 50–70 kpc, depending

on the galaxy (see details in Monachesi et al. 2016b and Harmsen et al. 2017). The projected minor axis surface brightness profiles of the halos are broadly consistent with power laws, with a slope that varies between  $-2 < \alpha < -3.5$ . We find steep color/metallicity gradients in three out of seven of the halos of the GHOSTS galaxies, whereas the other four show rather flat color profiles. From the RGB star counts we calculate the present-day stellar-halo mass by using isochrones between 10 and 40 minor axis equivalent radii. Within this radial range on the minor axis we have good and reliable coverage for all the GHOSTS galaxies. We scale the 10–40 kpc mass to total stellar halo mass using simulations (see details in Harmsen et al. 2017).

With all this information, we can provide then statistics on galaxy stellar outskirts beyond M31 and MW. Fig. 1 shows the results and correlations we find between the stellar halo properties for GHOSTS galaxies together with those of M31 and the MW stellar halos. We find that the GHOSTS stellar halos are diverse, with variations of a factor of  $\sim 20$  in stellar halo mass fractions with the addition of the Milky Way and M31 to the sample, more than an order of magnitude range in metallicities and significant variation in color gradients and density profile slopes. In addition, we find a factor of about 100 spread in stellar halo mass. Thus, there is significant scatter in all halo properties in a narrow range of stellar mass or rotation velocity.

Interestingly, as important as the diversity that we found in stellar halo properties, we find a strong correlation between the stellar halo metallicity at 30 kpc along the minor axis and the stellar halo mass, highlighted in the red panel in Fig. 1. This is the strongest correlation we find between stellar halo parameters. This very tight correlation indicates that larger stellar halos form from larger more metal-rich satellites, which is in agreement with accretion-only based models (see Harmsen et al., 2017; Bell et al., 2017) and we explore this further in the next section with the Auriga simulations.

### 2.2. Simulations

These observational results motivate the analysis of a large set of simulations in order to interpret the data and understand how we can use the stellar halo properties to learn about the merger and accretion history of galaxies. We use the Auriga simulation as it represents one of the largest datasets to study individual stellar halos with high-mass particle resolution. This is required to be able to quantify the scatter in halo-to-halo properties observed in nearby galaxies.

By analyzing the stellar halos of the Auriga galaxies in the same way as we did for the observations, we find that the Auriga simulations reproduce the diversity found in observed stellar halos of MW-mass galaxies (see Monachesi et al. 2019 for details). In particular, the Auriga galaxies reproduce the stellar halo mass–metallicity relation discovered empirically with the observations.

We then investigate the accretion history of these simulated galaxies to see if we can relate their accretion history to their stellar halo properties, more specifically with the observable properties that can be estimated,

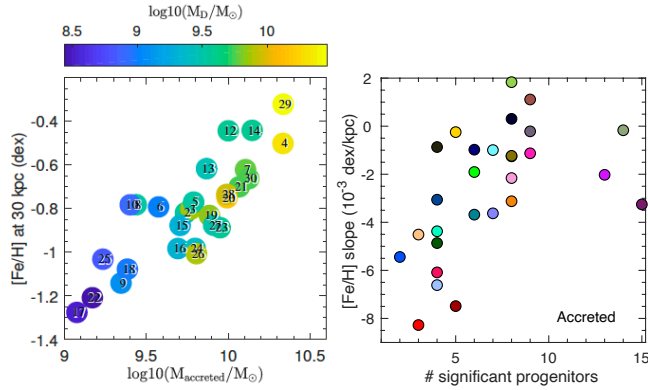


Figure 2: *Left panel:* Stellar halo mass–metallicity relation for Auriga galaxies, color coded by the stellar mass of the most dominant (more massive) accreted satellite. *Right panel:* Minor axis metallicity profile slopes as a function of the number of significant progenitors. Adapted from *The Auriga Stellar Haloes: Connecting stellar population properties with accretion and merging history*, Monachesi et al. (2019), Oxford University Press.

such as metallicity and stellar mass, metallicity gradients and stellar density profiles. We find that the build up of the accreted stellar halo varies quite significantly from galaxy to galaxy. The number of satellites that contribute to 90% of the accreted stellar mass, i.e. the number of significant progenitors, varies from 1 to 14 among the Auriga galaxies, with a median of 6.5. This variation is due to stochasticity in the accretion history. It is worth mentioning, however, that in most cases only one accreted satellite contributes to more than 50% of the stellar halo mass (see Monachesi et al. 2019 and Fattahi et al. 2020).

Fig. 2 shows, on its left panel, the stellar halo mass–metallicity relation of the Auriga galaxies, color coded by the stellar mass of the dominant (most massive) accreted satellite. We can see that larger halos accrete more massive dominant satellites. In addition, because of the galaxy metallicity–mass relationship, the most massive satellite imprints a stellar halo mass–metallicity relation. This implies that we can use the stellar halo mass or stellar halo metallicity to quantify the dominant (largest) merger that a galaxy has had (see Bell et al., 2017; D’Souza & Bell, 2018; Monachesi et al., 2019). The broad range in halo properties is therefore driven by the diversity in merger history.

On the right panel of Fig. 2 we show the metallicity gradient of the Auriga stellar halos as a function of the number of significant progenitors, i.e. satellites that contribute to 90% of the accreted stellar mass. We find an interesting trend, with larger gradients when fewer significant progenitors build up the stellar halo. Thus, halo metallicity gradients may quantify the degree of dominance of the largest accretion, which is reflected in the stellar halo mass–metallicity relationship.

### 3. Conclusions

Stellar halos offer unique information to decipher the merger history of galaxies. In this proceeding we present

results from observational and theoretical work on stellar halos of MW-mass galaxies, which have provided insight on how we can use stellar halo properties as a quantitative measure of merger history.

We conclude here with the most important results presented:

- Minor axis studies of resolved stars in nearby MW-mass galaxies from the GHOSTS survey reveal diverse stellar halo properties. Galaxies with stellar masses similar to the MW have an order of magnitude range in characteristic minor axis halo metallicities, power-law profiles with best slopes varying between  $-2$  and  $-3$ , and a variety of metallicity gradients, where half of the sample have little to no measurable metallicity gradient.
- We find a strong correlation between stellar halo metallicity and mass. This tight relation discovered empirically allows us to quantify the dominant accretion event. Larger halos are formed from a few larger satellites. The broad range in stellar halo properties is driven by the diversity in merger history.
- Metallicity (and possibly stellar density) gradients may better characterize the merger history.

Studies of stellar halos as those shown here will become increasingly important in the next decade, with the next generation of ground-based giant telescopes such as GMT, TMT and ELT as well as space telescopes as *JWST* and *WFIRST*. These new facilities will allow us to expand the sample of individual galaxies studied and will be excellent to sample diversity in halos as well as in galaxy types, allowing studies of resolved stellar populations in hundreds of galaxies. This will increase by at least an order of magnitude the number of galaxies for which we have resolved studies of stellar halos.

*Acknowledgements:* AM acknowledges the organizers of the LARIM 2019 conference for their financial support. The author is thankful for the fruitful collaboration over the years and inspiring discussions with E. F. Bell, R. de Jong, J. Bailin and the GHOSTS collaboration, F. A. Gómez, R. J. J. Grand, S. White, V. Springel and the Auriga team. AM acknowledges financial support from FONDECYT Regular 1181797 and funding from the Max Planck Society through a Partner Group grant.

### References

- Bell E.F., et al., 2010, *AJ*, 140, 1850  
 Bell E.F., et al., 2017, *ApJL*, 837, L8  
 Bullock J.S., Johnston K.V., 2005, *ApJ*, 635, 931  
 D’Souza R., Bell E.F., 2018, *MNRAS*, 474, 5300  
 Fattahi A., et al., 2020, arXiv e-prints, arXiv:2002.12043  
 Gilbert K.M., et al., 2014, *ApJ*, 796, 76  
 Grand R.J.J., et al., 2017, *MNRAS*, 467, 179  
 Harmsen B., et al., 2017, *MNRAS*, 466, 1491  
 Ibata R.A., et al., 2014, *ApJ*, 780, 128  
 Monachesi A., et al., 2016a, *MNRAS*, 459, L46  
 Monachesi A., et al., 2016b, *MNRAS*, 457, 1419  
 Monachesi A., et al., 2019, *MNRAS*, 485, 2589  
 Radburn-Smith D.J., et al., 2011, *ApJS*, 195, 18  
 Searle L., Zinn R., 1978, *ApJ*, 225, 357  
 Xue X.X., et al., 2015, *ApJ*, 809, 144



# 100th anniversary of the International Astronomical Union

S. Torres-Peimbert<sup>1</sup>

<sup>1</sup> *Instituto de Astronomía, Universidad Nacional Autónoma de México, México*

Contact / [silvia@astro.unam.mx](mailto:silvia@astro.unam.mx)

**Abstract** / A brief review of the history and present activities of the International Astronomical Union is presented.

**Keywords** / general: miscellaneous

## 1. Introduction

The International Astronomical Union was founded in 1919, since then it has enlarged its mission, it has multiplied its membership, and has expanded its projects. Its mission is to promote and safeguard the science of astronomy in all its aspects, including research, communication, education and development, through international cooperation.

The key activity of the IAU is the organization of scientific meetings. Among the responsibilities of the IAU are the definition of fundamental astronomical and physical constants; unambiguous astronomical nomenclature and informal discussions on the possibilities for future international large-scale facilities. It also serves as the internationally recognized authority for assigning designations to celestial bodies and surface features on them.

At present it is composed of 13,675 astronomers (of which 543 are junior members), of 103 countries. Its funding is provided by the contribution of 86 countries. The basic information presented here can be found at [iau.org](http://iau.org)<sup>\*</sup>. The fraction of women members of IAU in November 2019 was 18.1% of all membership.

## 2. Executive Committee

The Union is guided by the Executive Committee composed of 12 members: 4 officers, 6 vice-presidents and 2 counselors. The officers election is for 3 years; currently they are: President: Ewine van Dishoeck (Netherlands); President elect: Debra Elmegreen (USA); General Secretary: Teresa Lago (Portugal); and Assistant General Secretary: José Miguel Rodríguez Espinosa (Spain). There are six Vice-presidents who are in office during six years: Laura Ferrarese (Canada); John Hearshaw (New Zealand); Ajit Kembhavi (India); Daniela Lazzaro (Brasil), Boris Shustov (Russia); and Junichi Watanabe (Japan). The past President and past General Secretary act as counselors: namely, Silvia Torres-Peimbert (Mexico), and Piero Benvenuti (Italy).

<sup>\*</sup><http://www.iau.org/>

## 3. Organization

To carry out its activities the Union is organized in 9 Divisions, 35 Commissions and 54 Working Groups. These Divisions cover in general the different topics of interest. They are: A. Fundamental Astronomy; B. Facilities, Technology and Data Science; C. Education, Outreach and Heritage; D. High Energy Phenomena and Fundamental Physics; E. Sun and Heliosphere; F. Planetary Systems and Astrobiology; G. Stars and Stellar Physics; H. Interstellar Matter and Local Universe; and J. Galaxies and Cosmology.

The Commissions encompass various astronomical sub-disciplines; and form part of the Divisions. Finally, the working groups are established to undertake certain well-defined tasks for limited time periods.

## 4. Main tasks

Some of the Union commitments are: I. to stimulate astronomical knowledge among professional astronomers, II. to coordinate professional tasks and interact with other fields of professional level; and III. to recognize excellence in astronomy through prizes. Examples of some of these activities that have been carried out during its first 100 years of existence are listed below.

- In general, its objective is to stimulate participation of astronomers in all countries.
- Every three years it hosts a General Assembly (GA). Altogether there have been 30 GAs in sites around the world.
- IUA sponsors meetings. Among them there are: Symposia (totalling 356); Focus Meetings, Divisions, Commissions & Working group meetings at the GA.
- It hosts Regional meetings every 3 years per geographical region (42 regional events have taken place); and it co-sponsors other meetings (e.g., COSPAR and Annual Young Astronomers conference).
- It aims to promote changes that benefit professional astronomy.
- It publishes Symposia proceedings, Colloquia proceedings (discontinued), Highlights of Astronomy,

Transactions, Information Bulletins/Catalyst, E-Newsletters, etc.

- It represents astronomy at the International Science Council (ISC) – resulting from the merging of the International Council for Science (ICSU) and the International Social Science Council (ISSC).
- It participates in the selection of different prize recipients: (a) The Gruber Prize of Cosmology and The Kavli Astrophysics Prize; (b) The Gruber Foundation Fellowships in Astrophysics; and (c) The IAU PhD Prize for each Division.
- it organizes the International School for Young Astronomers (ISYAs). This program was established in 1967; it is a three-week international postgraduate school. So far 42 ISYAs have taken place.

## 5. Strategic Plan

The 2009 International Year of Astronomy succeeded in exciting the imagination and creativity of an unprecedented numbers of individuals. In this project 148 IYA2009 National Nodes participated; the total amount spent around the world was €10 900 000; and the number of people that attended any form of this celebration was of 791 600 000. It was such a successful program that it gave rise to the approval of “IAU Strategic Plan 2010-2020” at the GA in Rio de Janeiro (2009) \*\*.

Among its projects was the creation of an “Office of Astronomy for Development”(OAD); which was established with the task of stimulating tools for development in every country. Its headquarters are in Cape Town, South Africa. In order to increase regional involvement “OAD Nodes” were established. It has been very successful and well received in all continents. \*\*\*

Not much later, the “Office of Astronomy Outreach” was created, with the mission to build networks to support and disseminate information to the amateur astronomy and public outreach communities, and to ultimately make it easier for the public to access information about the universe. Its headquarters are in Tokyo, Japan. In this case, the IAU network of National Outreach Coordinators was organized. \*\*\*\*.

Expanding on the experience gained, at the 2018 GA the “IAU Strategic Plan 2020-2030” was approved. †. In it five goals were delineated:

- To lead the worldwide coordination of astronomy and the fostering of communication and dissemination of astronomical knowledge among professional astronomers.
- To promote the inclusive advancement of the field of astronomy in every country.
- To promote the use of astronomy as a tool for development in every country.
- To engage the public in astronomy through access to astronomical information and communication of the

\*\*[https://www.iau.org/static/education/strategicplan\\_2010-2020.pdf](https://www.iau.org/static/education/strategicplan_2010-2020.pdf)

\*\*\*[www.astro4dev.org](http://www.astro4dev.org)

\*\*\*\*<https://www.iau.org/public/>

†[https://www.iau.org/static/administration/about/strategic\\_plan/strategicplan-2020-2030.pdf](https://www.iau.org/static/administration/about/strategic_plan/strategicplan-2020-2030.pdf)

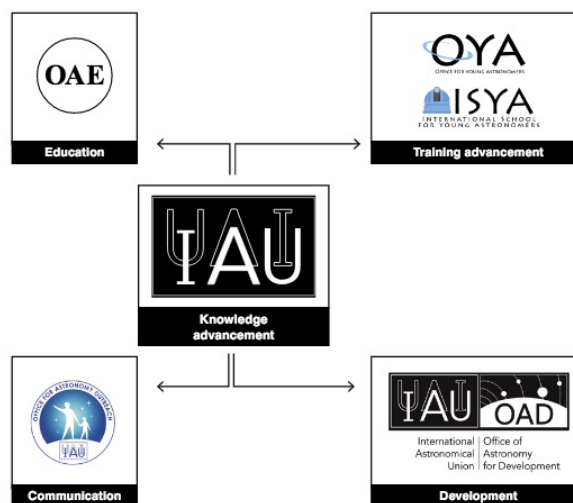


Figure 1: Relationships between the various IAU components and offices. Figure taken from IAU Strategic Plan 2020-2030.

science of astronomy.

- To stimulate the use of astronomy for teaching and education at school level.

At present, in addition to the OAD and OAO offices, an “Office for Young Astronomers” (OYA) has been formalized. It is a virtual office in Oslo, Norway, sponsored by the Norway Academy of Science that hosts ISYA activities and is devoted to develop the next generation of astronomers and scientists. ‡

More recently, on November 2019, a new office was launched, the “Office of Astronomy for Education” (OAE). The location for its new Office of Astronomy for Education will be Haus der Astronomie, HdA, an astronomy outreach centre based in Heidelberg, Germany. §

The overall structure of the activities of IAU is presented schematically in Figure 1.

## 6. Impact in Latin America

As it has happened elsewhere, Latin America has improved significantly its astronomical resources, both in infrastructure and in the number of scientists devoted to this activity. IAU has helped to catalyze this increment through its several programs.

Several IAU sponsored meetings have been held in the region; namely: 2 General Assemblies, 33 Symposia, 2 Colloquia, and 15 Regional meetings.

In particular, in addition to the 9 ISYAs that have been held in this region, it has sponsored Central American Schools of Astronomy, and many outreach activities through National teamworks of people interested in the dissemination of astronomy; it has favored better contact with amateur astronomers, and it has triggered

‡[https://www.iau.org/education/office\\_for\\_young\\_astronomers/](https://www.iau.org/education/office_for_young_astronomers/)

§<https://www.iau.org/education/oe/>

collective activities like ‘Noche de las Estrellas’ which has unified up to 100 sites for simultaneous star parties.

The number of IAU members in Latin America and the Caribbean is of 744 which comprise 5.4 % of the total membership. They are distributed as follows: Argentina, 156; Brazil, 216; Chile, 129; Colombia, 30; Costa Rica, 2; Cuba, 5; Honduras, 3; Mexico, 171; Peru, 2; Uruguay, 5; Venezuela, 21; Ecuador, 2; Puerto Rico, 1; and Trinidad & Tobago, 1.

It is worth noting that in the ‘Name Exoworlds’ project, 20 of the more than one hundred that participated were from Latin America and the Caribbean.

## 7. 100 years of IAU

We are celebrating the IAU centennial and the goal was for it to be celebrated around the world. The theme has been “100 years: under one sky”, “100 años IAU - Bajo el mismo cielo”. It has been a very successful celebration so far. ¶

There is a long list of astronomical inspired events related to the centennial celebration which can be found in its web page ¶. I will only point out some centennial highlights:

- Exhibit ‘Above and Beyond’ which shows the advances per decade on: (a) astronomy and space exploration, (b) technology and (c) cultural displays related to the topic \*\*;
- Exhibit ‘Inspiring Stars’ for people with special abilities††;
- The Flagship Ceremony, at the Palace of the Academy in Brussels April 11 and 12;
- Dark skies for all‡‡;

- 100 Hours of Astronomy (with the participation of 85 countries), January 10–13;
- Women and Girls in Astronomy Day, February 11 (and throughout the month);
- 100th Anniversary of the total solar eclipse of 1919 which confirmed the Theory of General Relativity, May 29;
- 50th Anniversary of Moonlanding, July 29;
- Total Solar eclipse in Chile and Argentina, July 2nd;
- 100th Anniversary Book (See Andersen et al. (2019));
- Name ExoWorlds Campaign, June to December.

The Union has always been very concerned about incorporating young astronomers. Since 2017 it has established an annual prize for the best PhD thesis in each one of the Divisions. In addition, at the 2018 GA, IAU incorporated as temporary members astronomers that have recently obtained a PhD.

Recently the project ‘IAU100 NameExoWorlds’ gave every country in the world the opportunity to name an exoplanet and its host star, where a star–planet system was assigned to each country. The selected stars could be observed with a small telescope from the latitude of the capital of each country. The names were chosen by public voting. Again this scheme turned out to be a success, as 112 countries participated in this selection. The resulting names are available on line.

*Acknowledgements:* Support from CONACyT project 241732 is gratefully acknowledged.

## References

Andersen J., Baneke D., Madsen C., 2019, *The International Astronomical Union*, Springer

¶<https://www.iau-100.org/events>

¶<https://www.iau-100.org/>

\*\*[100exhibit.iau.org/](https://100exhibit.iau.org/)

††<https://aorgil.blogs.uv.es/>

[iau100-inspiring-stars-exhibition/](https://iau100-inspiring-stars-exhibition/)

‡‡[darkskies4all.org/](https://darkskies4all.org/)



# Solar corona tomography

A.M. Vásquez<sup>1</sup>

<sup>1</sup> *Instituto de Astronomía y Física del Espacio, CONICET-UBA, Argentina*

Contact / albert@iafe.uba.ar

**Abstract** / The study of the Sun is of interest for both practical and fundamental reasons. It is the ultimate driver of space weather conditions, whose accurate prediction relies on advancing our understanding of solar dynamics. It provides a solid base of knowledge on which other types of stars can be modeled, hence it is of central interest to stellar astrophysics. Solar tomography is currently the only observational technique capable of providing an empirical three-dimensional description of the solar corona at a global scale. As such, it is of relevance to the aforementioned topics. In this short article we summarize the methodology and the diagnostics it provides, review examples of results, and discuss future projects.

*Keywords* / Sun: corona — Sun: UV radiation — Sun: fundamental parameters — Sun: magnetic fields

## 1. Introduction

The corona is the region of the solar atmosphere where plasma is heated to million degree temperatures and accelerated, forming the solar wind. It is where solar flares release their energy and coronal mass ejections are energized. Improving knowledge of the physics of the corona is essential to advance our understanding of the Sun-Earth relation, for which empirical data is key.

Being the corona optically thin in spectral ranges such as white light (WL) and extreme-ultraviolet (EUV), its images are two-dimensional (2D) projections of an underlying three-dimensional (3D) emitting structure. Tomography is a global inversion technique that, applied to coronal images, allows determination of the 3D distribution of some of the fundamental parameters of the radiating coronal plasma.

## 2. Tomography of the solar corona

Most of our empirical knowledge on the corona is based on its remote sensing and imaging over a wide range of wavelengths. This will continue to be the case in the era of the Parker Solar Probe (PSP, launched August 2018) and the Solar Orbiter mission (Solo, launched February 2020). Solar corona stereoscopy (Feng et al. 2007) and tomography (Aschwanden 2011; Vásquez 2016) are powerful observational techniques of the corona that allow to infer quantitative 3D information of some of its fundamental plasma parameters, such as the direction of its magnetic field, or the distribution of the electron density and temperature.

### 2.1. White-light tomography

The intense WL radiation of the Sun's photosphere is Thompson scattered by the free electrons of the solar corona, providing a direct diagnostic for its density. The theory, originally developed by Minnaert (1930), allows

determination of the 3D distribution of the coronal electron density from WL images. Based on eclipse images of the corona, the first reconstruction of its electron density structure at a global scale was carried out by van de Hulst (1950), assuming full azimuthal symmetry. Later on, Leblanc et al. (1970) developed the first tomographic reconstruction relaxing that assumption.

Altschuler & Perry (1972) developed the first actual *solar rotational tomography* (SRT), based on time series of WL coronagraph images, relying on the solar rotation to provide different view angles of the solar corona. Frazin (2000) and Frazin & Janzen (2002) developed a robust, regularized, positive method for tomographic inversion from time series of WL images, works in which reviews on WL SRT can be found.

Existing WL tomography studies are based on data provided by both ground and space-borne WL coronagraphs. In the case of space-borne instruments, tomographic reconstructions are so far based on data provided by the Large Angle and Spectrometric Coronagraph instrument on board the SOLar and Heliospheric Observatory (SOHO) mission, and the WL COR coronagraphs on board the Solar TERrestrial RELations Observatory (STEREO) twin-spacecraft mission. These different space-borne instruments provide observations of the corona in the range of heliocentric heights  $r \approx 1.5 - 6.0 R_{\odot}$ . Ground based coronagraphs, such as the High Altitude Observatory (HAO) KCOR instrument, can currently provide observations at lower heights, in the range  $\approx 1.1 - 1.5 R_{\odot}$ .

### 2.2. EUV tomography

Heavy elements present in the million degree solar corona emit in the UV and EUV ranges, providing diagnostics for both electron density and temperature of the solar corona. Frazin et al. (2005) introduced the *differential emission measure tomography* (DEMT) tech-

nique, that uses time series of EUV images to determine the 3D distribution of the *local differential emission measure* (LDEM) in the solar corona. The LDEM is the temperature distribution of the coronal plasma in each tomographic grid cell (or voxel). DEMA was originally implemented by Frazin et al. (2009), and first applied by Vásquez et al. (2009) to study the 3D structure of coronal prominence cavities.

The time series of full-Sun EUV images is used to pose a tomographic inversion problem that can be solved for the 3D distribution of the *filter band emissivity* (FBE). The FBE is the wavelength-integrated coronal spectral emissivity multiplied by the passband of the respective EUV filter. The tomographic FBE found for all bands in each voxel are jointly used as a constraint to infer the LDEM of the voxel. The determination of the LDEM is implemented by modeling it with functions depending on a small number of free parameters and then finding its values to best reproduce the tomographic FBEs. By computing moments of the LDEM in each voxel, global 3D maps of the coronal electron density and temperature are obtained as a final product.

A thorough description of DEMA technique can be found in Frazin et al. (2009) and a recent review in Vásquez (2016). Discussion and calculation on the dominating uncertainty sources and error bars of the tomographic products can be found in Vásquez et al. (2009, 2010, 2011); Nuevo et al. (2015); Lloveras et al. (2017, 2020). Initial applications of DEMA studies involved its use to characterize the thermodynamic state of the global corona at solar minimum (Vásquez et al. 2010, 2011), as well as first efforts of using its results to validate 3D-MHD models (Vásquez et al. 2008; van der Holst et al. 2010; Jin et al. 2012; Evans et al. 2012).

Existing DEMA studies are based on data taken by the Extreme ultraviolet Imaging Telescope (EIT) instrument on board the SOHO mission, the Extreme Ultraviolet Imager (EUVI) instruments on board the STEREO twin spacecrafts, and the Atmospheric Imaging Assembly (AIA) instrument, on board the Solar Dynamics Observatory (SDO) mission. These space-borne instruments provide observations of the corona at heliocentric heights in the range  $r \approx 1.0 - 1.3 R_{\odot}$ .

### 2.3. Static and time-dependent tomography

EUV tomography has been so far applied under the static corona assumption. In this framework, tomographic reconstructions provide a quantitative description of the average state of the solar corona over the data acquisition time, allowing to study regions which exhibit a stable magnetic structure during their observation, such as the diffuse quiet corona, coronal streamers, and coronal holes. Active regions exhibiting fast changes in their structure can not be reconstructed with these techniques. Best suited for solar minimum conditions, tomographic reconstructions allow nonetheless reconstruction of extended regions of the corona even in periods of larger activity of the solar cycle (SC).

Time dependent SRT has been applied to WL data by means of different techniques, such as Kalman filtering (Butala et al., 2010), or spatial-temporal regu-

larization (Vibert et al., 2016). The type of detail and dynamics captured by WL images is quite different to those seen in EUV images. While for WL data time-dependent SRT has been shown to improve the reconstructions to some extent, it is yet not clear what benefits would be obtained in the case of EUV tomography.

### 2.4. Tomography, magnetic models, and coronal heating

Combined with global magnetic models of the solar corona, such as potential field source surface (PFSS) models, DEMA allows statistical study coronal thermodynamic properties in distinct magnetic structures. This approach was first developed and applied by Huang et al. (2012) to study the global coronal thermodynamic structure for a solar minimum between solar cycles (SC) 23/24. They found the core of the equatorial streamer belt to be characterized by the ubiquitous presence of magnetic loops with downward gradients of temperature, dubbed *down loops*. First observed by that work, down loops were theoretically predicted by Serio et al. (1981) and Aschwanden & Schrijver (2002). Down loops can be expected if the heating deposition is strongly confined near the coronal base of a magnetic loop.

Nuevo et al. (2013) studied a sequence of rotations around the solar minimum between SCs 23 and 24. Their study revealed an anti-correlation between the global coronal activity level and the presence of down loops in the corona. They also found down loops to be characterized by plasma  $\beta \gtrsim 1$  (where  $\beta$  is the ratio of thermal to magnetic pressure), which favors Alfvén wave damping and plasma heating at the base of the corona. A recent theoretical study by Schiff & Cranmer (2016) successfully reproduced down and up loops by means of numerical simulations of a 1D steady state model that considers time-averaged heating rates.

Nuevo et al. (2015) extended DEMA to make use of the SDO/AIA instrument, which has a broader temperature sensitivity range, compared to the previous generation of instruments. Their study allowed to determine that the global quiet Sun corona at solar minimum is characterized by two distinct (warm and hot) characteristic temperatures, whose mean values were found to be  $\approx 1.5$  and  $\approx 2.6$  MK, respectively. These results are consistent with independent determinations of the characteristic temperatures of the solar corona based on spectral analysis (Feldman & Landi 2008).

Lloveras et al. (2017) carried out a detailed comparative analysis of the thermodynamic 3D structure of the corona for two solar rotations representative of the solar minima between SCs 22/23 and SCs 23/24. They found the SCs 23/24 minimum to be characterized by smaller values of both electron density and temperature compared to the SCs 22/23 minimum. Their results are consistent with the fact that the last three solar cycles have shown a systematic decrease in activity level, with the SCs 23/24 minimum having shown a much more quiet and extended minimum. Lloveras et al. (2020) recently expanded that study to the current minimum between SCs 24/25, using also the DEMA reconstructions to validate state-of-the-art 3D magnetohydrodynamic (MHD)

simulations developed by Sachdeva et al. (2019) in the context of space weather prediction modeling.

Mac Cormack et al. (2017) computed magnetic loop integrated radiative losses and heat conduction energy flux, to determine the energy input flux  $\Phi$  required at the coronal base of each loop for stability. They found characteristic values in the range  $\Phi \sim 0.5 - 2.0 \times 10^5 \text{ erg sec}^{-1} \text{ cm}^{-2}$ . A large fraction of this energy input, even its totality, could be accounted for by dissipation of Alfvén waves, as recently shown by Hahn & Savin (2014) through spectral analysis of the base of quiet-Sun coronal regions. Mac Cormack et al. (2020) firstly used this novel tomographic product to investigate scaling laws in quiet-Sun coronal loops. This tomographic product can be used for validation of coronal heating models in 3D-MHD simulations of the global corona.

### 3. Current and future developments

#### 3.1. Tomography with the Parker Solar Probe

Coronal tomographic reconstructions have so far relied on solar rotation to provide the different view angles required to pose the inversion problem. The payload of the PSP mission includes the Wide-field Imager (WISPR) WL telescopes (Vourlidas et al., 2016). Its high orbital eccentricity and record approach to the Sun, make PSP the fastest orbiting object around the Sun. The different view angles will thus be provided by the spacecraft orbital motion. Also due to the orbital high eccentricity, the observational sequences of WISPR are geometrically more complicated than those of any previous WL telescope.

Vásquez et al. (2019) investigated the potential use of WISPR data for tomography. Using the PSP orbital information and a 3D-MHD coronal model, WISPR images were synthesized and tomographic reconstructions simulated. As the PSP perihelion progressively decreases, the range of observed heights shifts to smaller values, and the data-gathering lapse shortens. As a result, reconstruction of vast coronal regions will be possible in the second half of the mission's lifetime (2021-2025). By 2025 tomographic reconstruction of about half coronal longitudes will be possible within heights  $r \approx 3 - 10 R_{\odot}$ , with data gathered over just  $\approx 3$  days.

#### 3.2. Multi-instrument tomography

We recently extended our tomographic codes to be applied to visible emission line coronagraph data provided by the Coronal Multichannel Polarimeter (CoMP) at the HAO, and the (soon to be operative) Upgraded CoMP (HAO/UCoMP) instrument (Landi et al., 2016). A new tomographic methodology, dubbed Multi-Instrument Tomography (MIT), is currently being developed by our group. The technique will involve joint analysis of tomographic products based on data provided by multiple wavelength instruments: WL coronagraphs (HAO/KCOR), EUV telescopes (SDO/AIA), and visible emission line coronagraphs (HAO/UCoMP). MIT will allow joint determination the 3D distribution of the coronal electron density and temperature, electron-temperature correlation, and iron abundance.

## 4. Conclusions

Solar corona tomography is a powerful tool that allows determination of the 3D distribution of fundamental plasma parameters of the solar corona at a global scale. Successfully applied to both WL and EUV data to study the thermodynamic structure of the corona, tomography has provided key validation data for 3D-MHD coronal models, such as those oriented to space weather prediction. Current and future instrumentation for observing the solar corona will provide continued opportunity for development and application of tomographic techniques.

*Acknowledgements:* Thanks to the LOC of the XVI LARIM meeting, specially to its chair Dr. Eduardo Unda-Sanzana, for their hard and careful work to make it a success in the midst of very difficult times for Chile. Thanks also to the SOC, specially to its chair Dr. Patricia B. Tissera, for their scientific interest in this work and kind invitation. Thanks to all for their support.

## References

- Altschuler M.D., Perry R.M., 1972, *SoPh*, 23, 410  
 Aschwanden M.J., 2011, *Living Reviews in Solar Physics*, 8, 5  
 Aschwanden M.J., Schrijver C.J., 2002, *ApJ*, 142, 269  
 Butala M.D., et al., 2010, *SoPh*, 262, 495  
 Evans R.M., et al., 2012, *ApJ*, 756, 155  
 Feldman U., Landi E., 2008, *Physics of Plasmas*, 15, 056501  
 Feng L., et al., 2007, *SoPh*, 241, 235  
 Frazin R.A., 2000, *ApJ*, 530, 1026  
 Frazin R.A., Janzen P., 2002, *ApJ*, 570, 408  
 Frazin R.A., Kamalabadi F., Weber M.A., 2005, *ApJ*, 628, 1070  
 Frazin R.A., Vásquez A.M., Kamalabadi F., 2009, *ApJ*, 701, 547  
 Hahn M., Savin D.W., 2014, *ApJ*, 795, 111  
 Huang Z., et al., 2012, *ApJ*, 755, 86  
 Jin M., et al., 2012, *ApJ*, 745, 6  
 Landi E., Habbal S.R., Tomczyk S., 2016, *Journal of Geophysical Research (Space Physics)*, 121, 8237  
 Leblanc Y., Leroy J.L., Poulain P., 1970, *A&A*, 5, 391  
 Lloveras D.G., et al., 2017, *SoPh*, 292, 153  
 Lloveras D.G., et al., 2020, *arXiv e-prints*, arXiv:2004.06815  
 Mac Cormack C., et al., 2017, *ApJ*, 843, 70  
 Mac Cormack C., et al., 2020, *Advances in Space Research*, 65, 1616  
 Minnaert M., 1930, *ZA*, 1, 209  
 Nuevo F.A., et al., 2013, *ApJ*, 773, 9  
 Nuevo F.A., et al., 2015, *ApJ*, 811, 128  
 Sachdeva N., et al., 2019, *ApJ*, 887, 83  
 Schiff A.J., Cranmer S.R., 2016, *ApJ*, 831, 10  
 Serio S., et al., 1981, *ApJ*, 243, 288  
 van de Hulst H.C., 1950, *BAN*, 11, 135  
 van der Holst B., et al., 2010, *ApJ*, 725, 1373  
 Vásquez A.M., 2016, *Advances in Space Research*, 57, 1286  
 Vásquez A.M., Frazin R.A., Kamalabadi F., 2009, *SoPh*, 256, 73  
 Vásquez A.M., Frazin R.A., Manchester IV W.B., 2010, *ApJ*, 715, 1352  
 Vásquez A.M., et al., 2008, *ApJ*, 682, 1328  
 Vásquez A.M., et al., 2011, *SoPh*, 274, 259  
 Vásquez A.M., et al., 2019, *SoPh*, 294, 81  
 Vibert D., et al., 2016, *Astronomy and Computing*, 17, 144  
 Vourlidas A., et al., 2016, *SSRv*, 204, 83

# Chemodynamic structures in dwarf galaxy Leo I

## Chemodynamical tracers for the formation of dSph

A.G. Alarcón Jara<sup>1</sup>, M. Fellhauer<sup>1</sup>, J.D. Simon<sup>2</sup>, A. del Pino<sup>3</sup>

<sup>1</sup> *Universidad de Concepción, Concepción, Chile*

<sup>2</sup> *Observatories of the Carnegie Institution for Science, Pasadena, CA, USA*

<sup>3</sup> *Space Telescope Science Institute, Baltimore, MD, USA*

Contact / alexralarconj@udec.cl

**Abstract** / We present a chemokinematic analysis of the Leo I dwarf spheroidal galaxy using BEACON to find chemo-kinematic patterns among stars of different stellar populations using their metallicity and velocity along the line of sight. We compare our results with the prediction of the dissolving star cluster model.

**Keywords** / galaxies: dwarf — galaxies: kinematics and dynamics — galaxies: Local Group — galaxies: structure

According to the dissolving star cluster scenario proposed by Assmann et al. (2013a,b) and Alarcón Jara et al. (2018), a dSph galaxy is formed by the fusion and dissolution of several star clusters, formed within a dark matter halo. The main prediction of this model is that stars forming in the same star cluster follow similar orbits after dissolution. This motivates us to search for streaming motions or circular orbits of stars with similar chemical compositions in dSph galaxies. For this purpose we use BEACON (del Pino et al., 2017), a code optimized to find groups of stars with similar chemo-kinematic properties in resolved stellar systems. As input for BEACON we need the positions, line-of-sight velocities  $V_{LOS}$ , and metallicities  $[Fe/H]$ .

We apply BEACON to a Leo I data set which contains 943 stars taken from the Keck/DEIMOS instrument by Sohn et al. (2007) and Kirby et al. (2010) and new data acquired with Magellan/IMACS in March 2018. We find 329 stars classified in 13 different rotating stream candidates that share similar metallicities. We calculate the angular momentum and then normalize it by the number of stars in each group, representing the angular momentum per unit of stellar mass. Those 13 different streams show different angular momentum directions (Fig. 1 left panel) distributed randomly inside the galaxy. This result is similar to the angular momentum distribution of the streams that the dissolving star cluster scenario shows in Fig. 1 (right panel).

Our results indicate that the overall structure of dSph galaxies is due to the superposition of different stellar populations with different orbits as it is predicted by the dissolving star cluster model. It is necessary to apply BEACON to other dSphs, in order to search for chemo-dynamical substructures in those systems and obtain a better understanding of the origin of dSphs.

*Acknowledgements:* AA acknowledges funding from Carnegie Observatories through their Carnegie-Chile Fellowship. MF acknowl-

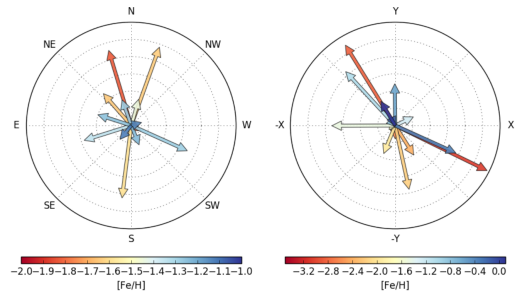


Figure 1: Angular momentum per unit stellar mass: Left panel shows the projected angular momentum of Leo I recovered by BEACON. The right panel shows the angular momentum for a simulation of the dissolving star cluster model with 16 star clusters. Circles have radii from  $0 \text{ pc}^2\text{s}^{-1}$  to  $3 \times 10^3 \text{ pc}^2\text{s}^{-1}$  with steps of  $0.5 \times 10^3 \text{ pc}^2\text{s}^{-1}$  for each concentric circle. There is not net rotation signal, in agreement with the predictions of the dissolving star cluster model.

edges funding through the Concurso Proyectos internacionales de Investigación, Convocatoria 2015 (project code PII20150171), BASAL Centro de Astrofísica y Tecnologías Afines (CATA) AFB-170002 and Fondecyt regular No. 1180291.

## References

- Alarcón Jara A.G., et al., 2018, MNRAS, 473, 5015
- Assmann P., et al., 2013a, MNRAS, 432, 274
- Assmann P., et al., 2013b, MNRAS, 435, 2391
- del Pino A., et al., 2017, MNRAS, 465, 3708
- Kirby E.N., et al., 2010, ApJS, 191, 352
- Sohn S.T., et al., 2007, ApJ, 663, 960

# STARHORSE photo-astrometric distances, extinctions, and astrophysical parameters for *Gaia* DR2 stars

F. Anders<sup>1,2</sup>, A. Khalatyan<sup>2</sup>, C. Chiappini<sup>2</sup>, A.B.A. Queiroz<sup>2</sup>, B.X. Santiago<sup>3</sup>

<sup>1</sup> *Institut de Ciències del Cosmos, Universitat de Barcelona (IEEC-UB), Barcelona, Spain*

<sup>2</sup> *Leibniz-Institut für Astrophysik Potsdam (AIP), Potsdam, Germany*

<sup>3</sup> *Universidade Federal do Rio Grande do Sul, Instituto de Física (IF/UFRGS), Porto Alegre, RS, Brazil*

Contact / fanders@icc.ub.edu

**Abstract** / By combining the precise data delivered by *Gaia* DR2 with the photometric catalogues of PanSTARRS-1, 2MASS, and AllWISE, we recently derived Bayesian stellar parameters, distances, and extinctions for 265 million stars. The results are available to the community through the *Gaia* mirror at [gaia.aip.de](http://gaia.aip.de). We remind the community to pay attention to the flags provided with the data.

*Keywords* / Galaxy: general

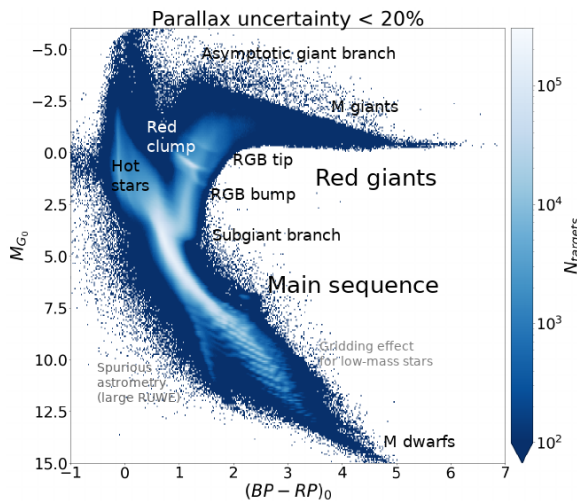


Figure 1: Extinction-corrected colour-magnitude diagram for stars with parallaxes more precise than 20%.

## 1. The *Gaia* DR2 STARHORSE catalogue

In a recent work (Anders et al., 2019), we took advantage of the spectacular astrometric precision achieved by *Gaia*'s second data release (*Gaia* DR2; Gaia Collaboration et al. 2018) and combined these optical data with additional wide-angle photometric catalogues from the optical to the mid-infrared (PanSTARRS-1, 2MASS, and AllWISE). Using the Bayesian tool STARHORSE (Queiroz et al., 2018), we rederived Bayesian distances, extinctions, and stellar parameters for 265 million stars brighter than  $G = 18$  (137 million of which we consider most reliable). We achieved a median precision of 5% in distance, 0.20 mag in  $V$ -band extinction, and 245 K in effective temperature for  $G \leq 14$ , degrading slightly with  $G$ . The results were tested against asteroseismic surface gravities, spectroscopic results from

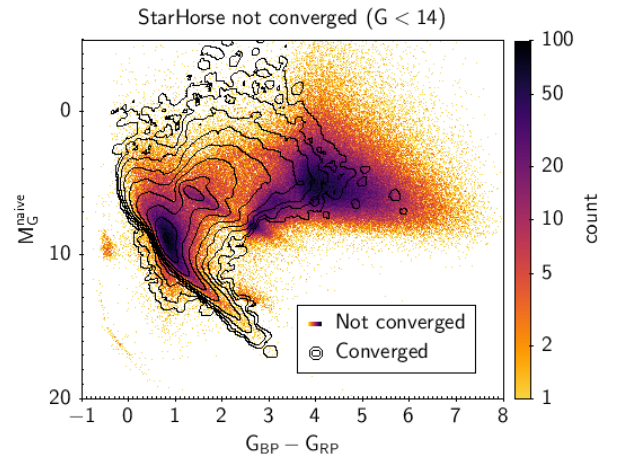


Figure 2: Parallax-corrected *Gaia* DR2 colour-magnitude diagram, highlighting the distribution of stars for which STARHORSE converged (black contours) and for which not (density).

APOGEE, and distances to star clusters. All results are available through the ADQL query interface of the *Gaia* mirror at the Leibniz-Institut für Astrophysik Potsdam ([gaia.aip.de](http://gaia.aip.de)), and as binary tables at [data.aip.de](http://data.aip.de).

Figure 1 shows an example of a well-selected subsample of the STARHORSE dataset, while Fig. 2 highlights the parameter space in which the catalogue is incomplete (e.g. white dwarfs, highly reddened giants, AGB stars). We stress that flagged results (see columns SH\_OUTFLAG, SH\_GAIAFLAG and discussion in Anders et al. 2019) should be used with utmost care.

## References

- Anders F., et al., 2019, A&A, 628, A94
- Gaia Collaboration, et al., 2018, A&A, 616, A1
- Queiroz A.B.A., et al., 2018, MNRAS, 476, 2556

# Characterizing the iron $K\alpha$ line variability in a large sample of AGNs

C. Andonie<sup>1,2</sup>, F. Bauer<sup>1,2</sup>

<sup>1</sup> *Instituto de Astrofísica, Facultad de Física, Pontificia Universidad Católica de Chile, Chile*

<sup>2</sup> *Instituto Milenio de Astrofísica, Santiago, Chile*

Contact / cpandonie@uc.cl

**Abstract** / We present a preliminary study of iron  $K\alpha$  line and continuum variability in AGNs. On hour-to-year scales, the variability of these two emission features are well correlated in some AGNs yet not at all in others, implying distinct morphological/structural distributions of reflecting clouds among local AGNs.

**Keywords** / galaxies: active — galaxies: nuclei — X-rays: galaxies

## 1. Introduction

X-ray emission is a universal characteristic of Active Galactic Nuclei (AGN) which originates within a few Schwarzschild radii, and hence allows us to test physical conditions very close to the central supermassive black hole. Two important features in the X-ray spectra of AGNs are the iron 6.4 keV  $K\alpha$  fluorescence line and the 30 keV Compton hump, due to absorption and Compton scattering of  $> 10$  keV X-rays by 'cold' (neutral) gas, respectively. Both features are thought to arise from the broad line-emitting and torus regions, although recent studies of local AGNs show that at least some narrow iron  $K\alpha$  photons appear spatially extended (on 0.1–1 kpc scales, Wang et al., 2014). On the other hand, a number of studies (Iwasawa et al., 1996; Lamer et al., 2003) have investigated the timing properties of AGNs and found correlations between the primary X-ray continuum and the iron  $K\alpha$  line fluxes, indicating that some fraction of the iron  $K\alpha$  line tracks the continuum variability with lags of tens of days, and hence originates in the innermost part of the accretion disc or the broad line region. The aim of this project is to understand where the Fe  $K\alpha$  arises from, and relate it to the other AGN and host properties.

## 2. Data, results and conclusions

We analysed over 1000 ACIS-I/S *Chandra* observations, many in HETG mode, for more than 100 hard X-ray selected AGNs, of which 32 yielded  $> 5$  reliable measurements. Most of these AGNs are 'local', with  $z < 0.1$ , while a small subsample have  $0.1 < z < 0.3$ . We computed the Fe  $K\alpha$  6.4 keV line ( $F_{6.4\text{keV}}$ ) and 2–10 keV continuum ( $F_{2-10\text{keV}}$ ) fluxes and assessed whether these quantities were correlated in each AGN by fitting a 1st order polynomial:  $F_{6.4\text{keV}} \propto mF_{2-10\text{keV}}$ .

We expect the slope,  $m$ , should lie between 0 (the Fe  $K\alpha$  line flux does not respond quickly to a change in the continuum flux) and 1 (the Fe  $K\alpha$  line flux responds

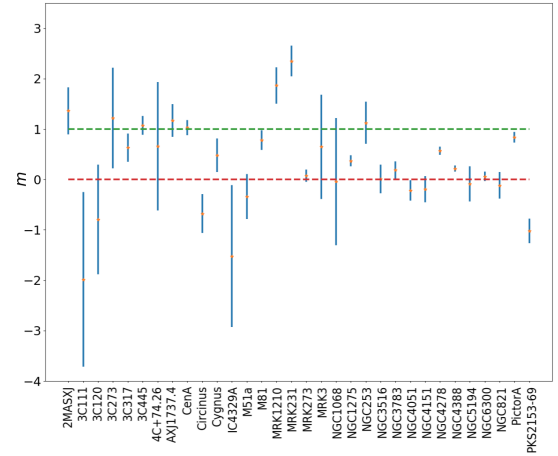


Figure 1: Slopes for 32 AGNs. The green and red lines denote  $m = 1$  and  $m = 0$ , respectively. We observe that 9 slopes are consistent with 1 ( $< 2\sigma$ ), 12 slopes are consistent with 0 ( $< 2\sigma$ ); 2 slopes are intermediate (excluding  $m = 0$  and  $m = 1$  at  $> 2\sigma$ ); and 7 are inconclusive.

quickly to a change in the continuum). The best-fit slopes for the 32 AGNs are shown in Fig. 1. We interpret the variety of slopes to indicate that a constant ( $m = 0$ ) fraction arises from clouds residing further away than the typical continuum variation time scale, such that the variations get washed out by the time delays (e.g. an extended torus or circumnuclear clouds;  $>$  light-months), while a variable portion results from clouds close enough to react to continuum variations in a unified way (e.g. from the broad line region or the inner walls of the torus; light-days to light-months). Fig. 1 thus implies a broad diversity of cloud distributions amongst local AGNs.

## References

- Iwasawa K., et al., 1996, MNRAS, 282, 1038
- Lamer G., et al., 2003, MNRAS, 338, 323
- Wang J., et al., 2014, ApJ, 781, 55

# The formation of ultra-faint dwarf spheroidal galaxies

C.A. Aravena<sup>1</sup>, M. Fellhauer<sup>1</sup>, F. Urrutia Zapata<sup>1</sup>, A.G. Alarcón Jara<sup>1</sup>

<sup>1</sup> *Departamento de Astronomía, Universidad de Concepción, Concepción, Chile*

Contact / cataaravena@udec.cl

**Abstract** / Ultra-faint dwarf spheroidal galaxies, discovered in recent years, are a continuation of the dwarf spheroidal sequence to smaller and fainter objects. These galaxies exhibit similar properties such as old, metal-poor populations, patchy and distorted shapes and high velocity dispersions. They might be amongst the first galaxies in the early Universe and are therefore interesting probes of early structure formation. The standard formation scenarios involve strong destructive processes which finally let to the shape we see today. We propose an alternative formation channel, in continuation to our successful dissolving star cluster model for classical dwarf spheroidals, in which these ultra-faint dwarfs have formed from a turbulent star formation event producing a fractal distribution of stars inside a dark matter halo. We show that our scenario, using Segue 1 as example, is able to reproduce all kinematical and structural features of ultra-faint dwarfs we see today.

*Keywords* / methods: numerical — galaxies: dwarf — galaxies: formation — galaxies: kinematics and dynamics

Ultra-faint dwarf (UFD) spheroidal galaxies are a sub-class of the classical dwarf spheroidals (dSph), with very similar physical properties. They do not contain any gas at the present time and their stars are very iron-poor, with ages  $\gtrsim 10 - 12$  Gyr (Vincenzo et al., 2014). These systems are the most dark matter (DM) dominated systems, do not show recent star formation activity and have a high ( $> 100$ ) mass-to-light ratio. They show different morphologies; most of the dwarfs are elongated, demonstrating that they are not spherically symmetric systems, and probably do not have an isotropic velocity dispersion.

We perform numerical simulations using the Astrophysical Multipurpose Software Environment (AMUSE) to study a star formation scenario for UFDs galaxies, originally proposed by Assmann et al. (2013a,b). For our simulations of Segue 1 we produce a fractal initial distribution of stars from a turbulent gas cloud. The filamentary star formation region is formed by 700 particles in virial equilibrium, with equal masses ( $M_{\star} = 0.5 M_{\odot}$ ). We assume a physical size  $r_{\text{fractal}}$  of the system between 20 to 200 pc. We follow the evolution of the initial fractal distribution within an analytical halo for 5 Gyr.

We conclude that our models are able to reproduce all kinematical and structural properties of UFDs (e.g. patchy structure, ellipticity, effective radius and velocity dispersion, see Fig. 1, bottom panel). It is very clearly visible that our formation scenario produces objects that have the distorted shapes of UFD intrinsically, without the need of and external influence.

Our main result is that using cored haloes, we need fractal distributions of 70–100 pc to reproduce Segue 1 (see Fig. 1, top panel). On the other hand, our results show that large halo scale lengths exhibit stellar distributions still out of the equilibrium after 5 Gyr.

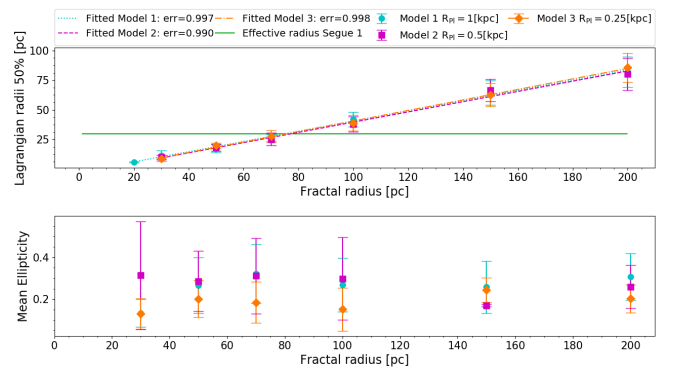


Figure 1: *Top panel:* Half-mass radius against the initial size of the fractal for each Plummer distribution after 5 Gyr of evolution. *Bottom panel:* Mean ellipticity against the initial size of the fractal for each Plummer distribution. Cyan circles, purple squares, and orange diamonds represent models with  $R_{P1} = 1, 0.5,$  and  $0.25$  kpc, respectively.

*Acknowledgements:* CA, FUZ and AAJ acknowledge funding through Fondecyt Regular No. 1180291 and the Chilean BASAL Centro de Excelencia en Astrofísica y Tecnologías Afines (CATA) grant PFB-06/2007. FUZ acknowledges support through CONICYT PAI/INDUSTRIA 79090016. MF acknowledges support through Fondecyt regular 1180291, Basal PFB-06/2007 and PII20150171.

## References

- Assmann P., et al., 2013a, MNRAS, 432, 274  
 Assmann P., et al., 2013b, MNRAS, 435, 2391  
 Vincenzo F., et al., 2014, MNRAS, 441, 2815

# Analytical solutions for radiation-driven winds in massive stars. II: The $\delta$ -slow regime

I. Araya<sup>1</sup>, A. Christen<sup>2</sup>, M. Curé<sup>3</sup>, L. Cidale<sup>4,5</sup>, H. Clavería<sup>2</sup>, R. Venero<sup>4,5</sup>, M. Haucke<sup>4,5</sup>, C. Arcos<sup>3</sup>

<sup>1</sup> *Centro de Investigación DAiTA Lab, Universidad Mayor, Chile*

<sup>2</sup> *Instituto de Estadística, Pontificia Universidad Católica de Valparaíso, Chile*

<sup>3</sup> *Instituto de Física y Astronomía, Facultad de Ciencias, Universidad de Valparaíso, Chile*

<sup>4</sup> *Dpto. de Espectroscopía, Fac. de Cs. Astronómicas y Geofísicas, Univ. Nacional de La Plata, Argentina*

<sup>5</sup> *Instituto de Astrofísica La Plata, CCT La Plata, CONICET-UNLP, La Plata, Argentina*

Contact / ignacio.araya@umayor.cl

**Abstract** / Accurate mass-loss rates and terminal velocities from line-driven winds are important to obtain synthetic spectra from radiative transfer calculations. From a theoretical point of view, analytical expressions for the wind parameters and velocity profile would have many advantages over numerical calculations, that solve the complex non-linear set of hydrodynamic equations. In our previous work, we obtained an analytic description for the fast wind regime. Now, we propose a new analytical expression for the line-force term and obtain a velocity profile closed-form solution for the  $\delta$ -slow regime. Using this analytical expression, we describe a methodology to obtain the mass-loss rates. Moreover, we establish a relation between our line-force term with the known stellar and m-CAK line force parameters. To this purpose, we calculate a grid of numerical hydrodynamical models and perform a multivariate multiple regression. The numerical and analytical descriptions lead to almost the same synthetic spectra.

**Keywords** / hydrodynamics — methods: analytical — stars: early-type — stars: mass-loss — stars: winds, outflows

Müller & Vink (2008, hereafter MV08) proposed a mathematical expression for the radiative line acceleration  $\hat{g}_L(\hat{r})$  as a function of stellar radius  $\hat{r}$ , but it does not fit the  $\delta$ -slow solution (Curé et al., 2011). For this reason, we modify the expression, namely:

$$\hat{g}_L(\hat{r}) = \frac{\hat{g}_0}{\hat{r}^{1+\delta_1}} \left(1 - \frac{1}{\hat{r}^{\delta_2}}\right)^\gamma \quad (1)$$

where  $\hat{g}_0$ ,  $\delta_1$ ,  $\delta_2$  and  $\gamma$  are the fitted parameters. Using the methodology of MV08, it is possible to obtain a dimensionless differential equation of motion for the radial velocity, where the solution of this equation is based on the Lambert  $W$  function. In Araya et al. (2014) a relationship between the MV08 line-force parameters and the stellar and m-CAK line-force parameters was given for fast solutions. To derive a similar relationship, now for the  $\delta$ -slow solutions, we create a grid of m-CAK hydrodynamic models in which the grid points are selected to cover the region of the  $T_{\text{eff}}-\log g$  diagram where the B- and A-type supergiants are located. Then, we develop the relationship applying a multivariate multiple regression (Rencher & Christensen, 2012). Once we know the relationship (estimated model) for the new line acceleration parameters as a function of the stellar and m-CAK line-force parameters, we can obtain the velocity profile of the  $\delta$ -slow wind solution in terms of the Lambert  $W$ -function. Because the velocity profile is not an observable quantity, we use both the analytical and numerical solutions as input of the radiative transfer code FASTWIND (Puls et al., 2005) in

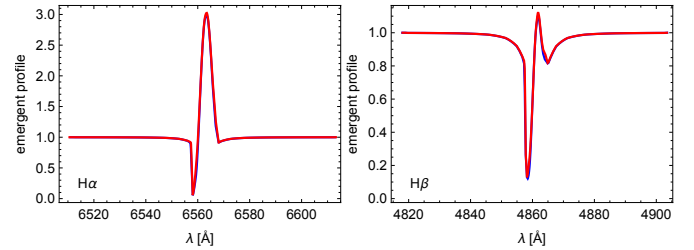


Figure 1: H $\alpha$  and H $\beta$  profiles calculated with FASTWIND. Blue and red lines correspond to the line profiles obtained using the numerical and analytical solutions, respectively.

order to obtain synthetic line profiles and compare them (Fig. 1). The results show an excellent agreement.

**Acknowledgements:** I.A. thanks the support from CONICYT FONDECYT/Iniciación project N° 11190147. C.A thanks to CONICYT FONDECYT/Iniciación project N° 11190945. I.A., M.C. and C.A. are thankful for support from the project CONICYT FONDECYT/Regular project N° 1190485.

## References

- Araya I., Curé M., Cidale L.S., 2014, ApJ, 795, 81  
 Curé M., Cidale L., Granada A., 2011, ApJ, 737, 18  
 Müller P.E., Vink J.S., 2008, A&A, 492, 493  
 Puls J., et al., 2005, A&A, 435, 669  
 Rencher A., Christensen W., 2012, *Methods of Multivariate Analysis*, Wiley Series in Probability and Statistics, Wiley



# A MaNGA-View on how isolated galaxies formed and evolved

M. Argudo-Fernández<sup>1</sup>, M. Boquien<sup>2</sup>, F. Yuan<sup>3</sup>, S. Shen<sup>3</sup>, J. Yin<sup>3</sup>, R. Chang<sup>3</sup>

<sup>1</sup> *Instituto de Física, Pontificia Universidad Católica de Valparaíso, Valparaíso, Chile*

<sup>2</sup> *Centro de Astronomía (CITEVA), Universidad de Antofagasta, Antofagasta, Chile*

<sup>3</sup> *Shanghai Astronomical Observatory, Chinese Academy of Sciences, Shanghai, China*

Contact / maria.argudo@pucv.cl

**Abstract** / Integral Field Spectroscopy (IFS) provides us with a 3-dimensional view of galaxies (one spectral, two spatial) that encodes the processes driving their evolution. MaNGA (Mapping Nearby Galaxies at APO) is an IFS survey designed to investigate an unprecedented sample of 10,000 nearby galaxies. We use MaNGA data to investigate how exactly do galaxies build their disk when they grow in isolation, unaffected by external influences.

*Keywords* / galaxies: general — galaxies: formation — galaxies: evolution

## 1. MaNGA and isolated galaxies

MaNGA (Bundy et al., 2015; Drory et al., 2015; Blanton et al., 2017) is an Integral Field Spectroscopy (IFS) survey which aims to observe 10,000 galaxies in the local universe ( $z < 0.15$ ) by 2020, using the 2.5-meter telescope at the Apache Point Observatory (Gunn et al., 2006) and the BOSS spectrograph (Smee et al., 2013). This legacy dataset will address urgent questions in our understanding of galaxy formation, including the nature of present-day galaxy growth via merging and gas accretion, the processes responsible for terminating star formation in galaxies, the nature of nuclear activity in galaxies, or the broad formation history of galaxy sub-components, including the disk, bulge, and dark matter halo.

However, these processes may be affected by the environment in which galaxies reside. Galaxy evolution is driven by intrinsic and secular processes, but their local and large-scale environments also play an important role. To understand the effects of the environment on galaxy properties it is necessary to have a reference sample where the effects of the environment are minimised and quantified. Isolated galaxies (i.e. galaxies with no physical neighbours within a volume of  $d \leq 1$  Mpc projected radius and a line-of-sight velocity difference  $\Delta v \leq 500$  km s<sup>-1</sup>; Argudo-Fernández et al., 2015), which represent about 11% of the total number of galaxies in the local Universe ( $z \leq 0.08$ ), are unique laboratories to understand the formation and evolution of galaxies.

In this work we focus on spiral, star-forming isolated galaxies, to explore how do galaxies build their disk, and to compare with the prediction of state-of-the-art chemical evolution models (CEMs).

## 2. Exploring the SFH in isolated galaxies

To explore the disk growth of isolated galaxies we require to constraint their star formation history (SFH). We found 176 isolated galaxies observed with MaNGA in the SDSS-DR15 (Aguado et al., 2019). Of them, we focused on 18 almost face-on spirals, without any signs of interaction, with a MaNGA bundle coverage up to  $2.5 R_e$  (with  $R_e$  the effective radius) and where more than 90% of the spaxels are classified as star-forming (from spatially-resolved BPT diagrams obtained using MARVIN, Cherinka et al., 2019).

We use a novel method (under development) based on CIGALE (Code Investigating GALaxy Emission, Boquien et al., 2019) to perform spectral energy distribution fitting and a Bayesian-like analysis on the stacked spectra in each radial bin (created with the MaNGA Data Analysis Pipeline, Westfall et al., 2019), to get the parameters of the SFH such as the age, timescale  $\tau$ , stellar metallicity  $[Z/H]$ , and dust attenuation  $A_V$ .

We find that in general isolated galaxies show gradients in age and  $\tau$  in agreement with the inside-out disk growth, and almost flat gradients in stellar metallicity. It is necessary to further explore these results comparing with gas-phase metallicity gradients and CEMs to understand this general trend.

## References

- Aguado D.S., et al., 2019, ApJS, 240, 23
- Argudo-Fernández M., et al., 2015, A&A, 578, A110
- Blanton M.R., et al., 2017, AJ, 154, 28
- Boquien M., et al., 2019, A&A, 622, A103
- Bundy K., et al., 2015, ApJ, 798, 7
- Cherinka B., et al., 2019, AJ, 158, 74
- Drory N., et al., 2015, AJ, 149, 77
- Gunn J.E., et al., 2006, AJ, 131, 2332
- Smee S.A., et al., 2013, AJ, 146, 32
- Westfall K.B., et al., 2019, AJ, 158, 231

# Helium abundance in horizontal branch stars in M28

D. Barría<sup>1</sup>, C. Moni Bidin<sup>1</sup>

<sup>1</sup> Instituto de Astronomía, Universidad Católica del Norte, Antofagasta, Chile

Contact / daniela.barría@ucn.cl

**Abstract** / We intend here to determine fundamental properties for a sample of blue horizontal branch (HB) stars in the poorly studied bulge globular cluster M28. We analysed 66 low-resolution spectra from FLAMES@VLT collected during 2013. Fundamental stellar parameters and surface helium abundance were obtained fitting hydrogen and helium lines to synthetic spectra. All studied HB stars hotter than Grundhal jump show helium depletion at some level. We found that the helium surface abundance as a function of stellar temperatures follows the tendency observed in HB stars in other globular clusters like M22, NGC 6752, M80, NGC 5986 and  $\omega$  Cen.

**Keywords** / stars: horizontal-branch — stars: atmospheres — stars: abundances — stars: fundamental parameters — globular clusters: individual: NGC 6626 (M28)

## 1. Introduction

M28 (NGC 6626) is a poorly studied globular cluster (GC) located at only 2.7 kpc from the Galactic center. It is a very old ( $\sim 13.5$  Gyr), metal poor ( $[\text{Fe}/\text{H}] = -1.29 \pm 0.01$ ) object (Villanova et al., 2017), and exhibits a blue and extended horizontal branch (HB). As a consequence of gravitational diffusion, blue HB stars show helium-depleted atmospheres (Greenstein, 1967). Diffusion is also responsible for erasing chemical differences between HB stars of different metallicities (Pace et al., 2006). Thus, a similar trend in the helium abundance as a function of stellar temperatures has been found for HB stars in GCs of different metallicities (Salgado et al., 2013; Moni Bidin et al., 2007, 2009, 2012). In this work, we aim to determine fundamental properties and surface helium abundances for a sample of 66 HB stars in M28 and compare these results to other studied GCs.

## 2. Data collection and analysis

HB star candidates were pre-selected from photometric observations of M28 collected from the VVV survey (Minniti et al., 2010). Data were obtained between 2010 and 2011 with the VIRCAM camera in the  $YZJHK_s$  bands and reduced with the VIRCAM pipeline. Spectroscopic data of selected HB stars were collected during 2013 with the ESO multifibre spectrograph FLAMES/GIRAFFE mounted at the VLT-UT2. Typical spectral resolution was  $R \sim 6500$ . Stellar atmospheric parameters such as effective temperature, surface gravity and helium abundance were derived by fitting hydrogen and helium lines to synthetic spectra.

## 3. Results

Fig. 1 shows the measured surface helium abundance of target stars as a function of their temperature. As comparison, the inner plot exhibits the trend found in other five galactic GCs. We found that HB stars in M28 follow

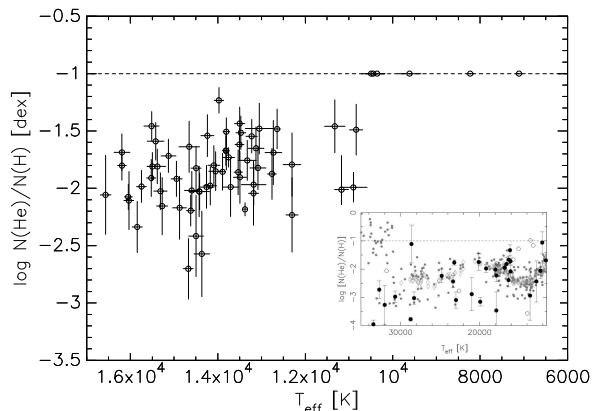


Figure 1: Surface helium abundance vs. effective temperature for HB stars in M28. *Inner plot*: the trend observed in M22 (circles), NGC 6752, M80, NGC 5986 and  $\omega$  Cen (grey dots). Credit: Salgado et al. (2013), reproduced with permission ©ESO.

the tendency observed in other GCs in the 12 000 K to 17 000 K temperature range analysed here. A smooth decrease of helium abundance is observed up to  $T_{\text{eff}} \sim 14 500$  K, where a minimum is found. Beyond that, a slight increase in the helium abundance is identified.

**Acknowledgements:** This work was based on observations collected at the European Southern Observatory under ESO programme 091.D-0535. This work was supported by FONDO COMITE MIXTO ESO-CHILE 2015.

## References

- Greenstein G.S., 1967, Nature, 213, 871
- Minniti D., et al., 2010, NewA, 15, 433
- Moni Bidin C., et al., 2007, A&A, 474, 505
- Moni Bidin C., et al., 2009, A&A, 498, 737
- Moni Bidin C., et al., 2012, A&A, 547, A109
- Pace G., et al., 2006, A&A, 452, 493
- Salgado C., et al., 2013, A&A, 559, A101
- Villanova S., et al., 2017, MNRAS, 464, 2730



# Scaling relations for globular cluster systems in early-type galaxies

J.P. Caso<sup>1,2,3</sup>, B.J. De Bórtoli<sup>1,2,3</sup>, A.I. Ennis<sup>1,2,3</sup>, L.P. Bassino<sup>1,2,3</sup>

<sup>1</sup> *Facultad de Ciencias Astronómicas y Geofísicas de la Universidad Nacional de La Plata, Argentina*

<sup>2</sup> *Instituto de Astrofísica de La Plata (CCT La Plata – CONICET, UNLP), Argentina*

<sup>3</sup> *Consejo Nacional de Investigaciones Científicas y Técnicas, Ciudad Autónoma de Buenos Aires, Argentina*

Contact / jpcaso@fcaglp.unlp.edu.ar

**Abstract** / We studied a sample of globular cluster systems belonging to elliptical galaxies located in different environments. This sample was supplemented with literature results, in order to analyze different parameters derived from the radial profiles in terms of several properties of the host galaxy.

**Keywords** / galaxies: star clusters: general — galaxies: elliptical and lenticular, cD — galaxies: evolution — galaxies: halos

## 1. Introduction and data

It is believed that the mass accretion history of a galaxy has a main role in the build up of its globular cluster system (GCS), favouring the formation and survival of globular clusters (GCs) by different processes (e.g Kruijssen, 2015; Choksi & Gnedin, 2019). Moreover, in the case of massive galaxies a large fraction of their GCs were not formed in situ, but obtained through mergers (Forbes et al., 2011; Caso et al., 2017). In particular, their radial distributions scale with the properties of the galaxies and their halos (Escudero et al., 2015).

We carried on the photometry of HST/ACS images from several elliptical galaxies with intermediate luminosity, obtained from the HST Data Archive. In addition, we used the photometric catalogues of GC candidates from the Virgo and Fornax clusters (Jordán et al., 2009, 2015). We fitted the radial profiles for a sample of 27 GCSs, using a modified Hubble profile. We also compiled the parameters of the radial profiles available in the literature for a sample of GCSs hosted by early-type galaxies.

## 2. Results

In agreement with previous studies (Forbes, 2017; Hudson & Robison, 2018), our results suggest that the parameters of the GCSs radial profiles correlate with several properties of the host galaxy. The exponent of the Hubble profile inversely correlates with both the stellar mass of the galaxy and the number of GCs, with giant ellipticals presenting more flattened GCSs than their less massive counterparts.

Regarding the extension of the GCS as a function of the stellar mass of the galaxy, it was fitted by a bi-linear relation, with a pivot mass of  $\approx 4 \times 10^{10} M_{\odot}$ . It also correlates with the richness of the GCS, but in this case a quadratic function results in an accurate representa-

tion. This is probably due to the non-linear relation between the stellar mass and the number of GCs (Harris et al., 2013). The effective radius of the host galaxy and the extension of the GCS might be correlated, but presenting a large scatter. The central velocity dispersion seems to correlate with the extension of the GCS for central galaxies, but its behaviour is different for satellites, pointing to the relevance of the late evolution of the two groups, probably due to the different mass accretion histories in central and satellite galaxies.

Based on a statistical comparison with the halos from the SMDPL dark-matter simulation, part of the Multidark project Klypin et al. (2016), the effective radius and the extension of the GCS scale with the projected effective radius and the virial radius of the halo, respectively.

## References

- Caso J.P., Bassino L.P., Gómez M., 2017, MNRAS, 470, 3227
- Choksi N., Gnedin O.Y., 2019, MNRAS, 488, 5409
- Escudero C.G., et al., 2015, MNRAS, 0, 0
- Forbes D.A., 2017, MNRAS, 472, L104
- Forbes D.A., et al., 2011, MNRAS, 413, 2943
- Harris W.E., Harris G.L.H., Alessi M., 2013, ApJ, 772, 82
- Hudson M.J., Robison B., 2018, MNRAS, 477, 3869
- Jordán A., et al., 2009, ApJS, 180, 54
- Jordán A., et al., 2015, ApJS, 221, 13
- Klypin A., et al., 2016, MNRAS, 457, 4340
- Kruijssen J.M.D., 2015, MNRAS, 454, 1658



# Kinematic asymmetries in dark matter dominated galaxies

L. Chemin<sup>1</sup>, P. Amram<sup>2</sup>, C. Carignan<sup>3</sup>, C. Balkowski<sup>5</sup>, B. Épinat<sup>2</sup>

<sup>1</sup> *Centro de Astronomía, Universidad de Antofagasta, Chile*

<sup>2</sup> *Laboratoire d'Astrophysique de Marseille, Aix-Marseille Univ., CNRS, UMR 7326, Marseille, France*

<sup>3</sup> *Department of Astronomy, University of Cape Town, South Africa*

<sup>4</sup> *GEPI, Observatoire de Paris, Université PSL, CNRS, Meudon, France*

*Contact* / laurent.chemin@uantof.cl

**Abstract** / We are completing a Fabry-Pérot interferometry survey of the ionized gas in low mass surface density galaxies in order to measure the asymmetric and non-circular gas motions in their velocity fields. The goal of this work is to investigate whether the importance of such motions can impact the mass distribution and the structure of dark matter haloes of low mass disks. We describe here preliminary results of the analysis, reporting motions significantly larger than in previous works.

*Keywords* / galaxies: kinematics and dynamics — dark matter

## 1. Context

The mass profiles of low mass surface density disks (LSDDs) are supposedly dominated by the dark matter (DM) component. Studies of the kinematics of LSDDs have become important over the last  $\sim 25$  years to test the validity of numerical simulations made in the framework of the standard cosmological Cold Dark Matter model. Numerical simulations predict cuspy mass profiles at the centre of haloes. However, this finding has generated a tension with observational data because the rotation curves of LSDDs are observed to be shallow in their inner regions (de Blok, 2010). Among the solutions proposed to explain this cusp-core discrepancy, two of them stand out. On one hand, outflows from strong star-forming events are thought to reshape initial DM cusps into shallower mass profiles (the cusps are destroyed, e.g. Governato et al., 2012). On the other hand, dynamical perturbations and/or physical processes in the gas component are thought to alter significantly the inner kinematics so that rotation curves look artificially shallower than expected (the cusps are hidden in cores, e.g. Oman et al., 2019).

The objective of this project is to test the validity of the second hypothesis. We study the kinematics of samples of nearby LSDDs to search for asymmetric and non-circular motions of gas which are supposed to trace the perturbations, and whose amplitude ( $\lesssim 20 \text{ km s}^{-1}$ ) should explain the difference between the cuspy and the core-dominated inner kinematics.

## 2. Importance of asymmetric and non-circular motions

Until now, the search of asymmetric motions in the ionized gas of LSDDs have been made with fiber-fed integral field spectroscopy (IFS) at resolutions of  $\sim 3''$  and  $\sigma_{\text{inst}} = 15 - 25 \text{ km s}^{-1}$ , which is barely appropriate to

allow the detection of weak asymmetries. Studies based on this technique have naturally failed to detect motions significant enough to alleviate the cusp-core tension (Kuzio de Naray et al., 2006, 2008; Adams et al., 2014).

As of today, we have observed the  $\text{H}\alpha$  kinematics of 30 LSDDs by means of Fabry-Pérot (FP) interferometry at the Canada-France-Hawaii Telescope, ESO/La Silla 3.6m telescope, Observatoire du mont Mégantic 1.6m telescope, and Observatoire de Haute-Provence 1.93m telescope. The high-quality FP data ( $\sim 0.5 - 1.6''$  sampling,  $\sigma_{\text{inst}} \sim 5 - 15 \text{ km s}^{-1}$ ) make it possible to detect important asymmetric gas motions without ambiguity.

As illustrative results, we measure average asymmetric motions of  $21 \text{ km s}^{-1}$  in NGC 2552,  $\sim 13 \text{ km s}^{-1}$  in DDO 64, and  $15 \text{ km s}^{-1}$  in NGC 4395. This is twice larger than previously found in the same galaxies (8, 6 and  $10 \text{ km s}^{-1}$  respectively, Kuzio de Naray et al., 2006, 2008). The difference is explained by the coarser resolution and sampling of IFS data than for FP interferometry. The asymmetries keep that amplitude all throughout the disks, even in the inner regions important for the study of the cusp-core problem. The  $\text{H}\alpha$  velocity fields and random motions of this first sample of 30 LSDDs (Chemin et al., 2020) will allow us to study for the first time the real impact of significant kinematic perturbations on the mass distribution of LSDDs.

## References

- Adams J.J., et al., 2014, ApJ, 789, 63
- Chemin L., et al., 2020, submitted
- de Blok W.J.G., 2010, Advances in Astronomy, 2010, 789293
- Governato F., et al., 2012, MNRAS, 422, 1231
- Kuzio de Naray R., McGaugh S.S., de Blok W.J.G., 2008, ApJ, 676, 920
- Kuzio de Naray R., et al., 2006, ApJS, 165, 461
- Oman K.A., et al., 2019, MNRAS, 482, 821

## Feeding and feedback in local radio galaxies

G.S. Couto<sup>1</sup>, T. Storchi-Bergmann<sup>2</sup>, A. Robinson<sup>3</sup>, R.A. Riffel<sup>4</sup>, P. Kharb<sup>5</sup>, D. Lena<sup>5</sup>, A. Schnorr-Müller<sup>2</sup>

<sup>1</sup> *Centro de Astronomía, Universidad de Antofagasta, Antofagasta, Chile*

<sup>2</sup> *Universidade Federal do Rio Grande do Sul, Porto Alegre, Brazil*

<sup>3</sup> *School of Physics and Astronomy, RIT, Rochester, USA*

<sup>4</sup> *Universidade Federal de Santa Maria, Santa Maria, Brazil*

<sup>5</sup> *Indian Institute of Astrophysics, Bangalore, India*

<sup>6</sup> *SRON Netherlands Institute for Space Research, Utrecht, The Netherlands*

Contact / guilherme.couto@uantof.cl

**Abstract** / We summarize our results using optical integral field spectroscopy (IFS) of four nearby ( $z < 0.07$ ) radio galaxies obtained with the GMOS instrument at Gemini North and South telescopes. The galaxies in our sample present extended radio jets and have in common signatures of interactions or merger events. The presence of more than one kinematic component in the galaxies of our sample indicate that feedback is disturbing the gas in the central regions, and this is usually traced by high velocity dispersions and high line ratios. Although we estimate a low energetic input of the radio jet in the circumnuclear gas, jet–cloud interaction seems to be connected with extended emission-line regions. We also present resolved diagnostic diagrams for these galaxies using the optical emission-lines, and the comparison with shocks and photoionization models, which suggests the presence of shocks in regions closer to the radio jet, but also a contribution from AGN photoionization.

**Keywords** / galaxies: active — galaxies: jets — galaxies: kinematics and dynamics — galaxies: Seyfert

We analyzed optical IFS data on the radio galaxies Arp 102B (Couto et al., 2013), Pictor A (Couto et al., 2016), 3C 33 (Couto et al., 2017) and 4C +29.30 (Couto et al., in prep.) to study jet–gas interactions and inflowing scenarios. We observe high line ratios such as  $[\text{N II}]/\text{H}\alpha$ ,  $[\text{S II}]/\text{H}\alpha$  and  $[\text{O I}]/\text{H}\alpha$  related to shock signatures, such as high velocity dispersions and centroid velocities, indicating outflowing shocked gas, result of the interaction between the radio jet and the circumnuclear gas in these galaxies. One clear example is 3C 33 (Fig. 1, left), where we can observe a region with high velocity dispersion ( $\sigma > 150 \text{ km s}^{-1}$ ) almost perpendicularly to the radio jet orientation (blue line). We conclude that this region in 3C 33 presents outflowing gas in lateral expansion due to the passage of the radio jet.

We observe disturbed kinematics in the sample, with more than one component present. For some galaxies a rotation model does not converge, indicating that rotation is not the dominant component in the gas kinematics. Fig. 1 (right) shows the centroid velocity field of 4C +29.30, displaying a complex pattern. We can observe a blueshifted and a redshifted region in a disturbed morphology. These features present high velocities in the channel maps ( $\sim -600$  and  $\sim 400 \text{ km s}^{-1}$ , respectively), and we interpret them as being part of a bipolar outflow. Indications of inflowing mechanisms are observed in the sample, such as a linear feature in Pictor A resembling a nuclear bar, and nuclear spirals in 3C 33. We interpret that the activity in our sample could be explained by inflowing gas due to galaxy interaction, for which there are signatures for all galaxies

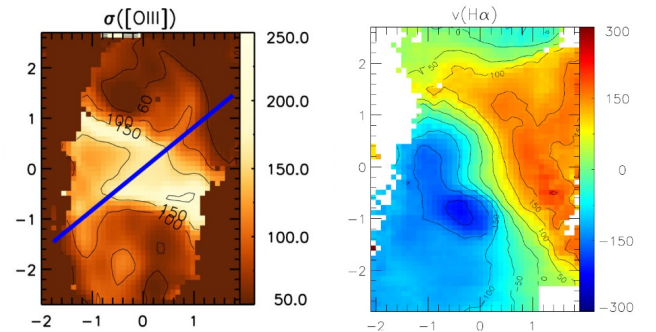


Figure 1: *Left:*  $[\text{O III}]$  velocity dispersion map of 3C 33. *Right:*  $\text{H}\alpha$  centroid velocity map of 4C +29.30. Velocity in  $\text{km s}^{-1}$ ,  $(x, y)$  positions in arcsec. Taken from *Gas rotation, shocks and outflow within the inner 3 kpc of the radio galaxy 3C 33*, Couto et al. (2017), Oxford University Press.

in the sample. The high ionized-gas masses observed ( $0.7 - 4.6 \times 10^8 M_{\odot}$ ) seem to agree with this scenario.

*Acknowledgements:* GC acknowledges the support by the Comité Mixto ESO-Chile and the DGI at University of Antofagasta, and from the Brazilian institutions CNPq and CAPES. Based on observations obtained at the Gemini Observatory.

### References

- Couto G.S., Storchi-Bergmann T., Schnorr-Müller A., 2017, MNRAS, 469, 1573
- Couto G.S., et al., 2013, MNRAS, 435, 2982
- Couto G.S., et al., 2016, MNRAS, 458, 855



# Search, spectral classification and benchmarking of brown dwarfs

M. dal Ponte<sup>1,2</sup>, B. Santiago<sup>1,2</sup>, A. Carnero Rosell<sup>3,2</sup>, B. Burningham<sup>4</sup>

<sup>1</sup> *Instituto de Física, UFRGS, Porto Alegre, RS, Brazil*

<sup>2</sup> *Laboratório Interinstitucional de e-Astronomia - LIneA, Rio de Janeiro, RJ, Brazil*

<sup>3</sup> *Centro de Investigaciones Energéticas, Medioambientales y Tecnológicas (CIEMAT), Madrid, Spain*

<sup>4</sup> *Center for Astrophysics Research, University of Hertfordshire, Hatfield, UK*

Contact / marina.ponte@ufrgs.br

**Abstract** / Here we present our search for brown dwarfs using the Dark Energy Survey (DES). We developed a selection method based on color criteria. We also performed spectral classification using photometry only. We used this sample of brown dwarf candidates and the stellar data from *Gaia* DR2 and DES DR1 to search for wide ( $> 5''$ ) binary systems. We found 255 wide binary pairs composed by a brown dwarf companion to a star and 6 multiple systems containing substellar members. We also found 9 binary systems composed by two brown dwarfs. We estimate the fraction of wide binaries with a brown dwarf secondary in the range 2–4%.

**Keywords** / binaries: general — brown dwarfs — surveys

## 1. Introduction

Brown dwarfs are substellar objects with masses that bridge the gap between H-burning low-mass stars and giant planets. These objects are common in our Galaxy, but due to their very low luminosity currently known samples are still largely restricted to a distance of few tens of parsecs.

## 2. Methodology

We developed a color selection method and applied it to DES (Abbott et al., 2018) to find new L and/or T candidates. We used these data for spectral classification closely following the approach by Skrzypek et al. (2015) and Skrzypek et al. (2016).

For the benchmark systems, our approach was to use our sample of brown dwarfs and search for possible stellar companions using the *Gaia* DR2 and DES DR1 data. We also searched for binary systems made up of two brown dwarfs. For the primary stars, distances were computed using the STARHORSE code (Queiroz et al., 2018). For the L and T dwarfs, distances were computed photometrically.

## 3. Results

The L-dwarf scale height was estimated with the aid of a brown dwarf simulation code, which we call GALMODBD, by comparing the observed and simulated number counts of objects for a grid of models of varying spatial distributions. A scale height of  $h_{z,\text{thin}} \sim 450$  parsecs was found. More details are available in Carnero Rosell et al. (2019).

We discovered 255 wide binary and 6 multiple system candidates composed by L or T dwarfs companions to

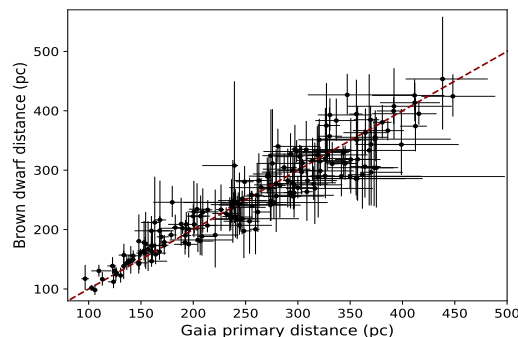


Figure 1: The common distance pair candidates identified using the brown dwarf sample and *Gaia* DR2 primary stars. The error bars correspond to a distance uncertainty of  $2\sigma$ .

stars. These systems are useful to improve brown dwarf evolutionary models, since their chemical composition and age constraints may be taken from the primary star assuming coevality. The pair candidates composed by a brown dwarf companion to a *Gaia* DR2 primary star are shown in Fig. 1. In our search, we also found 9 double brown dwarf systems. More details are available in dal Ponte et al. (in prep).

## References

- Abbott T.M.C., et al., 2018, ApJS, 239, 18
- Carnero Rosell A., et al., 2019, MNRAS, 489, 5301
- Queiroz A.B.A., et al., 2018, MNRAS, 476, 2556
- Skrzypek N., Warren S.J., Faherty J.K., 2016, A&A, 589, A49
- Skrzypek N., et al., 2015, A&A, 574, A78

# A panchromatic study of the stellar populations in NGC 4303

N.Z. Dametto<sup>1</sup>, R. Riffel<sup>2</sup>, L. Colina<sup>3</sup>, R.A. Riffel<sup>4</sup>, M. Boquien<sup>1</sup>

<sup>1</sup> *Centro de Astronomía (CITEVA), Universidad de Antofagasta, Antofagasta, Chile*

<sup>2</sup> *Universidade Federal do Rio Grande do Sul, Porto Alegre, RS, Brazil*

<sup>3</sup> *Centro de Astrobiología (CAB, CSIC-INTA), Madrid, Spain*

<sup>4</sup> *Universidade Federal de Santa Maria, Santa Maria, RS, Brazil*

Contact / natacha.dametto@uantof.cl

**Abstract** / Star formation (SF) tracers in the optical spectral range are considerably well known nowadays and had been used to identify SF in galaxies over the years. The near-infrared (NIR) regime, on the other hand, remains poorly explored, even though this is an important wavelength range which is less affected by dust obscuration than the optical and will be the regime probed by future observational facilities such as JWST, ELT/MOSAIC and GMT/NIRS. Thus, one can use the well-studied visible regime to anchor the simple stellar population (SP) models, determine ages and compare the resulting predictions for the NIR. In this work, the SP synthesis technique was applied from the UV to the NIR using spectra from STIS/*HST* and SINFONI/VLT of the low-luminosity active galactic nuclei NGC 4303.

*Keywords* / galaxies: star formation — infrared: galaxies — galaxies: individual: NGC 4303

We performed a panchromatic SP synthesis of the low-luminosity active galactic nuclei NGC 4303 with four different configurations: using the whole spectra from UV to NIR spectral range normalized in the optical (at  $\lambda_0 = 5510 \text{ \AA}$ , Pan $\lambda_0$ 5510), and near infrared (at  $\lambda_0 = 2.067 \mu\text{m}$ , Pan $\lambda_0$ 20670). Since young (old) stars emit most of their energy output in the UV-optical (NIR) range, an additional analysis was done using only the blue (NIR) part of the spectrum, extrapolating the results to the complete wavelength range.

Preliminary results indicate the need of the three SPs (young:  $t \leq 50 \text{ Myr}$ , intermediate-age:  $50 \text{ Myr} < t \leq 2 \text{ Gyr}$ , and old:  $t > 2 \text{ Gyr}$ ) in the nuclear region of the galaxy to fit the entire wavelength range spectrum, from the UV to the NIR (Pan $\lambda_0$ 5510 and Pan $\lambda_0$ 20670 in Fig. 1). Fitting only the blue part will spread the intermediate-age SP into the other two bins, probably because the stars that populate the intermediate-age bin ( $\sim 1 \text{ Gyr}$ ) emit the majority of their light in the NIR. On the other hand, when fitting only the NIR range, a high contribution of young and reddened stars appears, outshining the contribution of the old SP found in the other three sets. This can be explained by either of two scenarios: one is related to our incapability to properly distinguish between a young reddened stellar population and a dust free old stellar population; the other could be related to the fact that young hot stars in this region are still embedded in the cold gas in which they were born (Calzetti et al., 1994). In this sense, using the NIR, which penetrates deeper into the dust layers, one would be able to access these stellar populations. Moreover, no signature of non-thermal and hot dust components were necessary in order to reproduce the nuclear continuum of this source. From these preliminary tests, the inclusion of the NIR adds valuable information to the

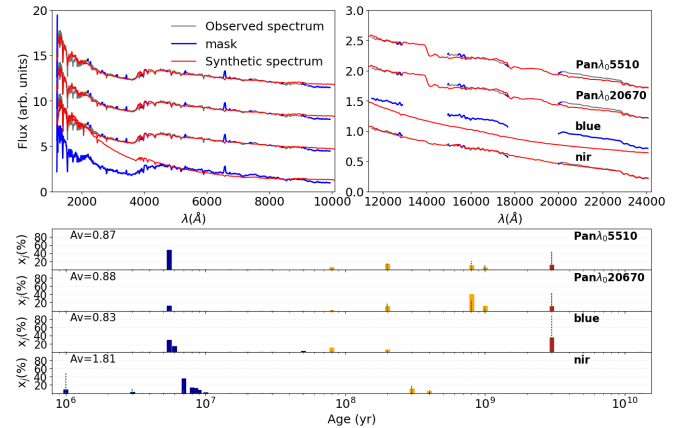


Figure 1: Top: Nuclear synthetic spectrum (in red) overlapping the observed spectrum (in gray). Bottom: Age histograms for each configuration, displaying the flux-weighted ( $x_j$ , colored bars) and mass-weighted (dotted green lines) SP contributions. Blue, orange and red represent young, intermediate-age and old SPs, respectively.

fits, because it penetrates deeper into the dust layers, unveiling obscured sources that would be missed using only the bluer region of the spectrum (UV/optical).

*Acknowledgements:* ND acknowledges the support by the FONDECYT project 3190769, and from the Brazilian institution CNPq.

## References

Calzetti D., Kinney A.L., Storchi-Bergmann T., 1994, *ApJ*, 429, 582



# The role of radiation backgrounds in the direct collapse scenario

V.B. Díaz<sup>1</sup>, D.R.G. Schleicher<sup>1</sup>, S. Bovino<sup>1</sup>, S. Vanaverbeke<sup>2</sup>, R. Riaz<sup>1</sup>, M.Z.C. Vergara<sup>1</sup>

<sup>1</sup> *Departamento de Astronomía, Facultad Ciencias Físicas y Matemáticas, Universidad de Concepción, Chile*

<sup>2</sup> *Centre for mathematical Plasma-Astrophysics, Department of Mathematics, KU Leuven, Heverlee, Belgium*

Contact / [vdiazd@udec.cl](mailto:vdiazd@udec.cl)

**Abstract** / The discovery of massive quasars at very high redshift ( $z > 6$ ) raises a fundamental question about the formation and nature of their seeds in the early Universe. Through the pathways that have been proposed to answer this question, one promising model seems to be the direct collapse scenario. This scenario requires an efficient accretion of the gas onto the central object and also assumes the suppression of fragmentation to form a massive black hole seed early on. Previous works have shown that to achieve these requirements, we need to use a strong radiation background. In this work, we study the role of the radiation during the gravitational collapse in a primordial gas cloud using the code GRADSPH-KROME to explore the chemical conditions and determine the required value of  $J_{21}$  for an atomic collapse. We found that, to keep the gas in an atomic state the value of  $J_{21}$  should be  $\sim 10^5$  which is very high. Also, increasing the rotation of the cloud, it is even higher. Previous work has shown that these high values are difficult to achieve, so the direct collapse scenario could hardly explain the formation of the quasars observed at high redshift.

**Keywords** / black hole physics — cosmology: theory — early Universe — stars: formation — hydrodynamics

Numerous quasars at very high redshift had been discovered through many surveys in the last years (Bañados et al., 2018; Schleicher, 2019) and different pathways have been proposed to explain their formation in the early Universe. The direct collapse scenario (Loeb & Rasio, 1994) seems the most plausible way to assemble a supermassive black hole (SMBH) because it provides the most massive black hole seeds, which then can grow due to moderate accretion rates to form SMBHs (Latif et al., 2013). To create these massive seeds, a strong radiation background is necessary to suppress  $H_2$  cooling, the main cooling mechanism in the early universe (Bromm & Loeb, 2003). The flux is measured in units of  $J_{21}$ , where  $J_{21} = 1$  corresponds to a flux of  $10^{-21}$  erg cm<sup>-2</sup> s<sup>-1</sup> Hz<sup>-1</sup> sr<sup>-1</sup> at the Lyman limit.

To study the impact of the radiation field in a primordial gas cloud, we modeled a spherical and turbulent gas cloud in solid body rotation using the coupling of the smoothed particle hydrodynamics code GRADSPH (Vanaverbeke et al., 2009) with the chemistry package KROME (Grassi et al., 2014).

We varied the values of  $J_{21}$  from  $10^2$  to  $10^5$ , and the rotation factor  $\beta$  (ratio of rotational to gravitational energy) from 3% to 10%. Using  $\beta = 3\%$  and the weaker values of  $J_{21}$  we found that at higher densities the temperature decreases rapidly due to the  $H_2$  formation producing cooling, then the temperature becomes quite constant because the  $H_2$  cooling rate becomes less efficient at higher densities. For  $J_{21} = 10^4$ , it takes longer for  $H_2$  to build up compared to the latter case, and also, we start to appreciate the presence of two gas phases (cold and hot phase) at the same density. For  $J_{21} = 10^5$ , most of the gas is in a hot phase keeping the

gas atomic because the high radiation dissociates the  $H_2$  according to theoretical expectation. With these results, we found that the value of  $J_{21}^{\text{crit}}$ , i.e. the minimum value of  $J_{21}$  required for keeping the gas atomic during collapse, is in the range of  $10^4 - 10^5$ , which is very high, and such high values rarely occur (Dijkstra et al., 2014). Furthermore, if we start to increase the rotation factor, we see that it is harder to destroy  $H_2$ ; therefore, more radiation is needed to destroy it. We conclude that black hole formation via direct collapse is efficiently suppressed and could hardly explain the formation of the first SMBHs.

*Acknowledgements:* VBD thanks Conicyt for financial support (CONICYT-PFCHA/MagisterNacional/2017-22171293 and CONICYT PIA ACT172033).

## References

- Bañados E., et al., 2018, *Nature*, 553, 473
- Bromm V., Loeb A., 2003, *ApJ*, 596, 34
- Dijkstra M., Ferrara A., Mesinger A., 2014, *MNRAS*, 442, 2036
- Grassi T., et al., 2014, *MNRAS*, 439, 2386
- Latif M.A., et al., 2013, *MNRAS*, 436, 2989
- Loeb A., Rasio F.A., 1994, *ApJ*, 432, 52
- Schleicher D.R.G., 2019, M. Latif, D. Schleicher (Eds.), *Formation of the First Black Holes*, 223–239, World Scientific
- Vanaverbeke S., et al., 2009, *Comput. Phys. Commun.*, 180, 1164



# Neutron escape from microquasar jets

G.J. Escobar<sup>1</sup>, L.J. Pellizza<sup>1</sup>, G.E. Romero<sup>1</sup>

<sup>1</sup> *Instituto Argentino de Radioastronomía, CONICET-CICPBA, Argentina*

Contact / gescobar@iar.unlp.edu.ar

**Abstract** / The launching mechanism and composition of astrophysical jets are still open problems. If relativistic protons are present in these jets, then energetic neutrons should be produced. Since neutrons are not affected by magnetic fields, they should escape the jet and decay outside. In this work we introduce the relativistic neutron component in the model of a microquasar jet. We find that observable signatures are too weak for current instruments, but a steady escape of secondary charged particles from the decay region might contribute to the population of Galactic cosmic rays.

*Keywords* / stars: jets — relativistic processes

## 1. Introduction

Astrophysical jets are collimated flows of matter and radiation. They are present in several astrophysical sources such as active galactic nuclei, microquasars (MQs), and gamma-ray bursts. The launching mechanism and composition of these jets are still not well understood. One approach to study the composition of these systems consists in modelling the spectral energy distribution that different particle populations in the jet would produce. Previous works (e.g., Pepe et al., 2015) usually include mainly relativistic protons and electrons. Neutrons, however, would be produced by the interaction of energetic protons with ambient ones. The dynamics of this component is different from that of charged particles, because neutrons do not interact with the magnetic field that collimates the flow. Therefore, they may escape freely, decaying outside the jet, and possibly giving rise to a rich phenomenology. In this work, we introduce the neutron component in MQ jet models, and explore the observable consequences.

## 2. General scheme

Our jet model is based on that of Romero & Vila (2008). We consider a lepto-hadronic model in which relativistic protons and electrons of energy  $E_i$  are injected in the jet at a rate  $Q_i(E_i) \propto E_i^{-\alpha} \exp(-E_i/E_{\max,i})$ , for  $i = e, p$ , with maximum energy  $E_{\max,i}$  and spectral index  $\alpha$ . The fraction of the jet kinetic power in relativistic particles is 10%, most of which is carried by protons. Protons radiate via synchrotron and pion decay from proton-proton collisions. Relativistic neutrons are introduced through the interaction channel  $p+p \rightarrow p+n+\pi^+(\dots)$ . Charged-particle populations may evolve also through escape and advection, whereas neutrons may escape and decay. The steady spectral density for the three species is obtained by solving the system of three coupled transport equations, as described in Escobar et al. (2018).

Almost all neutrons escape from the jet. These

free neutrons inject energetic particles in the interstellar medium (ISM) through beta decay, following an exponential law in distance from the source. We study the propagation and emission of these particles considering synchrotron radiation of electrons, proton-proton inelastic collisions with the ambient medium, as well as diffusion and thermalization by coupling with matter and waves in the ISM.

## 3. Results and conclusions

We apply the model to a typical microquasar system (Cygnus X-1, e.g., Pepe et al., 2015). Neutrons carry only about  $10^{-7}$  of the power of the jet, and decay at typical distances of  $10^{16} - 10^{17}$  cm, far from the source (whose typical size is  $\sim 10^{12} - 10^{13}$  cm). As the jet bulk velocity is non-relativistic (Lorentz factor  $\Gamma \sim 1.25$ ), we consider the neutron flux to be spherically symmetric. Because of the low ISM magnetic field ( $\sim 10^{-5}$  G), the synchrotron spectrum of secondary electrons peaks at a much lower energy than that of the jet. However, even at low energies the jet flux is still higher, and secondary-electron emission would not be observable. The main energy-loss mechanism of secondary protons is elastic Coulomb scattering, producing no radiation.

Both secondary protons and electrons travel long distances before cooling. Therefore, they would escape from the system with some fraction of their initial energy, and propagate through the interstellar medium. This result suggests that microquasars may be cosmic-ray sources (cf. Heinz & Sunyaev, 2002). Future work will focus on the main features of this cosmic-ray population, and its impact on the surrounding medium.

## References

- Escobar G.J., et al., 2018, BAAA, 60, 95
- Heinz S., Sunyaev R., 2002, A&A, 390, 751
- Pepe C., Vila G.S., Romero G.E., 2015, A&A, 584, A95
- Romero G.E., Vila G.S., 2008, A&A, 485, 623



## Formation scenarios of dSph galaxies

M. Fellhauer<sup>1</sup>, A.G. Alarcon Jara<sup>1</sup>, C. Aravena<sup>1</sup>, F. Urrutia Zapata<sup>1</sup>, D.R. Matus Carrillo<sup>1</sup>, M.C.B. Morales Inostroza<sup>1</sup>

<sup>1</sup> *Departamento de Astronomía, Universidad de Concepción, Chile*

*Contact / mfellhauer@astro-udec.cl*

**Abstract** / In this short review we show the different formation scenarios for dwarf spheroidal galaxies (dSphs) and focus on the two scenarios we are investigating at the Theory Group in Concepción. We have established the dissolving star cluster scenario, in which the dSph galaxies form in situ as they are now, using star forming events inside the central area of a dark matter (DM) halo, and furthermore, the dwarf galaxy in dissolution scenario in which we explain the structural and dynamical properties of dSph galaxies without the need of DM.

*Keywords* / methods: numerical — galaxies: formation — galaxies: dwarf

Dwarf spheroidal galaxies (dSphs) are the smallest galaxies known and most likely the most numerous type of galaxies. Many dozens of them are found around the Milky Way (MW) and Andromeda with perhaps several hundreds of them still to be detected. As galaxy formation is hierarchical these galaxies are probably the basic building blocks, i.e. the first galaxies which have formed. Within the standard cosmology scenario, they are furthermore believed to be the most dark matter (DM) dominated objects known.

There are three main pathways of their formation and evolution discussed in the literature. The most accepted scenario finds the dSph galaxies at the endpoint of a destructive evolution, but still well embedded in DM haloes. In this scenario the building blocks are dwarf disc galaxies, which get destroyed by ram pressure—which removes the gas—, galactic tides or resonant stripping. These processes are able to transform a system with ordered rotation into a pressure supported object like the dSphs we see today. Meanwhile the nature of the stellar component changes dramatically, the DM halo staying more or less intact in this scenario.

We propose a different scenario (dissolving star cluster scenario; DSCS) in which the dSph galaxies form as we see them now. The gas in the central region of a small DM halo forms stars in the form of small star clusters and associations. These objects orbit the central region of the DM halo and slowly dissolve, spreading their stars in the inner region and building up the luminous component of the galaxy.

Finally, there is a third scenario. Here again dSph galaxies are at the endpoint of a destructive process happening while they orbit a major galaxy like the MW. Here, they start out as pressure supported systems, with or without DM, and get destroyed by the tidal forces of the host galaxy. To explain the high velocity dispersions measured in dSph galaxies, the fact which gives rise to the claim that they are the most DM dominated objects known, the remnants have to be close to the apocentre

of their orbits and the measurement of the dispersion gets completely falsified by unbound stars around the remnant.

Our group is successfully working in the latter two scenarios and is able to reproduce with our simulations all kinematical and structural features of dSph galaxies. The DSCS was introduced in 2013. The results of our simulations show high velocity dispersions, twisted contours, colder central areas, off-centre nuclei or multiple density peaks very similar to the observed dSph galaxies. Meanwhile our models account for the variety of star formation histories seen in dSph galaxies. Furthermore we have extended our models into the realm of faint and ultra-faint dSph galaxies. Our models predict streaming motions which should be still detectable in these objects. Analysing the best observational data with a new tool does indeed reveal these streaming motions in dSph galaxies. If the first scenario is true we would expect to measure the remnants of the ordered rotation; in our scenario, the angular momentum of the streaming motions can point in any direction. Indeed the latter is the case.

In the third scenario we have so far successfully reproduced the shape and kinematics of Bootes, Ursa Major II, Canes Venatici I, Segue 1 and Coma Berenice, showing that no matter which dSph galaxy we try, there is always a DM free solution possible.

*Acknowledgements:* MF acknowledges financial support for him and his students from Fondecyt regular No. 1180291, Basal (CATA) AFB-170002 and Quimal 170001.

# Deuteration chemistry in massive star-forming regions

S. Ferrada-Chamorro<sup>1</sup>, S. Bovino<sup>1</sup>, A. Lupi<sup>2</sup>, D.R.G. Schleicher<sup>1</sup>

<sup>1</sup> *Departamento de Astronomía, Universidad de Concepción, Concepción, Chile*

<sup>2</sup> *Scuola Normale Superiore, Pisa, Italy*

Contact / [siferrada@udec.cl](mailto:siferrada@udec.cl)

**Abstract** / We present here the results of 3D magneto-hydrodynamical (MHD) simulations of collapsing massive clumps in conjunction with a state-of-the-art chemical network, including time-dependent freeze-out processes, to follow the evolution of depletion and deuteration of molecules of interest. We find both processes to be very efficient, and deuteration values close to previous results which followed a full depletion approach.

**Keywords** / astrochemistry — methods: numerical — stars: formation — stars: massive

Deuterium fractionation (or deuteration), i.e. the ratio of deuterated to non-deuterated species, has been proposed to be an appropriate chemical clock (Fontani et al., 2011), which can help to assess the time scales of key phases of high-mass star formation. Deuteration is heavily linked to the degree of freeze-out of heavy molecules, as its main driver, the  $\text{H}_3^+$  and  $\text{H}_2\text{D}^+$  ions, easily react with other molecules, CO in particular. Previous works followed a full-depletion approach for the chemistry, but this can be improved and expanded upon adding time-dependent depletion processes. Here we aim to see how efficient depletion is when treated consistently and how it affects the degree of deuteration when changing the initial conditions. We employ the MHD code GIZMO (Hopkins, 2015) coupled with KROME (Grassi et al., 2014) using an updated chemical network, simulating the collapse of massive star-forming clumps.

Results are shown on Fig. 1, where the different realizations followed different parameters: initial  $\text{H}_2$  ortho-to-para ratio (OPR), cosmic-ray ionization rate (CRIR), and grain-size ( $\langle a \rangle$ ). The comparison between different runs is done with our fiducial conditions as a reference (CRIR =  $2.5 \times 10^{-17} \text{ s}^{-1}$ , OPR = 3.0, and  $\langle a \rangle = 0.035 \mu\text{m}$ ). We have found high levels of CO depletion in all runs, and a consecutive fast increase of deuteration levels, with  $\text{H}_3^+$  deuteration values in good agreement with previous results reported by Körtgen et al. (2017).  $\text{N}_2$  depletion, on the other hand, is seen to be less efficient, due to its formation channel involving slow neutral-neutral reactions. These results help support the idea that a high level of deuteration can be built up over a very short time, as long as depletion is treated consistently. Despite this, degeneracy on the results due to uncertainties on the initial conditions should be kept into account and further explored (Bovino et al., 2019).

*Acknowledgements:* SFC thanks funding from CONICYT Programa de Astronomía Fondo ALMA-CONICYT 2017 Project #31170002 and the SNS, where part of this work was pursued. SB is financially supported by CONICYT Fondecyt Iniciación

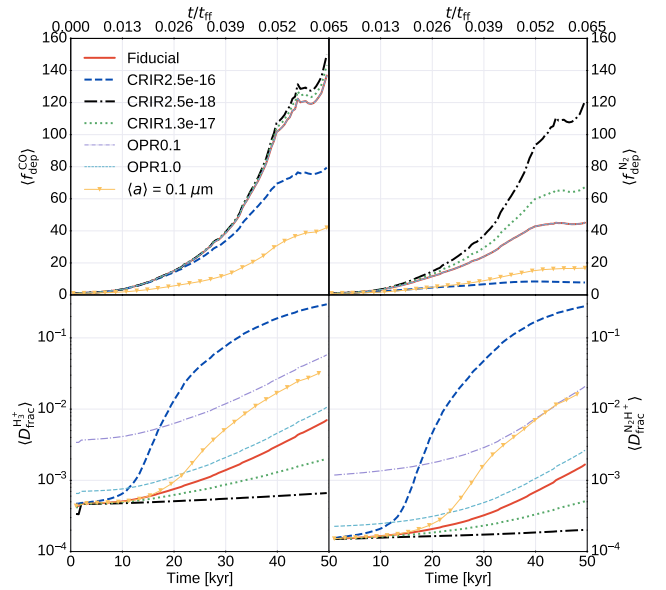


Figure 1: Time evolution of the column density-weighted average for the CO and  $\text{N}_2$  depletion factor,  $\langle f_{\text{dep}}^{\text{CO}} \rangle$  and  $\langle f_{\text{dep}}^{\text{N}_2} \rangle$ , respectively, and  $\text{H}_3^+$  and  $\text{N}_2\text{H}^+$  deuterium fractionation. Adapted from *The 3D structure of CO depletion in high-mass prestellar regions*, Bovino et al. (2019), doi:10.3847/1538-4357/ab53e4, ©AAS. Reproduced with permission.

(project 11170268), CONICYT programa de Astronomía Fondo Quimal 2017 QUIMAL170001, and BASAL Centro de Astrofísica y Tecnologías Afines (CATA) AFB-17002.

## References

- Bovino S., et al., 2019, ApJ, 887, 224
- Fontani F., et al., 2011, A&A, 529, L7
- Grassi T., et al., 2014, MNRAS, 2419, 2386
- Hopkins P.F., 2015, MNRAS, 000
- Körtgen B., et al., 2017, MNRAS, 2625, 2602

# Comparative study of activity of the near-parabolic orbit comet C/1977 R1 (Kohler)

L.F. de Araújo<sup>1</sup>, A.A. de Almeida<sup>1</sup>, G.C. Sanzovo<sup>2</sup>

<sup>1</sup> Instituto de Astronomia, Geofísica e Ciências Atmosféricas, USP, São Paulo, Brasil

<sup>2</sup> Departamento de Física, UEL, Paraná, Brasil

Contact / loreanyfa@usp.br

**Abstract** / Kohler is considered a case of young, nearly parabolic comet. In this work we deduce, semi-empirically, water and hydroxyl production rates from the photometric observations of this comet taken from the Archive of Photometric Data on Comets and British Astronomical Society archives. Our results are being compared with those obtained from radio observations at 18 cm, and with observations of water production in a sample of several recent comets observed by the SWAN all-sky camera on the *SOHO* spacecraft.

**Keywords** / comets: individual: Kohler — comets: general — astrochemistry

## 1. Introduction

Comets are the most primitive members of the Solar System. Their composition has a variety of information about their origin and evolution, as well as the origin and evolution of the Solar System itself. Hence, they are generally referred to as cosmic fossils. The knowledge of cometary properties is necessary in order to establish a complete description of the physical chemical evolution along their orbits.

In this work, we study the comportment of the comet Kohler and make comparisons to understand the behavior of comets of different taxonomic classes.

## 2. Theoretical considerations and results

Being the main topic of this work, the water production rate is calculated from the ratio obtained through the semi-empirical method of visual magnitudes given by De Almeida et al. (1997). We know that 0.85% of water result in the daughter molecule, hydroxyl (OH). Therefore, we take this as our key component.

In Fig. 1 we can see that the production rates found by Crovisier et al. (1981) and Despois et al. (1981), from observations made in radio ( $\lambda = 18$  cm), agree well with the visual observations in the range shown. The power laws of the pre- and post-perihelic phases of the comet are  $r^{5.48}$  and  $r^{-5.62}$ , respectively. Through the analyses of the active area of the comet, we estimate the effective radius of the comet to be close to 3 km, with an active fraction of 11% and minimum radius of 0.98 km.

Making comparisons with other comets observed with the SWAN all-sky camera on the *SOHO* spacecraft and arranged in (Combi et al., 2019), we start to see the flat power law of comets from the Oort Cloud. Comet Kohler is considerably steeper, characteristic of long period comets.

To continue this work, we will increase the sample of

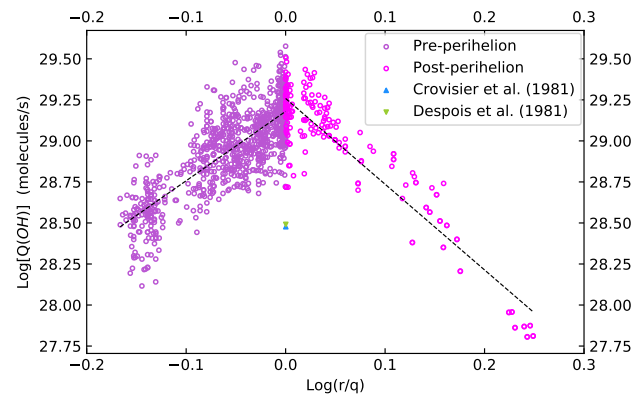


Figure 1: Correlation between hydroxyl production rate  $Q(\text{OH})$  and heliocentric and perihelic distance ratio  $r/q$  for visual and radio observations.

comets to work on, study the behavior of the power law with respect to the 3 taxonomic classes and relate the rate of hydroxyl production to that of other chemical components present in the Kohler comet spectrum.

*Acknowledgements:* To my advisor and CAPES, Brazil, for the master's scholarship.

## References

- Combi M., et al., 2019, *Icarus*, 317, 610
- Crovisier J., et al., 1981, *A&A*, 97, 195
- De Almeida A., Singh P., Huebner W., 1997, *Planet. Space Sci.*, 45, 681
- Despois D., et al., 1981, *A&A*, 99, 320

# Kepler photometry and spectroscopic observations of the $\delta$ Scuti / $\gamma$ Doradus hybrid candidate star KIC 4920125

L. Fox-Machado<sup>1</sup>, J. Higuera<sup>1</sup>

<sup>1</sup> *Instituto de Astronomía, Universidad Nacional Autónoma de México*

Contact / lfox@astro.unam.mx

**Abstract** / We present a preliminary report on the ground-based spectroscopic observations and *Kepler* photometry of KIC 4920125 —a  $\delta$  Scuti /  $\gamma$  Doradus hybrid candidate. The radial velocity analysis suggests that KIC 4920125 is a single-lined spectroscopic binary with an orbital period of 50 days. A Fourier analysis of *Kepler* light curves was performed.

**Keywords** / stars: oscillations — stars: variables: Scuti — stars: variables:  $\gamma$  Doradus

## 1. Introduction

The *Kepler* high-precision photometry has revealed a large number of hybrid candidate stars in which  $\delta$  Scuti ( $\delta$  Sct) and  $\gamma$  Doradus ( $\gamma$  Dor) type pulsations are present, and that occupy the entire region between the blue edge of the  $\delta$  Sct instability strip and the red edge of the  $\gamma$  Dor instability strip and beyond (Uytterhoeven et al., 2011). As we know, the  $\delta$  Sct stars pulsate in low radial order  $p$ - and mixed  $p$ - $g$  modes with periods in the 0.01–0.3 d range, driven by the  $\kappa$  mechanism operating in the He II ionization zone. On the other hand, the  $\gamma$  Dor stars pulsate in high-order  $g$ -modes with periods in the 0.3–3.0 d range driven by the convective blocking at the base of their envelope convection zone. A number of outstanding questions on the structure, evolution and excitation pulsation mechanism in A–F stars are expected to be answered by studying such hybrid candidate stars. KIC 4920125 (= BD+42 3370, GSC 03143-00305), with a *Kepler* magnitude of 11.1 mag, was identified as a hybrid candidate by Uytterhoeven et al. (2011).

## 2. Observations, analysis and discussion

We obtained 15 optical spectra of KIC 4920125 over three seasons in June 2017, July 2018 and August 2019 using the Echelle spectrograph attached to the 2.12 m telescope of the San Pedro Mártir Observatory in Mexico, covering a wavelength range of 3800–7300 Å with a resolution of  $R = 18000$  at 5000 Å. The radial velocities were measured with the IRAF task `fxcor`, by cross-correlating the spectra against spectra of radial-velocity standard stars acquired with the same setup and in the same night. The atmospheric parameters of the star were computed with the `iSPEC` code (Blanco-Cuaresma et al., 2014). A preliminary fit to radial velocity data gives  $P = 50.4$  d,  $\gamma = -18.2$  km s<sup>-1</sup> and  $K_1 = 4.2$  km s<sup>-1</sup>.

A Fourier analysis of the all available *Kepler* data

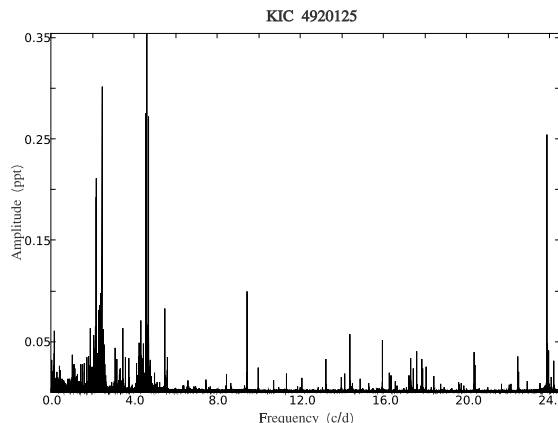


Figure 1: Amplitude spectrum of KIC 4920125.

was performed using the PERIOD04 package (Lenz & Breger, 2005). The raw time series data which include 65183 data points from quarters 0 to 17 (Q0 - Q17) with 30 min exposures have been processed as explained in Baran et al. (2011). The full amplitude spectrum out to the Nyquist frequency for KIC 4920125 is shown in Fig. 1. A detailed analysis of these observations will be given elsewhere.

*Acknowledgements:* This work received financial support from the DGAPA-UNAM grant PAPIIT IN100918.

## References

- Baran A.S., et al., 2011, *AcA*, 61, 325
- Blanco-Cuaresma S., et al., 2014, *A&A*, 569, A111
- Lenz P., Breger M., 2005, *Communications in Asteroseismology*, 146, 53
- Uytterhoeven K., et al., 2011, *A&A*, 534, A125



# Orbital light-curve changes in DPVs related with the long cycle

J. Garcés<sup>1</sup>, R.E. Mennickent<sup>1</sup>, G. Djurašević<sup>2,3</sup>

<sup>1</sup> *Universidad de Concepción, Departamento de Astronomía, Casilla160-C, Concepción, Chile*

<sup>2</sup> *Astronomical Observatory, Belgrade, Serbia*

<sup>3</sup> *Isaac Newton Institute of Chile, Yugoslavia Branch, Belgrade, Serbia*

Contact / juangarcés@udec.cl

**Abstract** / We present the case of two binaries that show cyclic changes in the morphology of their orbital light curves. These would be key to test the recently proposed magnetic dynamo theory for semi-detached Algol binaries that show a long photometric cycle.

**Keywords** / binaries: eclipsing — stars: close binaries

## 1. Introduction

Double Periodic Variables (DPVs) show a long photometric cycle that is in average 33 times the orbital period (Mennickent et al., 2003). They consist of a giant star (secondary), which has filled its Roche lobe, and which is in the phase of mass transfer to the hot B-dwarf star (primary) surrounded by an accretion disc (Mennickent et al., 2016a). In the case of the DPV V393 Sco, emission lines of chromospheric activity (Mg II and C I) from the secondary component have been found, in addition to variable high-altitude bipolar jets (Mennickent et al., 2012). Other case, HD 170582, shows changes of H $\alpha$  and H $\beta$  emissions during the long cycle. Doppler tomography reveals that the hot-spot is brighter during the minimum of the long cycle, product of variations in the mass transfer rate (Mennickent et al., 2016). This could be explained by the presence of a magnetic dynamo acting on the secondary star, which would produce changes in its equatorial radius (Applegate, 1992), modulating cyclically the mass transfer rate as indicated by the dynamo theory for DPVs (Schleicher & Mennickent, 2017). Also, this phenomenon could explain the recent changes in the orbital light curves that have been found in some DPVs and that we report here.

## 2. Orbital light-curve changes

The most surprising case is that of OGLE-LMC-DPV-097. It has an orbital period of 7<sup>d</sup>751749 and a long sinusoidal cycle of 302 d (Poleski et al., 2010). During the maximum stage of the long cycle, a light curve with an evident primary and secondary eclipse is observed. During the minimum stage, the secondary minimum disappears. These changes were analyzed for the first time, using a theoretical light curve model (Djurašević, 1992a,b) that includes an accretion disc with active areas such as a bright/hot spot (Djurašević et al., 2010). These indicate that the accretion disc would be colder

and extended during the maximum of the long cycle and smaller and hotter during the minimum, explaining the disappearance of the secondary minimum (Garcés L. et al., 2018).

Another case is OGLE-BLG-ECL-157529. It shows an orbital period of 24<sup>d</sup>799 and a variable long period that decreases from 880 to 750 d. During the maximum stage of the long cycle, the primary minimum reaches its greatest depth, while the secondary minimum becomes less deep. An opposite case is shown in the minimum stage. The theoretical models show a thinner accretion disc in the maximum and thicker in the minimum stage, hiding the primary star (brighter) and producing the reversal of the primary minimum observed at some observation epochs (Mennickent et al., 2020).

Both objects might be crucial to understand the DPV phenomenon and to test the theory of the magnetic dynamo.

*Acknowledgements:* JG and REM acknowledge support by VRID-Enlace 216.016.002-1.0, the BASAL (CATA) and FONDECYT 1190621. GD acknowledges the financial support of the Ministry of Education and Science of the Republic of Serbia through the project 176004 "Stellar Physics".

## References

- Applegate J.H., 1992, ApJ, 385, 621
- Djurašević G., 1992a, Ap&SS, 196, 267
- Djurašević G., 1992b, Ap&SS, 197, 17
- Djurašević G., et al., 2010, MNRAS, 409, 329
- Garcés L. J., et al., 2018, MNRAS, 477, L11
- Mennickent R.E., Otero S., Kołaczkowski Z., 2016a, MNRAS, 455, 1728
- Mennickent R.E., et al., 2003, A&A, 399, L47
- Mennickent R.E., et al., 2012, MNRAS, 427, 607
- Mennickent R.E., et al., 2016, MNRAS, 461, 1674
- Mennickent R.E., et al., 2020, MNRAS, Submitted
- Poleski R., et al., 2010, AcA, 60, 179
- Schleicher D.R.G., Mennickent R.E., 2017, A&A, 602, A109

# Gas velocity structure of the Orion A integral-shaped filament

V. González Lobos<sup>1</sup>, A.M. Stutz<sup>1,2</sup>

<sup>1</sup> *Departamento de Astronomía, Facultad de Ciencias Físicas y Matemáticas, Universidad de Concepción, Chile*

<sup>2</sup> *Max-Planck-Institute for Astronomy, Heidelberg, Germany*

Contact / [vgonzalezl@udec.cl](mailto:vgonzalezl@udec.cl)

**Abstract** / This is a kinematic study of the Orion A integral-shaped filament at different gas densities, aiming to understand the underlying physical process of star formation. We describe the velocity structure of the filament through intensity-weighted position–velocity diagrams, and non-thermal velocity dispersion radial profiles.

**Keywords** / stars: formation — ISM: clouds — ISM: individual objects: Orion A

In González Lobos & Stutz (2019) we present a kinematic analysis of the integral-shaped filament (ISF, e.g. Bally et al. 1987), a massive filament with ongoing star formation in an embedded cluster, located in the nearby Orion A giant molecular cloud. We aim to understand the physical process that regulates star formation, and particularly to study the previously reported wave-like properties of the ISF (Stutz & Gould, 2016; Stutz, 2018). We use public spectral imaging observations of different molecular transitions ( $^{12}\text{CO}$ ,  $^{13}\text{CO}$ ,  $\text{NH}_3$  and  $\text{N}_2\text{H}^+$ ) to trace the gas at different critical densities. See González Lobos & Stutz (2019) for details on the datasets and analysis.

We extract the kinematic parameters of the line emission (integrated intensity, central velocity, and velocity dispersion) to describe the velocity structure of the ISF. With these parameters we first construct intensity-weighted position–velocity diagrams (see Figs. 3–4 of González Lobos & Stutz, 2019), which highlight global and smaller-scale structures. The radial velocity structure is characterized by a north-to-south velocity gradient terminating with a peak near the cluster center, and by smaller scale velocity fluctuations reminiscent of torsional waves. Then, using the velocity dispersion, we obtain non-thermal velocity dispersion radial profiles for each tracer (see Fig. 5 of González Lobos & Stutz, 2019). The profiles show that the velocities are supersonic and depend on the tracer, that is, higher density tracers ( $\text{NH}_3$ ,  $\text{N}_2\text{H}^+$ ) are ‘kinematically colder’ than lower density tracers ( $^{12}\text{CO}$ ,  $^{13}\text{CO}$ ). With the velocity dispersion we estimate the specific kinetic energy profiles of the gas, shown in Fig. 1, and compare them with the gravitational potential of the filament (Stutz & Gould, 2016) and cluster (Stutz, 2018). These profiles show that the cloud is deeply gravitationally bound, suggesting that either the cloud is undergoing gravitational collapse or that forces other than supersonic turbulence (such as magnetic fields and rotation) are needed to provide support against gravity.

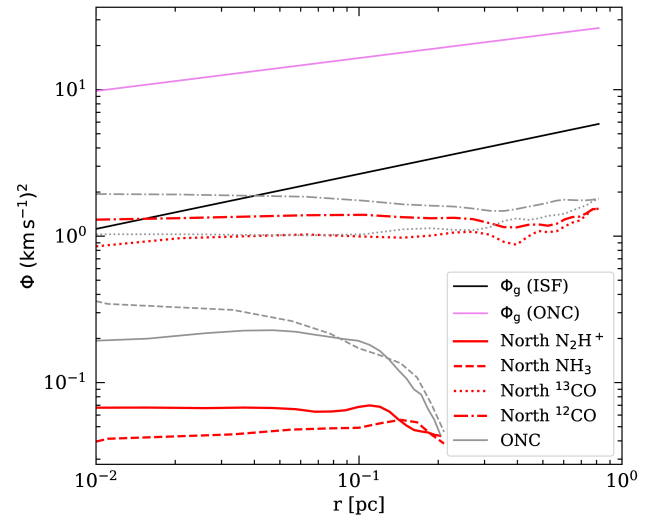


Figure 1: Specific kinetic energy radial profiles of the ISF, red (gray) curves represent the northern (cluster) region of the ISF. The black (pink) line represents the ISF (cluster) gravitational potential profile (Stutz & Gould, 2016; Stutz, 2018). Taken from *Gas velocity structure of the Orion A Integral Shaped Filament*, González Lobos & Stutz (2019), Oxford University Press..

*Acknowledgements:* VGL acknowledges funding from CONICYT Magister 2018 grant 22182160, CATA BASAL grant PFB-06/2007 and Dominik Schleicher. AS acknowledges funding from Fondecyt regular PII20150171 and CATA BASAL grant AFB-170002.

## References

- Bally J., et al., 1987, ApJL, 312, L45
- González Lobos V., Stutz A.M., 2019, MNRAS, 489, 4771
- Stutz A.M., 2018, MNRAS, 473, 4890
- Stutz A.M., Gould A., 2016, A&A, 590, A2



# Collisional blue stragglers as the “top of the iceberg” of modified stars in globular clusters

V.V. Kravtsov<sup>1</sup>

<sup>1</sup> *Shternberg Astronomical Institute, Lomonosov Moscow State University, Moscow, Russia*

*Contact / vkravtsov1958@gmail.com*

**Abstract** / Stellar populations (SPs) in Galactic globular clusters (GCs) exhibit specific dissimilarities as compared to those in open clusters. These are the manifestations of so-called multiple SPs in monometallic GCs, which are not observed in other environments, neither in open clusters nor in the field. We focus on stellar collisions, an unexplored factor which could at least be one of the key contributors to these dissimilarities. The stellar collisions do occur in the densest part of GCs but are of much lower probability in open clusters or improbable at all in the field. We draw attention and argue that the collisional blue stragglers (CBSs) observed in GCs are just the top of the iceberg of main sequence stars modified via collisions and accumulated in GCs during the cluster lifetime. We consider the expected impact of stellar collisions/merging on the characteristics of the modified stars in GCs and discuss the observed effects compatible with this process.

*Keywords* / globular clusters: general — Hertzsprung-Russell and colour-magnitude diagrams — stars: low-mass

## 1. Introduction

Two different mechanisms responsible for the origin of two SPs with different elemental abundances in monometallic GCs were proposed: (i) fast rotating massive stars (Decressin et al., 2007, 2010) and/or (ii) intermediate-mass asymptotic giant branch stars (Ventura & D’Antona, 2009). Valcarce & Catelan (2011) proposed another scenario. However, no single scenario is able to adequately interpret the variety of observational manifestations. The old age of SPs implied by the proposed processes is in agreement with the observational evidence that the multiple SPs in GCs are nearly coeval within 0.5 Gyr. This means very unlikely radial segregation between the SPs within the majority of GCs, given both the cluster relaxation time at the half-mass radius (Harris, 1996) and the old age of their SPs.

## 2. Stellar collisions and the implied outcome

However, a body of evidence about unrelaxed states in the form of different radial distribution between homologous stars of the red giant branch or main sequence turnoff (MSTO) in GCs has been accumulated to date. We suggest a causal relationship between stellar collisions/merging forming modified main sequence (MS) stars in GCs and the respective observational manifestations. This mechanism should primarily be responsible for the formation of modified MS stars from lower-mass primordial ones, in a wide MS luminosity range, at and below the present day MSTO, as opposed to mass transfer in binary systems (Stępień & Kiraga, 2015) leading preferentially to the formation of blue stragglers. Such modified MS stars are referred to by us as the lower-mass counterparts (LOMACOs) of the CBSs presently

observed in GCs (Ferraro et al., 2009; Dalessandro et al., 2013). LOMACOs have formed and accumulated in the MS of GCs during the cluster lifetime,  $\sim 13$  Gyr,

LOMACOs are expected to differ from the primordial MS stars of the same mass by: (i) the superficial elemental (CNO) abundance (Glebbeek et al., 2008), (ii) a longer timescale of the MS evolution, and (iii) a faster rotation during at least some time after the collision happens (Sills, 2015). The LOMACOs are probably much more numerous than the presently observed CBSs. The reservoir of the primordial MS stars (i.e., with  $M < 0.45 M_{\odot}$ ), from which the LOMACOs are typically formed, is approximately ten times the number of more massive MS stars, the potential targets for the formation of CBSs. Moreover, the timescale of LOMACOs MS evolution is not only somewhat longer than that of the primordial MS stars of the same mass, but it is much longer than the timescale of the presently observed CBSs. Therefore, even at the same formation rate of LOMACOs and the presently visible CBSs, the LOMACOs should be much more numerous in view of (much) different timescales of their MS evolution.

## References

- Dalessandro E., et al., 2013, *ApJ*, 778, 135
- Decressin T., et al., 2007, *A&A*, 464, 1029
- Decressin T., et al., 2010, *A&A*, 516, A73
- Ferraro F.R., et al., 2009, *Nature*, 462, 1028
- Glebbeek E., Pols O.R., Hurley J.R., 2008, *A&A*, 488, 1007
- Harris W.E., 1996, *AJ*, 112, 1487
- Sills A., 2015, *Models of Individual Blue Stragglers*, 277
- Stępień K., Kiraga M., 2015, *A&A*, 577, A117
- Valcarce A.A.R., Catelan M., 2011, *A&A*, 533, A120
- Ventura P., D’Antona F., 2009, *A&A*, 499, 835



# Link between filaments and star formation: kinematics

H.-L. Liu<sup>1</sup>, A. Stutz<sup>1,2</sup>

<sup>1</sup> *Departamento de Astronomía, Universidad de Concepción, Chile*

<sup>2</sup> *Max-Planck-Institute for Astronomy, Heidelberg, Germany*

Contact / hongliliu2012@gmail.com

**Abstract** / Kinematics is a useful probe to internal motions and structures of filaments as demonstrated in a number of studies, and our recent APEX kinematic observations on several filamentary clouds mainly in  $^{13}\text{CO}$  and  $\text{C}^{18}\text{O}$  at a resolution of  $0.1 \text{ km s}^{-1}/28''$ . Our immediate results suggest that more detailed studies of filament kinematics are still required to understand filament-scale physical processes related to filament formation and evolution, and core (star) formation. Particularly, we found in the filamentary cloud G345.51+0.84 that not all of non-thermal motions are necessarily to act against gravity along the filament.

*Keywords* / ISM: clouds — ISM: structure — ISM: molecules — stars: formation

## 1. Introduction

The critical role of filamentary clouds in the processes of star formation has been demonstrated thanks to long-wavelength *Herschel* observations. In turn, increasing analysis on filament kinematics has been carried out in a number of studies as the kinematics is a key factor in understanding some physical processes linked to filaments, such as core formation (e.g., Hacar & Tafalla 2011, Liu et al. 2019), filament formation (e.g., Palmeirim et al. 2013) and evolution (e.g., small-scale multiple velocity-coherent fibres Hacar et al. 2018), and other potential large-scale motions (e.g., Stutz et al. 2018; González Lobos & Stutz 2019; Liu et al. 2019, 2020). With limited kinematic observations so far, it is, however, still challenging to incorporate all of these observed physical processes into a simple and universal model aimed to describe the link between filaments and star formation. Therefore, we are observing kinematics of six filaments at distances of  $< 3.0 \text{ kpc}$  mainly in  $^{13}\text{CO}$  and  $\text{C}^{18}\text{O}$  (2–1) with APEX at a resolution of  $0.1 \text{ km s}^{-1}/28''$ . One of the merits of our samples is their simple morphologies, which reduce the kinematic ambiguities resulting from projection effects. In addition, the broad spectrum of masses in our samples would allow us to build up the bridge between low and high-mass filamentary star formation. Below, some immediate results on analysis of kinematics are presented for two selected filamentary clouds, G350.54+0.69 and G345.51+0.84, both of which have similar distances,  $\sim 1.4 \text{ kpc}$ .

## 2. Filament kinematics

G350.54+0.69 has an average mass per unit length ( $M/L$ ) of  $\sim 100 M_{\odot} \text{ pc}^{-1}$  along its  $\sim 8 \text{ pc}$  length, and hosts two separate filaments: G350.5-N and G350.5-S (Liu et al. 2018). The  $\text{C}^{18}\text{O}$  observations by APEX show a large-scale periodic velocity oscillation along the G350.5-N filament with a wavelength of  $\sim 1.3 \text{ pc}$  and an

amplitude of  $0.12 \text{ km s}^{-1}$ . Comparing with theoretical models, we conjectured that the periodic velocity oscillation could be driven by a combination of longitudinal gravitational instability and a large-scale periodic physical oscillation along the filament. The latter may be an example of an MHD transverse wave (see Liu et al. 2019 for more details).

G350.54+0.69 has an average  $M/L$  of  $\sim 370 M_{\odot} \text{ pc}^{-1}$  along its  $\sim 3 \text{ pc}$  length, and consists of blue and red-shifted velocity subclouds with respect to the entire filamentary system. Detailed diagnostics on the intensity maps suggests that they could be physically connected through cloud-cloud collision. The velocity gradients evidence global infall motions from cloud to filament, and finally to clump scales. Moreover, analysis of the internal kinematics of the main filament led us to conclude that not all of non-thermal turbulent motions necessarily provide support against gravity in the G350.54+0.69 filamentary cloud — for example, cloud-cloud collisions and global infall motions both can generate such non-thermal motions to facilitate the collapse of cloud (Liu et al., 2020).

*Acknowledgements:* H.L. Liu acknowledges the funding from Fondecyt Postdoctoral (project code 3190161).

## References

- González Lobos V., Stutz A.M., 2019, MNRAS, 489, 4771
- Hacar A., Tafalla M., 2011, A&A, 533, A34
- Hacar A., et al., 2018, A&A, 610, A77
- Liu H.L., Stutz A., Yuan J.H., 2018, MNRAS, 478, 2119
- Liu H.L., Stutz A., Yuan J.H., 2019, MNRAS, 487, 1259
- Liu H.L., et al., 2020, MNRAS, in prep.
- Palmeirim P., et al., 2013, A&A, 550, A38
- Stutz A.M., Gonzalez-Lobos V.I., Gould A., 2018, arXiv e-prints, arXiv:1807.11496



# Introducing the new photometric PYTHON3 package SKZPIPE

F. Mauro<sup>1</sup>

<sup>1</sup> *Instituto de Astronomía, Universidad Católica del Norte, Chile*

*Contact* / francesco.mauro@ucn.cl

**Abstract** / Nowadays, big sky surveys and the availability of large amounts of photometric data are flooding astronomers with data, making relevant having tools to process their data in an efficient, accurate and easy way, minimizing reduction time. We introduce SKZPIPE, a PYTHON3 package designed to process generic data. This first version is designed to use the DAOPHOT suite to perform point-spread function (PSF) fitting photometry. The photometric algorithms of this software have already demonstrated its accuracy and efficiency with the adaptation VVV-SKZ\_PIPELINE for the 'VISTA Variables in the Via Lactea' ESO survey. The new versions are even improved, with a solid parallelism. The package helps the user also in the matching and stacking processes, avoiding repetitive interaction in all the operations, retaining all of the benefits of the power and accuracy of the photometric software, detaching them from the burden of data processing. This software provides not only a pipeline, but also all the tools to run easily each atomic step of the whole photometric procedure, from photometry to matching the results, including the information retrieval from fits headers and an internal instrumental database. The following version will add the support to other photometric softwares (as SExtractor).

*Keywords* / techniques: image processing — miscellaneous

## 1. Introduction

In the last decades the available amount of photometric data was increasing, while generic users can be refrained from accessing the available photometric datasets since they have to learn the details about how to process them. So they wait for catalogs from others.

Performing PSF-fitting photometry is a complex process that requires to follow several steps, a quite good knowledge of the selected photometric program, and several details about the instrument. All these points are time consuming because of elaboration, training and data collection.

Previously, we have tried to improve the situation developing several pipelines with different degrees of automation and usability.

*Acknowledgements:* F.M. is thankful for the financial support from FONDECYT for project 3140177.

## References

Stetson P.B., 1987, PASP, 99, 191

## 2. SKZPIPE

In 2014, thanks to Fondecyt Postdoctoral project 3140177, a completely rewriting of the code started, to have a more useful, and complex, system. It is easier to use, permitting a perfect and complete wrapper of photometric software (DAOPHOT, Stetson, 1987, up to now, but not only it in the future), giving the opportunity to create a user's own pipeline. It covers all the steps in the photometric process (e.g. information collection, multiprocessing, matching) and is designed with a real high level of generality. It is a modern PYTHON3 module with C extensions, completely autonomous (reducing the external code as possible), dependent only on external modules that are easily installable.

The alpha version of the SKZPIPE package is available at [github.com/skz5k2/SkZpipe](https://github.com/skz5k2/SkZpipe).



# A speckle survey of binary stars in the southern sky

R.A. Mendez<sup>1,2</sup> and E. Costa<sup>1,2</sup>

<sup>1</sup> *Departamento de Astronomía, Facultad de Ciencias Físicas y Matemáticas, Univ. de Chile, Santiago, Chile*

<sup>2</sup> *Observatorio Astronómico Nacional, Universidad de Chile, Santiago, Chile*

Contact / rmendez@uchile.cl

**Abstract** / In the year 2014 we started a systematic astrometric monitoring of  $\sim 2000$  close southern binary systems within 250 pc of the Sun using the HRCAM speckle interferometer camera at the SOAR 4.1m telescope. The unique data set from this survey will be combined with published data and *Gaia* astrometry to accurately measure stellar masses in a wide range of parameter space with the purpose of testing stellar models, in particular, to determine a precise empirical mass-to-luminosity relationship for low metallicity systems, which at present is not very well constrained. Tight systems not resolved by *Gaia* and/or HRCAM@SOAR are being observed with the newly commissioned Zorro speckle camera at the 8.1m Gemini South telescope. We are also conducting ad-hoc monitoring to derive radial velocity curves for the spectroscopic binaries among our visual binaries.

**Keywords** / binaries: visual — binaries: spectroscopic — stars: fundamental parameters — stars: luminosity function, mass function — astrometry — surveys — catalogues — techniques: high angular resolution

## 1. Introito & finale

The scope and main goals of our survey have been described in Mendez et al. (2017). In that paper we also present some early results from our survey. The reader is referred to that paper for further details (see also Claveria et al., 2019).

Given the frantic pace of current research driven by a fierce competition for scarce funding, and a desire to “be the first”\*, it might seem somewhat suicidal to carry out a ground-based astrometric research that, by its very nature, requires sustained observations over long time scales. And, in some sense, it is, and certainly not recommended for young researchers in early stages of their career. In this case, in particular, astrometric observations of the longer period systems (e.g., those with periods over 100 yr) would be useful only for future generations of astronomers. However, a survey of this nature is very timely now (specially for shorter period systems), due to the availability of exquisite trigonometric parallaxes from *Gaia*, a traditional deterrent and limiting factor in visual binary star research (for masses).

*Acknowledgements:* We feel very fortunate to count with the support and wise advice of Dr. Andrei Tokovinin (Cerro Tololo Inter-American Observatory) in all aspects of our research, and specially in matters related to the use and calibration of HRCAM\*\* at the SOAR 4.1m telescope (an extremely efficient instrument for double star research designed, commissioned, maintained, and operated by him along with the support staff at CTIO, see e.g., Tokovinin et al., 2019), and also from Dr. Elliott Horch who had the original idea and initiated this survey in the Northern Sky using the WIYN telescope (Horch & van Altena, 2011). We are also collaborating with Dr. José Ángel Docobo and his team at

the Universidad de Santiago de Compostela (Spain). Their extensive expertise in the computation of orbital parameters has been a tremendous help to our research (Docobo et al., 2019). Finally, we are grateful to Dr. Steve Howell (NASA Ames Research Center) for building and making available to the general community the Zorro Speckle camera at the Gemini South telescope\*\*\*, and to the Zorro instrument Scientist at Gemini Dr. Ricardo Salinas. This recently commissioned instrument (semester 2019A) is superb, delivering precisions of 1 mas routinely, and which will allow the study of much tighter systems (diffraction limit at  $\sim 10$  mas down to  $V \sim 16$ ), including many spectroscopic binaries with available radial velocity curves. We are indebted to the Chilean Time Allocation Committee (responsible of allocating the reserved 10% Chilean time on all telescopes in Chilean territory as per international agreements) for decidedly supporting our legacy program, and for understanding the long-term nature of this type of observations; of course without their continued trust, this survey will not be possible. Last, but not least, \$ issues: Support for this research is being provided by the Chilean Centro de Excelencia en Astrofísica y Tecnologías Afines (CATA) BASAL AFB-170002, and FONDECYT/CONICYT grant # 1190038.

## References

- Claveria R.M., et al., 2019, PASP, 131, 084502
- Docobo J.A., et al., 2019, MNRAS, 482, 4096
- Horch E.P., van Altena W.F., 2011, J.A. Docobo, V.S. Tamazian, Y.Y. Balega (Eds.), *American Institute of Physics Conference Series, American Institute of Physics Conference Series*, vol. 1346, 21–35
- Mendez R.A., et al., 2017, AJ, 154, 187
- Tokovinin A., et al., 2019, AJ, 158, 48

\*Instead of the natural motivation in science, which should be to try to advance on fundamental questions about nature, or –even– mere curiosity.

\*\*<http://www.ctio.noao.edu/~atokovin/speckle/index.html>

\*\*\*<https://www.gemini.edu/sciops/instruments/alopeke-zorro/>

# Cluster galaxies in the cosmic afternoon with SpARCS and GOGREEN

J. Nantais<sup>1</sup>, R. Demarco<sup>2</sup>, P. Cerulo<sup>2</sup>, G. Wilson<sup>3</sup>, M. Balogh<sup>4</sup>, A. Muzzin<sup>5</sup>, G. Rudnick<sup>6</sup>, A. Noble<sup>7</sup>,  
L. Old<sup>8</sup>, R. van der Burg<sup>9</sup>, SpARCS Collaboration, GOGREEN Collaboration

<sup>1</sup> *Departamento de Ciencias Físicas, Universidad Andrés Bello, Santiago, RM, Chile*

<sup>2</sup> *Departamento de Astronomía, Universidad de Concepción, Concepción, Biobío, Chile*

<sup>3</sup> *Department of Physics and Astronomy, University of California Riverside, Riverside, CA, USA*

<sup>4</sup> *Department of Physics and Astronomy, University of Waterloo, Waterloo, Ontario Canada*

<sup>5</sup> *York University, Toronto, Ontario, Canada*

<sup>6</sup> *Department of Physics and Astronomy, The University of Kansas, Lawrence, KS, USA*

<sup>7</sup> *School of Earth and Space Exploration, Arizona State University, Tempe, AZ, USA*

<sup>8</sup> *European Space Agency, European Space Astronomy Center, Madrid, Spain*

<sup>9</sup> *European Southern Observatory, Garching, Germany*

Contact / julie.nantais@unab.cl

**Abstract** / Galaxy clusters at high-intermediate redshifts,  $0.8 < z < 2$ , are very active sites of both the growth of the clusters themselves and the evolution of galaxies within them. The SpARCS and GOGREEN collaborations have amassed and are continuing to analyze some of the richest datasets available on mostly infrared-selected clusters in the northern and southern skies in this dynamic redshift range. Recent and in-progress findings of SpARCS and GOGREEN provide important constraints on quenching timescales for the early type-to-late type transition and, more recently, characterization of star formation with optical, near-infrared, and ALMA radio spectroscopy.

*Keywords* / galaxies: evolution — galaxies: clusters: general

## 1. Introduction and results

Although a relationship between the star-forming properties of galaxies and their environments is well established in the literature (Dressler, 1980; Kauffmann et al., 2004), exactly how this came to be is a matter of ongoing debate. The SpARCS (Wilson et al., 2009; Muzzin et al., 2009) and GOGREEN Balogh et al. (2017) surveys focus specifically and in unprecedented detail on very dense environments — clusters and rich groups — at redshifts above 0.8, the early years of cosmic star formation decline and cluster growth. Our latest research seeks to resolve questions left unanswered by earlier research at slightly lower redshifts.

Our recent results include analyses of the star formation rate–stellar mass relation at  $z \sim 1.6$  (Nantais et al., in prep.) and  $1 < z < 1.4$  (Old et al., 2020). The preliminary results of these studies, shown in Fig. 1, could be explained by the recent formation of clusters at  $z > 1.5$  and a recent onset of environmental quenching at very slightly lower redshifts ( $\sim 1$  Gyr of difference).

## References

- Balogh M.L., et al., 2017, MNRAS, 470, 4168  
Dressler A., 1980, ApJ, 236, 351  
Kauffmann G., et al., 2004, MNRAS, 353, 713  
Muzzin A., et al., 2009, ApJ, 698, 1934  
Old L.J., et al., 2020, MNRAS, 493, 5987  
Wilson G., et al., 2009, ApJ, 698, 1943

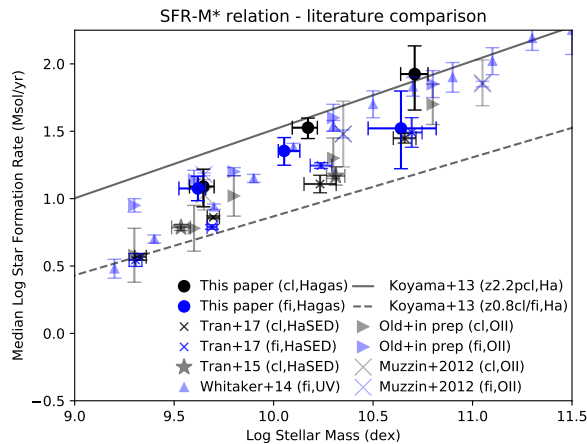


Figure 1: Comparison of star formation rate–stellar mass relations in the literature and our preliminary SpARCS (Nantais et al., in prep., filled circles) and GOGREEN (Old et al., 2020, large sideways triangles) studies. While Nantais et al. (in prep.) find no significant difference between the clusters and field, Old et al. (2020) find a mild suppression of star formation in low-mass cluster galaxies, probably indicating an early stage of environmental quenching that may not yet be taking effect in the SpARCS clusters at  $z \sim 1.6$ .



# The Orion luminosity/mass function revisited

K. Peña Ramírez<sup>1</sup>

<sup>1</sup> *Centro de Astronomía (CITEVA), Universidad de Antofagasta, Chile*

Contact / karla.pena@uantof.cl

**Abstract** / I present an analysis of the luminosity/mass function of the largest groups identified towards the Orion Complex. Those groups were determined using spectroscopic and astrometric data from APOGEE-2 and *Gaia* DR2 by applying a hierarchical clustering algorithm to the six-dimensional stellar data. I used Gaussian mixture models to represent the sample, and have found luminosity/mass function sub-structures in the explored regions. I have tested the approach with the most recent member list of 25 Ori cluster as a verification sample, reproducing the found sub-structures in its luminosity/mass function.

**Keywords** / open clusters and associations: general — stars: kinematics and dynamics — stars: pre-main sequence

## 1. Introduction

Although the research on the topic of the Initial Mass Function (IMF) has been extensive in the last  $\sim 70$  years, most of the observational efforts has been focused in the IMF low- and high-mass ends. It has been established that the rest of the IMF is well described either by continuous functions or power-law segments. Nevertheless, in the literature there are scarce reports of additional IMF substructures. This is the case of the Wielen dip/bump, first reported by Wielen et al. (1983) using the catalog of solar neighbourhood stars of Gliese (1969). The author reported a dip at about  $M_V \sim 7$  mag corresponding to mid-K type stars. Wielen et al. (1983) stated that most people explain the so-called Wielen dip in the luminosity function of field stars as a consequence of a special property of the relation between stellar mass and stellar luminosity in the region of the dip.

If the IMF would be universal and valid for clusters too, then we should see the dip also in the luminosity function of clusters. Lee et al. (1997); D'Antona & Mazzitelli (1994); Luhman et al. (2003); Luhman (2007); Elsanhoury et al. (2011); Luhman (2018), among others, have reported the presence or absence of the IMF feature in different open clusters such as Pleiades, Hyades, Perseus, and Taurus. Theoretically Kroupa et al. (1990) and Kroupa & Boily (2002) acknowledged the existence of the so called 'Wielen Dip' and relate the depression/plateau in the luminosity function due to  $H^-$  opacity becoming increasingly important in the atmospheres of K dwarfs, reducing then their luminosities. Recently, using *Gaia* DR2 (Gaia Collaboration et al., 2018) and complementary data from the DANCE project (Bouy & Alves, 2015), Olivares et al. (2019) reported the IMF feature in Ruprecht 147.

(2018), I have identified the presence of the IMF Wielen dip/bump in a set of Orion regions. I have applied Gaussian mixture models plus bootstrapping to disentangle the peak accounting for the IMF characteristic mass, and a secondary peak at about  $0.7 M_\odot$ . The potential contamination of field giants was discarded as well as a possible instrumental bias. The same IMF structure was identified in the most recent IMF determination of the 25 Ori cluster (Suárez et al., 2017). There is no clear correlation with the estimated ages of the regions, although the most prominent structures dilute considering groups of groups.

## References

- Bouy H., Alves J., 2015, *A&A*, 584, A26
- D'Antona F., Mazzitelli I., 1994, *ApJS*, 90, 467
- Elsanhoury W.H., et al., 2011, *ISRN Astronomy and Astrophysics*, 2011, 127030
- Gaia Collaboration, et al., 2018, *A&A*, 616, A1
- Gliese W., 1969, *Veröffentlichungen des Astronomischen Rechen-Instituts Heidelberg*, 22, 1
- Kounkel M., et al., 2018, *AJ*, 156, 84
- Kroupa P., Boily C.M., 2002, *MNRAS*, 336, 1188
- Kroupa P., Tout C.A., Gilmore G., 1990, *MNRAS*, 244, 76
- Lee S.W., Sung H., Cho D.H., 1997, *Journal of Korean Astronomical Society*, 30, 181
- Luhman K.L., 2007, *ApJS*, 173, 104
- Luhman K.L., 2018, *AJ*, 156, 271
- Luhman K.L., et al., 2003, *ApJ*, 593, 1093
- Olivares J., et al., 2019, *A&A*, 625, A115
- Suárez G., et al., 2017, *AJ*, 154, 14
- Wielen R., Jahreiß H., Krüger R., 1983, A.G.D. Philip, A.R. Upgren (Eds.), *IAU Colloq. 76: Nearby Stars and the Stellar Luminosity Function*, 163–170

## 2. The Wielen dip/bump in Orion

From the analysis of the largest groups identified by the six-dimensional study presented in Kounkel et al.



# Chemical gradients in the disk galaxies M33 and NGC 300

M. Peña<sup>1</sup>, S. Flores-Durán<sup>1</sup>

<sup>1</sup> *Instituto de Astronomía, Universidad Nacional Autónoma de México, Ciudad de México, México*

Contact / miriam@astro.unam.mx

**Abstract** / The chemical gradients in the disk of the late type galaxies M33 and NGC 300, obtained from H II regions (representing the chemistry of the present interstellar medium) and planetary nebulae (PNe, representing the chemistry of the interstellar medium a few Gyr ago), are discussed. It is found that PNe gradients are flatter than the ones from H II regions. A brief analysis is presented.

*Keywords* / galaxies: spiral — galaxies: abundances

## 1. Introduction

It is well known that spiral galaxies show chemical inhomogeneities. In most spirals the chemical abundances in the disc present a negative gradient with the galactocentric distance. These gradients have been derived by means of different indicators: young stars, stellar clusters, H II regions, and other objects. In many cases, the abundances derived from H II regions, which represent the chemistry of the interstellar medium (ISM) at present, are employed to calculate the gradient and such an information has been used to compute models of chemical evolution of the galaxy. According to the models, the negative slope of metallicity indicates that the disc has been formed inside-out.

In this work we have used the chemical abundances of planetary nebulae which, by means of the elements not perturbed by stellar nucleosynthesis, represent the chemistry of the ISM at the time of the central star formation, a few Gyr ago. With this we intend to analyze if the chemical gradient in the disc has evolved with time. The galaxies analyzed are M33 (SA(s)cd) and NGC 300 (SA(s)d), two late-type, low-mass, low-metallicity, nearby spirals.

## 2. Data analysis and results

For M33, the data employed for H II regions were adopted from Magrini et al. (2009), and the data employed for PNe were reported by Bresolin et al. (2009). The galactocentric distances of the objects were obtained from the same references. In the case of NGC 300, for H II regions and PNe we used the chemical abundances and galactocentric distances published by Stasińska et al. (2013). Several elements (O, Ne, A) were analyzed for both galaxies.

In Table 1 we present the oxygen abundances at  $R = 0$ ,  $12 + \log(\text{O}/\text{H})$ , and the gradients derived from H II regions and planetary nebulae (PNe), in units of dex  $\text{kpc}^{-1}$ , for both galaxies.

It is found that the slopes of gradients from PNe are flatter than the slopes of gradients from H II regions.

Table 1: Gradients of O/H

Object	O/H <sup>(a)</sup>	H II gradient dex $\text{kpc}^{-1}$	PNe gradient dex $\text{kpc}^{-1}$
M33	8.5	-0.047	-0.038
NGC 300	8.6	-0.077	-0.030

(a)  $12 + \log(\text{O}/\text{H})$  is the value at  $R = 0$  from H II regions.

This is particularly true for NGC 300 where the gradient from PNe is a factor of two less steep than the value from H II regions. It is worth mentioning that the same results are found for the elements Ne and Ar.

This result can indicate that the gradients steepen with time, in the sense that, as said above, PNe gradients represent the chemistry of the ISM a few Gyr ago. However, other effects such as migration of objects in the disc of the galaxy and merging of galaxies of different metallicities can flat the gradients with time, as migration moves the objects from their original place of birth outside or inside the disc, and mergings mix the objects of different galaxies with different metallicities.

Analysis of a large sample of galaxies of different Hubble type and different metallicities will shed more light on this subject. A complete version of this work can be found in Peña & Flores-Durán (2019).

*Acknowledgements:* This work received partial support from DGAPA-PAPIIT UNAM, grant IN103117, and CONACyT-México Project #241732.

## References

- Bresolin F., et al., 2009, ApJ, 700, 309
- Magrini L., Stanghellini L., Villaver E., 2009, ApJ, 696, 729
- Peña M., Flores-Durán S.N., 2019, RMxAA, 55, 255
- Stasińska G., et al., 2013, A&A, 552, A12



# Non-porphyrific chondrules in unequilibrated chondrites (CO) from Atacama Desert

G.A. Pinto<sup>1,3</sup>, M.E. Varela<sup>2</sup>, R. Martínez<sup>3</sup>

<sup>1</sup> *Instituto de Astronomía y Ciencias Planetarias de Atacama, Universidad de Atacama, Copiapó, Chile*

<sup>2</sup> *Instituto de Ciencias Astronómicas, de la Tierra y el Espacio, ICATE-CONICET, San Juan, Argentina*

<sup>3</sup> *Museo del Meteorito, San Pedro de Atacama, Chile*

Contact / gpinto.mo@gmail.com

**Abstract** / Chondrules belong to the protoplanetary disc (PPD). According to their texture they can be divided in non-porphyrific and porphyritic, as a consequence of rapid or slow cooling rate, respectively. We performed a petrographic and chemical composition study of three glass-rich chondrule, one radial pyroxene and four barred olivine samples from three unequilibrated carbonaceous (CO3) chondrite. The presence of volatile elements and SiO<sub>2</sub> can provide information to understand the low temperature processes that modify the bulk chemical composition of chondrules, acquired at the moment of formation at the PPD, when acting as open systems.

*Keywords* / meteorites, meteors, meteoroids — protoplanetary disks

## 1. Introduction

Chondrules are spherical objects composed of Fe-Mg silicates and a glass rich phase, called mesostasis. They are formed during the first stage of Solar System formation (Bollard et al., 2017). The process/es involved in chondrule formation cover a wide range of mechanisms whose nature is still unknown (Connolly Jr & Jones, 2016). This study focus on petrographic and chemical composition of eight chondrules from the unequilibrated CO3 chondrites, Catalina 008 [CO3.0], El Médano 216 [CO3.0] and Los Vientos 123 [CO3.1]. These chondrites were found in the Atacama Desert and belong to the Museo del Meteorito collection.

## 2. Methods

Optical microscopy was used to describe the petrographic texture and select the object. Major element composition of the constituent phases of the chondrules were performed using a JEOL 6400 analytical scanning electron microscope (NHM, Vienna). The apparent chondrule diameters, mass balance calculation and total sample porosity were obtained using IMAGEJ program.

## 3. Results and discussion

The apparent chondrule diameter, in the three CO3 samples, has a mean of 210  $\mu\text{m}$ . The most common petrographic texture in chondrules is porphyritic (95%), whereas the amount of non-porphyrific objects is just 5%. The studied chondrules have an apparent diameter up to 400  $\mu\text{m}$ . Among the eight selected objects, one is radial pyroxene (RP), three are glass-rich chondrules (GRC), and four are barred olivine (BO) objects. The results show that olivine composition is Fo 44.04

to 98.64, with low contents in Al (0.06 to 0.91 wt%). Two GRC are Mg-rich (up to 13.2 wt%) while the third displays a high bulk content of Ca (14.7 wt%). The mesostasis is Si-Al-Ca rich (Si: 19.66 to 28.21 wt%; Al: 4.86 to 11.84 wt%; Ca: 7.87 to 16.65 wt%), with low content in Mg (2.26 to 4.66 wt%).

Most objects have high content of refractory lithophile elements (Al, Ti, Ca) showing a continuous range of concentration varying from  $\sim 1 \times \text{CI}$  to  $10 \times \text{CI}$ . Volatile elements are present in the glass phase, with high contents of Na. The enrichment of Si in all studied objects (compared to CI composition) could be due a late process, within a cooling nebular reservoir characterized by solar composition and chondritic dust. In such reservoir gaseous SiO is expected to be present (Ebel & Grossman, 2000). These gas-melt interactions could explain the negative correlation observed between SiO<sub>2</sub> and refractory elements in chondrule mesostasis (Libourel et al., 2006). In addition, the study of volatile elements (Na, K, Rb) of non-porphyrific chondrules from the CH chondrite Acfer 182 (Varela, 2019) indicates that at low temperatures, while cooling of the nebula, chondrules could have different evolution paths. The presence of volatile elements in mesostasis, as well as the enhancement of Si, could indicate signatures of secondary low-temperature process.

## References

- Bollard J., et al., 2017, *Science advances*, 3, e1700407
- Connolly Jr H.C., Jones R.H., 2016, *Journal of Geophysical Research: Planets*, 121, 1885
- Ebel D.S., Grossman L., 2000, *Geochim. Cosmochim. Acta*, 64, 339
- Libourel G., Krot A.N., Tissandier L., 2006, *Earth and Planetary Science Letters*, 251, 232
- Varela M.E., 2019, *Geochim. Cosmochim. Acta*, 257, 1

# Design and analysis of a prototype antenna for the low-frequency radio telescope MIST

O.A. Restrepo<sup>1,2</sup>, F.I. Lucero<sup>1</sup>, R. Molina<sup>1</sup>, G. Chaparro<sup>2</sup>, F.P. Mena<sup>1</sup>, R. Bustos<sup>3</sup>

<sup>1</sup> *Electrical Engineering Department, Universidad de Chile, Chile*

<sup>2</sup> *Vicerrectoría de Investigación, Universidad ECCI, Colombia*

<sup>3</sup> *Laboratorio de Astro-Ingeniería y Microondas, Universidad Católica de la Santísima Concepción, Chile*

Contact / orestrepog@ecci.edu.co

**Abstract** / A low frequency dipole antenna for the MIST radio telescope was proposed and tested using both simulation and laboratory measurements. The antenna is composed of two identical aluminum planes and located at a height of  $\lambda/4$  over a ground plane. The simulation results are compared with laboratory measurements showing that the half-power beam width is  $114^\circ$ , according to the expected values.

**Keywords** / instrumentation: miscellaneous — site testing

## 1. Introduction

The Mapper of the IGM Spin Temperature (MIST), currently in the development stage, is a radio telescope that will be installed in Chile next year. MIST consists of one dipole antenna that will explore the Universe in the 50–120 MHz frequency band. A candidate antenna for MIST is a 'blade' antenna consisting of two plane elements made of sheet aluminum. This antenna was proposed by the EDGES group for the observations of the epoch of the reionization (Bowman et al., 2018). However, its gain shows a dependence with frequency and elevation angle that should be studied and possibly improved. In this paper, we present a study of a blade antenna scaled at a factor of 1/10 with respect to the original antenna used in the EDGES project.

## 2. Simulations and laboratory measurements

The dipole-type blade antenna consists of two rectangular panels located at a height relative to the ground plane corresponding to  $\lambda/4$  (Mozdzen et al., 2016). The physical dimensions of the antenna were scaled to 63 mm width and 49 mm length, corresponding to a 1.5 GHz design frequency.

This antenna was simulated with the software HFSS, obtaining the radiation pattern. These simulations were done considering an infinite ground plane. The size of the feed initially corresponds to 2.2 mm and the thickness of the panels is 3 mm. Once the blade antenna was characterized through simulations, a prototype was constructed for laboratory testing. The objective of the laboratory test is to verify these results with the simulations.

Fig. 1 shows the radiation patterns of the two measurements made in separate dates. We can see that they exhibit similar radiation pattern characteristics in both situations. For example, the half-power beam width is

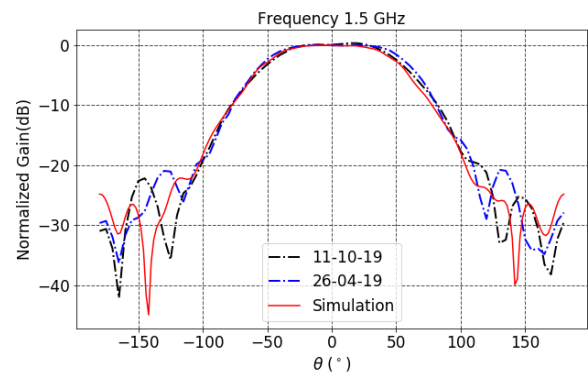


Figure 1: Comparison between simulations and laboratory measurements of the gain as a function of zenith distance  $\theta$ . The radiation pattern corresponds to the plane that contains the electric field vector.

$110^\circ$  for the simulation and  $\sim 114^\circ$  for measurements in both dates. These results allow us to extrapolate them to lower frequencies and thus to be able to characterize our real antenna for the radiotelescope MIST.

*Acknowledgements:* This work was supported by QUIMAL/CONICYT 180003 and BASAL A-F-B 170002. We would also like to thank Federico Santa María University for allowing us to occupy their anechoic chamber in the laboratory measurements.

## References

- Bowman J.D., et al., 2018, *Nature*, 555, 67
- Mozdzen T.J., et al., 2016, *MNRAS*, 455, 3890



# A MUSE study of the Seyfert 1 galaxy NGC 7469: Spatially resolved star-formation and AGN-driven winds

A.C. Robleto-Orús<sup>1</sup>, J.P. Torres-Papaqui<sup>1</sup>, A.L. Longinotti<sup>2</sup>, R.A. Ortega-Minakata<sup>3</sup>, S.F. Sánchez<sup>4</sup>, Y. Ascasibar<sup>5</sup>, E. Bellocchi<sup>5</sup>, L. Galbany<sup>6</sup>, M. Chow-Martínez<sup>7,1</sup>, J.J. Trejo-Alonso<sup>8</sup>, A. Morales-Vargas<sup>1</sup>,  
F.A. Romero-Cruz<sup>1</sup>

<sup>1</sup> *Departamento de Astronomía, Universidad de Guanajuato, Mexico*

<sup>2</sup> *Instituto Nacional de Astrofísica, Óptica y Electrónica, Mexico*

<sup>3</sup> *Instituto de Radioastronomía y Astrofísica, Universidad Nacional Autónoma de México, Mexico*

<sup>4</sup> *Instituto de Astronomía, Universidad Nacional Autónoma de México, Mexico*

<sup>5</sup> *Departamento de Física Teórica, Universidad Autónoma de Madrid, Spain*

<sup>6</sup> *PITT PACC, Department of Physics and Astronomy, University of Pittsburg, USA*

<sup>7</sup> *Instituto de Geología y Geofísica IGG-CIGEO, Universidad Nacional Autónoma de Nicaragua, Nicaragua*

<sup>8</sup> *Facultad de Ingeniería, Universidad Autónoma de Querétaro, Mexico*

Contact / aitorrobleto@gmail.com

**Abstract** / NGC 7469 is a nearby luminous infrared galaxy hosting a type-1 active galactic nucleus for which X-ray nuclear winds have been detected. We use archival data from MUSE to look for extended winds using the [O III] $\lambda$ 5007 emission line. We found a blue-shifted wind ( $\sim -900$  km s<sup>-1</sup>) at scales of 10<sup>2</sup> pc possibly associated with the active galactic nucleus and a slower wind ( $-200$  to  $-350$  km s<sup>-1</sup>) associated with the massive circumnuclear star forming regions.

**Keywords** / galaxies: Seyfert — galaxies: nuclei

NGC 7469 is a well-known luminous infrared galaxy (LIRG) hosting a Seyfert 1 active galactic nucleus (AGN). It is tidally interacting with IC 5283, causing a starburst, mostly concentrated in a circumnuclear ring located between 0.4 to 1.6 kpc from the centre (Genzel et al., 1995) with stellar population ages under 20 Myr (Diaz-Santos et al., 2007). Studies in some AGN found extended emission from ionized gas at distances up to kiloparsecs from their nuclei, at velocities of  $\sim 10^2$  to  $10^3$  km s<sup>-1</sup> (Cicone et al., 2018). Nevertheless, only in a few cases such winds have been confirmed as energy-conserving and driven by the AGN (e.g., Feruglio et al., 2015; Tombesi et al., 2015; Longinotti et al., 2018). In the case of NGC 7469, nuclear winds have been observed in X-rays (warm absorbers) and UV with velocities of 500 to 2000 km s<sup>-1</sup> by different authors (e.g., Mehdipour et al., 2018; Grafton-Waters et al., 2019). Such winds have been associated with the AGN. We aim to find extended optical counterparts through the kinematics of optical emission lines in the circumnuclear region using integral field spectroscopy (IFS).

We use archival IFS observations by MUSE (ESO/VLT). For these, we separate the central AGN from the host galaxy contribution to the observed spectra using the QDEBLEND3D software (Husemann et al., 2014). In the resulting host galaxy spectra we look for extended emission with asymmetries in the [O III] $\lambda$ 5007 emission line. We subtract a synthetic continuum fitted

with the STARLIGHT code (Cid Fernandes et al., 2005) resulting in pure-emission spectra. The [O III] $\lambda$ 5007 line is fitted with two Gaussian components; one identifies the systemic (central) component of the gas in the host galaxy while the other corresponds to the (blue-shifted) wind.

While spatially resolved line-of-sight velocity (LoSV) maps of the central component show a typical disc rotation pattern, the blue-shifted component shows an extended wind with LoSV up to  $\sim -900$  km s<sup>-1</sup> reaching  $\sim 750$  pc from the AGN, covering most of the western region in between the AGN and the circumnuclear ring. Over the ring position a slower wind is detected with LoSV from  $-200$  to  $-350$  km s<sup>-1</sup>. The former may be originated by the AGN while the latter could be associated with the star formation of the ring.

## References

- Cicone C., et al., 2018, *Nature Astronomy*, 2, 176
- Cid Fernandes R., et al., 2005, *MNRAS*, 358, 363
- Diaz-Santos T., et al., 2007, *ApJ*, 661, 149
- Feruglio C., et al., 2015, *A&A*, 583, A99
- Genzel R., et al., 1995, *ApJ*, 444, 129
- Grafton-Waters S., et al., 2019, arXiv:1907.01946
- Husemann B., et al., 2014, *MNRAS*, 443, 755
- Longinotti A.L., et al., 2018, *ApJL*, 867, L11
- Mehdipour M., et al., 2018, *A&A*, 615, A72
- Tombesi F., et al., 2015, *Nature*, 519, 436



# Improving FOF galaxy group finder

F. Rodríguez<sup>1,2</sup>, M. Merchán<sup>1,2</sup>

<sup>1</sup> *Universidad Nacional de Córdoba. Observatorio Astronómico de Córdoba. Córdoba, Argentina*

<sup>2</sup> *CONICET. Instituto de Astronomía Teórica y Experimental, Córdoba, Argentina.*

Contact / facundo.rodriguez@unc.edu.ar

**Abstract** / The identification of galaxy groups allows us to link the galaxies with the halos in which they reside and, in this way, link their formation and evolution with the large-scale structure of the Universe. For this reason, it is necessary to have group finders as accurate as possible. Here we present a work in progress on an algorithm that improves the performance of Friends-of-Friends identifications by including halo-based technique.

**Keywords** / galaxies: groups: general — galaxies: haloes — galaxies: luminosity function, mass function

## 1. Introduction

The most used method to identify galaxy groups is Friends-of-Friends (FOF; e.g. Huchra & Geller, 1982; Merchán & Zandivarez, 2002, 2005). This method is based on spatial criteria for assigning galaxies to groups and it is, by far, the most used to search for groups. However, some studies indicate that this technique has low reliability for low-number groups and, on the other hand, those that are numerous could have many intruders (e.g. Stothert et al., 2019; Davies et al., 2019).

On the other hand, the halo-based group finder developed by (Yang et al., 2005) was intensively used in recent years, mainly because it can find groups with few members. Thus, the group catalogs from these identifications allow the study of the halo occupation distribution in a wide range of masses and luminosities. This algorithm relates the galaxy group luminosity with the mass of the dark matter halo, assigning the mass by the abundance matching technique on luminosity. However, the resulting groups' catalog has, in general, less numerous systems. Nowadays, several observational studies need reliable galaxy groups that have both poor as numerous systems. Besides that, enhancing the performance of galaxy groups identification allows us to make more accurate simulations. In this work, we propose an algorithm that combines the two methods described above: in the first step a FOF identification is implemented and, in the second, from the resulting groups, we implement an algorithm that uses the halo-based method.

## 2. Proposed group finder

We start our group identification using the FOF algorithm implemented by Merchán & Zandivarez (2002, 2005). After the accomplishment of this algorithm, we have a sample of galaxy systems with two or more members, i.e., we have the center of these groups, the galaxies that compose them, and the properties of each one of them. To improve this group sample, we take only those

that have at least one bright galaxy (absolute magnitude in  $r$ -band  $M_r < -19.5$ ). Taking this into account, we discard all groups that do not meet this criterion, and also add all bright galaxies as potential groups for the next step.

The second part of the method is run based on the halo-based group finder proposed by Yang et al. (2005), which is iterative and based on an adaptive filter modeled according to the general properties of dark matter halos. Since this method requires a catalog of potential groups, we began with the resultant galaxy groups of the last procedure and, based on their properties, we implement a halo-based iterative algorithm.

## 3. Algorithm performance

In this work, we test if the luminosity threshold improves FOF groups, and then compare if the second part of our procedure (halo based) improves the effectiveness of our method. To evaluate this we measure the purity ( $P$ ) and completeness ( $C$ ) of the sample.  $P$  indicates the numbers of interlopers that the systems have, and we obtained that the second part of our method improves this quantity. On the other hand,  $C$  gives us information about the number of members that we lose in the identification process, and we show that this quantity is very high and similar in both parts of our method.

As a result of our tests we conclude that implementing the complete algorithm that we proposed, we obtain a very reliable galaxy group sample.

## References

- Davies L., et al., 2019, MNRAS, 483, 5444
- Huchra J.P., Geller M.J., 1982, ApJ, 257, 423
- Merchán M., Zandivarez A., 2002, MNRAS, 335, 216
- Merchán M.E., Zandivarez A., 2005, ApJ, 630, 759
- Stothert L., Norberg P., Baugh C.M., 2019, MNRAS, 485, L126
- Yang X., et al., 2005, MNRAS, 356, 1293



# Hierarchical star formation in nearby galaxies

M.J. Rodríguez<sup>1</sup>, G. Baume<sup>1,2</sup>, C. Feinstein<sup>1,2</sup>

<sup>1</sup> *Instituto de Astrofísica de La Plata, UNLP-CONICET, Argentina*

<sup>2</sup> *Facultad de Ciencias Astronómicas y Geofísicas, UNLP, Argentina*

Contact / jimenaro@fcaglp.unlp.edu.ar

**Abstract** / We study the hierarchical structure of the young stellar populations in five nearby galaxies by means of the fractal dimension and the  $Q$  parameter.

*Keywords* / stars: early-type — galaxies: star formation — galaxies: star clusters: general

## 1. Introduction

Star formation proceeds in a hierarchical way, as is revealed by the wide range of length scales of the stellar structures, from large stellar complexes and aggregates to small associations and clusters. The study of the different structures shows that they exhibit self-similar and fractal properties. These features are also found in the structures formed by the interstellar medium (ISM). This similarity suggests that the stellar structures may originate from those in their parental molecular clouds, which are in turn associated with turbulence and self gravity.

We study the hierarchical stellar structure of the young population in five nearby galaxies (NGC 300, NGC 247, NGC 2403, NGC 253 and NGC 2366), located between almost 2 and 3.5 Mpc. For this purpose, we used multi-band images and photometric data obtained with the *Hubble Space Telescope* (HST) ACS Camera, available in the HST archive\*.

## 2. Procedure

We built the star density maps of the young population for each galaxy. We selected this population identifying the bright and blue stars, that is the upper main sequence stars, in the color magnitude diagrams. On these maps it was possible to detect several structures; most of them presented internal sub-structures pointing to a hierarchical behavior of the young population in the studied galaxies. By means of the perimeter–area ( $P - A$ ) relationship:  $P \propto A^{(D_2/2)}$  (Sun et al., 2018), we estimated the projected fractal dimension  $D_2$  (Mandelbrot, 1982) of the detected structures. We obtained the following values of  $D_2$ :  $1.44 \pm 0.02$  for NGC 2403,  $1.56 \pm 0.01$  for NGC 300,  $1.3 \pm 0.01$  for NGC 253 and  $1.58 \pm 0.02$  for NGC 247.

We also studied the internal structure of the young stellar associations detected in previous works (Rodríguez et al., 2019, 2018, 2016) by means of the  $Q$  parameter introduced by Cartwright & Whitworth

(2004) to distinguish a fractal sub-clustered distribution from a radial distribution of stars. We found that most of the stellar associations presented a fractal distribution of stars, and only a very small percentage presented  $Q$  values according with a homogeneous distribution, but they can be explained by the uncertainty of these values.

## 3. Results

We detected young stellar structures in the five studied galaxies. Most of them presented internal substructures, revealing a hierarchical behavior with a high degree of clustering. We estimated the fractal dimension for these structures obtaining values between 1.3 and 1.58. These values are similar to the typical fractal dimension obtained for the ISM and for the young stellar structures in the Magellanic Clouds (e.g. Lee et al., 2016; Sun et al., 2018). They are also consistent with a scenario of hierarchical star formation regulated by supersonic turbulence and self gravity.

The internal structure of thousands of young stellar associations detected in previous works was studied by means of the  $Q$  parameter. We found that almost all the associations present subclumpings. This fact suggests that the studied population is very young and the groups still preserve the same structure of the molecular clouds from which they form.

## References

- Cartwright A., Whitworth A.P., 2004, MNRAS, 348, 589
- Lee Y., et al., 2016, JKAS, 49, 255
- Mandelbrot B.B., 1982, *The fractal geometry of nature*, vol. 1, WH freeman New York
- Rodríguez M.J., Baume G., Feinstein C., 2016, A&A, 594, A34
- Rodríguez M.J., Baume G., Feinstein C., 2018, MNRAS, 479, 961
- Rodríguez M.J., Baume G., Feinstein C., 2019, A&A, 626, A35
- Sun N.C., et al., 2018, ApJ, 858, 31

\*<https://archive.stsci.edu>

# Uncertainties in quantitative spectroscopy of O-type stars

C. Sabín-Sanjulián<sup>1</sup>

<sup>1</sup> *Departamento de Astronomía, Universidad de La Serena, Chile*

Contact / cssj@dfuls.cl

**Abstract** / We evaluate the effects of spectrum quality, continuum normalisation and line broadening characterisation on the determination of stellar parameters of a set of synthetic O-type spectra. We convolve the synthetic spectra with different resolving powers ( $R$ ), signal-to-noise ratios (S/N) and rotational velocities, and estimate effective temperature and surface gravity with the IACOB-GBAT tool. We find that (1) accurate stellar parameters are obtained for  $S/N > 100$ –150 and  $R > 2500$ , (2) continuum renormalisation does not have a critical effect, and (3) errors higher than 20% in line broadening of fast rotating dwarfs can affect significantly the results.

*Keywords* / stars: massive — stars: atmospheres — stars: fundamental parameters — techniques: spectroscopic

## 1. Context and method

Recent large surveys such as GOSSS (Maíz Apellániz et al., 2017), IACOB (Simón-Díaz et al., 2011b) and VFTS (Evans et al., 2011) have collected thousands of spectra of OB stars. However, this numerous and diverse spectroscopic material poses a challenge for the quantitative analysis of massive stars. Multiple sources of error are present and a thorough control of the accuracy of the analyses becomes necessary. In this work, we intend to quantify the effects of spectrum quality, continuum normalisation and line broadening characterisation on the analysis of O-type stars.

A set of synthetic optical spectra were computed using FASTWIND (Puls et al., 2005) with the typical stellar parameters of O-type stars at solar metallicity (see Holgado et al., 2018). They were convolved with different resolving powers, signal-to-noise ratios and line broadenings, and analysed quantitatively using the IACOB-GBAT automatic tool (Simón-Díaz et al., 2011a; Sabín-Sanjulián et al., 2014; Holgado et al., 2018), which requires projected rotational velocity ( $v \sin i$ ) as input parameter and provides mean values and uncertainties for effective temperature ( $T_{\text{eff}}$ ) and surface gravity ( $\log g$ ).

## 2. Results

In a first test, the synthetic spectra were convolved with  $v \sin i = 50 \text{ km s}^{-1}$  and different S/N and  $R$  values in order to evaluate the effects of spectrum quality (see Fig. 1). For  $S/N \gtrsim 100$ –150 and  $R \geq 2500$  the tool reproduces accurately the input parameters within the expected error ranges. For lower S/N and  $R$  the analyses are not trustworthy.

Secondly, random renormalisations to H Balmer lines were applied in two synthetic spectra to evaluate the effects of a wrong continuum normalisation. No critical effects on the stellar parameters were found.

The last test was devoted to errors in the characterization of line broadening. We convolved a dwarf and a

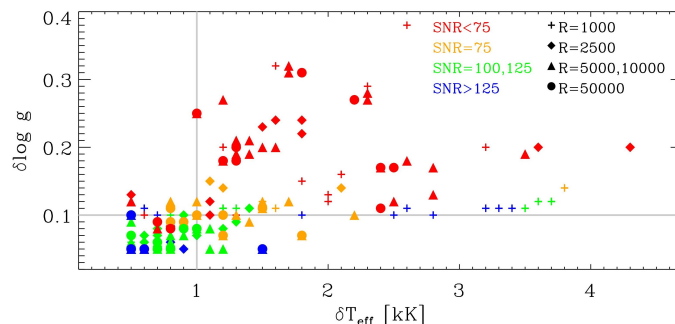


Figure 1: Uncertainties in  $\log g$  as a function of uncertainties in  $T_{\text{eff}}$  for different S/N and  $R$  values. Typical errors are indicated with grey lines.

supergiant with  $v \sin i = 50, 100, 200 \text{ km s}^{-1}$  and analysed them using different input values for  $v \sin i$ . We found that errors higher than 20% can lead to large errors in  $T_{\text{eff}}$  and  $\log g$ , specially in fast rotating O dwarfs.

*Acknowledgements:* CS-S acknowledges support from CONICYT-Chile through the FONDECYT Postdoctoral Project 3170778.

## References

- Evans C.J., et al., 2011, *A&A*, 530, A108
- Holgado G., et al., 2018, *A&A*, 613, A65
- Maíz Apellániz J., et al., 2017, *HSA IX*, 509–509
- Puls J., et al., 2005, *A&A*, 435, 669
- Sabín-Sanjulián C., et al., 2014, *A&A*, 564, A39
- Simón-Díaz S., et al., 2011a, *Journal of Physics Conference Series*, *Journal of Physics Conference Series*, vol. 328, 012021
- Simón-Díaz S., et al., 2011b, C. Neiner, G. Wade, G. Meynet, G. Peters (Eds.), *Active OB Stars: Structure, Evolution, Mass Loss, and Critical Limits*, *IAU Symposium*, vol. 272, 310–312

# Evaluating ‘twin’ parallaxes for binary stars

A. Samadi-Ghadim<sup>1</sup>, P. Jofré<sup>1</sup>

<sup>1</sup> Núcleo de Astronomía, Facultad de Ingeniería y Ciencias, Universidad Diego Portales (UDP), Santiago, Chile

Contact / anya.samadi@mail.udp.cl

**Abstract** / Employing *Gaia* DR2 stellar parallaxes, we tried to first evaluate how ‘twin parallaxes’ are compared with *Gaia* parallaxes. In the meantime, we checked how different is the performance of twin/*Gaia* parallaxes for binary stars than for single stars. Our study on a sample of *Gaia* DR2-RAVE DR5 stars shows that for 70% of them, the twin parallaxes agree well with *Gaia* parallaxes (both for single and binary stars). However, for binary candidates we detected larger scatter between two values than we found for single stars.

*Keywords* / stars: general — parallaxes — binaries: general

## 1. Introduction

Stellar parallax is a key parameter to determine stellar distances. It is mostly driven by spectroscopic methods that are mostly model-dependent. Our ability to accurately place stars on the HR diagram is limited by the observed flux of the distant stars. However, the ‘twin’ method (Jofré et al., 2015) is a method that helps us to resolve this limitation, by only using the difference of apparent magnitudes of two stars, having the same spectra and hence the same luminosity (twins), to derive the unknown parallax of the other star. In the case of binary stars the observed light, consequently the luminosity, is a contribution of both companions and hence the derived parallax may not be accurate. Here, we present how is the performance of ‘twin’ compared to *Gaia* DR2 parallaxes, in general, and how it is for binary stars, in particular. In Sec. 2., firstly, we describe our selected stellar sample and then we present the results obtained from this study.

## 2. Selected sample and results

Jofré et al. (2017) used part of RAVE DR5 (Kunder et al., 2017) stars with TGAS parallaxes as reference stars to derive twin parallaxes for the other part without measured parallaxes. In this study, we selected the cross-matching of the mentioned list with *Gaia* DR2 (Gaia Collaboration et al., 2018). To check the twin method for binary stars, we applied the method of Bouber et al. (2020, in prep.) to detect candidate binary stars. Their method, mainly, considers the stars with large uncertainty in radial velocities as binary candidates. In the end, we have 11 905 targets in each of the binary and single stars sample. As the first step, we calculated the correlation coefficient between *Gaia* and twin parallaxes for both single and binary stars. We derived a correlation equal to  $\sim 0.9$  for single stars and  $\sim 0.8$  for the candidate binaries, for the two parallaxes that show a high agreement between them. However, there is a larger scatter between the

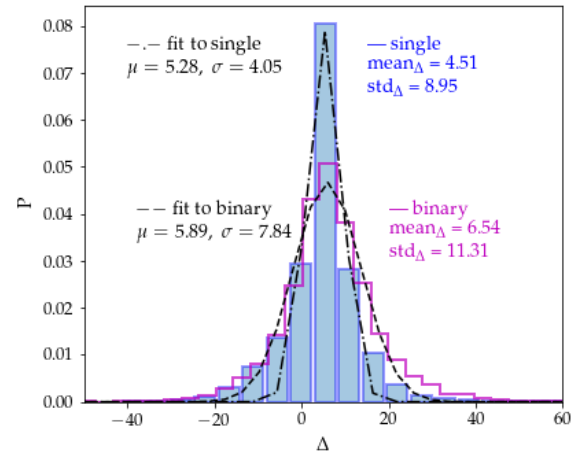


Figure 1:  $\Delta$  for single (bars) and binary (steps) candidate stars. The dashed (dot-dashed) lines show the Gaussian fits to both distributions.

values for binaries. As the next step, we evaluated the difference between the two parallaxes by means of  $\Delta = (\varpi_{\text{twin}} - \varpi_{\text{Gaia}})(\epsilon_{\varpi_{\text{Twin}}}^2 + \epsilon_{\varpi_{\text{Gaia}}}^2)^{-1/2}$ . Fig. 1 shows the distribution of  $\Delta$  for both binary and single stars, along with the Gaussian fits to these distributions ( $\varpi$ : the parallax,  $\epsilon$ : the parallax error). We conclude that for 70% of both binary and single stars  $\Delta$  is less than  $\sigma_{\Delta}$  (the standard deviation).

*Acknowledgements:* We acknowledge the financial support of ALMA-CONICYT grant number 31170029 for this research.

## References

- Gaia Collaboration, et al., 2018, A&A, 616, A1
- Jofré P., et al., 2015, MNRAS, 453, 1428
- Jofré P., et al., 2017, MNRAS, 472, 2517
- Kunder A., et al., 2017, AJ, 153, 75



# Torques on low-mass objects embedded in discs in eccentric orbits

F.J. Sánchez-Salcedo<sup>1</sup>

<sup>1</sup> *Instituto de Astronomía, Universidad Nacional Autónoma de México, México City, Mexico*

Contact / jsanchez@astro.unam.mx

**Abstract** / We consider a gravitational perturber on an eccentric orbit, embedded in a gaseous disc. We compare the eccentricity damping timescale  $t_e$  measured in numerical simulations with the value predicted using the dynamical friction framework. We find that the analytic estimate of  $t_e$  based on considerations of dynamical friction is more accurate than previously thought.

**Keywords** / accretion, accretion discs — black hole physics — planet–disc interactions — hydrodynamics — protoplanetary discs

## 1. Introduction

The orbital parameters of a gravitational perturber, such as a protoplanet or a stellar-mass black hole, embedded in an accretion disc, may evolve due to the exchange of angular momentum and energy with the disc. Using the FARGO3D code (Benítez-Llambay & Masset, 2016), we study the eccentricity damping timescale,  $t_e$ , of a perturber of mass  $M_p$  that revolves around a central massive object  $M_c$  in the midplane of a gaseous disc. We consider low-mass perturbers (i.e.  $q \equiv M_p/M_c \ll 1$ ) having orbital eccentricities  $e$  larger than the disc’s aspect ratio  $h$ . We assume that both the perturber and the accretion disc rotate in the same direction (prograde orbit). Our aim is to test analytical estimates of  $t_e$  derived using a dynamical friction approach (Muto et al., 2011). For further details, readers are referred to Sánchez-Salcedo (2019).

## 2. Eccentricity damping timescale: results

Here we present the results of a 2D simulation of a perturber with  $q = 2 \times 10^{-5}$  and  $e = 0.15$  embedded in a disc with  $h = 0.02$  and constant surface density  $\Sigma_0$ . This value of  $h$  is representative of AGN discs. The perturber is modeled using a Plummer sphere with softening radius  $R_{\text{soft}} = 0.3hR$ , where  $R$  is the distance of the perturber to the central object. From the two components of the force acting on the perturber, we infer the eccentricity damping timescale  $t_e$ . In Fig. 1, we compare  $t_e$  measured in our simulation with the value predicted in the linear approximation of dynamical friction as described in Muto et al. (2011). We have assumed that  $q_d \equiv \pi a^2 \Sigma_0 / M_c = 5 \times 10^{-3}$ , where  $a$  is the semimajor axis of the orbit. We see that the local approximation predicts reasonably well, with an error of  $\sim 16\%$ , the value of  $t_e$ .

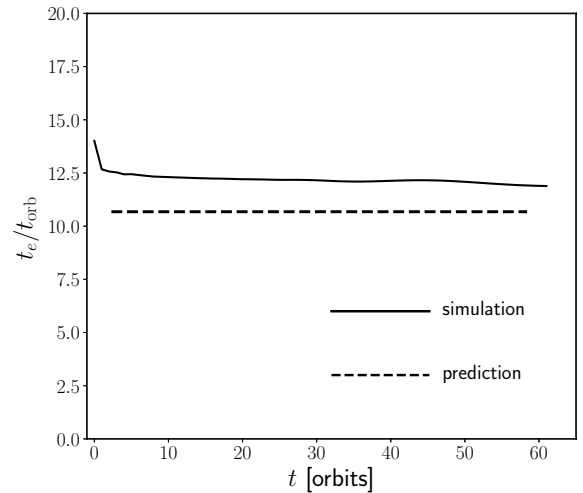


Figure 1: Comparison of the eccentricity damping timescale (in units of the orbital period  $t_{\text{orb}}$ ) as measured in the numerical simulation (solid curve), with the predicted value (dashed line).

111118 is greatly appreciated.

## References

- Benítez-Llambay P., Masset F.S., 2016, ApJS, 223, 11
- Muto T., Takeuchi T., Ida I., 2011, ApJ, 737, 37
- Sánchez-Salcedo F.J., 2019, ApJ, 885, 152

*Acknowledgements:* Financial support from project PAPIIT



# Tidal effects in potentially habitable planets at the sub-stellar mass limit

M.B. Sánchez<sup>1,2</sup>, G.C. de Elía<sup>1,2</sup>, J.J. Downes<sup>3</sup>

<sup>1</sup> *Facultad de Ciencias Astronómicas y Geofísicas, Universidad Nacional de La Plata, La Plata, Argentina.*

<sup>2</sup> *Instituto de Astrofísica de La Plata, CCT La Plata-CONICET-UNLP, La Plata, Argentina.*

<sup>3</sup> *Centro Universitario Regional del Este, Universidad de la República, Uruguay.*

Contact / msanchez@fcaglp.unlp.edu.ar

**Abstract** / We studied the relevance of tidal effects along the formation and early evolution of rocky planets near a star with a mass close to the sub-stellar mass limit. We developed a set of  $N$ -body simulations that included the early contraction and spin up of the star, the distortions and dissipation from tidal forces and general relativistic effects, and neglected the interaction between the bodies involved and the gas during the first Myr. We found that the tidal effects allow the survival of a close-in planet population with masses  $0.001 < M/M_{\oplus} < 0.012$ .

**Keywords** / planets and satellites: terrestrial planets — planets and satellites: formation — astrobiology

## 1. Introduction

There is observational and theoretical evidence of rocky planet formation around very low mass stars (VLMSs) and brown dwarfs (BDs) (e.g. Payne & Lodato, 2007; Gillon et al., 2017). This is relevant because VLMSs are the most common stars in our Galaxy and together with the BDs, the closest objects in the solar neighbourhood (e.g. Bastian et al., 2010). Moreover, planets around VLMSs are thought to form close-in to their hosts (e.g. Mulders et al., 2015). Because the habitable zone (HZ) is also close to the VLMSs (Barnes et al., 2013), such close-in planets make these stars main targets for the detection of potentially habitable planets. The close-in planets are exposed to a strong tide with the central star. So far, we know tidal effects are relevant during the late dynamical evolution of such population (Bolmont et al., 2011).

## 2. Numerical model: $N$ -body simulations

We developed a set of 10  $N$ -body simulations with the MERCURY code by adding as external forces tidal distortions and dissipation terms (Hut, 1981; Eggleton et al., 1998) and general relativistic (GR) effects (Anderson et al., 1975), and including the contraction and spin up of the central star (Bolmont et al., 2011), which occurs during its pre-main sequence phase. The simulations include a central object with a mass of  $0.08 M_{\odot}$  and a set of planetary embryos with a total mass of  $0.25 M_{\oplus}$  and initially located between  $0.015 < a/a_{\text{u}} < 1$  in almost circular and co-planar orbits. We compared the results from this new version of the code with those from the original MERCURY code by running another 10 simulations that consider only purely gravitational interactions. In this way we evaluated the relevance of tidal effects during the first 100 Myr over the rocky protoplanetary embryo distribution.

## 3. Results and conclusions

We found 11 candidates to potentially habitable planets in 9 of the 10 simulations including tidal and GR effects, while only 2 candidates were found in 2 of 10 simulations neglecting both effects. Our results shows that tidal effects are relevant during the formation and early evolution of such systems and must be included to explain the close-in body population located inside the HZ of a system around stars with masses close to the sub-stellar mass limit. A detailed description of motivations, procedures, results and implications can be found in Sánchez et al. (2020).

*Acknowledgements:* MBS and GCdeE acknowledge support from the XVI LARIM LOC.

## References

- Anderson J.D., et al., 1975, ApJ, 200, 221
- Barnes R., et al., 2013, Astrobiology, 13, 225
- Bastian N., Covey K.R., Meyer M.R., 2010, ARA&A, 48, 339
- Bolmont E., Raymond S.N., Leconte J., 2011, A&A, 535, A94
- Eggleton P.P., Kiseleva L.G., Hut P., 1998, ApJ, 499, 853
- Gillon M., et al., 2017, Nature, 542, 456
- Hut P., 1981, A&A, 99, 126
- Mulders G.D., Pascucci I., Apai D., 2015, IAU General Assembly, 22, 2256025
- Payne M.J., Lodato G., 2007, MNRAS, 381, 1597
- Sánchez M.B., de Elía G.C., José Downes J., 2020, A&A, 637, A78



# What obscures a galaxy?

J.H. Barbosa-Santos<sup>1</sup>, G.B. Lima Neto<sup>1</sup>

<sup>1</sup> *Instituto de Astronomia, Geofísica e Ciências Atmosféricas, IAG-USP, Brasil*

Contact / jullian.santos@usp.br

**Abstract** / Dust-obscured galaxies (DOGs) are the larger stellar nursery in the Universe and key objects to understand cosmic star formation history. We use a chemodynamical galaxy model and a dust production model to investigate the process that rules dust production in galaxies. We simulated forty galaxy models with initial baryonic mass  $M_{G,0}$  from  $7.5 \times 10^7 M_{\odot}$  to  $2.0 \times 10^{12} M_{\odot}$ , varying star formation and dust production efficiency. We compared our results with observational data from low and high redshift. We find that dust production in high star formation systems is almost insensible to stellar dust production efficiency, since grain accretion in cold ISM rules dust accumulation in them. Dust accretion is also enough to explain reionization DOGs, even for low dust production efficiencies. We argue that a  $M_{\text{Dust}}/M_{\text{Gas}}-M_{\text{Dust}}/M_{*}$  diagram is a good tracer to investigate both galaxy evolution and dust production.

**Keywords** / ISM: dust, extinction — ISM: evolution — ISM: abundances — galaxies: evolution — galaxies: high-redshift

## 1. Introduction

Dust-obscured galaxies (DOGs) are observed since redshift  $\sim 8$  (the reionization epoch), with a cosmic density peak coinciding with the cosmic star formation peak at  $z \sim 2$ . They are the larger and most intense star factories in the Universe, ruling star formation for high stellar mass galaxies. However, since low stellar mass galaxies seem to be dominated by unobscured star formation, it is unclear which processes are dominant for dust enhancement.

## 2. Simulations and data

In this work, we investigate the dominant dust formation process required to obscure a galaxy, by means of a chemodynamical galaxy model from Friaca & Terlevich (1998) coupled with a dust production recipe from Dwek (1998). We simulate galaxies with initial baryonic mass,  $M_{G,0}$ , in the range  $7.5 \times 10^7 M_{\odot}$  to  $2.0 \times 10^{12} M_{\odot}$ , adopting four different star formation efficiencies and two dust production efficiencies. Combining all variables, we ran forty galaxy models.

We compare our simulations with data from the literature. For the local Universe, we have irregular dwarf galaxies and blue compact dwarfs from Lisenfeld & Ferrara (1998), elliptical galaxies from Lianou et al. (2016), miscellaneous galaxy types from De Vis et al. (2017), and KINGFISH, DGS and G11 catalogs from Rémy-Ruyer et al. (2014) and Rémy-Ruyer et al. (2015). For the high- $z$  sample, we use a SMG sample from da Cunha et al. (2015), with redshifts between  $z = 1.58$  and  $5.82$ , LBGs from Magdis et al. (2017), at  $z \sim 3$ , and the reionization galaxies A1689-zD1 at  $z \sim 7.5$  (Knudsen et al., 2016) and A2744 YD4 at  $z \sim 8.3$  (Laporte et al., 2017).

## 3. Results

We find that dust production in high star formation systems is almost insensible to stellar dust sources, since grain accretion in cold ISM is considered and SNe driven outflows are also always present, especially in low mass galaxies. Dust accretion is also enough to explain reionization DOGs, even for small dust production efficiency. Low star formation rate galaxies are not efficient to accrete ISM material, being the most suitable place to investigate stellar dust sources. We also argue that  $M_{\text{Dust}}/M_{\text{Gas}} - M_{\text{Dust}}/M_{*}$  diagram is a good tracer for both galaxy evolution model and dust formulation, due to link between gas, stars, dust and star formation rate.

## References

- da Cunha E., et al., 2015, ApJ, 806, 110
- De Vis P., et al., 2017, MNRAS, 464, 4680
- Dwek E., 1998, ApJ, 501, 643
- Friaca A.C.S., Terlevich R.J., 1998, MNRAS, 298, 399
- Knudsen K., et al., 2016, MNRAS, 466
- Laporte N., et al., 2017, ApJLett, 837, L21
- Lianou S., et al., 2016, MNRAS, 461, 2856
- Lisenfeld U., Ferrara A., 1998, ApJ, 496, 145
- Magdis G.E., et al., 2017, A&A, 603, A93
- Rémy-Ruyer A., et al., 2014, A&A, 563, A31
- Rémy-Ruyer A., et al., 2015, A&A, 582, A121



# Formation of massive black holes: interplay of collisions and accretion

D.R.G. Schleicher<sup>1</sup>, P.J. Alister Seguel<sup>1</sup>, B. Reinoso<sup>1</sup>, M.Z.C. Vergara<sup>1</sup>, T. Boekholt<sup>2</sup>, M.A. Fellhauer<sup>1</sup>,  
R.S. Klessen<sup>3,4</sup>, N. Leigh<sup>1</sup>, C. Olave<sup>1</sup>, V.B. Díaz<sup>1</sup>, C. Bravo-Castillo<sup>1</sup>, R. Riaz<sup>1</sup>, B. Bandyopadhyay<sup>1</sup>, L.  
Haemmerle<sup>5</sup>

<sup>1</sup> *Departamento de Astronomía, Facultad Ciencias Físicas y Matemáticas, Universidad de Concepción, Chile*

<sup>2</sup> *CIDMA, Departamento de Física, Universidade de Aveiro, Campus de Santiago, Portugal*

<sup>3</sup> *Universität Heidelberg, Zentrum für Astronomie, Institut für Theoretische Astrophysik, Heidelberg, Germany*

<sup>4</sup> *Universität Heidelberg, Interdisziplinäres Zentrum für Wissenschaftliches Rechnen, Heidelberg, Germany*

<sup>5</sup> *Observatoire de Genève, Université de Genève, Sauverny, Switzerland*

Contact / dschleicher@astro-udec.cl

**Abstract** / More than 100 supermassive black holes are known to exist at redshifts larger than 5.6, but their initial formation pathways are still uncertain. As fragmentation seems almost inevitable in high-redshift gas clouds, and gas is expected to be present at early times in our Universe, we explore formation scenarios based on the interplay of collisions and accretion. We briefly discuss the masses that are potentially achievable, as well as the main uncertainties.

*Keywords* / black hole physics — stars: Population III — methods: numerical

More than 100 supermassive black holes have been observed at redshifts larger than 5.6 (Bañados et al., 2016), and their number is continuously increasing. Their potential formation scenarios have been laid out by Rees (1984), including the direct collapse of very massive gas clouds, collisions in dense stellar clusters as well as scenarios involving supermassive stars. Our group has explored several of these scenarios, including the direct collapse, which may produce objects with up to  $10^5 M_{\odot}$  under the right conditions (Latif et al., 2013). This however requires the gas to be primordial, and to be exposed to a very strong UV background (Latif et al., 2015), as even small amounts of gas and molecular hydrogen can trigger strong fragmentation (Omukai et al., 2008; Latif et al., 2016).

If fragmentation occurs, a cluster of protostars forms, which can still produce a central massive object via collisions (e.g. Sakurai et al., 2017; Reinoso et al., 2018). It is very likely that also gas is still present, at least in the early stages, which may considerably enhance the masses of the resulting protostars. Particularly, one may expect the gas to increase the protostellar velocity dispersion due to its contribution to the gravitational potential, it may be accreted onto the protostars, and it may enhance the collision rate via gravitational friction. Using simulations with AMUSE (Pelupessy et al., 2013) that include a realistic mass-radius relation (Haemmerlé et al., 2018) for different accretion rates ( $10^{-5} - 10^{-1} M_{\odot} \text{ yr}^{-1}$ ), we have explored the effect of the gas onto the cluster in simplified scenarios, showing that central objects of  $\sim 10^5 M_{\odot}$  may form

(Boekholt et al., 2018).

We are currently extending these models including flattening and rotation, to understand how the results depend on the geometry and the presence of ordered motion within the cluster. In addition, we have explored the effect of mass loss during collisions. Indeed, our results show that the latter may have a relevant effect on the final masses that can be achieved, potentially reducing it by about a factor of 10 (Alister Seguel et al., 2019). In the future, we plan to pursue a more realistic modeling of the gas, and the expected mass loss during collisions needs to be quantified further.

## References

- Alister Seguel P.J., et al., 2019, arXiv e-prints, arXiv:1912.01737
- Bañados E., et al., 2016, ApJS, 227, 11
- Boekholt T.C.N., et al., 2018, MNRAS, 476, 366
- Haemmerlé L., et al., 2018, MNRAS, 474, 2757
- Latif M.A., et al., 2013, MNRAS, 436, 2989
- Latif M.A., et al., 2015, MNRAS, 446, 3163
- Latif M.A., et al., 2016, ApJ, 823, 40
- Omukai K., Schneider R., Haiman Z., 2008, ApJ, 686, 801
- Pelupessy F.I., et al., 2013, A&A, 557, A84
- Rees M.J., 1984, ARA&A, 22, 471
- Reinoso B., et al., 2018, A&A, 614, A14
- Sakurai Y., et al., 2017, MNRAS, 472, 1677



# Star formation history of Canis Major OB1 II: a bimodal X-ray population revealed by *XMM-Newton*

T. Santos-Silva<sup>1</sup>, J. Gregorio-Hetem<sup>1</sup>, T. Montmerle<sup>2</sup>, B. Fernandes<sup>1</sup>

<sup>1</sup> *Instituto de Astronomia, Geofísica e Ciências Atmosféricas da Universidade de São Paulo, Brasil*

<sup>2</sup> *Institut d'Astrophysique de Paris, France*

Contact / thaisfi@gmail.com

**Abstract** / Using X-rays (from *XMM-Newton*) and infrared (WISE and 2MASS) observations, we could characterize about 250 X-ray sources and find indications of at least two star formation episodes that took place in the same region, CMa R1, separated by at least  $\sim 5$  Myr. Considering the ages of the CMa R1 members, the masses of the molecular cloud complex and their spatial distribution, we suggest that this association is going through the final stages of the star formation process.

**Keywords** / X-rays: stars — infrared: stars — stars: early-type — open clusters and associations: general — stars: formation — stars: pre-main-sequence

## 1. Introduction

The Canis Major OB1 is an association of young stars and clusters with different ages coexisting in a molecular cloud, including the ionized region called Canis Major R1 (CMa R1) that has been studied in different wavelengths by our group (Gregorio-Hetem et al., 2009; Fernandes et al., 2015; Santos-Silva et al., 2018; Fernandes et al., 2019) in order to explore its enigmatic scenario of star formation. Our previous results from ROSAT (Gregorio-Hetem et al., 2009), had revealed two stellar groups with different ages by optical and near-infrared counterparts, suggesting a possible mixing of populations originated from distinct star formation episodes.

## 2. Methodology

Motivated by these results, our group proposed more sensitive X-ray data, from *XMM-Newton* satellite, in order to improve the identification of the entire young stellar population of CMa R1. Observations of four fields (see Fig. 11 of Santos-Silva et al., 2018) provided us a catalog of 387 sources that were characterized according to hardness ratios, light curves and spectra. On the other hand, 2MASS counterparts of these sources were used to estimate their masses and ages, and used to define a complete sub-sample of stellar counterparts for statistical purposes.

## 3. Results

Among the 387 X-ray sources, we observed flares (or similar events) in 13 sources. For 21 bright sources we obtained spectra that could be fitted by a thermal plasma model. The mean values of the fit parameters were used to estimate X-ray luminosities. Moreover,

78% of the sample sources are confirmed as members or probable members of CMa R1. Our complete sub-sample (defining our ‘best sample’) is composed of 250 objects with ages among 0.3 and 55 Myr and masses varying from  $0.5 M_{\odot}$  to  $9 M_{\odot}$ . Most of them (171) are found to the East of the cloud, inside the dense molecular gas (near Z CMa). Among them only 30% are old ( $> 10$  Myr), while  $\approx 50\%$  are young ( $< 5$  Myr). The opposite scenario happens at the West site, in areas lacking molecular gas (near GU CMa): among 79 objects, almost 50% of the population are old and only 30% are young.

## 4. Conclusions

Our results confirm at least two distinct episodes of star formation in CMa R1: the first one occurred slowly in the whole studied region about 10 Myr ago and dispersed the molecular gas, while the second episode ( $< 5$  Myr) took place in the regions where molecular gas is still present. However, recently, based on runaway stars, Fernandes et al. (2019) suggested the existence of three more recent star-forming episodes (6 Myr, 2 Myr and 1 Myr ago).

*Acknowledgements:* TSS thanks FAPESP financial support (Proc. No. 2018/06822-6).

## References

- Fernandes B., et al., 2015, MNRAS, 448, 119
- Fernandes B., et al., 2019, A&A, 628, A44
- Gregorio-Hetem J., et al., 2009, A&A, 506, 711
- Santos-Silva T., et al., 2018, A&A, 609, A127



# With a view to ELT: the *Primera Luz* outreach initiative

E. Unda-Sanzana<sup>1</sup>

<sup>1</sup> *Centro de Astronomía (CITEVA), Universidad de Antofagasta, Chile*

*Contact* / eduardo.unda@uantof.cl

**Abstract** / In preparation for the opportunities that Extremely Large Telescope (ELT) will offer not only for science but also for education and tourism, the Centro de Investigación, Tecnología, Educación y Vinculación Astronómica (CITEVA) at Universidad de Antofagasta (UA) has developed a pioneer alliance of education and astroengineering to work on a long-term program supported by the Regional Government of Antofagasta (GORE) to produce a series of innovative educational materials. Also, thanks to funding from other sources and contributions from UA staff, we have engaged in high-impact programs to work with specific groups, such as blind and visually-impaired people.

*Keywords* / general: miscellaneous

## 1. Introduction

The European Southern Observatory (ESO) is currently building the 39-m ELT on top of Cerro Armazones in the Region of Antofagasta (Chile). The expectation for this modern landmark, as well as the worldwide interest in the scientific output of VLT and ALMA in the same region of the country, have moved GORE to strengthen the public funding devoted to local astronomical education. The aim of GORE is that eventually much of the personnel and users of the new facilities will be of local origin. In this encouraging context, the author has led a group of CITEVA researchers and professionals working since 2014 on a 10-year vision to improve the educational materials and experiences available to schools. The initiative is called *Primera Luz* (First Light, PL from now on) as an acknowledgement that its first horizon to deliver high-quality educational products has been, since its conception, the first light of ELT.

## 2. Main work on the initiative

Several GORE-funded projects have made possible to develop educational products and to run high-impact activities of direct contact with schoolchildren and the general public. As a guideline, every year GORE expects that the activities will reach at least 5 000 people, although in some cases that figure has nearly doubled. In the development of the educational products an inclusive and international approach has been used, often providing English subtitles or translations when applicable. The main products have been:

- An astrophotography exhibition of 30 panels depicting regional sites by night.
- A collection of educational PL videos explaining why Astronomy is important from a regional perspective.
- A series of Astronomy lessons and accompanying activity boxes and videos to be used by local schools.

In several cases the strength of astroengineering techniques (e.g. for testing and prototyping) has been used to support the development of a high-quality educational tool. Also, the Ckoirama Observatory and the Astroengineering Lab have been centerpieces of the interaction with schoolchildren and the general public since their opening.

At the institutional level the UA signed in 2015 a collaboration agreement with ESO to carry out a series of public outreach and education activities which exploit the availability of materials produced by PL. This agreement enables CITEVA to train communicators of Astronomy (teachers, touristic guides, journalists) on a yearly basis, as well as offering a program of public astronomical observations and talks open to any interested person. All the activities are free of charge for the participants and all the PL products are available to the public in <http://www.astro.uantof.cl/primeraluz>.

## 3. Beyond PL

Original efforts by permanent and temporary CITEVA colleagues have increased the reach and scope of PL. Of particular notice is the IAU-supported AstroBVI project, by María Argudo-Fernández et al., focused on the blind and visually impaired population, which she started while completing a postdoctoral stay in CITEVA. AstroBVI benefited from the application of astroengineering techniques already used by PL.

*Acknowledgements:* The author acknowledges Juan Pablo Colque as his main collaborator in PL, as well as the contributions by many other researchers and professionals who have supported his work throughout the years. Christian Nitschelm has been fundamental in running successful public observation programs.

# A new formation scenario for compact ellipticals

F. Urrutia Zapata<sup>1</sup>, M. Fellhauer<sup>1</sup>, A.G. Alarcón Jara<sup>1</sup>, D.R. Matus Carrillo<sup>1</sup>, C.A. Aravena<sup>1</sup>

<sup>1</sup> *Departamento de Astronomía, Universidad de Concepción, Concepción, Chile.*

Contact / feurrutia@udec.cl

**Abstract** / Compact elliptical (cE) galaxies have high central surface brightnesses and exhibit a high compactness. The prototype of this class of galaxies is M32, a satellite of Andromeda. Using numerical simulations, we investigate the formation of a cE using the “merging star cluster scenario” (MSCS), i.e. the merging of dozens or hundreds of star clusters inside a cluster complex (CC). The MSCS has proven successful in reproducing less massive objects like extended star clusters and ultra-compact dwarf galaxies (UCDs). Our simulations show that we can obtain objects like cEs in this scenario as well, opening up a new formation channel for cEs.

**Keywords** / galaxies: formation — galaxies: evolution — galaxies: dwarf — galaxies: star clusters: general — methods: numerical

We have demonstrated that the merging star cluster scenario (MSCS) is able to explain the formation of extended star clusters and ultra-compact dwarf galaxies (UCDs, Fellhauer & Kroupa, 2002a,b; Brüns et al., 2009). In this scenario, dozen or hundreds of star clusters born inside a small region called cluster complex (CC) merge on a short time scale and form a more massive and extended object. Our work tries to explain the formation of compact ellipticals (cEs). These objects are a relatively new type of object; their most important characteristics are small effective radii ( $R_{\text{eff}}$ ) and high central surface brightnesses. The typical formation scenario of cEs points to a galaxy origin. cEs are the result of tidal stripping and truncation of nucleated larger systems, or they could have an intrinsic origin. We propose a new formation scenario for cEs. We model cEs using the MSCS, considering higher sizes and masses than in the previous works mentioned above. We claim that the early Universe could have produced very strong star bursts, which form those big and massive CCs.

For our cE models we divide the total mass of the cluster complex of  $10^9 M_{\odot}$  into 64 or 128 UCDs. We perform a large parameter study to see which are the initial conditions of CCs that lead to final objects resembling cEs: the distance to the center of the galaxy of the CC ( $R_{\text{gal}}$ ), the Plummer radius of the UCDs ( $R_{\text{sc}}$ ), the Plummer radius of the CC ( $R_{\text{cc}}$ ) and the initial number of UCDs in the CC ( $N_0$ ).

All simulations lead to a stable object. We determine the number of constituents  $N_{\text{merger}}$ , the mass, the  $R_{\text{eff}}$ , the ellipticity, the central velocity dispersion and the surface brightness of our resulting objects.

The left panel of Fig. 1 shows the histogram of the ellipticities of the final merger objects. The black line at  $\epsilon = 0.2$  denotes the adopted value for cE galaxies. Most simulations exhibit objects with  $\epsilon$  values below or equal to 0.2. The middle panel shows  $R_{\text{eff}}$  as function of the distribution size  $R_{\text{cc}}$ . The upper curve is for  $R_{\text{sc}} = 4$  pc, and for the lower curve both  $R_{\text{sc}}$  values of 10 and 20 pc

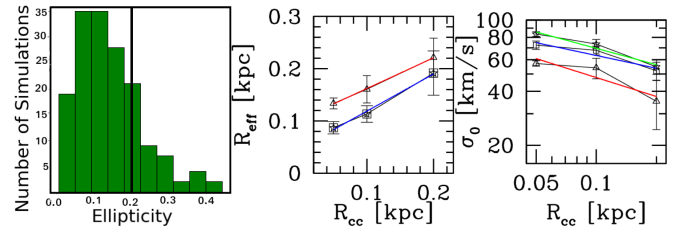


Figure 1: Left panel: Histogram of the ellipticities. Middle panel:  $R_{\text{eff}}$  vs.  $R_{\text{cc}}$ . Right panel:  $\sigma_0$  vs.  $R_{\text{cc}}$ . Taken from *The formation of compact dwarf ellipticals through merging star clusters*, Urrutia Zapata et al. (2019), Oxford University Press.

are used. Linear fits are shown in red and blue. The right panel shows  $\sigma_0$  as function of  $R_{\text{cc}}$ . The bottom line (red) is for  $R_{\text{sc}} = 4$  pc, the middle line (blue) for  $R_{\text{sc}} = 10$  pc, and the top line (green) for  $R_{\text{sc}} = 20$  pc. The fitting lines shown in color are power laws.

We analyse the resulting objects and all dynamical properties match the observational values of compact ellipticals found in the literature. The main result of this study is that indeed it is possible to obtain a cE galaxy in the merging star cluster scenario.

*Acknowledgements:* This work was funded by the CONICYT PAI/INDUSTRIA 79090016. FU, AA, CA and DM acknowledges support through regular No. 1180291 and Chilean BASAL Centro de Excelencia en Astrofísica y Tecnologías Afines (CATA) grant PFB-06/2007. MF acknowledges support through Fondecyt regular 1180291, Basal PFB-06/2007 and PII20150171.

## References

- Brüns R.C., Kroupa P., Fellhauer M., 2009, *ApJ*, 702, 1268
- Fellhauer M., Kroupa P., 2002a, *MNRAS*, 330, 642
- Fellhauer M., Kroupa P., 2002b, *AJ*, 124, 2006
- Urrutia Zapata F., et al., 2019, *MNRAS*, 489, 2746



# Asteroseismic analysis of subdwarf B variable stars: what we have learned from the recent space missions

M. Uzundag<sup>1</sup>, M. Vučković<sup>1</sup>

<sup>1</sup> *Instituto de Física y Astronomía, Universidad de Valparaíso, Valparaíso, Chile*

Contact / murat.uzundag@postgrado.uv.cl

**Abstract** / Over the last decade the space missions, in particular *Kepler*, then *K2* and now NASA mission of *Transiting Exoplanet Survey Satellite (TESS)* have completely transformed our understanding of hot subdwarf B variable stars (sdBVs). In this proceeding, I will give a brief overview of the current state-of-the-art analysis of hot sdB pulsating stars from the perspective of the recent space missions.

**Keywords** / asteroseismology — methods: observational — techniques: photometric — stars: subdwarfs

## 1. Overview

With the advance of high precision ( $\sim 0.01 \mu\text{Hz}$ ) and high duty cycle ( $> 90\%$ ) photometric monitoring from space, unprecedented asteroseismic measurements and tools have become available for sdB pulsators.

The non-radial oscillations observed in pulsating sdBs offer a unique way to probe these stars resolving their pulsation geometry, which is described by three quantized numbers:  $l$  (the modal degree) defines total surface nodes,  $n$  (the radial order) characterizes radial nodes from the core to the surface and  $m$  (the azimuthal order) describes surface nodes which pass through the pulsation axis.

During the nominal *Kepler* mission, 18 pulsating subdwarf B stars were monitored in short-cadence mode (for a review see Reed et al., 2018). The majority of the stars (16) are long period g-mode pulsators, while just two of them are short period p-mode pulsators. Additionally, 3 known sdBs stars in the old open cluster NGC 6791 were found to pulsate. In 2013, the *Kepler* mission was re-initiated after the second reaction wheel failure and it continued as *K2* mission observing along the ecliptic. In the *K2* mission more than 25 sdBs have been found to pulsate and the analysis are still ongoing.

For all the sdBVs observed with the abovementioned missions the asymptotic period sequences for g-mode pulsations have been successfully applied, especially for dipole and quadrupole modes, as more than 60% of the periodicities are associated with these modes. The asymptotic approximation can be perfectly applied for homogeneous stars. However, sdB stars are stratified and diffusion processes (gravitational settling and radiative levitation) contribute significantly to compositional discontinuities, which disturb the pulsational modes and could break the sequences. This effect has been shown in several sdBV stars. Furthermore, when the compositional discontinuities become stronger in transition zones, some modes are trapped, which was also detected

for few sdBV stars observed with *Kepler*.

Another asteroseismic tool, rotational multiplets, became useful both for the identification of pulsation modes and for the derivation of rotation periods of the core and the surface of these stars. Single sdB stars tend to have long rotation periods, from 16 d to 289 d (for a review see Charpinet et al., 2018), while sdBs in binaries have shorter rotation periods, between 2.42 h and 14.16 d.

Thanks to the continuous, long baseline datasets, we are now able to examine how the frequencies and amplitudes of the pulsation modes change over time by producing sliding Fourier Transforms of the light curves. That the amplitudes and frequencies of sdBVs change in time was known before space observations. However, with continuous observations, non-linear interactions become discernible via resonant mode coupling phenomena.

Now with the latest NASA *Transiting Exoplanet Survey Satellite (TESS)* dedicated to high-precision photometric monitoring of stars from space we are continuing to discover new sdBVs. Thus far, *TESS* has monitored thousands of sdB stars with 2-min cadence in 17 sectors. Few sectors at high latitude regions, close to the ecliptic caps, will be observed continuously, and for several sdBs found in this zone, one year continuous baseline photometry will be available. For these targets similar achievements can be reached as with *Kepler* sdBVs.

*Acknowledgements:* MU gratefully acknowledges financial support from the organizing committee.

## References

- Charpinet S., et al., 2018, *Open Astronomy*, 27, 112  
Reed M.D., et al., 2018, *Open Astronomy*, 27, 157



# New cycle period in chromospherically active stars, characterized by some activity index

F.A. Villegas<sup>1</sup>, R.E. Mennickent<sup>1</sup>, J. Garcés<sup>1</sup>

<sup>1</sup> *Universidad de Concepción, Departamento de Astronomía, Chile*

Contact / [fabrivillegas@udec.cl](mailto:fabrivillegas@udec.cl)

**Abstract** / From a robust long-term observational monitoring, in which we have collected around 6500 photometric data in filters C, i, g, and r for 5 targets, it has been possible to obtain the long-term photometric cycle length related to the apparition and vanishing of superficial stellar spots in some binary stars and singles of low mass. The analysis of these measurements has allowed us to delimit periods of rotation (in the case of binary systems assuming synchronous rotation). A spectroscopic study of the Ca II, H(396.8 nm) and K(393.3 nm) line emissions has allowed us to confirm the chromospheric activity.

*Keywords* / binaries: eclipsing — techniques: photometric — stars: chromospheres

## 1. Introduction

From different approaches, the chromospherically active stars are recognized. This phenomenon is present in different types of stars, such as RS Canum Venaticorum (RS CVn) and BY Draconis (BY Dra) variables, described by Berdyugina (2005). In them there is a cyclic internal movement, which induces an electric current necessary to maintain the magnetic field.

From a spectroscopic context, Wilson (1978) measured the change in the emission lines of Ca II, H (3968 Å) and K (3933 Å), from the Mt. Wilson survey. This periodic change is associated with S-Index which indicates the different levels of chromospheric activity. On the other hand, Phillips & Hartmann (1978) identified variations in BY Dra produced by starspots in the surface, using photographs over a time scale of 50–60 years. These methods are the pioneers in photometric and spectroscopic studies.

## 2. Observations

Using about 4500 photometric data, we obtained the final light curve for five RS CVn and BY Dra stars (which present some previously identified activity indicator), from the TAROT telescope, a 25-cm telescope located in the La Silla Observatory, Chile, with g, r, i and c filters. Data were reduced in a standard way using IRAF tasks CCDRED and PHOT, and photometric observations provided by the All Sky Automated Survey (Pojmanski, 2003). These observations consist of simultaneous photometry in the V filter through five apertures (we chose the database labeled with quality ‘A’, that means good quality data).

## 3. Results

From the Fourier series analysis it was possible to identify the rotational period of the system, reporting a new, more precise measure. Additionally in the periodograms, there are secondary peaks to the orbital period, showing possible signals related to stellar spots product of the differential rotation. Using these results we disentangled the light curve into an orbital and long-cycle part with the aid of a Fourier decomposition algorithm described by Mennickent et al. (2012).

We find in 4 of the 5 stars analyzed, and in some cases determine for the first time, the presence of a long photometric cycle associated with chromospheric activity. The results allows us to complement previous investigations and, in some cases, contribute to **understand** the link between rotation and magnetic cycles of stars with low mass, of spectral type K1 III, K3 III y K4 V. Our results will help to understand the dynamo mechanism driving the long photometric cycles in these objects.

*Acknowledgements:* Acknowledgements to Fondecyt 1190621 and funding by Departamento de Astronomía and Fac. C. F. y M., Udec.

## References

- Berdyugina S., 2005, Living Reviews in Solar Physics, 2
- Mennickent R.E., et al., 2012, MNRAS, 421, 862
- Phillips M.J., Hartmann L., 1978, ApJ, 224, 182
- Pojmanski G., 2003, AcA, 53, 341
- Wilson O., 1978, ApJ, 226, 379



## Cosmic magnetic fields from cosmological simulations

S. Adduci Faria<sup>1</sup>, P. Barai<sup>2</sup>, E.M. de Gouveia Dal Pino<sup>1</sup>

<sup>1</sup> *Instituto de Astronomia, Geofísica e Ciências Atmosféricas, IAG-USP, Brasil*

<sup>2</sup> *Universidade Cruzeiro do Sul, Unicsul, Brasil*

Magnetic fields are believed to be dragged from galaxies into the intracluster medium via winds and jets, and amplified by turbulent dynamo action. However, magnetic fields  $> 10^{-15}$  G have been inferred from gamma-ray observations in the low density intergalactic medium (IGM), though this evaluation is highly uncertain. The origin of such Intergalactic Magnetic Fields is still unknown. They could be either generated primordially in the early Universe, or be simply transported out of the galaxies and amplified according to the process above. The properties of magnetic fields are very difficult to measure directly, especially in the low density diffuse regions of the IGM. Cosmological hydrodynamical (HD) and magneto-hydrodynamical (MHD) simulations are very helpful in order to compute the contributions from the galaxies along their evolution and that of the black holes that grow inside them. The aim of this work is to investigate the origin of cosmic magnetic fields in the diffuse intergalactic medium and clusters of galaxies by means of cosmological numerical simulations. We present cosmological simulations of clusters of galaxies starting at  $z = 8$  and show how turbulent magnetic fields in equipartition with the pressure distribution of primordial gas evolve in galaxies and clusters. Preliminary results indicate that their distribution is similar both in HD and MHD simulations at the densest regions, such as galaxies and halo cores, but they are over-estimated in diffuse regions, such as filaments and voids. Interestingly, the densest regions, according to recent MHD simulations, do not follow magnetic flux conservation due to magnetic field amplification by dynamo processes and feedback from structure formation. Therefore our results indicate that such amplification processes lead to magnetic field equipartition with the gas.

*Keywords* / MHD — cosmic rays — cosmology: miscellaneous

*Contact* / stela.faria@usp.br

---

## Massive open clusters in VVV data using unsupervised clustering algorithms

J. Anais Vilchez<sup>1</sup>, S. Ramírez-Alegría<sup>1</sup>, K. Peña-Ramírez<sup>1</sup>

<sup>1</sup> *Centro de Astronomía (CITEVA), Universidad de Antofagasta, Antofagasta, Chile*

We test a technique for searching massive clusters based on an unsupervised clustering algorithm to be applied on the VISTA Variables in the Via Lactea (VVV) data. The explored space parameters are the apparent position in the sky, infrared magnitudes, colors and the reddening-free parameter  $Q_{\text{IR}}$ , a linear combination of  $(J - H)$  and  $(H - K_s)$ . In this poster we present the results of using DBSCAN on the cluster VVV CL0888, reviewing the stellar population detected by this clustering algorithm. Our strategy was able to find a structure whose position, size, color and shape are similar to those found in the literature.

*Keywords* / surveys — open clusters and associations: general — Galaxy: disc

*Contact* / jorge.anais@uamail.cl



## Heating of protostellar accretion discs associated with plasma inhomogeneities

N.F.S. Andrade<sup>1</sup>, V. Jatenco-Pereira<sup>1</sup>

<sup>1</sup> *Instituto de Astronomia, Geofísica e Ciências Atmosféricas, IAG-USP, Brazil*

The magnetorotational instability (MRI) is the most promising mechanism in driving angular momentum transport in the radial direction in accretion discs associated to T Tauri stars. However, the fact that this instability requires a minimum ionization fraction, makes it ineffective in the inner regions (i.e. at the midplane of the regions close to the central object) of these discs. In this work, we consider damping of Alfvén waves as a possible source of extra heating in the disc and analyse its effects for the occurrence of the MRI in these systems. In particular, we focus on how the Kelvin-Helmholtz instability (KHI), associated with the presence of surface Alfvén waves, can develop, enhancing the energy dissipation due to a cascading of the wave energy. We take the Keplerian shear to be the main responsible for the onset of KHI and study how the development of such instability can influence the wave dissipation. Our results confirm that the triggering of this instability can greatly amplify the amount of energy released, as previously stated in the literature, and thus make MRI effective in a larger region of the disc. Finally, we argue that this mechanism, when applied to T Tauri discs, can couple both resonant absorption and turbulent damping of Alfvén waves.

*Keywords* / stars: formation — accretion, accretion discs — magnetohydrodynamics

*Contact* / natalia.fernanda.andrade@usp.br

## The lithium–rotation connection in the Psc–Eri stream

J. Arancibia<sup>1,2</sup>, J. Bouvier<sup>3</sup>, A. Bayo<sup>1,2</sup>, P.A.B. Galli<sup>4</sup>, W. Brandner<sup>5</sup>, H. Bouy<sup>4</sup>, D. Barrado<sup>6</sup>

<sup>1</sup> *Instituto de Física y Astronomía, Universidad de Valparaíso, Chile*

<sup>2</sup> *Núcleo Milenio Formación Planetaria - NPF, Univ. de Valparaíso, Chile*

<sup>3</sup> *IPAG, Univ. Grenoble Alpes, Grenoble, France*

<sup>4</sup> *Laboratoire d'Astrophysique de Bordeaux, Univ. Bordeaux, CNRS, Pessac, France*

<sup>5</sup> *Max Planck Institute for Astronomy, Heidelberg, Germany*

<sup>6</sup> *Depto. Astrofísica, Centro de Astrobiología (INTA-CSIC), Villanueva de la Cañada, Spain*

The evolution of lithium abundance over a stellar lifetime is indicative of transport processes operating in stellar interiors. These non-standard transport processes could be affected by structural changes induced by rotation, magnetic activity, metallicity, or accretion. In this work, we study the connection between lithium content and rotation in low-mass stars belonging to the recently discovered Psc–Eri stellar stream, which has an age similar to the Pleiades (125 Myr). We obtained the rotational periods from the literature and complemented this data with optical spectra for 40 candidate members of the Psc–Eri stream. The spectra were obtained with the FEROS high-resolution spectrograph at the ESO/MPG 2.2m telescope at La Silla Observatory. To estimate the lithium content, we measured the equivalent width of the 607.8 nm Li I line. We found that a clear relation exists between the lithium content and rotation rate for a restricted range of spectral types (from late-G to early-K), where slow rotators are more lithium depleted compared with faster rotators at similar temperatures. This connection is notably similar to that previously reported for the Pleiades cluster. The two main implications of this results are: 1) the lithium–rotation relation seems to be universal for low-mass stars close to the zero-age main sequence over a specific effective temperature range; and 2) given the probably different initial conditions and evolution of the Psc–Eri stellar stream respect to that of the Pleiades, it seems that the lithium–rotation connection does not depend on environmental effects.

*Keywords* / stars: low-mass — stars: pre-main-sequence — stars: abundances — stars: rotation — open clusters and associations: individual: Psc–Eri

*Contact* / javier.arancibia@postgrado.uv.cl



## Atmospheric chemistry of a free-floating planet's exomoon

P.J. Ávila<sup>1</sup>, S. Bovino<sup>1</sup>, T. Grassi<sup>2</sup>

<sup>1</sup> *Departamento de Astronomía, Facultad Ciencias Físicas y Matemáticas, Universidad de Concepción, Chile*

<sup>2</sup> *Ludwig Maximilian University of Munich, Munich, Germany*

A free-floating planet (FFP) is a planetary-mass object that does not orbit a star but orbits a galactic center directly or a non-star massive object (like a brown dwarf or other FFP). It has been suggested that a FFP might conserve its companion moon in the ejection from a forming planetary system. The existence of life on a FFP's moon depends on the capability to reach (in the absence of a companion star) a temperature that allows relevant processes for life to take place. With a considerable atmosphere, this may ensure the long-term thermal stability of liquid water on the surface of that body. We employ the one-dimensional radiative-convective code PATMO to model the thermal structure of planetary atmospheres, coupled to gas-phase chemical kinetics. Opacity plays an important role in the thermal profile of an atmosphere. In this specific case, we employ a frequency averaged gray opacity function. We consider cosmic rays chemistry and molecular/eddy diffusion, and include tidal and radiogenic heating. Our ultimate goal is to assess the conditions under which liquid water might exist on the surface of such a moon. We explore different initial conditions and find that liquid water could exist if we consider that orbital parameters can be stable over time. The chemical evolution in a low-temperature environment can be slow, but it is plausible. The next step in our investigation is to further analyze the time evolution of water formation and include the rain-out process, which is important to estimate the amount of water.

*Keywords* / astrochemistry — planets and satellites: atmospheres

*Contact* / patricioavila@udec.cl

---

## Alternative classification diagrams for AGN/SBGs

C.P. Aydar<sup>1</sup>, J.E. Steiner<sup>1</sup>, D. May<sup>1</sup>

<sup>1</sup> *Instituto de Astronomia, Geofísica e Ciências Atmosféricas da Universidade de São Paulo (USP), Brazil*

The aim of BPT Diagnostic Diagrams is to use emission-line ratios to distinguish starburst regions from nuclear activity in the central region of galaxies. The active galactic nuclei (AGN) can be divided into Seyferts if their ionization rate is high, or LINERs if this parameter is low. However, the three traditional diagrams can sometimes be ambiguous with regards to a single object when it lies near the boundaries of the different classifications. We propose alternative diagnostic diagrams, using combinations of the emission lines commonly employed in the literature — for example  $[\text{O III}]\lambda 5007/\text{H}\beta$  with  $[\text{O I}]\lambda 6300/\text{H}\alpha$  and  $[\text{N II}]\lambda 6583/\text{H}\alpha$  with  $[\text{S II}]\lambda\lambda 6716,6731/\text{H}\alpha$ . We consider observational data from Palomar Survey and objects simulated with CLOUDY and STARBURST99. The combination of line ratios ( $\log([\text{S II}]/\text{H}\alpha) + 0.7 \times \log([\text{N II}]/\text{H}\alpha)$ ) can be a useful axis, particularly for separating LINERs from starburst regions. The line ratio  $[\text{O III}]/[\text{O I}]$  may also be a useful ratio, particularly for separating LINERs from Seyferts. The ionization parameter and the metallicity of an object with emission-lines are fundamental to describe the position of such object in a diagnostic diagram, and so, they are crucial to characterize a class of objects. The alternative diagnostic diagrams proposed are useful to classify AGNs (as Seyferts or LINERs) and star forming regions, suggesting that combining all four traditional line ratios in a single diagram avoids the possibility of multiple classification. Therefore, with these new diagrams, we find that it is possible to distinguish the ionizing source and also to study the parameters that are relevant when considering both kinds of objects, starburst regions and active galactic nuclei.

*Keywords* / galaxies: active — galaxies: nuclei — galaxies: starburst

*Contact* / catarina.aydar@gmail.com



## Stellar magnetic activity in the Orion star-formation complex

M.G. Batista<sup>1,2</sup>, G. Pinzón<sup>1</sup>, J. Hernández<sup>3</sup>

<sup>1</sup> *Universidad Nacional de Colombia*

<sup>2</sup> *Universidad de los Andes, Bogotá, Colombia*

<sup>3</sup> *Instituto de Astronomía, Universidad Autónoma de México, Ensenada, Baja California*

The impact of magnetic activity during the earliest stages of the formation of stars is an important open issue still not understood. A very precise characterization of this activity is required because magnetic phenomena play an important role in the formation and early evolution of stars and planets. In this work, we present preliminary measurements of magnetic activity indicators in stars belonging to the Orion star-forming complex, located at  $\sim 400$  parsecs and with stellar populations with an age range of  $\sim 1$ – $10$  Myr. We conducted a detailed analysis of HECTOSPEC spectra obtained for 1780 stars belonging to this star forming region. We have measured different chromospheric activity indicators using the Ca II, K and H lines as well as the infrared triplet. Results reveal the presence of two populations among the sample, one active and another inactive. With this indicator we seek to measure the non-photospheric contribution in the Ca II lines, comparing the measured equivalent widths with those reported for stars with similar spectral types. Future work will be focused to search possible correlations of stellar activity with age, stellar rotation and mass.

*Keywords* / stars: magnetic field — stars: formation

*Contact* / mbatista@unal.edu.co

## Multiwavelength analysis of brightness variations in FSRQs

P.P.B. Beaklini<sup>1</sup>, T.P. Dominici<sup>2</sup>, Z. Abraham<sup>1</sup>, J.C. Motter<sup>3</sup>

<sup>1</sup> *Instituto de Astronomia, Geofísica e Ciências Atmosféricas, Universidade de São Paulo, São Paulo/SP, Brazil*

<sup>2</sup> *Museu de Astronomia e Ciências Afins (MAST/MCTIC), Rio de Janeiro, Brazil*

<sup>3</sup> *Departamento de Astronomia, Universidade Federal do Rio Grande do Sul, Porto Alegre/RS, Brazil*

We studied the correlation between multiwavelength brightness variability and  $R$ -band polarization variations in flat-spectrum radio quasars (FSRQs) 3C 279 and PKS 1510-089, spanning enough time to cover the time lags due to opacity effects. Original data were obtained monthly at 7 mm radio continuum (Itapetinga Radio Observatory) and  $R$ -band polarimetry (Pico dos Dias Observatory) between 2009 and 2014. We compared our observations to  $\gamma$ -ray *Fermi*/LAT and  $R$ -band SMARTS light curves. For PKS 1510-089, we detected at 7 mm a correlation between radio and four  $\gamma$ -ray flares with a delay of about 54 days between them, with the  $\gamma$ -ray counterpart occurring first. Using optical polarimetry, we also detected a large variation in polarization angle (PA) rotation within two days, associated with the beginning of a  $\gamma$ -ray flare. The variability in the polarimetric parameters can be reproduced with a model considering the differences in PA and polarization degree (PD) of the jet and of a new component ejected from the compact core. In 3C 279, we found a good correlation between 7 mm and  $R$ -band light curves, with a delay of  $170 \pm 30$  days in radio, but no correlation with the  $\gamma$  rays. We also detected an increase in the  $R$ -band polarization degree and rotation of the PA simultaneous to these flares. The variability of the polarization parameters during flares can be explained by the combination of the jet polarization parameters and those of newly formed jet components, as proposed for PKS 1510-089.

*Keywords* / galaxies: active — quasars: individual: 3C 279, PKS 1510-089 — radiation mechanisms: non-thermal — galaxies: jets

*Contact* / taniadominici@mast.br



## Time evolution of rotating and magnetized white dwarf stars

L. Becerra<sup>1,2</sup>, K. Boshkayev<sup>4,5</sup>, J.A. Rueda<sup>2,3,6</sup>, R. Ruffini<sup>2,3,6</sup>

<sup>1</sup> *Instituto de Astrofísica, Pontificia Universidad Católica de Chile, Santiago, Chile*

<sup>2</sup> *ICRANet, Pescara, Italy*

<sup>3</sup> *Dipartimento di Fisica and ICRA, Sapienza Università di Roma, Rome, Italy*

<sup>4</sup> *NNLOT, al-Farabi Kazakh National University, Almaty, Kazakhstan*

<sup>5</sup> *Department of Physics, Nazarbayev University, Astana, Kazakhstan*

<sup>6</sup> *ICRANet-Rio, CBPF, Rio de Janeiro, RJ, Brazil*

We have followed the structure and thermal evolution of isolated, massive, uniformly rotating and highly magnetized white dwarf stars (WDs). We studied the possibility that angular momentum losses driven by magnetic dipole braking developed the physical conditions inside the WD suitable to produce a thermonuclear explosion or the star gravitational collapse to a neutron star. We have assumed that the WD cools by neutrino emission processes and heats by carbon-burning reactions. In general, since the WD loses angular momentum by magnetic dipole braking and its mass remains constant, its central density and temperature increase and its main radius decreases. For sub-Chandrasekhar WDs (with mass less than  $\sim 1.4 M_{\odot}$ ) the star spins-down, and for super-Chandrasekhar WDs (with mass greater than  $\sim 1.4 M_{\odot}$ ) it spins-up. We consider WDs with surface magnetic fields from  $10^6$  to  $10^9$  G and found that the WD lifetime is inversely proportional both to the magnetic field and to the WD mass. We have defined the WD lifetime as the time the WD needs to reach some instability condition, i.e. until it reaches mass-shedding, secular axisymmetric instability, inverse  $\beta$  decay instability, or the carbon-ignition line (energy release from the carbon fusion equals the neutrino emissivity).

*Keywords* / white dwarfs — stars: magnetic field — supernovae: general

*Contact* / laura.marcela.becerra@gmail.com

## Five new young cluster candidates in VVVX disc area

S. Bernal<sup>1,2</sup>, J. Borissova<sup>1,2</sup>, R. Kurtev<sup>1,2</sup>

<sup>1</sup> *Instituto de Física y Astronomía, Universidad de Valparaíso, Chile*

<sup>2</sup> *Millennium Institute of Astrophysics, Santiago, Chile*

We are reporting the discovery and photometric investigation of five infrared star cluster candidates projected in the disc area covered by the ongoing “VISTA Variables in the Via Lactea eXtended (VVVX)” ESO Public Survey. The cluster candidates are discovered by visual inspection for the local overdensities with respect to the surrounding areas. They are projected in the ionized, H II regions BRAN 47, BRAN 44 and BRAN 45. Combining near-infrared  $JK_s$  photometry from VVVX with the *Gaia* DR2 proper motion and distance estimates, we determine some preliminary basic parameters of the clusters. The projected angular radius of the candidates is between 15 and 60 arcsec. The reddening  $E(J - K)$  values are determined between 0.7 and 1.5 mag and the distances are around  $\sim 3$  kpc. The existence of ionized gas constrains their ages to be less than 10 Myr.

*Keywords* / Galaxy: open clusters and associations: general — Galaxy: disc — infrared: stars

*Contact* / santiago.bernal@postgrado.uv.cl



## Atomic/molecular opacities and globular cluster spectra

V. Branco<sup>1</sup>, P.R.T. Coelho<sup>1</sup>

<sup>1</sup> *Instituto de Astronomia, Geofísica e Ciências Atmosféricas, IAG-USP, São Paulo, SP, Brazil*

Individual Galactic globular clusters (GCs) harbour two coeval generations of stars: the first one born with the “standard”  $\alpha$ -enhanced metal mixture, observed in field halo objects; and the second one characterized by an anticorrelated CNO<sub>Na</sub> abundance pattern overimposed on the first generation. Previous works have investigated the effect that such phenomena would have on the integrated properties of populations, for a metal-rich GC ( $[\text{Fe}/\text{H}] = -0.7$ ). They have found that some spectral indices were appreciably affected by the abundance anticorrelations. To study the effect of the CNO<sub>Na</sub> anticorrelation on GCs, we calibrated our synthetic stellar spectra using high spectral resolution observations of the Sun and Arcturus, as references, from 372 to 930 nm. To produce our synthetic spectra, we used the spectral synthesis program SYNTHE and ATLAS12. Calculating the mean absolute deviation of the predictions of different opacity lists, we produced two atomic line lists, one calibrated with the Sun and the other with Arcturus. We used our new list calibrated with the Sun to compute a grid of synthetic stellar spectra to study the GC 47 Tuc (NGC 104), using the empirical stellar library based on the work by Martins and the stellar models by Coelho. The performance of our two new atomic opacity line lists enhance the representation of the observed spectra by 15 to 25% in comparison to the other lists from the literature. Using the line list calibrated with the Sun to compute the stellar spectra grid for 47 Tuc, we investigated the impact of CNO<sub>Na</sub> anticorrelations on the integrated spectrum. It shows that when de CNO<sub>Na</sub> variation mixture is applied, the regions sensitive to those atomic lines change: C and O decrease whereas N and Na increase, as expected by the anticorrelation patterns of these abundances on GCs.

*Keywords* / globular clusters: individual: NGC 104 — stars: abundances — Sun: abundances — stars: individual: Sun, Arcturus — opacity

*Contact* / [vinicius.branco.silva@usp.br](mailto:vinicius.branco.silva@usp.br)

## Investigating the 21 cm signal from the reionization epoch

C. Bravo-Castillo<sup>1</sup>, D.R.G. Schleicher<sup>1</sup>

<sup>1</sup> *Universidad de Concepción, Departamento de Astronomía, Concepción, Chile*

Due to the presence of an enormous amount of neutral hydrogen during the pre-reionization epoch of the Universe, the intergalactic medium (IGM) can be characterized using the 21-cm line. This powerful tool will allow us to learn about the end of the ‘dark ages’ when the formation of the first structures and the first galaxies began. Once the first galaxies emerged, the IGM was affected by the associated radiative backgrounds. These galaxies have emitted ultraviolet radiation that carved out ionized regions around them until hydrogen became fully ionized, giving pass to the reionization era. We calculate the shape of the spin temperature and the brightness temperature as a function of redshift considering radiative heating. A particular black focus of this project will be to consider the contributions from X-ray photons produced by the first massive black holes.

*Keywords* / quasars: supermassive black holes — dark ages, reionization, first stars — intergalactic medium

*Contact* / [clbravoc@udec.cl](mailto:clbravoc@udec.cl)



## Ionospheric absorption with a 38 MHz ROACH-based array

G. Burgos<sup>1</sup>, R. Reeves<sup>1</sup>, A. Foppiano<sup>1</sup>, R. Rodríguez<sup>1,2</sup>, J. Parra<sup>1</sup>, K. Cortes<sup>1</sup>, D. Arroyo<sup>1</sup>, K. Makita<sup>3</sup>

<sup>1</sup> *Universidad de Concepción, Chile*

<sup>2</sup> *Universidad Austral de Chile*

<sup>3</sup> *Takushoku University, Japan*

Due to the presence of free electrons and ions among the many neutral particles high in the Earth's atmosphere (the ionosphere), signal perturbations from outer space can be detected at ground level throughout the day. These perturbations are caused mainly by Thomson scattering and collision of electrons with neutral particles. These mechanisms transfer the energy from the signal into kinetic energy of the neutral gas. The signal absorption caused by this phenomenon is proportional to the electron density in the ionosphere at any given height. The total ionospheric opacity can be determined with a passive receiver on the 30–45 MHz frequency range by measuring the intensity of cosmic noise which has an antenna temperature between 1 kK and 20 kK over this frequency range. This work is about the development and implementation of a measuring system which can help to characterize the absorption of the cosmic noise signals at low- and mid-latitudes. The system includes a 16 dipole antenna array, with a central frequency of 38 MHz and a 10 MHz bandwidth. The antenna is followed by an analog processing system that routes the signals to a set of analog-to-digital converters. The analog processing system has two components: a filter and an amplifier. A total gain of around 90 dB over a bandwidth of 12 MHz relative to the central frequency is achieved. The implementation consists of using surface-mount technology components. The signals from the 16 elements are fed to a beamforming system implemented in an FPGA-based ROACH digital platform, which essentially works like a spatial filter, improving the angular resolution of the system from approximately 120 degrees for a single dipole to 25 degrees for the full array. This, in turn, allows for the possibility to change the pointing direction of the receiving pattern, the implementation of multi-beam reception and the spectral analysis over the band of interest.

*Keywords* / radio continuum: general — opacity — instrumentation: miscellaneous

*Contact* / gburgos@udec.cl

---

## Best dSph candidates for indirect dark matter detection

C. Calderón-Galaz<sup>1</sup>, N.D. Padilla<sup>1</sup>, A. Reisenegger<sup>1</sup>

<sup>1</sup> *Pontificia Universidad Católica de Chile, Santiago, Chile*

Dwarf Spheroidal (dSph) galaxies are good candidates to detect the presence of dark matter (DM), due to their high mass-to-light ratio ( $M/L$ ), poor background, and close proximity to us. We aim to find dSphs that have a high astrophysical  $J$  and  $D$ -factors, which determine the strength of the signal for DM annihilation and decay, respectively, based on the dark-matter density profile. For classical dwarf galaxies, these have been well estimated. However, new ultrafaint dSphs are being found in ongoing surveys. Some of these have higher  $M/L$ , but poor kinematic data. We are developing a code that takes the new incoming kinematic information of dSphs and automatically calculates their  $J$  and  $D$ -factors. In this way we will update the values for the current and new dSphs. On the other hand, we are performing a statistical analysis to determine the minimum number of kinematic data points needed to obtain reliable  $J$ -factors, considering the ongoing debate on the dwarf galaxy Triangulum II, which has only 13 measured stars.

*Keywords* / dark matter — galaxies: dwarf — stars: kinematics and dynamics

*Contact* / ccalderon@astro.puc.cl



## Study of the binary system TYC 7398-2542-1

P.A. Calderón<sup>1</sup>, R.E. Mennickent<sup>1</sup>

<sup>1</sup> *Departamento de Astronomía, Universidad de Concepción, Chile*

Double periodic variables are a group of binary stars with an orbital period between 1 and 16 days, characterized by additional long cyclic variability in the range of 50 – 600 d. A photometric observation of TYC 7398-2542-1 was obtained from the third publicly available database ASAS-3. To calculate the orbital and long periods we used the LOMBSCARGLEFAST algorithm of the python library GATSPY. In order to separate the short- and long-term variability, we used the Fourier decomposition technique, applying the algorithm performed by Zbigniew Kolaczowski and explained by Mennickent, in which one extracts a periodic component with a specific frequency, leaving as residue a curve that could show a second periodic component. The periods found are  $P_0 = (2.7688 \pm 0.0003) \text{ d}$  and  $P_1 = (86.94 \pm 2.00) \text{ d}$ . On the other hand, it was possible to determine its ephemeris ( $\text{HJD}_1 = 2452794.78398 + 2.769 \times E$ ). Spectra were taken with the highly stable cross-dispersed échelle spectrometer (CHIRON) at the SMARTS 1.5 m telescope. A total of 6 spectra are available, which cover the orbital phase of the system. To obtain the radial velocities we used the cross-correlation technique implemented in the FXCOR IRAF task. This was done for H $\alpha$  lines in the range 6500 – 6700 Å. Through a Gaussian fit to the absorption lines, we obtained the absolute radial velocity from the spectrum taken at phase  $f = 0.022$ , which was considered as the radial velocity template in the cross-correlation technique. This was made through the calculation of the shift between the center of the Gaussian function and the laboratory rest wavelength for each line, and then applying the heliocentric correction. The weighted mean heliocentric velocity for these spectra is  $50.24 \pm 3.09 \text{ km s}^{-1}$  using H $\alpha$  lines. Once the absolute velocity of the template was calculated, it was possible to determine the velocities obtained by cross-correlation in the absolute radial velocity system. The speed covers the range from 17.4 to 121.4  $\text{km s}^{-1}$ .

*Keywords* / binaries: close — binaries: eclipsing — binaries: spectroscopic

*Contact* / pcalderon@udec.cl, rmennick@udec.cl

## Virial factor and Buckingham's II theorem

G. Cardona<sup>2</sup>, M.-A. Higuera-G<sup>1</sup>

<sup>1</sup> *Observatorio Astronómico Nacional, Universidad Nacional de Colombia*

<sup>2</sup> *Universidad Distrital Francisco José de Caldas, Bogotá, Colombia*

We apply the Buckingham's II theorem to determine the relation between some physical parameters and the virial factor, in the estimation of the black hole mass  $M_{\text{BH}}$  in type-1 AGNs. In this work, we contrast this relation with observational results and models. The analysis has shown that the virial factor is related to the FWHM and the luminosity of the source, following an inverse proportionality. This study identifies a general relation between the physical parameters and virial factor, when we estimate black hole masses  $M_{\text{BH}}$ . For the case in study we identify, using the Buckingham analysis, that  $f \propto \dot{M}$  and  $f_{\text{rad}} \propto \text{FWHM}^{-1}$ .

*Keywords* / galaxies: active

*Contact* / mahiguerag@unal.edu.co, gcardonar@udistrital.edu.co



## Recovering Algol-type eclipsing binaries in the CRTS

A. Carmo<sup>1</sup>, C.E. Ferreira Lopes<sup>1</sup>, A. Papageorgiou<sup>2,3</sup>, F.J. Jablonski<sup>1</sup>, C.V. Rodrigues<sup>1</sup>, A.J. Drake<sup>4</sup>,  
N.J.G. Cross<sup>5</sup>, M. Catelan<sup>2,3</sup>

<sup>1</sup> *Instituto Nacional de Pesquisas Espaciais, São José dos Campos - SP, Brazil*

<sup>2</sup> *Pontificia Universidad Católica de Chile, Facultad de Física, Instituto de Astrofísica, Santiago, Chile*

<sup>3</sup> *Millennium Institute of Astrophysics, Santiago, Chile*

<sup>4</sup> *California Institute of Technology, USA*

<sup>5</sup> *Institute for Astronomy, School of Physics and Astronomy, University of Edinburgh, UK*

Eclipsing binary systems are relevant to astronomy since they provide primary means of determining fundamental stellar astrophysical quantities such as mass, radius, and temperature of the components. Algol-type eclipsing binaries (EAs) have spherical or slightly ellipsoidal components and are generally systems that produce light curves with narrow eclipses and few points within the eclipse. The most current photometric surveys usually have observation cadences larger than these eclipses duration, which hinders the detection of EAs. The variability of these objects can even be detected, but the period is rarely found because an optimized constraint is required. Thereby, we used a new methodology to find new EAs in the Catalina Real-Time Transient Survey. As a result, we determined periodicity for 56% of EA<sub>up</sub> (EAs marked as having unknown period), which corresponds to 87 new EAs reported. Also, we use color criteria to select a subsample that contains 8 low-mass binary systems with spectral types K and M. To obtain the individual physical parameters of these components, each light curve was modeled with the Wilson & Devinney light curve synthesis code combined with a Monte Carlo Markov chain process. The results were examined in the scenario of radius inflation of low-mass stars in binary systems.

*Keywords / methods:* data analysis — techniques: photometric — astronomical databases: miscellaneous — stars: variables: general — stars: late-type — stars: low-mass

*Contact /* ayssedocarmo@gmail.com

## Material heritage of the history of radioastronomy in Brazil

T.P. Dominici<sup>1</sup>, D.A. da Silva Mesquita<sup>1,2</sup>, C.P. dos Santos<sup>1</sup>, M.C.M. Casimiro<sup>1,2</sup>, Y.C.P. Mariano<sup>1,2</sup>

<sup>1</sup> *Museu de Astronomia e Ciências Afins (MAST/MCTIC), Rio de Janeiro, Brazil*

<sup>2</sup> *Escola de Museologia, Universidade Federal do Estado do Rio de Janeiro, UNIRIO, Rio de Janeiro, Brazil*

The history of astronomy in Brazil is told with the bias of optical astronomy, which can be explained by the possibility of observing this spectral band with the human eye. Another reason is the historical use of observations of star positions in the determination of time and geographical coordinates; services that justified the creation of the Brazilian National Observatory. These activities implied the acquisition and development of a series of instruments and objects that are now recognized as science and technology (S&T) heritage, many of them belonging to the collection of the Museum of Astronomy and Related Sciences. Radioastronomy, in turn, has its development in the country marked by a series of institutional ruptures, but resulting in works of international relevance, such as the first observation of an extragalactic H<sub>2</sub>O maser, the discovery of a supermaser of H<sub>2</sub>O in Orion, and one of the first quasar variability studies at 22 and 43 GHz. Considering this scenario and trying to fill some of the historical shortcomings, we started a survey of the material heritage related to the development of radioastronomy in Brazil. The survey is focused on the objects that have been stored in the Pierre Kaufmann Radio Observatory during the last four decades. In operation since the 1970s, its main instrument is a 13.7 m diameter antenna, the largest one available exclusively for radioastronomy in Brazilian territory. We estimated that there are more than 500 instruments and objects out of use that have potential historical significance. They need to be cataloged, conserved, and organized on storage. They should compose a future historical collection of Brazilian radioastronomy, framed in recent heritage of S&T. Developing a set of criteria for the selection of recent heritage is a current debate in the international scenario, with which the present work collaborates. We intend to organize as soon as possible an exhibition of some of these objects representing the material heritage of radioastronomy in Brazil.

*Keywords /* history and philosophy of astronomy — miscellaneous

*Contact /* taniadominici@mast.br



## Deformations of NSs as a source of gravitational waves

F. Espinoza-Arancibia<sup>1</sup>, A. Reisenegger<sup>1</sup>

<sup>1</sup> *Instituto de Astrofísica, Pontificia Universidad Católica de Chile, Macul, Región Metropolitana*

Recently, the first direct detections of transient gravitational waves have been made using LIGO and VIRGO. Another expected type of signal, not yet detected, are continuous gravitational waves, emitted by rotating compact objects, such as neutron stars with non-axisymmetric deformations. In this work, we calculated the size of the maximum deformation that the crust can support before breaking, due to internal elastic stresses using a Newtonian model developed by Rencoret, Aguilera & Reisenegger (in preparation). We consider the difference in the displacements of mass elements between a state where the star is relaxed and a state where the star builds up stress in the crust due to the change of the centrifugal force by spin-down. Stress will build up in the crust until a failure criterion is met. Using this criterion, we can obtain the maximum size of the deformation until the crust breaks. The ellipticity associated with this deformation is  $\epsilon \approx 5 \times 10^{-7}$ . If this deformation were non-axisymmetric, the amplitude of the radiated gravitational waves can be compared to the estimated sensitivities of existing and planned ground based detectors. The calculated amplitude is below these sensitivities; thus, pulsars have a much smaller ellipticity. Increasing sensitivities and noticeably longer observation runs will increase the probability of a detection of continuous gravitational signals from spinning neutron stars.

*Keywords* / gravitational waves — stars: neutron

*Contact* / fespinoza@astro.puc.cl

## Optical classification and dynamical study of the OH megamaser galaxy *IRAS 11506-3851*

L.M. Gatto<sup>1</sup>, D. Sales<sup>1</sup>

<sup>1</sup> *Instituto de Matemática Estatística e Física, FURG, Brazil*

We present an optical spectroscopy study of the OH-megamaser galaxy (OHMG) *IRAS 11506-3851* using Gemini/GMOS and images taken from the *Hubble Space Telescope (HST)*. OHMGs form a sub-class accounting for approximately 20% of Luminous Infrared Galaxies (LIRGs), which emit OH maser lines at 1665 and 1667 MHz with a brightness of approximately  $10^{2-4} L_{\odot}$ . As these galaxies are found in gas-rich mergers, it has been suggested that OHMs can be used to trace galaxy merger rates and associated processes (dust obscured star formation and black hole growth). In addition, the OH lines often show broad asymmetric profiles and velocity shifts suggestive of outflows. OHMGs may therefore represent a critical, short-lived transition phase in which massive, dense concentrations of molecular gas are triggering intense episodes of star formation and the onset of AGN fueling, resulting in rapid black-hole growth. Our *HST* *i* band image of *IRAS 11506-3751* shows numerous compact regions of ongoing circumnuclear star formation. One-dimensional spectra of the OHMG show H $\beta$   $\lambda$ 4862.68, [O III]  $\lambda$ 5007, [O I]  $\lambda$ 6300, H $\alpha$  6564.61, [N II]  $\lambda$  6549.86 and 6585.27, and [S II]  $\lambda$ 6717.31 emission lines, and we also detect the NaD absorption line. The rotation curve close to the major axis of *IRAS 11506-3851* obtained through the H $\alpha$  emission line has an amplitude of approximately  $240 \text{ km s}^{-1}$ . A region located approximately 0.6 kpc from the nucleus of the galaxy in the eastern direction is blueshifted, suggesting an outflow of ionized gas. The BPT diagram was used to investigate the dominant excitation mechanism present in *IRAS 11506-3751*, and through it we conclude that in the center there is a composite Seyfert/star-forming region, whereas in the external regions of the galaxy there are star formation regions.

*Keywords* / line: identification — methods: observational — galaxies: active — galaxies: kinematics and dynamics

*Contact* / laragatto01@gmail.com



## A detailed re-analysis of the planetary system around Gl 832

P. Gorrini<sup>1</sup>, N. Astudillo-Defru<sup>2</sup>

<sup>1</sup> *Departamento de Astronomía, Universidad de Concepción, Chile*

<sup>2</sup> *Dpto. de Matemática y Física Aplicadas, Univ. Católica de la Santísima Concepción, Concepción, Chile*

M dwarfs make up about 70% of the stars in our Galaxy. Their small sizes and low masses make them ideal to search for terrestrial planets using the transit or radial velocity (RV) methods, as they produce enhanced signals compared to solar-like stars. However, a large fraction of M dwarfs have shown to be magnetically active, that combined with stellar rotation can induce RV variations that can mimic planetary signals, causing false planet detections, as seen in other investigations. In this work we re-analyse the RV time series of Gl 832 using archival RV data alongside new HARPS data, as well as stellar activity indicators. This M dwarf star hosts two planets, b and c, where the latter is reported as a super-Earth with  $5.4 M_{\oplus}$  located in the habitable zone in a planetary system only 4.95 pc away. A previous study shows that the orbital period of planet c is close to the stellar rotation period, casting doubts on the planetary origin of the signal. For our study we performed a Keplerian fit on the RV data and computed the generalized Lomb-Scargle periodogram (GLS) noticing a dominant periodicity near 3800 days, corresponding to planet b. After modeling and subtracting this signal, residual RV reveals two significant signals, near 35 days (which is the signal that corresponds to planet c) and near 184 days. In order to study the origin of the 35 days RV signal, we modeled the S-index, which is in activity tracer, improving by 89.78% the precision of the reported value of the stellar rotational period with a value of  $35.76 \pm 0.95$  days, being attributable to the 35 days RV signal. Afterwards, we made a Keplerian fit with Gaussian processes, observing in the resulting residual GLS periodogram that the two signals that appeared before were no longer present. In this sense, we conclude that none of both signals has a planetary nature, and therefore planet c is an artifact of stellar activity.

*Keywords* / stars: activity — planets and satellites: detection

*Contact* / pgorrini@udec.cl

## Terzan 5, a fossil relic of the Galactic bulge

V. Gotta<sup>1</sup>, F. Mauro<sup>1</sup>, C. Moni Bidin<sup>1</sup>, D. Geisler<sup>2</sup>, F. Ferraro<sup>3</sup>

<sup>1</sup> *Instituto de Astronomía, Universidad Católica del Norte, Antofagasta, Chile*

<sup>2</sup> *Departamento de Astronomía, Universidad de Concepción, Chile*

<sup>3</sup> *University of Bologna, Italy*

Terzan 5 is a Galactic cluster poorly studied until 2009 due the high extinction ( $E(B - V) = 2.38$ ) and the strong differential reddening ( $\Delta E(B - V) \approx 0.7$  mag), typical of the bulge area. Originally considered a globular cluster, previous works showed that this system has two horizontal branches (HBs) separated by 0.3 mag in the  $K_s$  band. It is thought that Terzan 5 can be a candidate for the building blocks of the Galaxy, due to their difference in age ( $\sim 7$  Gyr) and metallicity (0.5 dex), as these properties are not compatible with the evolution of a globular cluster. For this reason, our work is focused on observations in the  $J$  and  $K_s$  bands with GeMS/GSAOI and in the  $I$  band from VVV and *HST*. They allow us to observe the center of Terzan 5 and so, to analyze the two populations discovered, now in the central part, not previously observed with such precision. Analyzing the distribution of the stars in the two main HBs in the center of the cluster and the corresponding cumulative radial distributions, we can see that the bright HB is concentrated in the center, and it has an exponential distribution (although these results are still being evaluated), while the faint HB is more homogeneously distributed.

*Keywords* / Galaxy: bulge — Galaxy: formation — Galaxy: globular clusters: individual: Terzan 5

*Contact* / vanita.vane@gmail.com



## Effect of the inclination of the BLR on the virial factor

M.-A. Higuera-G.<sup>1</sup>, G. Cardona<sup>2</sup>

<sup>1</sup> *Observatorio Astronómico Nacional, Universidad Nacional de Colombia*

<sup>2</sup> *Universidad Distrital Francisco José de Caldas, Bogotá, Colombia*

In the last decade, observational relationships have been identified between the mass of supermassive black holes and the properties of their host galaxies, such as the star dispersion velocity, luminosity, or bulge mass. The structure and kinematics of the broad-line region (BLR) is a key problem in modern astrophysics, as properties of the broad emission lines are used to find the mass of the central black hole. In type-1 AGNs, the virial theorem is the tool to determine the black hole mass. In this approach, the cloud velocity is usually inferred from the width of the broad lines, and the size of the BLR is derived from reverberation measures. However, the virial method shows uncertainties that suggest to include a virial factor  $f$ . In this work, we take into account the effect of the BLR inclination  $i$ , assumed to have a planar distribution of radius  $R$  and height  $H$ , given by  $f = (4(\sin^2 i + (H/R)^2))^{-1}$ . We also assume that radiation pressure, determined by the luminosity, can diverge slightly from gravitational equilibrium and push the clouds of the BLR slightly outward. This effect offers a new way to obtain the BLR size,  $R_{\text{BLR}} = R_{\text{BLR}}^0 (a_1 L^{\alpha_{\text{Line}}} + a_2 L_{\lambda} / M_{\text{BH}})$ , where  $R_{\text{BLR}}^0$  is a typical size of the BLR,  $L$  the luminosity,  $\alpha_{\text{Line}}$  a dimensionless parameter,  $L_{\lambda}$  the luminosity at wavelength  $\lambda$ ,  $M_{\text{BH}}$  the mass of the black hole, and  $a_1$  and  $a_2$  are constants. Also we identify relations between inclination and the virial factor derived for radiation pressure  $f_{\text{rad}}$ . In this case, we obtain the relation  $f_{\text{rad}} \propto (2 \sin i)^{-1}$ , that takes into account the effects of the inclination in a planar distribution of BLRs, and of the radiation pressure.

*Keywords* / quasars: supermassive black holes — quasars: emission lines

*Contact* / mahiguerag@unal.edu.co, gcardonar@udistrital.edu.co

## LLAMA, a sub-mm radiotelescope in the Andes

J. Lepine<sup>1</sup>, Z. Abraham<sup>1</sup>, G.G. Castro<sup>2</sup>, J.J. Larrarte<sup>3</sup>, E. Rasztocky<sup>3</sup>, G. Gancio<sup>3</sup>, T. Dominici<sup>4</sup>, P. Beaklini<sup>1</sup>, F. Correr<sup>1</sup>, W. Beccari<sup>1</sup>, M. Luqueze<sup>1</sup>, S. Verri<sup>1</sup>, D. Zanella<sup>1</sup>, J. Kooi<sup>5</sup>, D. Ronsó<sup>1</sup>

<sup>1</sup> *Universidade de São Paulo, São Paulo, Brazil*

<sup>2</sup> *Universidade Presbiteriana Mackenzie, São Paulo, Brazil*

<sup>3</sup> *Instituto Argentino de Radioastronomía, CONICET, Argentina*

<sup>4</sup> *Museu de Astronomia e Ciências Afins, MAST-MCTI, Rio de Janeiro, Brazil*

<sup>5</sup> *California Institute of Technology, USA*

LLAMA is a joint Brazilian-Argentine Project of a 12 m mm/sub-mm radiotelescope similar to the ALMA antennas, at 4800 m altitude and 200 km from ALMA, financed in Brazil by FAPESP (São Paulo State), and in Argentina by MinCyT. The construction of the antenna by VERTEX (Germany) started in 2014. The access road to the site and a flat area were constructed. The antenna was transported to Argentina but is still waiting for the construction of a concrete foundation. We have two ALMA-like cooled receivers, in bands 5 and 9, and a cryostat with room for three cartridges constructed by NAOJ (Japan). We obtained significant contribution from NOVA-Groningen Lab and GARD (Gothenburg) for receiver construction and tests. A prototype IF processor has been constructed at NOVA. New ones are being constructed in São Paulo, with Total Power output for continuum observations and an 8-module FFT Spectrometer for line observations. An optical system has been constructed to transport the radio beam to the Nasmyth cabins, with ten remotely-controlled mirrors to select the receiver. It provides support to the cryostat and the calibration system, with two temperature-controlled loads. Its mechanical structure was built by ALFA Ferramentaria in Araraquara, São Paulo State. A refractor optical telescope mounted in a hole of the dish, with a protection tube and shutter, will be used for setting the parameters of the pointing model. For the alignment of the panels of the dish, near-field holography will be used, to reach a surface rms accuracy of 20  $\mu\text{m}$ . The holography receiver will be on loan from NRAO, and a transmitter is being developed in Brazil. The software will control remotely the motion of the dish, receivers, spectrometer, calibration loads. It will perform data acquisition and storage, quick view of the results, sensor monitoring, and more. We use the ACS infrastructure of ALMA for integration and specific local softwares for many instruments.

*Keywords* / instrumentation: miscellaneous

*Contact* / jacques.lepine@iag.usp.br



## IVIA: Ibero-American VLBI Initiative

J. Lepine<sup>1</sup>, J-P. Raulin<sup>2</sup>, T. Dominici<sup>3</sup>, G.G. Castro<sup>2</sup>, F. Roig<sup>4</sup>, A. Wiermann<sup>4</sup>, R. Hadano<sup>2</sup>, S. Lucena<sup>5</sup>, M. Garcia<sup>5</sup>, F. Correr<sup>1</sup>, W. Beccari<sup>1</sup>, M. Luqueze<sup>1</sup>, S. Verri<sup>1</sup>, D. Zanella<sup>1</sup>, K. Melendez-Delmestre<sup>6</sup>, T. Gonçalves<sup>6</sup>, U. Barres<sup>7</sup>, M. Borges<sup>4</sup>, M. Figueredo<sup>8</sup>

<sup>1</sup> *Universidade de São Paulo, São Paulo, Brazil*

<sup>2</sup> *Universidade Presbiteriana Mackenzie, São Paulo, Brazil*

<sup>3</sup> *Museu de Astronomia e Ciências Afins, MAST-MCTI, Rio de Janeiro, Brazil*

<sup>4</sup> *Observatório Nacional, OB-MCTI, Rio de Janeiro, Brazil*

<sup>5</sup> *Star One company, Rio de Janeiro, Brazil*

<sup>6</sup> *Universidade Federal de Rio de Janeiro, Brazil*

<sup>7</sup> *Centro Brasileiro de Pesquisas Físicas, Rio de Janeiro, Brazil*

<sup>8</sup> *Universidade Federal do Vale do São Francisco, Petrolina, Pernambuco, Brazil*

The IVIA groups plans to use large antennas in Ibero-America used for telecommunications in the past, to construct a VLBI network. In each country the effort will be in two steps: 1) Refurbish an antenna and install a 4–8 GHz receiver with Total Power detection and a spectrometer, and use the antenna for single dish observations; 2) Acquire the equipment for VLBI observations (atomic clock, IF processor and data storage system), then start VLBI observations. The expected benefits are many, like scientific and technical coordination between the institutions involved, organization of regional workshops and schools, approach to international entities for collaboration, and promotion of science with visibility for the public. The involved institutions and countries are Instituto de Radioastronomía y Astrofísica, UNAM, Mexico; Centro de Investigaciones Espaciales, Costa Rica; Observatorio Astronómico de Córdoba, Argentina; Universidad Nacional del Centro del Perú; Universidad ECCI y Oficina Regional Andina de Astronomía, Bogotá, Colombia; Universidad de São Paulo, Brazil; Ministerio de Industria, Energía y Minería, Uruguay; Observatorio Astronómico de Quito, Ecuador; Instituto Geográfico Nacional, Spain; and Instituto de Telecomunicações, Aveiro, Portugal. The Brazilian IVIA group obtained agreement from the director of Star One company to use one of their 32 m antennas. We inspected the antenna at Tanguá, 50 km North of Rio de Janeiro. We made a diagnostic of the work needed for refurbishment. The dish must be washed, some components replaced (motors, encoders), rust removed. The cost of refurbishment, not including receivers, will be about 200 000 USD. We still have to visit the Morungaba antenna, which may be in a better condition.

*Keywords* / instrumentation: miscellaneous

*Contact* / jacques.lepine@iag.usp.br

## Unveiling the properties of strong emission-line galaxies at redshift 2–4

M. Llerena<sup>1</sup>, R. Amorín<sup>1,2</sup>

<sup>1</sup> *Departamento de Astronomía, Universidad de La Serena, La Serena, Chile*

<sup>2</sup> *Instituto de Investigación Multidisciplinar en Ciencia y Tecnología, Universidad de La Serena, La Serena, Chile*

The first 2–3 Gyr of cosmic history ( $z > 2 - 3$ ) are key to understand how most present-day galaxies form and assemble and what is the role and relevance of star-forming galaxies in cosmic reionization at  $z > 6$ . According to recent observations, normal galaxies at these early epochs show more extreme stellar and nebular properties compared to their lower redshift counterparts, but the connection between these properties and the physical mechanisms facilitating galaxy growth and the escape of ionizing photons used for reionization still needs to be established. After the discovery of ten young, low-mass galaxies at  $z \sim 2.4 - 3.5$ , showing extremely compact HST morphologies and unusually strong Ly $\alpha$  emission and UV nebular lines (C IV, C III], He II, and O III]) in VIMOS Ultra Deep Survey spectra, deep near-IR X-shooter follow-up observations of four of them were conducted. With the goal of better constrain the emission-line properties from their rest optical spectrum, here we present the initial analysis of such dataset and the future plans to go ahead. We also present a first glance of a similar analysis which is being carried out using the unprecedented deep VANDELS survey, from which  $\sim 220$  C III]-emitting galaxies have been selected.

*Keywords* / galaxies: high-redshift — galaxies: evolution — galaxies: formation — cosmology: dark ages, reionization, first stars

*Contact* / mario.llerena@userena.cl



## Magnetic accretion in SW Sextantis stars

I.J. Lima<sup>1,2</sup>, C.V. Rodrigues<sup>1</sup>, P. Szkody<sup>2</sup>, C.E.F. Lopes<sup>1</sup>, F.J. Jablonski<sup>1</sup>, K.M.G. Silva<sup>3</sup>, A.S. Oliveira<sup>4</sup>, M.S. Palhares<sup>4</sup>, S. Shugarov<sup>5</sup>

<sup>1</sup> *Instituto Nacional de Pesquisas Espaciais (INPE/MCTIC), São José dos Campos - SP, Brazil*

<sup>2</sup> *Department of Astronomy, University of Washington, Seattle, WA, USA*

<sup>3</sup> *European Southern Observatory - Vitacura, Santiago de Chile, Chile*

<sup>4</sup> *IPED, Universidade do Vale do Paraíba, São José dos Campos, SP, Brazil*

<sup>5</sup> *Astronomical Institute of the Slovak Academy of Sciences, Slovakia*

Magnetic cataclysmic variables are compact binary systems in which mass transfer occurs from a low-mass star onto a magnetic white dwarf. In polars and intermediate polars sub-classes, the magnetic field of the white dwarf is strong enough to disrupt the inner accretion disc or even completely prevent disc formation. SW Sex stars are a type of nova-like cataclysmic variables, which show observational characteristics that indicate matter outside the orbital plane is distributed asymmetrically in azimuth. Many scenarios have been proposed to explain the SW Sex behavior; one of them is magnetic accretion. In order to search for evidence of magnetic accretion in SW Sex stars, we analyzed a set of photopolarimetric data of BO Cet, SW Sex, V442 Oph, V380 Oph, LS Peg, and UU Aqr. Polarized cyclotron emission is a distinguishing signal of magnetic accretion. If SW Sex stars have magnetic accretion, multi-periodicity can be a typical feature of these systems as the white dwarf spins asynchronously with the orbital period. In SW Sex, the prototype of the class, we found a period of 22.6 min in the photometry. In V442 Oph, we found a period of 12.4 min in the photometric data and its harmonics from circular and linear polarimetric data. Both systems have periods that can be related to the rotation of the magnetic white dwarfs, but a much larger data set will be needed to confirm or reject the periodicity. We found a strong peak centred at 138.2 min from a 14-year long photometric dataset of the V380 Oph. This period can be the spin period of the white dwarf, as well as the period of  $\sim 19$  min found in LS Peg from circular polarimetric data. This period was previously reported. In BO Cet, period analysis yields a period of 11.3 min in circular polarimetric data with the first harmonic at 22.6 min in linear polarization. In UU Aqr, we found a period of 4.2 h from photometric data, consistent with the positive superhump.

*Keywords* / accretion, accretion discs — methods: analytical — techniques: polarimetric — binaries: close — stars: novae, cataclysmic variables

*Contact* / isabellima01@gmail.com

## Cataclysmic variables with enhanced emission regions

P. Longa-Peña<sup>1</sup>, D. Barría<sup>2</sup>, H. Salas<sup>1</sup>, M. Romero<sup>1</sup>, D. Herrera<sup>2</sup>

<sup>1</sup> *Centro de Astronomía, Universidad de Antofagasta, Antofagasta, Chile.*

<sup>2</sup> *Instituto de Astronomía, Universidad Católica del Norte, Antofagasta, Chile.*

Doppler tomography is one of several methods used to detect and collect information about asymmetric emission sources detected at cataclysmic variables (CVs). It is currently understood that enhanced emission observed in the first quadrant of Doppler maps is due to the falling material impacting against the accretion disc (hot spot). There are, however, some systems which show an enhanced emission on the second and/or third quadrants. To date, these are emission features of unknown origin. In this work, we present a statistical analysis of a sample of 47 CVs showing asymmetric emission on the 2nd and 3rd quadrants of their Doppler maps. Main stellar and orbital parameters of the target binaries were collected from the literature in order to investigate if these systems are sharing common physical properties and thus explore on the physical mechanism(s) which might trigger these enhanced emissions. We found that the orbital periods, individual masses and mass ratio values are consistent with the general CV population. However, the studied sample exhibit higher mass transfer rate and primary temperature in comparison to their counterparts. These preliminary results shed light on a common property of the systems with atypical asymmetrical emission in their Doppler maps.

*Keywords* / stars: novae, cataclysmic variables — stars: dwarf novae — stars: emission-line, Be — stars: fundamental parameters

*Contact* / penelope.longa@uamail.cl



## Diffraction in stellar occultations reproduced in laboratory

L.E. Manzano<sup>1</sup>, J. H. Castro-Chacón<sup>2</sup>

<sup>1</sup> *Observatorio Astronómico, Universidad Tecnológica de Pereira, Colombia*

<sup>2</sup> *CONACYT - Instituto de Astronomía, Universidad Nacional Autónoma de México*

Kuiper Belt Objects (KBOs), as a consequence of their weak gravitational influence, as well as for their dynamical characteristics and composition, are key to understand the formation and evolution processes of the Solar System. Due to the distances and sizes of small KBOs, their direct observation is extremely challenging. In this sense, the Transneptunian Automated Occultation Survey (TAOS II) has the objective of detecting kilometer-sized KBOs through serendipitous stellar occultations. The theoretical models that predict the light curves which will be registered by this project, and from which the objects' characteristics will be determined, are based in the diffraction phenomena, taking instrumental effects into account as well. To date, a stellar occultation record by a kilometer-sized KBO has not been yet confirmed; this is why the only way to validate the computational models is in a laboratory. In this work, stellar occultations were reproduced with an experiment. An experimental assembly was set using a monochromatic light source, optical elements, a CNC machine and a high cadence camera to represent scaled different elements involved in a stellar occultation. The TAOS II operational parameters and the Fresnel scale were also taken into account. Once the captures were obtained, aperture photometry was implemented to derive the diffraction profiles, which were compared with the theoretical results of the simulator. As a result, it was possible to reproduce light curves of non-spherical objects obtained in the laboratory with the simulator, both for single and binary objects. Characteristic diffraction effects were reproduced in the laboratory, such as the Poisson spot, and brightness increase in profiles outside of the shadow path. We conclude that the TAOS II simulator correctly predicts the diffraction profiles obtained in the laboratory.

*Keywords* / occultations — Kuiper belt: general — instrumentation: miscellaneous

*Contact* / leksamz@utp.edu.co

## Binary interactions in a static filament

M.C. Morales<sup>1</sup>, M. Fellhauer<sup>1</sup>

<sup>1</sup> *Universidad de Concepción, Departamento de Astronomía, Concepción, Chile.*

From the observational data of Orion A Integral Shaped Filament (ISF), a previous work proposed an oscillatory motion of the gas filament called “Slingshot Mechanism” to explain the symmetric spread of older stars (Class II). The wave-like morphology of the filament and the kinematics of the gas and stars support this theory. Using the Astrophysical Multi-purpose Software Environment (AMUSE), it was possible to couple an accelerated cylindrical potential with an  $N$ -body solver to study the dynamics of the stars near the ISF. These simulations were able to reproduce the symmetric spread of the stars around the filament. We are now trying to see if an alternative scenario with a static filament can reproduce the same observational findings. Using MCLUSTER we generate binary systems distributed inside the ridgeline ( $r \sim 0.05$  pc) of a static analytic filament, to investigate if pure  $N$ -body interactions can lead to the same final distribution of older stars. Our first test with only 25 binary systems evolved for 2 Myr, and we find that a few stars are ejected from their initial locations to far away distances. However, one low-mass star ( $\sim 0.16 M_{\odot}$ ) was ejected perpendicular to the filament with  $v_x \sim -4.1 \text{ km s}^{-1}$ . As already mentioned in a previous work, using a crude back of the envelope calculation we see that simple  $N$ -body encounters are not enough to produce the observed symmetric distribution of stars. We still have to check our findings using the correct number of observed stars. These computationally-expensive simulations will be presented in the final thesis of MCM. We also want to check different initial conditions to make sure we can exclude the static filament hypothesis.

*Keywords* / methods: numerical — stars: kinematics and dynamics

*Contact* / matiascmorales@udec.cl



## Five-year spectral monitoring of Alpha Sco

B. Oostra<sup>1</sup>, M.G. Batista<sup>1</sup>, L.F. Rodríguez<sup>1</sup>

<sup>1</sup> *Universidad de los Andes, Bogotá, Colombia*

ESPARTACO is a high-resolution spectrograph designed and built in the Astronomical Observatory of the University of Los Andes in Bogotá, Colombia. Operating at a resolution of 31000, we have developed a spectral monitoring of Antares A since 2015, in order to assess its radial velocity variations at different timescales. From the observational data, we estimated its mean radial velocity around  $-3 \text{ km s}^{-1}$  with variations between  $+1 \text{ km s}^{-1}$  and  $-8 \text{ km s}^{-1}$  as evidence of its pulsation pattern. Previous works from other research groups have also carried out a spectral monitoring of Alpha Scorpii A, however, our work intends to enhance the temporal resolution and coverage. The data was obtained from 444 spectra along 108 nights employing a 40-cm telescope and the aforementioned high-resolution spectrograph. We observed some evidence of convective dynamics in the photosphere, consisting in systematic differences between the radial velocity accused by different absorption lines. The observations are expected to continue for a few more years because the fundamental oscillation period of Antares A is close to 2200 days.

*Keywords* / stars: individual: Antares — stars: oscillations

*Contact* / boostra@uniandes.edu.co, mg.batistar@uniandes.edu.co

## The 3D positions of gas and dust clouds in the Galactic centre

C. Ordenes-Huanca<sup>1</sup>, J. Cuadra<sup>1</sup>, Q.D. Wang<sup>2</sup>

<sup>1</sup> *Instituto de Astrofísica, Facultad de Física, Pontificia Universidad Católica de Chile, Chile*

<sup>2</sup> *Department of Astronomy, University of Massachusetts Amherst, USA*

Our work is focused on the nuclear star cluster and the nuclear disc of the Milky Way. More specifically, we consider the clouds of gas and dust that reside in this region and try to determine their 3D positions. Knowing the location of the clouds can tell us about, first, the recent history of Sgr A\*, as the clouds reflect the light that it emitted during its more active phases. Second, it can help us understand how star formation proceeds in extreme environmental conditions. The clouds are likely to form stars, a process which may well be regulated by the strong tidal field in the inner Galactic regions. To determine the clouds' 3D positions we consider that they obscure and redden the emission of the nuclear stars. As a first step in our project, we produce mock 3D distributions of clouds and stars and calculate the expected obscuration. We will discuss the results of recovering the 3D positions from the mock observations, and our plans to apply this method to actual observed data.

*Keywords* / Galaxy: centre — ISM: clouds

*Contact* / cordenes@astro.puc.cl



## Search of exoplanets around evolved binary stars

E.S. Pereira<sup>1</sup>, L.A. Almeida<sup>2</sup>, M.G. Pereira<sup>3</sup>, T.A. Michtchenko<sup>1</sup>

<sup>1</sup> *Instituto de Astronomia, Geofísica e Ciências Atmosféricas, IAG-USP, São Paulo-SP, Brazil.*

<sup>2</sup> *Universidade Estadual do Rio Grande do Norte, UERN, Mossoró-RN, Brazil.*

<sup>3</sup> *Universidade Estadual de Feira de Santana - UEFS, Feira de Santana-BA, Brazil.*

The planetary formation and evolution around binary systems is one of the open questions in the field of exoplanet research. Thanks to the *Kepler* mission, it is now known that some non-evolved binaries (systems with two main-sequence stars) host exoplanets. However, in recent years other questions have been raised: do exoplanets survive the most energetic phases of the host binary evolution? If so, what would be the dynamic evolution of these bodies? In the last years the presence of a few substellar candidates have been indirectly inferred around evolved post-common-envelope binaries using the eclipse timing variation method. These systems consist of either a white dwarf or a hot subdwarf as the primary star and a red dwarf companion in a close orbit ( $P < 1$  day). The method consists in searching for small but significant variations in the eclipse timings. These variations are usually explained by the light-travel-time effect which is a periodic effect caused by the gravitational interaction among the inner binary and circumbinary bodies. So in the last ten years, photometric observations have been carried out by our group using the Pico dos Dias Observatory (OPD/LNA) facilities for a selected sample of evolved short-term eclipsing binaries. In this work, we will present the current status of the observational program as well as the pilot project for the QS Vir system. This system consists of a white dwarf and a M3.5 red dwarf star in a short orbital period (3.618 hours). The variations of the orbital period of QS Vir have not been completely explained yet in the literature. Our good solution for the orbital period variation yields two circumbinary bodies (a brown dwarf and a giant planet) and possible mass transfer effects. Dynamical analysis has been performed to verify if the system has (or has not) long-term stability.

*Keywords* / binaries: eclipsing — white dwarfs — planetary systems — stars: individual: QS Vir

*Contact* / elielson.pereira@usp.br

## GW170817-like events in Chandra X-ray catalog

J. Quirola-Vásquez<sup>1,2</sup>, F.E. Bauer<sup>1,2,3</sup>

<sup>1</sup> *Instituto de Astrofísica, Pontificia Universidad Católica de Chile, Santiago, Chile*

<sup>2</sup> *Millennium Institute of Astrophysics (MAS), Santiago, Chile*

<sup>3</sup> *Space Science Institute, Boulder, Colorado 80301, USA*

The recent discovery of two fast X-ray transients in the *Chandra* Deep Field-South, potentially associated with magnetar wind interactions due to the merger of neutron stars, and X-ray counterparts of GW170817-like events, has sparked great interest in this type of transient. We developed a search for similar objects hidden in the *Chandra* Source Catalog (CSC 2.0), a database of  $\sim 220\,000$  serendipitous X-ray sources, as well as a cross-match with optical and infrared catalogs. Using two distinct methods, we found 17 transient candidates which could be related to extragalactic objects, 10 of which have clear optical/NIR counterparts ( $R < 23.5$ ) and 6 have only upper limits. These new candidates provide up to an order of magnitude increase in source statistics and should allow better constraints on the emission mechanisms for this emerging transient class.

*Keywords* / X-rays: general — gravitational waves

*Contact* / jquirola@astro.puc.cl



## The Universe as a statistical ensemble

N.B. Razo López, A.M. Cervantes Contreras

<sup>1</sup> *Universidad Autónoma de Querétaro, México*

Based on observational data from type Ia supernovae, an effective potential capable of generating the observed expansion of the Universe was built. Accordingly, the (non-geometric) Lagrangian and Hamiltonian for the Universe in terms of the energy were written. Through a statistical-mechanical approach, the Hamiltonian was analysed as a canonical ensemble to calculate the current temperature of the system (the Universe) and compare it to actual measurements of the Cosmic Microwave Background.

*Keywords* / cosmology: theory — cosmic background radiation

*Contact* / naela.r@hotmail.com

---

## Kinematical analysis of lines in high-ADF planetary nebulae

F. Ruiz-Escobedo<sup>1</sup>, M. Peña<sup>1</sup>

<sup>1</sup> *Instituto de Astronomía, UNAM, México*

In the aim to prove the validity of the theory of the two-coexistent plasmas in planetary nebulae (PNe) as the origin of the abundance discrepancy factor (ADF), we performed an analysis of the collisionally excited lines (CELs) and optical recombination lines (ORLs) for NGC 6891, NGC 6778 and Vy 2-2. For this work we used deep and high-resolution spectra, obtained with the ECHELLE-REOSC spectrograph attached to the 2.1 m telescope at OAN-SPM, to measure the fluxes and FWHM of the different CELs and ORLs available in their spectra. Then we computed their expansion velocities ( $v_{\text{exp}}$ ), as function of the distance to the central star; we also determined the physical conditions and abundances (ionic and total) for the three PNe. We found that CELs and ORLs of  $\text{O}^{+2}$  have different  $v_{\text{exp}}$  and FWHM. For NGC 6778,  $v_{\text{exp}}([\text{O III}]) > v_{\text{exp}}(\text{O II})$ , while for NGC 6891 and Vy 2-2,  $v_{\text{exp}}(\text{O II}) > v_{\text{exp}}([\text{O III}])$ .

*Keywords* / ISM: kinematics and dynamics — planetary nebulae: general

*Contact* / fdruiz@astro.unam.mx



## A new family of analytical potential–density pairs for galaxy models with thin disks and spheroidal halos

Y.F. Santos<sup>1</sup>, O.M. Pimentel<sup>1</sup>, G.A. González<sup>1</sup>

<sup>1</sup> *Universidad Industrial de Santander UIS, Escuela de Física, Bucaramanga, Colombia*

In this work a new family of galaxy models is constructed, which are characterized by having two components, a thin disk of matter and a large halo. The models were obtained considering the total gravitational potential. The gravitational potential generated by the spheroidal halo of matter is constructed considering a multipolar expansion, expressed in cylindrical coordinates. As this potential is a solution of the Laplace equation, a change of variables is done so that the Laplacian is nonzero over the  $z$  axis. So the new potential satisfies the Poisson equation and represents the potential distribution of three-dimensional material. From the gravitational potential we raised analytical expressions for the surface density of the disk, halo density of matter and the corresponding expressions for the curves of rotation. We found that the surface density of the disk presents a maximum at the center, vanishing at infinity. Also, we found that the halo density is maximum at the disk surface, also vanishing at infinity. The rotation curves obtained, for some values of the parameters, present a flat region for large values of the radial coordinate .

*Keywords* / galaxies: kinematics and dynamics

*Contact* / santosfabiany@gmail.com

---

## The VISCACHA survey - structure of outer MC star clusters

J.F.C. Santos Jr.<sup>1,2</sup>, F. Maia<sup>3</sup>, B. Dias<sup>4</sup>, L. Kerber<sup>5</sup>, A. Piatti<sup>6</sup>, E. Bica<sup>7</sup>, the VISCACHA team

<sup>1</sup> *Departamento de Física, ICEx - UFMG, Belo Horizonte, Brazil*

<sup>2</sup> *Departamento de Astronomía, Universidad La Serena, La Serena, Chile*

<sup>3</sup> *Instituto de Física - UFRJ, Rio de Janeiro, Brazil*

<sup>4</sup> *Departamento de Ciencias Físicas, Universidad Andrés Bello, Santiago, Chile*

<sup>5</sup> *Departamento de Ciências Exatas e Tecnológicas, UESC, Brazil*

<sup>6</sup> *Observatorio Astronómico, Universidad Nacional de Córdoba, Argentina*

<sup>7</sup> *Departamento de Astronomia, IF - UFRGS, Brazil*

The Magellanic Clouds (MCs) constitute an interacting pair of galaxies influenced by the Milky Way gravitational field. Several studies have shown the effects of the changing tidal field on the structure of both Clouds. How the varying tidal field affects their stellar populations may be gauged via star clusters, where this connection may be more confidently established due to the accurate determination of the clusters astrophysical properties. Our objective is to perform an analysis of the structural parameters of 56 Large Magellanic Cloud (LMC) and 34 Small Magellanic Cloud (SMC) clusters located in the galaxies outskirts searching for signatures of tidal-dynamical effects eventually altering their evolution. To achieve our goal, AO assisted observations in BVI bands with the 4.1m SOAR telescope have been carried out, in the scope of the VISCACHA (VIvisible Soar photometry of star Clusters in tApii and Coxi HuguA) survey, in which an homogeneous, deep and high quality photometry is being produced. The structural parameters central stellar density, central surface brightness, core and tidal radius were obtained from King model fittings to the surface brightness and radial density profiles. By grouping clusters according to different regions we found that (i) the westernmost LMC clusters, the nearest ones to the SMC, have a larger dispersion of their core radius than those of the clusters located elsewhere; (ii) older clusters present a spread of core radius, similar to results from studies of inner MCs populous clusters.

*Keywords* / galaxies: star clusters: general — Magellanic Clouds

*Contact* / jsantos@fisica.ufmg.br



## VHE $\gamma$ -rays from the Galactic center generated by cosmic rays

A. Scherer<sup>1</sup>, A. Reisenegger, J. Cuadra<sup>1</sup>

<sup>1</sup> *Instituto de Astrofísica, Pontificia Universidad Católica de Chile, Santiago, Chile*

Through observations in very-high-energy (VHE)  $\gamma$ -rays, the High Energy Stereoscopic System (HESS) allowed studying the properties of the VHE  $\gamma$ -ray emission from the Galactic center (GC) between 0.1 TeV and 100 TeV. HESS observed a  $\gamma$ -ray diffuse emission strongly correlated with the central molecular zone (CMZ) morphology, showing energies above 30 TeV. The best scenario to generate the  $\gamma$ -ray diffuse emission is hadronic interaction between cosmic rays (CR) and the ambient gas. The observed  $\gamma$ -ray spectrum implies that the intrinsic CR spectrum could extend to energies  $\sim 1$  PeV. The CR density profile in the CMZ shows an increased density towards the GC that is consistent with a source within the central 10 pc, with a continuous injection of CR over at least  $10^4$  years. Protons could be accelerated close to the supermassive black hole Sagittarius A\* or inside the clusters of young massive stars of Arches, Quintuplet and Nuclear. The problem is that current diffusion models are spherical and isotropic, but the CR diffusion in the CG is anisotropic. We plan to model the VHE  $\gamma$ -ray emission from the CMZ between 0.1 TeV and 100 TeV, generated by CR, considering different geometries, time dependence, and spectra of CR injection. We will include different diffusion coefficients, polar advection, and compute the interaction of CR with observed ambient gas. From the model, we will get the  $\gamma$ -ray morphology and spectrum observed by HESS in the CMZ, and predict  $\gamma$ -rays observation by the Cherenkov Telescope Array in the CMZ and other molecular clouds. Finally, we will identify multi-wavelength and multi-messenger contributions.

*Keywords* / gamma rays: general — cosmic rays — Galaxy: center

*Contact* / ascherer@uc.cl

---

## Characterization of young stellar clusters and star-forming regions using S-PLUS

T. Santos-Silva<sup>1</sup>, J. Gregorio-Hetem<sup>1</sup>, V. Jatenco-Pereira<sup>1</sup>, S-PLUS collaboration

<sup>1</sup> *Instituto de Astronomia, Geofísica e Ciências Atmosféricas da Universidade de São Paulo, Brasil*

The Galactic Survey (GS) of the S-PLUS collaboration is focused in the Milky Way plane, covering approximately a  $1420 \text{ deg}^2$  area of which  $\approx 400 \text{ deg}^2$  are in the bulge ( $-10^\circ < l < 10^\circ$ ,  $-15^\circ < b < +5^\circ$ ), and  $\approx 1020 \text{ deg}^2$  are in the disk ( $220^\circ < l < 278^\circ$ ,  $-15^\circ < b < +5^\circ$ ), dedicated mainly for the studies of open clusters and variable stars. In order to develop the methods that will be used in the studies of young stellar clusters and star forming regions in the GS, we are using S-PLUS observations of Canis Majoris R1 (CMa R1) star-forming region. CMa R1 harbors the ionized nebula Sh2-296, and shows a mixture of populations originated from distinct star formation episodes, which makes it a true laboratory for the study of star forming regions. Color magnitude (CMD) diagrams are being tested using PARSEC isochrones to determine mass, age, distance, and reddening of the young stellar population. While CMDs made with reddish bands (e.g., F515, F660, F861) break the degeneracy for low masses that occurs in other CMDs (e.g. F395, F430, F515 bands), the bluish bands CMDs help to better separate the older ages ( $< 10$  Myr). For this reason, we are developing an automated method for determining these parameters, which takes into account more than one type of CMD. On the other hand, color-color diagrams are being used to reveal indicators of the chromospheric activity of late-type dwarf active stars, and to diagnose accretion in classical T Tauri (CTT) stars. Our test sample was able to find most CTT stars revealed by X-ray observations and by optical spectroscopy. These previous results show that the large number of bands present in S-PLUS will be a great ally in the studies of star forming regions and young stellar objects.

*Keywords* / stars: early-type — open clusters and associations: general — stars: formation — stars: pre-main sequence

*Contact* / thaisfi@gmail.com



## Non-spherical distribution of rotational velocities of Be stars via Tikhonov deconvolution

M. Solar<sup>1</sup>, M. Curé<sup>1</sup>, D. Rial<sup>2</sup>, A. Christen<sup>3</sup>, J. Cassetti<sup>4</sup>

<sup>1</sup> *Universidad de Valparaíso, Chile*

<sup>2</sup> *Universidad de Buenos Aires, Argentina*

<sup>3</sup> *Pontificia Universidad Católica de Valparaíso, Chile*

<sup>4</sup> *Universidad Nacional de General Sarmiento, Argentina*

Be stars are the fastest rotators and its nature is not completely understood. We aim to determine the probability density function (PDF) and the cumulative density function (CDF) of true rotational velocities of Be field stars, and to study whether the rotation axes are non-uniformly distributed over the unit sphere. We deconvolve the true rotational velocities ( $v$ ) from a sample of 461 Be-star projected rotational speeds via Tikhonov regularization to obtain their PDF and CDF. For this purpose we developed a model with the apparent rotational velocity ( $v \sin i$ ) and a non-uniform projection of axes given by the power law  $1 + \alpha$  in the Fredholm integral. The  $\alpha$  parameter takes into account the non-sphericity and  $i$  is the inclination angle between the star's pole and the line of sight. A non-spherical distribution ( $\alpha = 75.8$ ) of rotational velocities fits better the data than the uniform case ( $\alpha = 0$ ). This is our first theoretical model to pick out if a sample comes from a non-spherical distribution of rotational axes. In the future, we will improve our description of non-spherical distribution of axes that consider a privileged direction of these axes. We also want to include more observations of Be stars and extend the study to rotational velocities in open clusters.

*Keywords* / stars: emission-line, Be — stars: rotation

*Contact* / msolar95@gmail.com

## Atacama region as a planetary analog for astrobiology

A. Tavernier<sup>1</sup>, M. Barbieri<sup>1</sup>, R. Osés<sup>1,2</sup>, A. Garcia<sup>1</sup>, C. Ulloa<sup>1</sup>

<sup>1</sup> *Universidad de Atacama, Copiapó, Chile*

<sup>2</sup> *Universidad de La Serena, La Serena, Chile*

One possible approach in astrobiology is to use the range of possibilities offered by the Earth to study geographical niches that could be similar to environments observed on planets or satellites of the Solar System. We will discuss the relevance of a particular region of the Atacama Desert in the Chilean Puna de Atacama, in the vicinity of the city of Copiapó (27°36 S / 70°33 W) in Chile, as a natural laboratory for astrobiology and planetary sciences. The environment of the mountain range in the Atacama region, with a stable cold desert climate for tens of millions years, includes hydrothermal springs, permafrost, glaciers and an interconnected water circulation between its salt lakes. The extreme physico-chemical characteristics of these different environments make the Chilean Puna de Atacama region a unique site in terms of the density of ecosystems that could be used for planetary analogy and astrobiology, especially for the study of extremophiles. Several tasks within the area of consideration will be carried out through the period 2020–2023: to search for sites with significant environmental gradients which can reproduce the current or past conditions observed on Mars or other bodies; to continue the microbiological inventory of the area and to do long-term monitoring of microbiological diversity in the most promising ecological niches. These experiments will benefit from the facilities of the Atacama high altitude laboratory, a multidisciplinary project led by the University of Atacama and including astronomical and planetary sciences projects. This laboratory will be built at the end of 2020 in the vicinity of the Salar de Maricunga (26°85 S / 69°03 W) at 3800 m asl. This scientific station will serve from 2021 to 2023, for 18 months, as a base camp for expeditions aimed at carrying out preparatory work. Then, in 2023, another laboratory and permanent measuring stations will be installed above 5200 m asl close to the Ojos del Salado (27°11 S / 68°54 W).

*Keywords* / astrobiology — Earth — methods: miscellaneous — planets and satellites: surfaces

*Contact* / adrien.tavernier@postgrados.uda.cl



## “Noche de las Estrellas”: a success story in Mexico and in other countries

S. Torres-Peimbert<sup>1</sup>, B. Arias<sup>1</sup>, E. Velarde<sup>1</sup>, J. Franco<sup>1</sup>

<sup>1</sup> *Instituto de Astronomía, Universidad Nacional Autónoma de México, México*

As part of the celebrations of the International Year of Astronomy 2009, collective star parties were organized to share with the general public the beauties of the sky. The effort was so well received and attracted such a large number of participants, that it has been repeated yearly. These star-gazing parties have been organized in several cities simultaneously; small telescopes are installed in selected places and other activities that highlight astronomy are presented. A specific date is selected in advance, and as many sites are invited to participate. Other countries that have participated in these star-parties are: Argentina (2015), Brasil (2015), China (2014), Colombia (from 2012 to 2018), Costa Rica (2015), Guatemala (2012), and Puerto Rico (2012). The most attended events have regularly taken place at Universidad Nacional Autónoma de México, UNAM in Mexico City.

*Keywords* / general: miscellaneous

*Contact* / [silvia@astro.unam.mx](mailto:silvia@astro.unam.mx)

---

## Revista Mexicana de Astronomía y Astrofísica:

S. Torres-Peimbert<sup>1</sup>, C.Allen<sup>1</sup>

<sup>1</sup> *Instituto de Astronomía, Universidad Nacional Autónoma de México, Mexico*

The Revista Mexicana de Astronomía y Astrofísica (RMxAA) was founded in 1974; it publishes original research papers in all branches of astronomy, astrophysics and closely related fields. No page charges nor submission or refereeing fees for publication are charged. Papers are published in English, with an abstract in Spanish. Two issues per year are published. The distribution has been free of charge and has included astronomical institutions in 50 countries. All papers are peer-reviewed. Until 1994 it also published as special volumes the proceedings of meetings held in Mexico and Latin America. In 1995 a separate journal, the Revista Mexicana de Astronomía y Astrofísica – Serie de Conferencias (RMxAC), was founded for this purpose. Both RMxAA and RMxAC are fully integrated into the ADS data base, which gives them wide visibility. They are open access journals, which can be found at <http://www.astrocu.unam.mx/RMxAA/> and <http://www.astrocu.unam.mx/RMxAC/>. From 1974 to 2019 it has published 1050 refereed articles. Its impact factor in 2018 was of 2.380. In 2018 Scopus classified it in the 5th place among all Latin Americans scientific journals and in the second quartile (Q2). The proceedings of 64 astronomical conferences have been published; 13 in RMxAA (prior to 1995) and 51 in RMxAC; 3 IAU Colloquia; 14 Latin American Regional IAU meetings; 4 “Astronomy with Gran Tecan” meetings, and 5 Dynamical Astronomy in Latin America –ADeLA– meetings.

*Keywords* / general: miscellaneous

*Contact* / [silvia@astro.unam.mx](mailto:silvia@astro.unam.mx)



## Pathway to black hole formation in protostar clusters

M.Z.C. Vergara<sup>1</sup>, D.R.G. Schleicher<sup>1</sup>, T. Boekholt<sup>2,3</sup>, B. Reinoso<sup>1</sup>, M. Fellhauer<sup>1</sup>, R.S. Klessen<sup>4,5</sup>, N. Leigh<sup>1</sup>, V.B. Díaz<sup>1</sup>

<sup>1</sup> *Departamento de Astronomía, Facultad Ciencias Físicas y Matemáticas, Universidad de Concepción, Chile*

<sup>2</sup> *CIDMA, Departamento de Física, Universidade de Aveiro, Campus de Santiago, Aveiro, Portugal*

<sup>3</sup> *Instituto de Telecomunicações, Campus Universitário de Santiago, Aveiro, Portugal*

<sup>4</sup> *Universität Heidelberg, Zentrum für Astronomie, Institut für Theoretische Astrophysik, Heidelberg, Germany*

<sup>5</sup> *Universität Heidelberg, Interdisziplinäres Zentrum für Wissenschaftliches Rechnen, Heidelberg, Germany*

In the early Universe and at low metallicities, the fragmentation often occurs in disk-like structures. Supermassive black holes (SMBHs) are astrophysical objects with an enigmatic origin, weighting millions of solar masses and residing in the centers of galaxies. An important formation scenario for the seed of SMBHs concerns the collisions and mergers of stars in a massive cluster with a high stellar density, in which the most massive star falls to the center of the cluster due to dynamical friction. This increases the rate of collisions and mergers since this new object has a larger collisional cross-section than other stars in the cluster. Once several collisions have occurred, a very massive star forms which may collapse to become an intermediate-mass black hole. Here we investigate the impact of rotation and flattening of dense protostellar clusters on the rate of formation of massive stars through collisions, which will later evolve into massive black holes. We use the Miyamoto-Nagai distribution to represent our model and employ  $N$ -body simulations to show, in detail, how flattening and rotation affect the number of collisions and the formation of a more massive object. Our preliminary results suggest that rotation keeps more stars in the system because fewer stars escape from it. However, the collisions are limited because they cannot sink to the center due to the ordered movement of the system. On the other hand, flattening increases the collisions due to the larger number density of the protostars.

*Keywords* / cosmology: theory — early Universe

*Contact* / marccortez@udec.cl

---

## Bayes-based estimation of orbital parameters in hierarchical triple stellar systems

C.L. Villegas<sup>1</sup>, R.A. Méndez<sup>2</sup>, M.E. Orchard<sup>1</sup>, J.F. Silva<sup>1</sup>

<sup>1</sup> *Departamento de Ingeniería Eléctrica, Facultad de Ciencias Físicas y Matemáticas, U. de Chile, Chile*

<sup>2</sup> *Departamento de Astronomía, Facultad de Ciencias Físicas y Matemáticas, U. de Chile, Chile*

This work presents a Bayesian methodology for estimating the orbital parameters in hierarchical triple stellar systems, using astrometry and radial velocity measurements, that considers the use of graphical models based on the system dynamics. Graphical models provide a novel way of performing the factorization of the joint distribution in terms of conditional independent components. Considering this factorization, certain orbital parameters get disjoint and, as a result, the estimation can be performed in a two-stage process independent of the available sources, that combines different observations sequentially. The method is employed in a few well-studied benchmark cases of triple systems and the results are very promising.

*Keywords* / methods: data analysis — stars: fundamental parameters

*Contact* / constanza.villegas@ug.uchile.cl

## Índice alfabético

- Abraham, Z., 83, 91  
Adduci Faria, S., 80  
Alarcón Jara, A.G., 37, 40, 51, 77  
Alistar Seguel, P.J., 74  
Allen, C., 101  
Almeida, L.A., 96  
Amorín, R., 92  
Amram, P., 45  
Anais Vilchez, J., 80  
Anders, F., 38  
Andonie, C., 39  
Andrade, N.F.S., 81  
Arancibia, J., 81  
Aravena, C.A., 40, 51, 77  
Araya, I., 41  
Arcos, C., 41  
Argudo-Fernández, M., 42  
Arias, B., 101  
Arroyo, D., 86  
Ascasibar, Y., 66  
Astudillo-Defru, N., 90  
Ávila, P.J., 82  
Aydar, C.P., 82
- Balkowski, C., 45  
Balogh, M., 61  
Bandyopadhyay, B., 74  
Barai, P., 16, 80  
Barbieri, M., 100  
Barbosa-Santos, J.H., 73  
Barría, D., 43, 93
- Barrado, D., 81  
Barrera-Ballesteros, J.K., 1  
Barres de Almeida, U., 19, 92  
Bassino, L.P., 44  
Batista, M.G., 83, 95  
Bauer, F.E., 39, 96  
Baume, G., 68  
Bayo, A., 81  
Beaklini, P.P.B., 83, 91  
Beccari, W., 91, 92  
Becerra, L., 84  
Bellocchi, E., 66  
Benvenuto, O.G., 6  
Bernal, S., 84  
Bica, E., 98  
Boekholt, T., 74, 102  
Boquien, M., 22, 42, 48  
Borges, M., 92  
Borissova, J., 84  
Boshkayev, K., 84  
Bouvier, J., 81  
Bouy, H., 81  
Bovino, S., 49, 52, 82  
Branco, V., 85  
Brandner, W., 81  
Bravo-Castillo, C., 74, 85  
Burgos, G., 86  
Burningham, B., 47  
Bustos, R., 65
- Calderón, P.A., 87

Calderón-Galaz, C., 86  
Cardona, G., 87, 91  
Carignan, C., 45  
Carmo, A., 88  
Carnero Rosell, A., 47  
Carraro, G., 11  
Casimiro, M.C.M., 88  
Caso, J.P., 44  
Cassetti, J., 100  
Castro, G.G., 91, 92  
Castro-Chacón, J. H., 94  
Catelan, M., 88  
Cerulo, P., 61  
Cervantes Contreras, A.M., 97  
Chang, R., 42  
Chaparro, G., 65  
Chemin, L., 45  
Chiappini, C., 38  
Chow-Martínez, M., 66  
Christen, A., 41, 100  
Cidale, L., 41  
Clavería, H., 41  
Coelho, P.R.T., 85  
Colina, L., 48  
Correra, F., 91, 92  
Cortes, K., 86  
Costa, R.A. Mendez and E., 60  
Couto, G.S., 46  
Cross, N.J.G., 88  
CTA Consortium, 19  
Cuadra, J., 95, 99  
Curé, M., 41, 100  
  
da Silva Mesquita, D.A., 88  
dal Ponte, M., 47  
  
Dametto, N.Z., 48  
de Almeida, A.A., 53  
de Araújo, L.F., 53  
De Bórtoli, B.J., 44  
de Elía, G.C., 25, 72  
de Gouveia Dal Pino, E.M., 80  
del Pino, A., 37  
Demarco, R., 61  
Dias, B., 98  
Djurašević, G., 55  
Dominici, T.P., 83, 88, 91, 92  
dos Santos, C.P., 88  
Downes, J.J., 72  
Drake, A.J., 88  
Díaz, V.B., 49, 74, 102  
  
Ennis, A.I., 44  
Épinat, B., 45  
Escobar, G.J., 50  
Espinoza-Arancibia, F., 89  
  
Feinstein, C., 68  
Fellhauer, M.A., 37, 40, 51, 74, 77, 94, 102  
Fernandes, B., 75  
Ferrada-Chamorro, S., 52  
Ferraro, F., 90  
Ferreira Lopes, C.E., 88  
Figueredo, M., 92  
Flores-Durán, S., 63  
Foppiano, A., 86  
Fox-Machado, L., 54  
Franco, J., 101  
  
Galbany, L., 66  
Galli, P.A.B., 81  
Gancio, G., 91

Garcés, J., 55, 79  
 Garcia, A., 100  
 Garcia, M., 92  
 Gatto, L.M., 89  
 Geisler, D., 90  
 GOGREEN Collaboration, 61  
 Gonçalves, T., 92  
 González Lobos, V., 56  
 González, G.A., 98  
 Gorrini, P., 90  
 Gotta, V., 90  
 Grassi, T., 82  
 Gregorio-Hetem, J., 75, 99  
  
 Hadano, R., 92  
 Haemmerle, L., 74  
 Haucke, M., 41  
 Herrera, D., 93  
 Hernández, J., 83  
 Higuera, J., 54  
 Higuera-G, M.A., 87, 91  
  
 Jablonski, F.J., 88, 93  
 Jatenco-Pereira, V., 81, 99  
 Jofré, P., 70  
  
 Kerber, L., 98  
 Khalatyan, A., 38  
 Kharb, P., 46  
 Klessen, R.S., 74  
 Kooi, J., 91  
 Kravtsov, V.V., 57  
 Kurtev, R., 84  
  
 Larrarte, J.J., 91  
 Leigh, N., 74, 102  
 Lena, D., 46  
  
 Lepine, J., 91, 92  
 Lima Neto, G.B., 73  
 Lima, I.J., 93  
 Liu, H.-L., 58  
 Llerena, M., 92  
 Longa-Peña, P., 93  
 Longinotti, A.L., 66  
 Lopes, C.E.F., 93  
 Lucena, S., 92  
 Lucero, F.I., 65  
 Lupi, A., 52  
 Luqueze, M., 91, 92  
  
 Maia, F., 98  
 Makita, K., 86  
 Manzano, L.E., 94  
 Mariano, Y.C.P., 88  
 Martínez, R., 64  
 Matus Carrillo, D.R., 51, 77  
 Mauro, F., 59, 90  
 May, D., 82  
 Melendez-Delmestre, K., 92  
 Mena, F.P., 65  
 Méndez, R.A., 102  
 Mennickent, R.E., 55, 79, 87  
 Merchán, M., 67  
 Michtchenko, T.A., 96  
 Molina, R., 65  
 Monachesi, A., 28  
 Moni Bidin, C., 43, 90  
 Montmerle, T., 75  
 Morales Inostroza, M.C.B., 51  
 Morales, M.C., 94  
 Morales-Vargas, A., 66  
 Motter, J.C., 83

Muzzin, A., 61

Nantais, J., 61

Noble, A., 61

Olave, C., 74

Old, L., 61

Oliveira, A.S., 93

Oostra, B., 95

Orchard, M.E., 102

Ordenes-Huanca, C., 95

Ortega-Minakata, R.A., 66

Oses, R., 100

Padilla, N.D., 86

Palhares, M.S., 93

Papageorgiou, A., 88

Parra, J., 86

Peña, M., 63, 97

Peña-Ramírez, K., 62, 80

Pellizza, L.J., 50

Pereira, E.S., 96

Pereira, M.G., 96

Piatti, A., 98

Pimentel, O.M., 98

Pinto, G.A., 64

Pinzón, G., 83

Queiroz, A.B.A., 38

Quirola-Vásquez, J., 96

Ramírez-Alegría, S., 80

Rasztocky, E., 91

Raulin, J-P., 92

Razo López, N.B., 97

Reeves, R., 86

Reinoso, B., 74, 102

Reisenegger, A., 86, 89, 99

Restrepo, O.A., 65

Rial, D., 100

Riaz, R., 49, 74

Riffel, R., 48

Riffel, R.A., 46, 48

Robinson, A., 46

Robleto-Orús, A.C., 66

Rodrigues, C.V., 88, 93

Rodriguez, F., 67

Rodríguez, L.F., 95

Rodríguez, M.J., 68

Rodríguez, R., 86

Roig, F., 92

Romero, G.E., 50

Romero, M., 93

Romero-Cruz, F.A., 66

Ronsó, D., 91

Rudnick, G., 61

Rueda, J.A., 84

Ruffini, R., 84

Ruiz-Escobedo, F., 97

S Klessen, R., 102

S-PLUS collaboration, 99

Sánchez, M.B., 72

Sánchez, S.F., 66

Sánchez-Salcedo, F.J., 71

Sabín-Sanjulián, C., 69

Salas, H., 93

Sales, D., 89

Samadi-Ghadim, A., 70

Santiago, B.X., 38, 47

Santos, Y.F., 98

Santos Jr., J.F.C., 98

Santos-Silva, T., 75, 99  
Sanzovo, G.C., 53  
Scherer, A., 99  
Schleicher, D.R.G., 49, 52, 74, 85, 102  
Schnorr-Müller, A., 46  
Shen, S., 42  
Shugarov, S., 93  
Silva, J.F., 102  
Silva, K.M.G., 93  
Simon, J.D., 37  
Solar, M., 100  
SpARCS Collaboration, 61  
Steiner, J.E., 82  
Storchi-Bergmann, T., 46  
Stutz, A.M., 56, 58  
Szkody, P., 93  
Tavernier, A., 100  
Torres-Papaqui, J.P., 66  
Torres-Peimbert, S., 31, 101  
Trejo-Alonso, J.J., 66  
Ulloa, C., 100  
Unda-Sanzana, E., 76  
Urrutia Zapata, F., 40, 51, 77  
Uzundag, M., 78  
Vásquez, A.M., 34  
van der Burg, R., 61  
Vanaverbeke, S., 49  
Varela, M.E., 64  
Velarde, E., 101  
Venero, R., 41  
Vergara, M.Z.C., 49, 74, 102  
Verri, S., 91, 92  
Villegas, C.L., 102  
Villegas, F.A., 79  
VISCACHA team, 98  
Vučković, M., 78  
Wang, Q.D., 95  
Wiermann, A., 92  
Wilson, G., 61  
Yin, J., 42  
Yuan, F., 42  
Zanella, D., 91, 92